



AALBORG UNIVERSITY
DENMARK

Aalborg Universitet

Mobility Management for Cellular Networks

From LTE Towards 5G

Gimenez, Lucas Chavarria

DOI (link to publication from Publisher):
[10.5278/VBN.PHD.ENGSCI.00101](https://doi.org/10.5278/VBN.PHD.ENGSCI.00101)

Publication date:
2017

Document Version
Publisher's PDF, also known as Version of record

[Link to publication from Aalborg University](#)

Citation for published version (APA):

Gimenez, L. C. (2017). *Mobility Management for Cellular Networks: From LTE Towards 5G*. Aalborg Universitetsforlag. Ph.d.-serien for Det Tekniske Fakultet for IT og Design, Aalborg Universitet
<https://doi.org/10.5278/VBN.PHD.ENGSCI.00101>

General rights

Copyright and moral rights for the publications made accessible in the public portal are retained by the authors and/or other copyright owners and it is a condition of accessing publications that users recognise and abide by the legal requirements associated with these rights.

- ? Users may download and print one copy of any publication from the public portal for the purpose of private study or research.
- ? You may not further distribute the material or use it for any profit-making activity or commercial gain
- ? You may freely distribute the URL identifying the publication in the public portal ?

Take down policy

If you believe that this document breaches copyright please contact us at vbn@aub.aau.dk providing details, and we will remove access to the work immediately and investigate your claim.

MOBILITY MANAGEMENT FOR CELLULAR NETWORKS

FROM LTE TOWARDS 5G

**BY
LUCAS CHAVARRÍA GIMÉNEZ**

DISSERTATION SUBMITTED 2017



AALBORG UNIVERSITY
DENMARK

Mobility Management for Cellular Networks: From LTE Towards 5G

Ph.D. Dissertation
Lucas Chavarría Giménez

Aalborg University
Department of Electronic Systems
Fredrik Bajers Vej 7
DK - 9220 Aalborg

Dissertation submitted: January 2017

PhD supervisor: Prof. Preben E. Mogensen
Department of Electronic Systems
Aalborg University

Assistant PhD supervisor: Prof. Klaus I. Pedersen
Department of Electronic Systems
Aalborg University

PhD committee: Professor Hans-Peter Schwefel (chairman)
Aalborg University

Associate Professor Henrik Lehrmann Christiansen
Technical University of Denmark

Research Engineer Berna Sayrac
Orange Labs France

PhD Series: Technical Faculty of IT and Design, Aalborg University

ISSN (online): 2446-1628
ISBN (online): 978-87-7112-891-8

Published by:
Aalborg University Press
Skjernvej 4A, 2nd floor
DK – 9220 Aalborg Ø
Phone: +45 99407140
aauf@forlag.aau.dk
forlag.aau.dk

© Copyright: Lucas Chavarría Giménez

Printed in Denmark by Rosendahls, 2017

Curriculum Vitae

Lucas Chavarría Giménez

Lucas Chavarría Giménez obtained his M.Sc. degree in Mobile Communications from Aalborg University, Denmark in 2011. From 2012 and 2014, he was employed as a research assistant at the Radio Access Technology (RATE) Section from the Department of Electronic Systems at Aalborg University. In February 2014, Lucas started pursuing the PhD degree in Wireless Communications within the Wireless Communication Networks (WCN) section at the Department of Electronic Systems at Aalborg University in collaboration with Nokia Bell-Labs. His research activities and interests are in the development of mobility management solutions for the next-generation of mobile networks.

Abstract

The ongoing design and standardization of the fifth generation (5G) new radio (NR) will enable new use cases and applications, imposing more challenging requirements in terms of mobility performance. As an example, 5G mobile networks should support seamless mobility with zero data interruption at each handover, even at high speeds.

A prerequisite for research towards new 5G mobility solutions is to first understand what current procedures can achieve. The initial work of this thesis is therefore focused on the analysis of field-measurements of an operational Long Term Evolution (LTE) network in both slow- and high-speed scenarios, observing rate of radio-link failures, handover failures, data interruption times, etc. It is found that the macro-cellular mobility performance is good with a low rate of failures. However, the measurements also reveal that the handover data interruption time can sometimes be hundreds of milliseconds and, therefore, presenting the first challenge to be addressed in order to fulfill the demanding 5G requirements. The field measurements are furthermore used to calibrate and validate system-level simulation models presented in the remainder of the thesis for benchmarking more sophisticated mobility solutions that are not yet implemented in the field.

Secondly, studies of the mobility performance and the data interruption time for the more evolved LTE-Advanced (LTE-A) versions with dual connectivity are addressed. These studies are conducted for a variety of environments, including generic scenarios with hexagonal network topologies, non-uniform site-specific scenarios, pedestrian mobility and high-speeds up to 130 km/h. The impact of using different network architectures for implementing dual connectivity are assessed as well. Simulations results of a site-specific high-speed scenario shows that when adopting dual connectivity with secondary cell group (SCG) architecture, the overall data interruption time increases by 42 % compared to single-node connectivity. While, if dual connectivity is realized with the split-bearer architecture, the interruption time is reduced by 83 %.

Furthermore, novel candidate solutions such as synchronous handover without random access (a.k.a. RA-less handover) and innovations with make-

before-break are explored. Complete elimination of the handover data interruption time is achieved by integrating both solutions, including new methods for synchronization and flow control between the data buffers at the source and target cells.

Additionally, the dissertation proposes further mobility enhancements for the next generation of mobile networks, including partly user-autonomous controlled mobility for reducing the control signaling overhead, and a user-association algorithm that selects the most suitable target cell based on throughput estimates (i.e. offering enhanced traffic steering capabilities). The concept of partly user-autonomous mobility is found to be particularly attractive for multi-connectivity scenarios where the device follows a predictable path, passing many cell sites with small to medium coverage. An example of the latter is the use case of highway vehicular devices, where it is found that the air interface Radio Resource Control (RRC) backhaul signaling can be reduced up to 92 % and 39 %, respectively.

Resumé

Den igangværende design og standardisering af den femte generation (5G) nye radio (NR) vil gøre det muligt for nye applikationer med mere udfordrende requirements med hensyn til mobilitet ydeevne. Som et eksempel, bør 5G mobilnet understøtte problemfri mobilitet med nul data afbrydelse ved hver overdragelse, selv ved høje hastigheder.

En forudsætning for forskning i retning af nye 5G mobile løsninger er først at forstå, hvad de nuværende løsninger kan opnå. Det indledende arbejde med denne afhandling er derfor fokuseret på analysen af field-målinger af en operationel Long Term Evolution (LTE) netværk i både langsom og høj hastighed scenarier, observere på radio-link fiaskoer, overdragelsen fiaskoer, data afbrydelse gange osv det er fundet, at makro-cellulære mobilitet præstation er god med en lav fiaskoer. Men målingerne viser også, at overdragelsen af data afbrydelse tid til tider kan være hundredvis af millisekunder, og derfor præsentere den første udfordring, der skal løses for at opfylde de krævede 5G krav. Målingerne felt er desuden bruges til at kalibrere og validere systemniveau simuleringer modeller præsenteret i resten af afhandlingen for benchmarking mere avancerede mobilitetsløsninger, der endnu ikke er gennemført på området.

For det andet er studier af mobilitet ydeevne og data afbrydelse tid til mere udviklet LTE-Advanced (LTE-A) versioner med dobbelt konnektivitet rettet. Disse undersøgelser er gennemført for en række forskellige miljøer, herunder generiske scenarier med sekskantede netværkstopologier, uensartede stedsspecifikke scenarier, fodgænger mobilitet og høje hastigheder på op til 130 km/t. Virkningen af at anvende forskellige netværksarkitekturer for gennemførelse dobbelt tilslutningsmuligheder vurderes som godt. Simuleringer resultaterne af en stedsspecifik højhastigheds-scenariet viser, at når det vedtager dobbelt tilslutning med sekundær celle gruppe (SCG) arkitektur, de samlede data afbrydelse tid stiger med 42 % i forhold til single-node-forbindelse. Mens, hvis dobbelt-forbindelse er realiseret med split bannerfører arkitektur, er afbrydelsen tid reduceret med 83 %.

Desuden er nye kandidat løsninger såsom synkron overdragelse uden random access (a.k.a RA-mindre overdragelsen) og innovationer med make-

før-break udforsket. Fuldstændig fjernelse af overdragelsen data afbrydelse tid opnås ved at integrere de to løsninger, herunder nye metoder til synkronisering og flowkontrol mellem data buffere på kilde- og target-cellerne.

Derudover afhandlingen foreslår yderligere mobilitet forbedringer til den næste generation af mobile netværk, herunder dels bruger-autonome kontrolleret mobilitet for at reducere kontrol signaleringsomkostninger, og en bruger-forening algoritme, der vælger den mest egnede målcellen baseret på throughput skøn (dvs. udbud forbedret trafik styreegenskaber). Begrebet delvis user-selvstændige mobilitet har vist sig at være særligt attraktive for multi-tilslutningsmuligheder scenarier, hvor indretningen følger en forudsigelig sti, passerer mange celle steder med små til mellemstore dækning. Et eksempel implementering af sidstnævnte er brugen tilfælde af motorvej køreveje enheder, hvor det er fundet, at luften grænsefladen Radio Resource Kontrol (RRC) signalering og netværk backhaul signalering kan reduceres op til 92 % og 39 %, henholdsvis.

Contents

Curriculum Vitae	iii
Abstract	v
Resumé	vii
List of Abbreviations	xix
Thesis Details	xxi
Acknowledgments	xxiii
I Introduction	1
Introduction	3
1 Architecture of a Cellular System	4
1.1 System Architecture of a 3G Network	5
1.2 System Architecture of a 4G Network	5
2 Mobility management in Cellular Networks	6
2.1 Mobility management in 3G networks	7
2.2 Mobility management in LTE	8
2.3 Mobility management in LTE-A	8
3 Towards the fifth generation of mobile networks	9
4 Scope of the Thesis	10
5 Research Methodology	10
6 List of Contributions	12
7 Thesis Outline	15
References	17
II Mobility Performance of Current Cellular Networks	19
1 Motivation	21

2	Objectives	22
3	Included Articles	22
4	Main Findings	23
	References	26
A	Validation of Mobility Simulations via Measurement Drive Tests in an Operational Network	27
1	Introduction	29
2	Simulations Methodology and Modeling	30
	2.1 Basic Methodology	30
	2.2 Aalborg Site-Specific Scenario	30
	2.3 User Movement Model	32
	2.4 Mobility Events Model	32
3	Drive Test Measurements	33
4	Performance Results	34
5	Conclusions	38
	References	39
B	Mobility Performance in Slow- and High-Speed LTE Real Scenarios	41
1	Introduction	43
2	Handover Timing and Key Performance Indicators	44
3	Scenario Description	45
4	Measurements	46
5	Experimental Results	47
	5.1 Coverage	47
	5.2 RRC Messages Analysis	48
	5.3 RLFs and HOFs	50
	5.4 Handover Events and Timing	50
6	Measurements and Simulations Comparison	52
7	Conclusions	53
	References	53
III	Mobility Performance of LTE-A with Dual Connectivity	55
1	Motivation	57
2	Objectives	58
3	Included Articles	58
4	Main Findings	59
	References	63

C	Mobility Sensitivity Analysis for LTE-Advanced HetNet Deployments with Dual Connectivity	65
1	Introduction	67
2	System Model And Mobility Concept	68
3	Scenarios and Related Modeling Assumptions	70
3.1	The Generic 3GPP Scenario	72
3.2	Site Specific Scenarios	72
4	Performance Results	73
5	Conclusions	77
	References	77
D	Analysis of Data Interruption in an LTE Highway Scenario with Dual Connectivity	79
1	Introduction	81
2	Scenario Description and Mobility Framework	82
2.1	Mobility with Single Connectivity	83
2.2	Mobility with Dual Connectivity	84
2.3	User-Plane Architectures for Dual Connectivity	85
2.4	Data Interruption Time	86
3	Simulation Methodology	86
4	Performance Results	87
5	Conclusions	91
	References	91
E	UE Autonomous Cell Management in a High-Speed Scenario with Dual Connectivity	93
1	Introduction	95
2	Network-Controlled and UE-assisted mobility	96
3	UE Autonomous Cell Management	97
3.1	Preparation strategy	100
4	Scenario and Simulation Methodology	102
5	Performance Results	105
6	Conclusions	108
7	Acknowledgments	108
	References	108
IV	Mobility Performance Towards 5G	111
1	Motivation	113
2	Objectives	114
3	Included Articles	114
4	Main Findings	115
	References	117

F	Towards Zero Data Interruption Time with Enhanced Synchronous Handover	119
1	Introduction	121
2	The LTE Baseline Handover	122
3	The Basic Synchronous RA-less Handover	125
4	Enhancements of the RA-less Handover	126
4.1	Early Data Forwarding During the Handover Preparation	126
4.2	Synchronous Make-Before-Break Handover	127
5	Evaluation of the Proposed Enhancements	129
5.1	Handover Timing with Typical Delays	129
5.2	UE and X2 Latency Sensitivity Analysis	130
5.3	Handover Timing Towards 5G	131
6	Conclusions	131
	References	134
G	Mobility Enhancements from LTE towards 5G for High-Speed Scenarios	135
1	Introduction	137
2	Mobility performance in current LTE networks	138
3	Mobility enhancements towards 5G	141
4	Overview of mobility enhancements	146
5	Conclusions	150
	References	150
H	Throughput-Based Traffic Steering in LTE-Advanced HetNet Deployments	153
1	Introduction	155
2	System Model and Performance Indicators	156
2.1	Scenario Modeling	156
2.2	Objectives and Performance Indicators	156
3	Throughput-Based Traffic Steering Algorithm	156
3.1	Signal-to-Interference and Noise Ratio Estimation	157
3.2	Throughput Estimation	157
3.3	Target Cells Selection	157
3.4	Theoretical Analysis of the Gain	158
3.5	Traffic Steering – Option 1	159
3.6	Traffic Steering – Option 2	160
4	Performance Evaluation	161
5	Simulation Results	162
5.1	Throughput Estimation Error	165
6	Conclusions	165
	References	165

V	Additional Studies and Collaborations	169
	References	176
VI	Conclusions	177
1	Summary of the Main Findings	179
2	Future Work	182
	References	182
	Appendix A	184
I	Comparison and Extension of Existing 3D Propagation Models with Real-world Effects Based on Ray-tracing. A Basis for Network Planning and Optimization	187
1	Introduction	189
2	Problem Formulation	191
	2.1 Tilt Dependency of Propagation Model	191
	2.2 Height Gain	192
3	Derivation of Tilt and Height Dependent propagation Model	193
	3.1 Tilt Dependent Shadow Model	193
	3.2 Height Gain Model	195
4	Ray Tracing Scenario Description and Statistics Extraction	195
	4.1 Ray Tracing Scenario	195
	4.2 Statistics Extraction	196
5	Model Coefficient Prediction and Performance Evaluation	199
	5.1 Shadowing Statistics and Predictor Coefficients	199
	5.2 Statistical Behavior of Height Gain	203
6	Impact of Tilt and Height Based Models in Network Planning and Optimization	204
7	Conclusion	206
	References	207
J	Verification of 3G and 4G Received Power Measurements in a Crowd-sourcing Android App	209
1	Introduction	211
2	The NetMap Application	212
3	Methodology	214
	3.1 Tools and Scenarios	214
	3.2 Data Processing and Evaluation	216
4	Results	219
5	Discussion	221
6	Conclusion	223
	References	224

K	From LTE to 5G for Connected Mobility	227
1	Introduction	229
2	Measurement Campaign	230
3	Latency Performance	233
4	Handover Execution Performance	236
5	Coverage Performance	237
6	Enabling Connected Mobility in 5G	239
7	Conclusion	241
	References	242
L	Measurement-based Evaluation of the Impact of Large Vehicle Shadowing on V2X Communications	245
1	Introduction	247
2	Measurement Campaign	248
	2.1 Measurement Scenario	248
	2.2 Setup, Calibration & Data Processing	251
3	Measurement Results	252
4	Comparison with Ray-tracing	255
5	Dynamic & Scalable Shadowing Model	258
6	Conclusions	263
	References	264
M	A Simple Statistical Signal Loss Model for Deep Underground Garage	267
1	Introduction	269
2	Measurement Campaign	270
	2.1 Scenarios	270
	2.2 Measurement Setup and Procedures	271
3	Result analysis	272
	3.1 Propagation into Underground Building Structure	272
	3.2 Floor Attenuation Factor	275
4	Conclusions	277
	References	277

List of Abbreviations

1G	First generation of mobile networks
2G	Second generation of mobile networks
3D	Three-dimensional
3G	Third generation of mobile networks
3GPP	Third generation partnership project
4G	Forth generation of mobile networks
5G	Fifth generation of mobile networks
AAU	Aalborg University
ACK	Acknowledgment
API	Application programming interface
AS	Active set
ASU	Arbitrary strength unit
C-RAN	Cloud-RAN
CA	Carrier aggregation
CAC	Composite available capacity
CDF	Cumulative density function
CN	Core network
CPICH	Common pilot channel
CQI	Channel quality indicator
CS	Circuit switched

CW	Continuous wave
DC	Dual connectivity
DL	Downlink
DPM	Dominant path model
E-RAB	E-UTRAN radio access bearer
E-UTRAN	Evolved UTRAN
E_c/I_o	Received signal per chip interference ratio
eNB / eNodeB	Evolved Node-B
EPC	Evolved packet system core network
FAF	Floor attenuation factor
FSPL	Free-space path loss
FTP	File transfer protocol
GPRS	General packet radio system
GPS	Global positioning system
HARQ	Hybrid-automatic-repeat-request
HetNet	Heterogeneous network
HO	Handover
HOF	Handover failure
HSPA	High-speed packet access
HSPA+	Evolved HSPA
ID	Identity
ISD	Inter-site distance
ITU	International telecommunication union
KPI	Key performance indicator
LOS	Line-of-sight
LR	Least-square
LTE	Long term evolution

LTE-A	LTE-Advanced
LTE-A Pro	LTE-Advanced professional
MAC	Medium access control
MBB	Mobile broadband
MCL	Maximum coupling loss
MeNB	Master eNB
MIMO	Multiple-input and multiple-output
MLB	Mobility load balancing
MME	Mobility management entity
MNO	Mobile network operator
MRO	Mobility robustness optimization
MSC	Mobile services sitwching centre
MTC	Machine-type communications
NB-IoT	Narrow-band internet-of-things
NLOS	Non-line-of-sight
NR	New Radio
PCell	Primary cell
PDCP	Packet data convergence protocol
PDSCH	Physical downlink shared channel
PP	Ping-pong
PRACH	Pyshical random access channel
PRB	Physical resource block
PS	Packet switched
QoS	Quality of service
RA	Random access
RACH	RA channel
RAN	Radio access network

RAT	Radio access technology
RE	Range extension
RF	Radio-frequency
RLC	Radio-link control
RLF	Radio-link failure
RMSE	Root mean square error
RNC	Radio network controller
RRC	Radio resource control
RRM	Radio resource management
RSCP	Received signal code power
RSRP	Reference signal received power
RSRQ	Reference signal received quality
RSSI	Received signal strength indicator
RSU	Road-side-unit
RTT	Round-trip-time
RX	Receiver
S-GW / SGW	Serving gateway
S-Synch	Secondary synchronization signal
SC	Small cell
SCell	Secondary cell
SCG	Secondary cell group
SeNB	Secondary eNB
SGSN	Serving GPRS support mode
SINR	Signal-to-interference-noise-ratio
TA	Time advance
TOS	Time-of-stay
TS	Traffic steering

TTI	Transmission time interval
TTT	Time-to-trigger
UDN	Ultra-dense network
UE	User equipment
UL	Uplink
UMi	Urban micro
UMTS	Universal mobile telecommunications system
UTRAN	UMTS terrestrial RAN
V2I	Vehicle-to-infrastructure
V2V	Vehicle-to-vehicle
V2X	V2V/V2I
WCN	Wireless Communication Networks
WLAN	Wireless local area network

Thesis Details

Thesis Title: Mobility Management for Cellular Networks: From LTE Towards 5G.

PhD Student: Lucas Chavarría Giménez.

Supervisors: Prof. Preben E. Mogensen. Aalborg University.
Prof. Klaus I. Pedersen. Aalborg University.

This PhD thesis is the result of three years of research at the Wireless Communication Networks (WCN) section (Department of Electronic Systems, Aalborg University, Denmark) in collaboration with Nokia – Bell Labs.

The main body of this thesis consist of the following articles:

- Paper A: Lucas Chavarría Giménez, Simone Barbera, Michele Polignano, Klaus I. Pedersen, Jan Elling, Mads Sørensen. "Validation of Mobility Simulations via Measurement Drive Tests in an Operational Network", *IEEE 81st Vehicular Technology Conference (VTC Spring)*. May 2015, pp. 1-5.
- Paper B: Lucas Chavarría Giménez, Maria Carmela Cascino, Maria Stefan, Klaus I. Pedersen, Andrea F. Cattoni. "Mobility Performance in Slow- and High-Speed LTE Real Scenarios". *IEEE 83rd Vehicular Technology Conference (VTC Spring)*. May 2016, pp. 1-5.
- Paper C: Simone Barbera, Lucas Chavarría Giménez, Laura Luque Sánchez, Klaus I. Pedersen, Per Henrik Michaelsen. "Mobility Sensitivity Analysis for LTE-Advanced HetNet Deployments with Dual Connectivity", *IEEE 81st Vehicular Technology Conference (VTC Spring)*. July 2015, pp. 1-5.

- Paper D: Lucas Chavarría Giménez, Per Henrik Michaelsen, Klaus I. Pedersen, "Analysis of Data Interruption Time in an LTE Highway Scenario with Dual Connectivity", *IEEE 83rd Vehicular Technology Conference (VTC Spring)*. May 20146, pp. 1-5.
- Paper E: Lucas Chavarría Giménez, Per Henrik Michaelsen, Klaus I. Pedersen, "UE Autonomous in a High-Speed Scenario with Dual Connectivity", *27th Annual IEEE International Symposium on Personal, Indoor and Mobile Radio Communications (PIMRC)*. September 2016, pp. 1-5.
- Paper F: Lucas Chavarría Giménez, Per Henrik Michaelsen, Klaus I. Pedersen, Troels E. Kolding, "Towards Zero Data Interruption Time with Enhanced Synchronous Handover", *IEEE 82nd Vehicular Technology Conference (VTC Spring)*. Submitted for publication. 2017.
- Paper G: Lucas Chavarría Giménez, Klaus I. Pedersen, Per Henrik Michaelsen, Preben E. Mogensen, "Mobility Enhancements from LTE towards 5G for High-Speed Scenarios", *IEEE Wireless Communications Magazine*. Submitted for publication. 2017.
- Paper H: Lucas Chavarría Giménez, István Z. Kovács, Jeroen Wigard, Klaus I. Pedersen, "Throughput-Based Traffic Steering in LTE-Advanced HetNet Deployments", *IEEE 82nd Vehicular Technology Conference (VTC Fall)*. September 2015, pp. 1-5.

In addition to the work here presented, and as part of the requirements for obtaining the PhD degree, mandatory courses and students supervision obligations were fulfilled.

This thesis has been submitted for assessment in partial fulfillment of the PhD degree. The thesis is based on the submitted or published scientific papers which are listed above. Parts of the papers are used directly or indirectly in the extended summary of the thesis. As part of the assessment, co-author statements have been made available to the assessment committee and are also available at the Faculty.

Acknowledgments

When I reflect upon the last three years, I feel particularly proud of what I have achieved. However, I would not have got this far without the support of many people. To all of them I dedicate this work.

There are two people in particular I would like to thank, my supervisors Professor Preben E. Mogensen and Professor Klaus I. Pedersen. I am extremely grateful for their unconditional support and constructive criticism offered throughout this thesis. It has been a pleasure to work with both of them.

I am also grateful to the co-authors of the papers included in this thesis. I have very much enjoyed the experience of working collaboratively and publishing together. A number of colleagues in particular offered important guidance at different times. Per Henrik Michaelsen provided helpful insights into the topics of this thesis and generously shared its wealth of experience with me. Also, his sense of humor was greatly appreciated particularly during the later part of this PhD. I would like to thank Laura Luque Sánchez for her advice and support, especially during the most stressful moments over the last few years and Troels E. Kolding for instilling the belief that anything is possible. Lastly, I would like to express my gratitude to Mads Brix who taught me how to work collaboratively on a system-level simulator.

I would also like to mention past and present colleagues from Aalborg University and Nokia – Bell Labs, who have made me feel part of both the academic community and the telecommunications industry, and have become great friends over the years.

Andrea F. Cattoni, Ali Karimi, Beatriz Soret, Benny Vejlgard, Claudio Rosa, Daniela Laselva, Davide Catania, Dereje A. Wassie, Erika Almeida, Fernando Tavares, Frank Frederiksen, Gilberto Berardinelli, Guillermo Pocovi, Huan C. Nguyen, Ignacio Rodríguez, István Z. Kovács, Jens Steiner, Jeroen Wigard, Mads Lauridsen, Michele Polignano, Panagiotis Fotiadis, Raphael Amarin, Renato Abreu, Simone Barbera, Thomas Jacobsen, Troels B. Sørensen, and Víctor Fernández.

I would also like to thank Dorthe Sparre and Linda Villadsen, section and project administrators from Aalborg University, for their friendly and professional assistance; my former Masters students, Maria Carmela Cascino and Maria Stefan, who I very much enjoyed supervising at Aalborg University; and Dr Germán Corrales, Pablo Fuentes and Patricia García de la Rosa for contributing on my success despite of the adversities. Lastly, I want to mention Dr Malayna Raftopoulos who spent innumerable hours proof-reading my articles and this thesis.

And of course, my family: Rosendo, Chendo, Alberto, Teresa, Judith and María Remedios who have supported and always believed in me despite being far away, and have encouraged me throughout the PhD to be the best I could be.

To all of them,

Thanks, tak, gracias.

Part I

Introduction

Introduction

In 1947 Douglas H. Ring and William R. Young described in a company memorandum the idea of providing wireless service to a metropolitan area by dividing it into a set of smaller regions covered by land transmitters [1]. These two engineers from Bell Laboratories gave birth to the now well-known concept of cellular networks. Unfortunately, the technology at that time was not mature enough and such visions had to remain on paper. It was some decades before these visions became a reality. Moreover, one important question remained unanswered:

"How to maintain a continuous connection if a moving user crosses the boundaries between cells?"

Twenty years later, in 1969, Bell Labs partially answered this question by implementing the first commercial cellular radio system, and materializing the ideas of Ring and Young. In this first cellular system, passengers of the *Metroliner* (illustrated in Figure 1.1) were able to make phone calls while traveling at 160 km/h [2]. The train line was divided into nine radio-zones with one base station each. As the train entered into a new radio-zone, any ongoing call was automatically transferred to the next base station. With this, the very first idea of providing service continuity for moving users was finally implemented and the concepts of *handover* and *mobility management* were born. However, the call transfer was only possible providing the same channel in the next radio-zone was available. Otherwise, the ongoing call was terminated.

The idea of transferring a call between cells for a moving mobile was further discussed in the articles published by Richard H. Frenkiel and Philip T. Porter in 1970 and 1971, respectively. Nonetheless, the procedures to carry out such mechanism did not come to light until Amos E. Joel Jr published the very first patent on handovers in 1972 [3].

Ideas regarding cells and handovers between cells were so revolutionary that following the *Metroliner* trial, and during the subsequent years, these concepts were implemented in all the generations of cellular networks. From

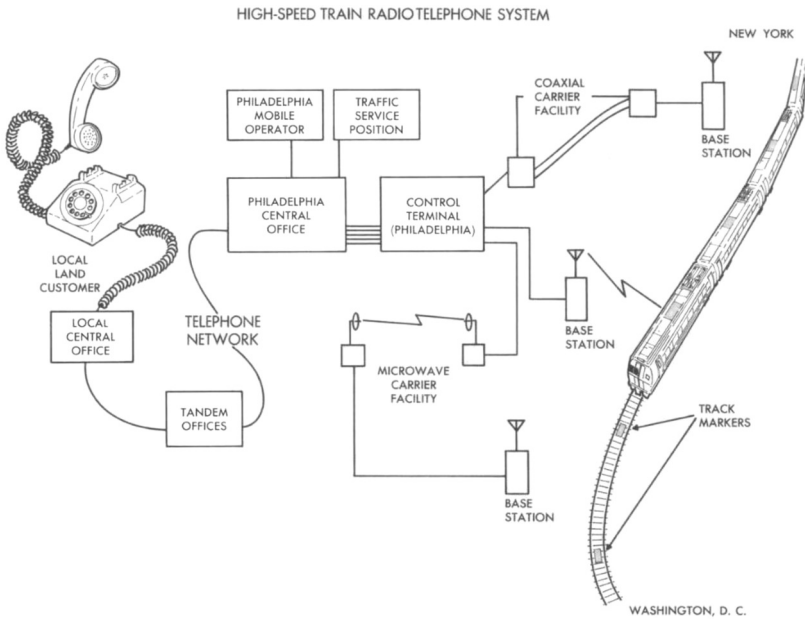


Fig. 1.1: Scheme of the first commercial cellular radio system deployed in January 1969 to provide service to the Metroliner train line. Image extracted from the Bell Laboratories record *Telephones Aboard the "Metroliner"* [2].

the first generation (1G) launched in Europe in 1981 [4], to the most recent fourth generation (4G) or Long Term Evolution (LTE).

This dissertation will closely analyze these well-known paradigms of cells, handover between cells, and the mobility management techniques implemented in current cellular networks and beyond: from the third generation (3G) of mobile networks –or Universal Mobile Telecommunications Systems (UMTS)–, the latest releases of LTE –LTE Advanced (LTE-A) and LTE-Advanced Professional (LTE-A Pro)–, towards the upcoming fifth generation (5G) of mobile networks. As a starting point, the following sections will provide a brief background of how the mobility management functionality is implemented in current mobile networks.

1 Architecture of a Cellular System

In order to understand the mobility management functionalities, it is first necessary to understand the architecture of a cellular system and the different implementations that can be found across the generations of our focus:

The architecture of a generic cellular system can be divided into three main parts:

- User Equipment (UE): Device that allows the end-user to access the services offered by the cellular network.
- Radio Access Network (RAN): Part of the cellular system in charge of the mobility management and of sustaining the connectivity between the UE and the core network. Moreover, the RAN is also in charge of guaranteeing an efficient utilization of the available radio resources.
- Core network (CN): Part of the system in charge of the access control, session control, and routing connections to external networks.

1.1 System Architecture of a 3G Network

The RAN in a 3G network is denominated UMTS Terrestrial RAN or UTRAN, whereas the CN is called Packet Core [5]. As can be seen in Figure 1.2(a), the 3G UTRAN consists of two main elements:

- The base station or **Node-B**, which performs the air interface Layer-1 processing, and implements some of the radio resource management (RRM) functionalities, like the inner-loop power control.
- The radio network controller (**RNC**) is the entity that manages the radio resources in the Node(s)-B that are connected to it. It is also responsible of controlling the load congestion and managing the buffer of the Nodes-B. It is also the entity that serves as the interface between the CN and the UTRAN. Generally speaking, a 3G network is based on a centralized architecture where the RNC orchestrates and hosts the majority of the functionalities, including the mobility management decisions.

1.2 System Architecture of a 4G Network

Whereas 3G supports circuit switching for voice and packet switching for data, LTE only supports packet switching. To this end, LTE defines a new RAN called evolved UTRAN (E-UTRAN) and a new packet-domain CN denominated evolved packet system core network (EPC) [6].

As illustrated in Figure 1.2(b), the LTE architecture was generally designed to be more flexible, simpler and flatter than the 3G architecture. As a result, the RNC is eliminated, and the RAN consists of a unique entity named evolved Node-B (**eNB**).

The eNB, therefore, integrates all the functionalities and protocols for providing the connectivity between the UE and the CN. These functionalities include those that were allocated in the RNC for 3G such as the mobility management and the efficient allocation of radio resources among the UEs.

Unlike 3G, LTE implements a distributed architecture where the eNBs can be connected to each other by means of the X2 interface.

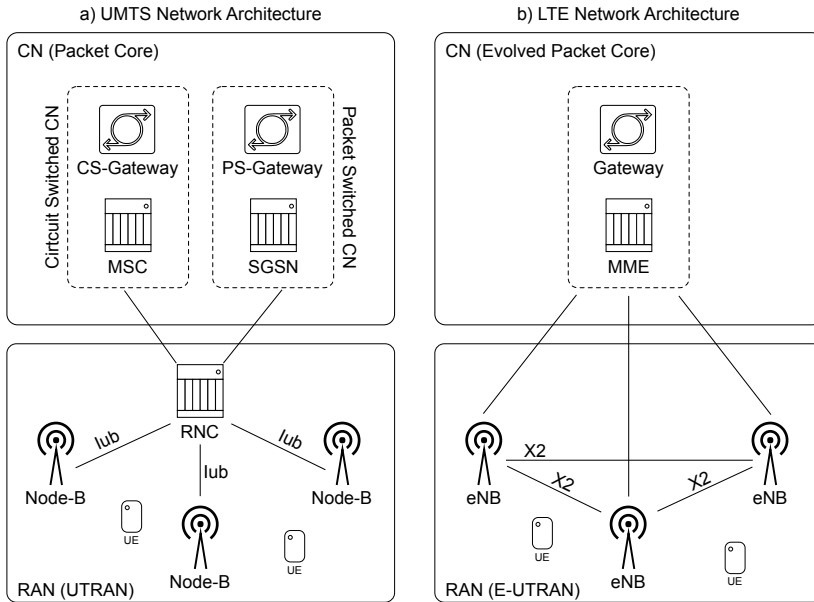


Fig. 1.2: Scheme of the network architectures of a) 3G (UMTS) system and b) 4G (LTE) system.

2 Mobility management in Cellular Networks

Among the different RRM functionalities, the mobility management is in charge of guaranteeing the continuation of the service as a user moves along the different cells. In general, the mobility of the UEs between the cells are managed by handovers or by cell re-selections, depending whether the UE is in connected- or idle-mode, respectively. The work compiled in this dissertation is mainly focused on connected-mode mobility.

The handovers can be typically classified into: **Intra-frequency** (between cells that share the same frequency band), **inter-frequency** (between cells which belong to different frequency bands), **intra-site** (between cells that belong to the same base station site) or **inter-site** (between cells that belong to different base station site). There are other types of classification, but they are beyond the scope of this thesis.

Handovers are normally based on a certain signal measured by the UE that is reported to the network with a certain periodicity, or when specific conditions are fulfilled. These measurements are commonly the received power or the signal quality perceived by the UE coming from the different cells. These observations are encapsulated in a measurement report and sent to the network. Afterwards, the network decides whether the handover should take place and which one is the best cell where the UE should connect

to. Thus, handovers are a **network-controlled and UE-assisted functionality**.

In order to measure the signals coming from cells that belong to different frequency bands, the UE should tune its filters. Due to the additional power consumptions that this operation entails, these measurements (called inter-frequency measurements) are not constantly performed and some cells operating in a different frequency bands may not be discovered by the UE. This is a common challenge in heterogeneous network (HetNet) scenarios, where a dense number of cells sizes coexist, operating at different frequency bands [7].

In general, the handover is a complex procedure that requires the following steps:

1. Radio measurements of the source and discovered neighboring cells at the UE side
2. Based on the measurements, the network takes the **handover decision** and determines the new target cell that will allocate the UE.
3. The network performs the **admission control**, by checking whether there are sufficient available resources for the target cell to accept the connection to the UE.
4. To guarantee a successful continuation of the service, the buffers at the target cell should be effectively managed. Thus, the target cell is ready to send data to the UE as soon as the handover process is complete. This step is critical in packet switched connections.
5. The radio bearers at the CN should be re-routed towards the new cell.

2.1 Mobility management in 3G networks

Connected mode mobility in 3G networks is based on the so-called **soft handovers**, where a UE is capable of maintaining several active connections to two or more adjacent cells simultaneously. The different cells a UE is connected to, constitute a list called active set (AS). As the UE approaches the boundaries of the current serving cell, a neighboring one becomes part of the AS, and the data transmission between the UE and the network follow different streams.

In the downlink, the signals from different cells are combined by the UE. In the uplink, if the cells in the AS belong to the same base station site, the data streams are received and combined by the Node-B. This situation is called **softer handover**. However, if the cells belong to different sites, the data streams must be combined at the RNC.

Due to the soft handover and the capabilities of having several simultaneous active links, the service continuity is guaranteed. Nevertheless, this

functionally can be only applied to intra-frequency handovers. In the cases of inter-frequency or inter-system handovers, the link with the previous cell must be terminated before establishing the connection towards a new cell. This process is called **hard handover** and because of its nature, the UE is unable to exchange any data with the network for the period of time this process lasts.

In all the cases, the RNC is the entity that decides what cells should serve each of the radio links, when the links should be terminated, executes the admission control, and decides when the handover should be performed. The RNC also terminates the radio resource control (RRC) protocol which is the one that defines the messages and procedures between the UE and the UTRAN. Moreover, the RNC is in charge of the buffer management to efficiently move the radio bearers between cells during a handover.

2.2 Mobility management in LTE

Due to the distributed nature of the network, LTE only implements hard handover procedures. In this type of handovers, the connection towards the serving cell should be "broken" before "making" the connection towards the new cell. Therefore, they also receive the name of **break-before-make** handovers. As will be further analyzed in this thesis, the hard handover functionality constitutes one of the most critical issues in the mobility performance for LTE, as during the handover process the UE is unable to exchange any data with the network.

The entity of the RNC does not exist in LTE. Therefore, the eNBs are in charge of performing the handover decisions and the admission control. Moreover, for continuous data transmission during handovers, the eNBs should support fast and efficient data forwarding mechanisms. To this end, the eNBs involved in the handover process can exchange signaling messages and user data during the handover via the X2 interface.

2.3 Mobility management in LTE-A

New features and mobility enhancements have appeared since the first version of LTE came to light with the 3rd Generation Partnership Project (3GPP) Release 8. The standardization of LTE Release 10 (under the branding name of LTE-A) included carrier aggregation (CA). With this feature, the UEs have the possibility of aggregating different component carriers within the same base station site, benefiting from additional allocated resources, hence increasing the end-user throughput.

This functionality was later extended to the aggregation of different carriers belonging to different sites. This enhancement appeared in LTE Release 12 under the name of dual connectivity (DC). DC was specifically design for

HetNet scenarios, where the UE can simultaneously consume radio resources from a macro-cell acting as the mobility anchor, and a small cell acting as a secondary cell that provides additional resources.

With these features, the UEs benefit from an increased throughput and enhanced mobility robustnesses [8]. Nevertheless, dual connectivity comes with the price of a large number of mobility events. Besides regular handovers, new events are defined for the aggregation, substitution, and release of the cells that serve the additional radio-links.

As will be described in the following parts of this thesis, the increased number of events becomes a challenging issue in high-speed HetNet scenarios. Additionally, the selected user-plane architecture for implementing DC has an impact on the mobility performance and on the data interruption time perceived by the UEs.

3 Towards the fifth generation of mobile networks

The LTE standard continues evolving: from the new features and enhancements included in LTE-A, to the most recent Release 13 under the commercial name of LTE-A Pro. However, the continuous demand for higher data rates and the appearance of new use cases (ranging from ultra-high definition media content to safety and ultra low-latency applications), calls for new capabilities that current mobile networks are unable to provide.

Therefore, a new generation of wireless networks is currently under development. The 5G new radio (NR) promises a completely new design that will meet more stringent and challenging requirements, allowing the implementation of the envisioned use cases. The design of new 5G NR includes the following mobility performance requirements:

- Seamless handovers between cells with zero data interruption time.
- Support for users moving at ultra-high speeds up to 500 km/h.
- Good mobility performance everywhere. The same good performance should be guaranteed for users in urban scenarios moving at pedestrian speeds and for users in high-speed scenarios such as highways or high-speed trains.

Table 1 shows a comparison between the current design recommendations for LTE-A [9] and the new target specifications for 5G [10]. These new stringent requirements are nowadays gaining momentum with the appearance of the new use cases. Consequently, these specifications are already being considered for the design of mobility enhancements in future releases of LTE. Therefore, LTE-A Pro is much more than a simple evolution of LTE-A.

Table 1: Comparison between the mobility requirements for LTE and 5G

Parameter	LTE [9]	5G [10]
HO interruption time	Intra-freq HO: 27.5 ms Inter-freq HO: [40-60] ms	0 ms
Max. UE speed supported	350 km/h	500 km/h

In fact, it can be considered as the standard that leads the way towards the design of mobility solutions for the 5G NR.

4 Scope of the Thesis

Inspired by the new and challenging mobility requirements, the main objectives of this thesis are:

- a) Understand what current mobility solutions can achieve by analyzing the mobility performance of current LTE networks.
- b) Based on the performance of the existing solutions, identify the critical issues that arise when considering the new mobility requirements.
- c) Propose new solutions that allows meeting the upcoming mobility requirements and user applications.
- c) Study and evaluate additional solutions that complement the proposed mobility enhancements for meeting the new design specifications.

5 Research Methodology

As depicted in Figure 1.3, the studies are carried out by an adopted research methodology that combines both, empirical and theoretical approaches. The overall working methodology can be summarized as follows:

- **Identify the main mobility problems in real scenarios:** The main problems and research questions have been identified by analyzing field-measurements of the mobility performance in operational 3G and 4G networks.
- **Identify the main hypothesis and possible solutions:** A more classical scientific approach was adopted for this task. First, the open literature was reviewed in search of additional research questions, any existing

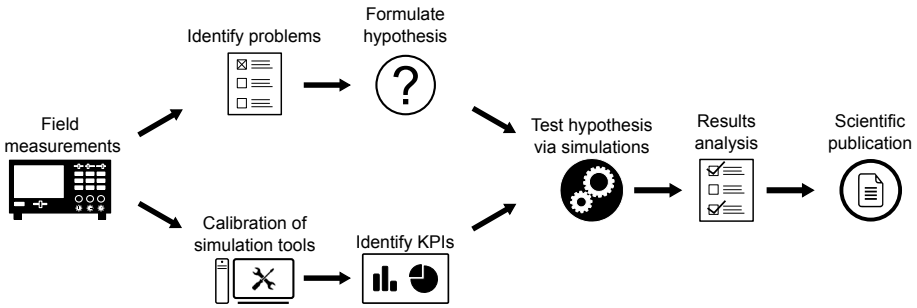


Fig. 1.3: Adopted research methodology during the course of these studies.

solutions, and new research directions. Then, the hypothesis were formulated followed by a proposal of new solutions to address the identified problems. During this process, the possible achievable benefits the proposed solutions could bring were also considered.

- **Calibration of simulation tools:** The outcome results of the measurements were utilized for calibrating, parameterizing, and validating the results provided by the simulation tools used for testing the hypothesis and the proposed solutions. Additionally, it was necessary to implement new capabilities in the simulation tools in order to import, replicate and simulate the scenarios analyzed during the field-measurements.
- **Identify the main key performance indicators (KPI):** In order to evaluate the performance of the proposed solutions, the main KPIs were identified. These included commonly accepted mobility performance KPIs and new ones that allowed us to fully understand the benefits of the proposals.
- **Validation and analysis of the solutions:** The majority of the hypothesis and proposed solutions were tested by means of Monte Carlo system-level simulations [11]. In order to create results of high degree of realism, the simulations were performed under commonly accepted 3GPP scenarios, or site-specific scenarios that model operational networks. With this methodology it was possible to work with quantities of data that are statistically significant, obtained by simulation campaigns with numerous users in the system. The time-based system-level simulator is developed in MATLAB and has been used for generating results for numerous 3GPP contributions and research projects, confirming is capable of producing trustful results [12–15]. The simulator also contributed on testing the latest state-of-the-art standardized features and mobility enhancements that are not yet available in the field.

- **Analysis of the results:** The postulated benefits of the proposed solutions were confirmed by an exhaustive analysis of the results. Moreover, the analysis of the results allow us to identify additional mobility problems that are not visible in the measurements.
- **Presentation of the results:** At the end of the entire process, the proposed solutions and their associated results were presented in the form of a scientific publication.

6 List of Contributions

The following publications has been authored or co-authored as part of the main core of the PhD studies:

- Paper A: Lucas Chavarría Giménez, Simone Barbera, Michele Polignano, Klaus I. Pedersen, Jan Elling, Mads Sørensen. "Validation of Mobility Simulations via Measurement Drive Tests in an Operational Network", *IEEE 81st Vehicular Technology Conference (VTC Spring)*. May 2015, pp. 1-5.
- Paper B: Lucas Chavarría Giménez, Maria Carmela Cascino, Maria Stefan, Klaus I. Pedersen, Andrea F. Cattoni. "Mobility Performance in Slow- and High-Speed LTE Real Scenarios". *IEEE 83rd Vehicular Technology Conference (VTC Spring)*. May 2016, pp. 1-5.
- Paper C: Simone Barbera, Lucas Chavarría Giménez, Laura Luque Sánchez, Klaus I. Pedersen, Per Henrik Michaelsen. "Mobility Sensitivity Analysis for LTE-Advanced HetNet Deployments with Dual Connectivity", *IEEE 81st Vehicular Technology Conference (VTC Spring)*. July 2015, pp. 1-5.
- Paper D: Lucas Chavarría Giménez, Per Henrik Michaelsen, Klaus I. Pedersen, "Analysis of Data Interruption Time in an LTE Highway Scenario with Dual Connectivity", *IEEE 83rd Vehicular Technology Conference (VTC Spring)*. May 2016, pp. 1-5.

- Paper E: Lucas Chavarría Giménez, Per Henrik Michaelsen, Klaus I. Pedersen, "UE Autonomous in a High-Speed Scenario with Dual Connectivity", 27th Annual IEEE International Symposium on Personal, Indoor and Mobile Radio Communications (PIMRC). September 2016, pp. 1-5.
- Paper F: Lucas Chavarría Giménez, Per Henrik Michaelsen, Klaus I. Pedersen, Troels E. Kolding, "Towards Zero Data Interruption Time with Enhanced Synchronous Handover", *IEEE 85th Vehicular Technology Conference (VTC Spring)*. Submitted for publication. 2017.
- Paper G: Lucas Chavarría Giménez, Klaus I. Pedersen, Per Henrik Michaelsen, Preben E. Mogensen, "Mobility Enhancements from LTE towards 5G for High-Speed Scenarios", *IEEE Wireless Communications Magazine*. Submitted for publication. 2017.
- Paper H: Lucas Chavarría Giménez, István Z. Kovács, Jeroen Wigard, Klaus I. Pedersen, "Throughput-Based Traffic Steering in LTE-Advanced HetNet Deployments", *IEEE 82nd Vehicular Technology Conference (VTC Fall)*. September 2015, pp. 1-5.

Additionally, during the course of these studies, the following articles has been published as part of a collaborative work within the Wireless Communication Networks (WCN) section or with other Nokia – Bell Labs sites:

- Collaboration 1 Dereje W. Kifle, Lucas Chavarría Giménez, Bernhard Wegmann, Ingo Viering, Anja Klein. "Comparison and Extension of Existing 3D Propagation Models with Real-World Effects Based on Ray-Tracing", *Wireless Personal Communications*. July 2014, num. 3, vol. 78, pp. 1719-1738.
- Collaboration 2 Mads Lauridsen, Ignacio Rodriguez Larrad, Lars Møller Mikkelsen, Lucas Chavarría Giménez, Preben E. Mogensen. "Verification of 3G and 4G Received Power Measurements in a Crowdsourcing Android App". *Wireless Communications and Networking Conference (WCNC)*. April 2016, pp. 1-6.

- Collaboration 3 Mads Lauridsen, Lucas Chavarría Giménez, Ignacio Rodríguez Larrad, Troels B. Sørensen, Preben E. Mogensen. "From LTE to 5G Connected Mobility", *IEEE Communications Magazine*. Accepted for publication. March 2017.
- Collaboration 4 Ignacio Rodríguez Larrad, Erika P. L. Almeida, Mads Lauridsen, Dereje A. Wassie, Lucas Chavarría Giménez, Huan C. Nguyen, Troels B. Sørensen, Preben E. Mogensen. "Measurement-based Evaluation of the Impact of Large Vehicle Shadowing on V2X Communications", *22th European Wireless Conference*. May 2016, pp. 1-8.
- Collaboration 5 Huan C. Nguyen, Lucas Chavarría Giménez, Istvan Z. Kovács, Ignacio Rodríguez Larrad, Troels B. Sørensen, Preben E. Mogensen. "A Simple Statistical Signal Loss Model for Deep Underground Garage", *IEEE 84th Vehicular Technology Conference (VTC Fall)*. September 2016, pp. 1-5.

Furthermore, three patent applications have been filled:

- Patent application 1 "Optimized synchronous RA-less handover without explicit handover confirmation message."
- Patent application 2 "Optimized Synchronous Handover in Radio Networks incl. Multi-Layer Cloud RAN by means of Early Admission."
- Patent application 3 "Buffer Management for Synchronous Cell Changes."

An overview of all the produced contributions and their classification into research topics is depicted in Figure 1.4.

The work developed during this PhD study also required executing additional activities that are not directly reflected in the aforementioned publications:

- To carry out the field-measurements, it was necessary to become acquainted with the use of the equipment, as well as to develop the necessary scripts and tools for exporting the collected samples and analyzing the results.
- The real-scenario information (such as terrain maps, base station locations, antenna patterns, tilts and orientations) were input into a ray-tracing tool for predicting and generating the path loss maps that were

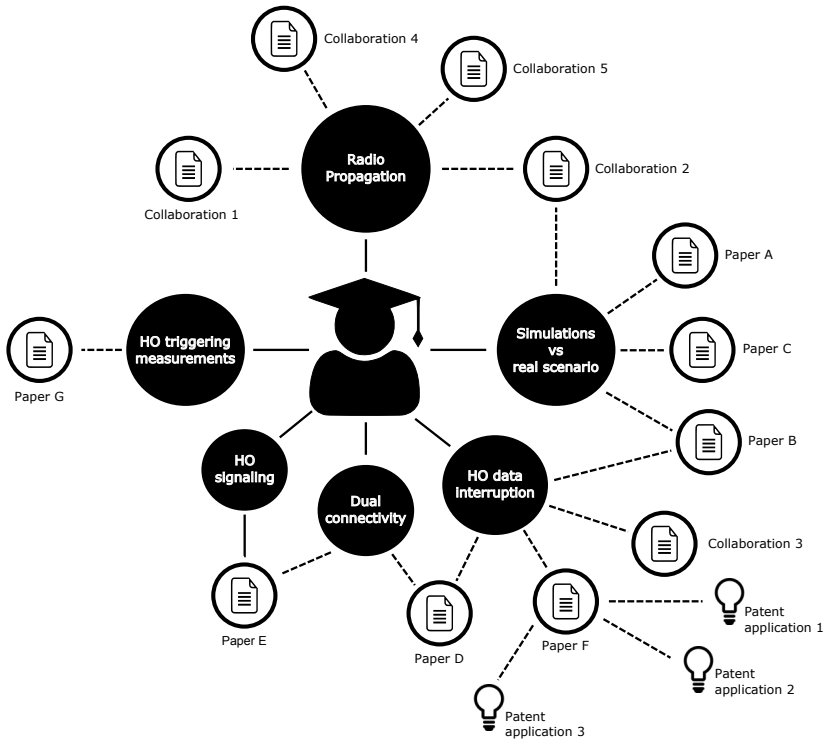


Fig. 1.4: Overview of all the contributions produced during the studies.

posteriorly used for the evaluation and the analysis of the solutions.

- The analyzed real-scenarios were also replicated into a system-level simulator. To this end, it was necessary to provide to the simulator new interfaces and capabilities for integrating and managing real network information, buildings and street layouts, terrain maps and the predicted path loss maps.

Finally, the PhD student participated in the supervision of student projects within the Wireless Communication Systems master of Aalborg University, for a total of 97 hours.

7 Thesis Outline

This dissertation is synthesized as a collection of publications. Therefore, the main contributions and findings of these studies are included in the articles that constitute the main core of the thesis. The dissertation is structured into six parts. Each of them include a short overview of the necessary background

and a summary of the main findings to help the reader in understanding how the different articles are related to each other. The thesis is outlined as follows:

- **Part I: Introduction** – Introductory chapter that presents the framework and the motivation for the study, explains the pursued goals, and describes the structure of this dissertation.
- **Part II: Mobility Performance of Current Cellular Networks** – This part is dedicated to identifying the main problems addressed in this thesis by analyzing field-measurements of the mobility performance under operational 3G and 4G networks. The measurements results identified one of the most critical limitations in LTE: the handover data interruption time. The outcome of the measurements is also used for calibrating a system-level simulator that replicates the studied real-scenarios. This step is relevant as the methodology of simulating real scenarios will be adopted throughout these studies. The main contributions of this part are collected in Paper A and Paper B.
- **Part III: Mobility Performance of LTE-A with Dual Connectivity** – This part presents the differences between the DC mobility performance results produced by the simulation of commonly adopted 3GPP scenarios, and the DC performance obtained by simulating a real-network. It also identifies the critical issues of the DC mobility performance of the highway scenario studied in Part I. Essentially, this part addresses the following questions: *Does the DC user-plane architecture have an impact in the experienced handover data interruption time? Can the signaling overhead produced by DC mobility events in a highway scenario be reduced?*. The outcome of these studies is presented in Paper C, Paper D, and Paper E.
- **Part IV: Mobility Performance Towards 5G** – This part presents an overview of the mobility enhancements that are currently under investigation for future LTE releases (from LTE-A Pro and onwards), leading the way to fulfilling the mobility performance requirements for 5G. Solutions for reducing and eliminating the handover data interruption time are presented. Moreover, is also proposes new handover decision algorithms that base their decisions on estimations of the user-throughput in the target cell. This part is composed by Paper F and Paper G.
- **Part V: Additional Mobility Challenges for Future Applications** – Based on the collaborative work with other research groups performed during the course of the PhD studies, this part summarizes additional

mobility challenges that may arise when considering the upcoming use-cases and applications. The articles that refer to this part are not in the main core of the thesis and are placed in an appendix at the end of this dissertation.

- **Part VI: Conclusions** – The dissertation is concluded by a summary of the main findings and recommendations for future research paths on the studied topics.

References

- [1] D. H. Ring, *Cover Sheet for Technical Memoranda. Mobile Telephony - Wide Area Coverage. Case 20564*, Bell Telephone Laboratories Incorporated, December 1947.
- [2] C. E. Paul, "Telephones aboard the metroliner," *Bell Laboratories Record*, vol. 77, March 1969.
- [3] A. E. Joel, "Mobile communication system," US Patent 3 663 762, 05 16, 1972.
- [4] A. Osseiran, J. Monserrat, and P. Marsch, *5G Mobile and Wireless Communications Technology*. Cambridge University Press, 2016.
- [5] H. Holma and A. Toskala, *WCDMA for UMTS. Radio Access for Third Generation Mobile Communications*. John Wiley & Sons Ltd, 2004.
- [6] —, *LTE for UMTS. OFDMA and SC-FDMA Based Radio Access*. John Wiley & Sons Ltd, 2009.
- [7] K. I. Pedersen, P. H. Michaelsen, C. Rosa, and S. Barbera, "Mobility enhancements for LTE-advanced multilayer networks with inter-site carrier aggregation," *IEEE Communications Magazine*, vol. 51, no. 5, pp. 64–71, May 2013.
- [8] S. C. Jha, K. Sivanesan, R. Vannithamby, and A. T. Koc, "Dual connectivity in LTE small cell networks," in *IEEE Globecom Workshops*, Dec 2014, pp. 1205–1210.
- [9] *Report ITU-R M.2134. Requirements related to technical performance for IMT-Advanced radio interface(s)*, 2008.
- [10] *3GPP Technical Report (TR) 38.913. Study on Scenarios and Requirements for Next Generation Access Technologies. V.0.4.0*, June 2016.
- [11] R. F. W. Coates, G. J. Janacek, and K. V. Lever, "Monte carlo simulation and random number generation," *IEEE Journal on Selected Areas in Communications*, vol. 6, no. 1, pp. 58–66, Jan 1988.
- [12] *FP7 SEMAFOUR project. Self-Management for Unified Heterogeneous Radio Access Networks*. [Online]. Available: <http://fp7-semafour.eu/>
- [13] *3GPP Technical Report (TR) 36.842. Study on Small Cell enhancements for E-UTRA and E-UTRAN. V.12.0.0*, Dec 2013.
- [14] *3GPP TSG-RAN WG1. R1-134528. Small Cell Detection Statistics and Related Considerations.*, Oct 2013.
- [15] *3GPP TSG-RAN WG2. R2-140368. Specifying Target Cell-Specific TTT.*, Feb 2014.

Part II

Mobility Performance of Current Cellular Networks

Mobility Performance of Current Cellular Networks

Before starting the analysis and design of new mobility solutions, it is necessary to understand what existing cellular networks can achieve. This part focuses on analyzing the experienced mobility performance of current 3G and 4G networks. The analysis is conducted by means of field-measurements under operational networks deployed by a major Danish operator. The outcome of the measurements is utilized for validating the simulation results provided by a system-level simulator that replicates the analyzed drive-test routes. This part identifies the main mobility issues that will be later addressed in the thesis.

1 Motivation

Conventionally, the performance of cellular networks and the evaluation of new features is carried out by means of link- and system-level simulations of specific scenarios, and network layouts. To this end, the 3GPP has standardized what nowadays constitutes the most commonly accepted scenarios and mathematical models for parameterizing the simulations of a mobile network [1].

This methodology is also typically adopted for analyzing the mobility performance of cellular networks and to evaluate possible enhancements [2]. Standard simulations provide a good understanding of the general behavior of the network and of the achievable gains and benefits that a feature can bring. Nonetheless, the standardized scenarios cannot always replicate all the conditions and phenomena that are present in the field. Consequently, there is growing tendency of modeling real scenarios in simulators to understand the behavior of operational networks. Instead of analyzing hexagonal network layouts, real base stations parameters, building databases, and terrain maps are imported into the simulators in order to evaluate the performance in, for instance, urban scenarios or specific hot-spot areas.

These advanced simulations not only require an exhaustive preparation to comprehensively replicate real environments, but also, depending on the complexity of the scenario, require a tremendous amount of computational resources. Therefore, the simulation models are designed based on a compromise between simulation time, processing power, and desired level of replicated details. Due to the limitations of the

simulation tools, the utilized models are commonly simplified, leaving behind specific dynamics which inclusion would consume an astronomic amount of resources. Thus, it is important to properly calibrate, parametrize, and posteriorly validate the simulation models to minimize the inaccuracies in the results.

In this part of the thesis, measurements of the mobility performance of operational 3G and 4G networks in the city of Aalborg, Denmark, are discussed. The main goal of this activity was to understand what current mobile networks can achieve, and to identify the mobility issues that should be addressed during the studies.

The outcome of the drive-tests was also utilized for calibrating and parameterizing a dynamic system-level simulator that was used in later studies of this PhD. To this end, it was necessary to provide new capabilities to the tool for importing, replicating and simulating real-network deployments that included not only the network configuration provided by the operator, but also building and street layouts, terrain information and path loss maps generated by a ray tracing tool.

A one-to-one comparison between the measurements and simulation results was performed in order to validate the simulation models and to evaluate whether the methodology of replicating a real-scenario in a system-level simulator was able to produce trustful mobility performance results, comparable to what can be experienced in the field.

2 Objectives

The aims of this part of the thesis are summarized as follows:

- Discover the most critical issues in the mobility performance of operational mobile networks by means of field drive-tests.
- Replicate the exact measured scenarios and the drive-test routes in a system-level simulator.
- Use the outcome of the measurements for validating the simulation models and evaluate whether the simulator is able to produce trustful and realistic results. Thereby, allowing the simulator to be used in later studies of the PhD.
- Analyze whether system level simulations of site-specific scenarios is a suitable methodology for analyzing the mobility performance of real networks.

Due to the pragmatical nature of the activities conducted in this part, additional secondary objectives are included:

- Learn who to operate the equipment required for conducting and analyzing field-measurements in an operational network.
- Provide the dynamic system-level simulator with the capability of importing and simulating real scenarios.

3 Included Articles

The articles that form the main body of this part of the thesis are:

Paper A. Validation of Mobility Simulations via Measurements Drive Tests in an Operational Network

This article analyzes measurements of the mobility performance of an operational 3G network deployed in the city center of Aalborg, Denmark. Measurements are performed using a commercial UE with a proprietary software that allows to collect different statistics, including the RRC messages exchanged with the network. The exact drive-test routes and scenario are afterwards imported in a system-level simulator including the network configuration provided by the operator, building and streets layout and propagation maps predicted by a ray-tracing tool. The measurements results are also utilized for configuring and parameterizing the simulator. The main observed KPIs are the number and location of handovers and radio-link-failures (RLFs), as well as, received signal strength and interference levels. Simulations and measurements results are then compared to each other, to validate the outcome of the simulator and evaluate whether the methodology of simulating site-specific scenarios is suitable for producing realistic mobility performance results of an operational cellular network.

Paper B. Mobility Performance in Slow- and High-Speed LTE Real Scenarios

This article extends the studies conducted in Paper A to LTE networks. In this case, the evaluation of the scenario of the city center is complemented with measurements of the highway stretch that encloses the city. The same methodology followed in Paper A is adopted. The analyzed scenarios are replicated in the simulator, and the mobility performance results are compared with the measurements to validate the outcome of the tool for further studies. Besides the KPIs analyzed in Paper A, this article also observes the number of handovers split into intra- and inter-site events, and pays particular attention to the handover data interruption time. The article also presents an exhaustive investigation of the mobility parametrization of the network by analyzing the Layer-3 signaling recorded during the measurements. The goal of this paper is to discover the most critical limitations present in current LTE networks.

4 Main Findings

Measurements of the mobility performance in operational networks

The post processing of the 3G measurements performed in Paper A shows that in the city center the majority of the handovers occur at street intersections, while turning a corner. Some problematic areas where RLFs are experienced are also identified in the 3G network. Further analysis of the measurements revealed that these RLFs were mainly due to low signal strength or high interference conditions. From the analysis of the results it was also observed the so-called *corner effect*. An UE turning a corner experiences a rapid decline of the received signal strength from the serving cell while the signal from another (interfering) cell increases, resulting in a decrease of the experienced signal-to-interference-and-noise-ratio (SINR). This effect is partic-

ularly perceptible while turning a corner due to a change from line-of-sight (LOS) to non-line-of-sight (NLOS) conditions. If the handover from the serving to the new stronger cell is not processed fast enough, the interference levels make it impossible to exchange the handover messages, ending up in a RLF or handover failure. In some of the drive-tests it was found that the UE was able to successfully perform the handover whereas in others, RLFs were experienced before the handover could finalize.

The studies conducted in Paper B shows better performance for the LTE macro-mobility with no handover and radio-link failures. A more sophisticated post processing of the measurements revealed that no intra-site handovers are experienced in the city center. The analysis suggested that this effect is due to the *street canyon effect* that makes the signal from farther sites to dominate over the signal received from closer ones. A close investigation of the recorded RRC messages exchanged between the UE and the network during the drive-tests, shows that the operator uses the same offset and hysteresis for configuring the handovers at the UE. Nevertheless, different values of time-to-trigger (TTT) are identified at each cell, indicating the use of mobility robustness optimization (MRO) at the network. In general, the operator use large values of TTT, being 1024 ms the most recurrent value. The timer T_{310} for detecting RLFs is measured generally large, parametrized with a value of 2 s, ensuring that the UE has enough time to recover after experiencing bad radio conditions. Analysis of the measurement results also identified one of the most critical issues in the mobility performance of current LTE networks: the data interruption time at each handover. The measurement results showed an average interruption time of 24-29 ms. However, extreme delays of more than 100 ms can be also experienced.

Additionally measurements of the handover interruption time were performed in Collaboration 3, extending the analysis to other scenarios and networks that cover rural, suburban and urban areas. In these cases, the measured median interruption time was observed within the range of 37-40 ms, with extreme cases up to several seconds. Additional details on these complementary results can be found in Part V. These findings of the measured handover interruption time clearly illustrates that current LTE networks are far away from fulfilling the 0 ms of handover data interruption time that is required by the upcoming applications for 5G [3].

Importing and Simulating a Real Scenario

The simulation of a real network and the drive-test routes requires a specific methodology for replicating the analyzed scenario. The base stations locations and configurations provided by the mobile operator, street and building layouts, and topographic maps are required for modeling the real environment. Furthermore, in order to produce similar radio-conditions compared to what can be experienced in the field, ray-tracing techniques are recommended for predicting the path loss map of each of the cells that provides coverage to the studied area.

To this end, a 3D version of the analyzed scenario was first modeled in a ray-tracing tool. During this process, it was identified that the resolution of the maps is a parameter that must be set carefully, as it has an impact on the simulations. A fine resolution increases the amount of time required for the path loss prediction. Additionally, it increases exponentially the amount of necessary computational resources for running the system-level simulations. However, if a course resolution is adopted,

the buildings footprint may penetrate the surrounding streets. In some cases, it was found that the buildings footprint may block completely the street, making impossible the simulation of a specific drive-test route. In other cases, due to the proximity of the buildings, a user moving along the simulated streets experienced an increase in the path loss due to the outdoors to indoors penetration loss, hence increasing the probability of experiencing a RLF. This effect was encountered while modeling the city center scenario due to the presence of narrow streets. A resolution of 5x5 m for each propagation map was found to be manageable by the computational resources, without excessively increasing the simulation time. The suitability of this resolution was later validated by the simulation results.

After creating the propagation maps, the real data was imported into the tool for performing the system-level simulations. Before initiating the studies collected in papers A and B, the tool was unable to run simulations of real-scenarios. Therefore, it was necessary to develop all the scripts and interfaces in order to provide the capabilities of importing and simulating the exact drive-test routes, including the predicted propagation maps, the network configuration and the building layouts. Several challenges were faced during this process, as the simulator must not only understand the imported data, but also efficiently manage the computational resources to avoid *out of memory* situations or long simulation times. This was identified as critical to simulate dense networks with large amount of cells because one cell generates one propagation map that covers the entire observed area. In some cases, the whole simulated area extends up to several kilometers, increasing the amount of computational resources and the simulation time.

Furthermore, the mobility parameterization (RRM measurements configuration and UE timers) should be in accordance to the values set by the operator that deployed the network, in order to obtain mobility statistics similar to what can be measured in the field. This network configuration was not provided in all the cases. Therefore, to obtain the mobility parametrization, it was necessary to analyze the Layer-3 messages collected during the drive-tests. Due to the limitations of the measurements software, it was not possible to automatize the process and all the signaling exchanged between the network and the equipment was manually inspected. This was found to be particularly beneficial for understanding the different RRC procedures apart from the ones related to mobility management.

Field Measurements VS. Simulations of a Real Scenario

A one-to-one comparison between the measurement results and the outcome of the simulations revealed that the high level of details replicated in the simulator generally produced only minor discrepancies in the results. The findings presented in Paper A demonstrated that the critical areas in terms of coverage and interference identified in the simulations were consistent with the ones identified in the measurements. The locations where the RLFs took place in the field matched relatively well with the simulation results, as the simulator was able to predict 6 out of 7 problematic areas in the city center scenario. Additionally, Paper A also concluded that the simulator was able to reproduce the corner effect found in the measurements.

In both papers A and B, the number of handovers in the simulations was discovered to be slightly different compared to the measurement results. This is explained

by the adopted 5x5 m resolution of the propagation maps and by the lack of specific dynamic effects in the simulator such as vehicles that may temporarily block dominant radio-paths to some cells, specific traffic conditions, and changes in the driving speed during the measurements. Nevertheless, no major differences in the comparison of the results were found, indicating that the resolution of 5x5 m for the propagation maps provides an acceptable balance between discrepancies in the results and computational cost.

Paper B also demonstrated that the simulator was able to predict the particular effect of not experiencing intra-site handovers in the city center. In the highway scenario, some intra-site handovers were found due to the presence of wider areas. However, as predicted by the simulator and extracted from the measurements, the inter-site handovers still dominated.

Essentially, the simulated handover rate, location of handovers, RLFs and signal/interference level statistics matched well with the measurements. Consequently, it can be concluded that the presented methodology for simulating site-specific scenarios is suitable for replicating trustful mobility results that are comparable with the ones observed in the field.

References

- [1] 3GPP Technical Report (TR) 36.814. *Further advancements for E-UTRA physical layer aspects. V.9.0.0*, March 2010.
- [2] 3GPP Technical Report (TR) 36.839. *Mobility enhancements in heterogeneous networks. v.11.1.0*, Dec 2012.
- [3] 3GPP Technical Report (TR) 38.913. *Study on Scenarios and Requirements for Next Generation Access Technologies. V.0.4.0*, June 2016.

Paper A

Validation of Mobility Simulations via Measurement Drive Tests in an Operational Network

Lucas Chavarría Giménez, Simone Barbera, Michele Polignano,
Klaus I. Pedersen, Jan Elling, Mads Sørensen

Published in
IEEE 81st Vehicular Technology Conference (VTC Spring), 2015.

© 2015 IEEE

Reprinted with permission. The layout has been revised.

Abstract

Simulations play a key role in validating new concepts in cellular networks, since most of the features proposed and introduced into the standards are typically studied by means of simulations. In order to increase the trustworthiness of the simulation results, proper models and settings must be provided as inputs to the simulators. It is therefore crucial to perform a thorough validation of the models used for generating results. The objective of this paper is to compare measured and simulated mobility performance results with the purpose of understanding whether simulation models are close to reality. The presented study is based on drive tests measurements and explicit simulations of an operator network in the city of Aalborg (Denmark) – modelling a real 3D environment and using a commonly accepted dynamic system level simulation methodology. In short, the presented results show that the simulated handover rate, location of handovers, radio link failures, and signal/interference level statistics match well with measurements, giving confidence that the simulations produce realistic performance results.

1 Introduction

Mobility performance and related enhancements are important topics for mobile wireless systems. In research, mobility improvements are typically first assessed by simple analytical considerations, followed by more complex dynamic simulation campaigns, before implementing and testing in the field. As an example, mobility performance and handover parameters optimization have been extensively analyzed by means of simulations for different Radio Access Technologies (RATs) in different studies. Optimized soft and softer handovers parameters for a realistic 3G network have been studied in [1]. Handover performance simulations on a realistic 3G scenario have been conducted in [2]. Examples of theoretical studies of 4G intra-frequency handover performance appears in [3], while [4] presents an algorithm to self-optimize handover parameters in a realistic 4G network. Field measurements of various handover statistics are presented in [5], while a comparison between the measured data interruption time in 3G and 4G is reported in [6]. Needless to say, the mobility performance results and conclusions from theoretical and simulation-based studies depend heavily on the underlying modeling assumptions. However, to the best of our knowledge, there are no studies available that present a one-to-one comparison of mobility performance observed in the field versus mobility performance simulation results for the exact same area. Such a study is needed in order to verify how accurate current simulation-based models reproduce mobility performance results, as simulation tools are a fundamental pillar in producing performance results for radio research and standardization purposes. The study is conducted for a 3G network, given the maturity and the widespread deployment of this technology. However the findings and working methodology can be extrapolated to other RATs, as the basic simulation methodology and underlying assumptions are to a large extent the same for 3G, 4G, and likely also the upcoming 5G. The experimental part of the study is based on drive tests in the city of Aalborg, Denmark, on the Telenor 3G network. The exact same network and drive tests are reproduced in a dynamic system level simulator by

importing the site positions, 3D building map, and using state-of-the-art ray tracing techniques to model the radio propagation effects. Hence, as the simulations and experimental data are from the same exact area, we are able to make a true one-to-one comparison to validate how accurately our simulations reproduce real-life effects. As it will be shown in this study, a good match of performance results is observed, which essentially confirms that the performance-determining modeling assumptions in the simulations are in coherence with reality, i.e. leading to trustworthy results.

The paper is organized as follows: In Section 2 the overall simulation methodology and modeling assumptions for the city of Aalborg are presented. Section 3 describes how the drive test measurements have been conducted, while Section 4 presents the comparison between the simulation and measurements results. Section 5 presents further discussion to put the findings into perspective. Finally, Section 6 summarizes the concluding remarks.

2 Simulations Methodology and Modeling

2.1 Basic Methodology

The basic simulation methodology follows the approach used in many 3rd Generation Partnership Project (3GPP) dynamic system level simulations characterized by multiple users generating dynamic traffic and moving according to fixed or randomly selected trajectories. For each time-step, the post detection Signal-to-Interference-Noise-Ratio (SINR) for each user is calculated, followed by a mapping to experienced throughput. The SINR to throughput mapping is according to the 3G High-Speed Packet Access (HSPA) performance, and includes the combined effect of scheduling, link adaptation, and hybrid automatic repeat request – also known as abstract physical layer to system level mapping. The downlink SINR is calculated from the base station transmitted powers and the radio propagation characteristics of all links. Additional details on the former and interference modeling are described in [7–11]. The utilized system level simulator has been used in numerous 3GPP simulation studies, and its performance results have been benchmarked against related results from other tools of other companies – both for 3G and 4G simulations. As an example of the former, see the 4G HetNet mobility performance results in [11]. Additional details on the applied modeling assumptions in the current study are outlined in the following subsections.

2.2 Aalborg Site-Specific Scenario

The environment modeling used in this study aims at reproducing a metropolitan area of the medium-size city of Aalborg (Denmark), using detailed data from a three dimensional (3D) map. The map contains 3D data for buildings and streets, as well as topography information such as terrain elevation. Path loss maps of the whole area are calculated by using ray-tracing techniques based on the Dominant Path Model (DPM), as described in [12] and [13], with a grid resolution of 5m x 5m. Thus, the radio propagation conditions are assumed to be constant within a 25m² area. Ray-tracing parameters have been calibrated according to previous studies in other Danish

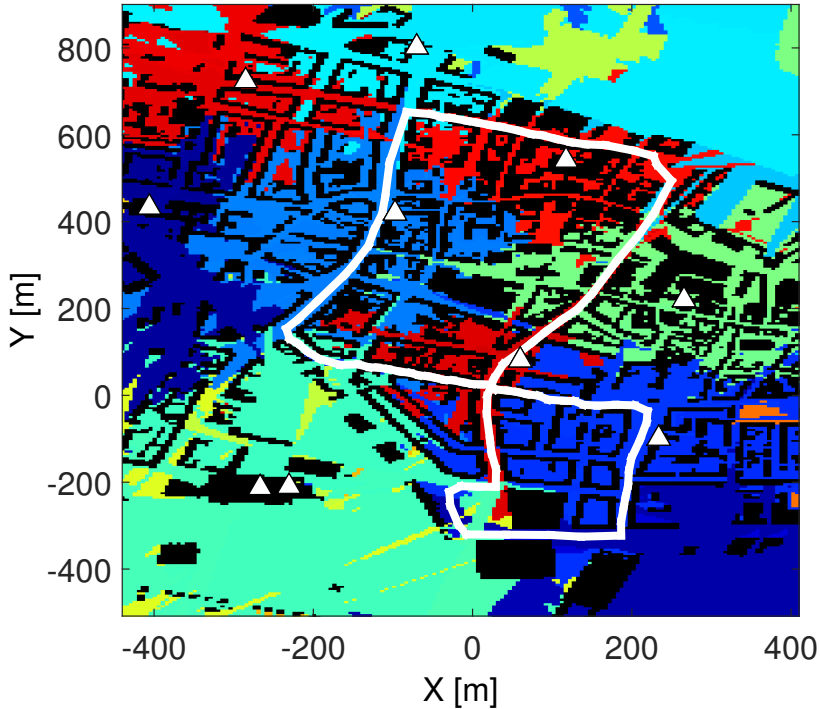


Fig. A.1: Zoom into the observation area of Aalborg. Buildings in black, macro sites locations and simulated streets in white. The other colors represent the simulated best server map.

cities, whose buildings layout is similar to Aalborg's, and under the network of the same mobile operator [14]. The 3D building map has the same resolution as the propagation maps. The considered urban scenario measures 5450 x 5335 meters. Although the whole network area performance is simulated, the results are collected only within a smaller selected area of the city center as depicted in Figure C.1. The observed area models street canyons surrounded by multiple buildings with an average height of 4 stories. Some open areas such as parks, squares and a fiord are also included.

The macro sites are placed according to the data provided by the operator. Throughout the whole city area a total of 64 3G macro sites are deployed. The majority of them have 3 sectors, while others have 2 sectors or a single sector. All of the considered macro sites operate at the 2100 MHz band. The average minimum Inter-Site Distance (ISD) is 368 meters with a standard deviation of 147 meters. The macro sites are deployed at different heights, pointing at different directions following the operator information. The antenna patterns are according to settings used in the field, including also the effects of electrical down-tilts for the sites where this is applied. Full load conditions are assumed for all the cells outside the observation area, i.e. those generate interference all the time. The scenario characteristics are summarized in Table A.1.

Table A.1: Aalborg Scenario Macro Sites Details

Parameter	Value
Scenario area	5450 m x 5335 m
Number of sites	64
Average ISD	368 m
Minimum ISD	35 m
ISD std. deviation	147 m
Average antenna height	22 m
Antenna height std. deviation	7 m
Average antenna tilt	7°
Antenna tilt std. deviation	2.7°

2.3 User Movement Model

In this study we limit only consider outdoor users in streets. The movement consists of linear trajectories with constant speed. At street-intersections, the new direction of movement is randomly selected with equal probability for each of the possible directions as dictated by the street grid. U-turns are not allowed in the movement of the user. In addition to the random movement, also deterministic user movement paths are simulated as illustrated in Figure C.1. As it can be seen in Figure C.1, the path can be divided into 2 loops. In the bigger loop the direction of the movement is clockwise while in the small loop the direction is counterclockwise. The two deterministic movement paths in Figure C.1 are the exact same ones as used in the experimental drive tests. Hence, statistics from these two drive paths are used for comparison against the experimental data.

2.4 Mobility Events Model

The simulator explicitly models the network controlled, terminal assisted, connected mode mobility procedures as defined by 3GPP for HSPA. Hence, terminal measurements, as well as the corresponding filtering, reporting of mobility events, etc is explicitly modeled in line with the Radio Resource Control (RRC) procedures [7]. More precisely, the handover events 1A, 1B, 1C, 1E, 1F are used as summarized in Table A.2. The handovers are mainly based on the Received Signal per Chip Interference Ratio (E_c/I_o). The parameterization of the mobility events used in the simulations is in line with those used in the real network. Thus, offsets, thresholds and Times to Trigger (TTTs) match the current configuration of the deployed network. Furthermore, declaration of Radio Link Failures (RLFs) in the simulator also follows the 3GPP specifications. In short, RLF is declared if the terminal experienced SINR is too low for certain time-period, see more details in [8–11].

Table A.2: Mobility Settings

Event 1A	<i>A primary CPICH enters the reporting range</i>	
	Reporting Range Constant	4 dB
	Hysteresis	0 dB
	TTT	500 ms
Event 1B	<i>A primary CPICH leaves the reporting range</i>	
	Reporting Range Constant	6 dB
	Hysteresis	0 dB
	TTT	640 ms
Event 1C	<i>A non-active primary CPICH becomes better than an active primary CPICH</i>	
	Offset	2 dB
	TTT	100 ms
Event 1E	<i>A primary CPICH becomes better than an absolute threshold</i>	
	Threshold	-105 dB
	TTT	200 ms
Event 1E	<i>A primary CPICH becomes worse than an absolute threshold</i>	
	Threshold	-105 dB
	TTT	200 ms

3 Drive Test Measurements

Terminal drive test measurement campaigns are conducted along the routes pictured in Figure C.1. The drive tests are repeated several times without stopping, starting and ending at the same position of the route. In order to emulate the traffic settings from simulations, measurements are taken during normal office working hours, walking or by car. The average speed is 6 kmph and 20 kmph respectively. Although it is intended to maintain a constant speed during each drive test, traffic conditions, pedestrians and traffic lights do not always allow traveling at the desired speed. Factors such as changes of the speed or different waiting times in traffic lights have an

Table A.3: Handovers per Minute in Real Measurements and Simulations

Speed (kmph)	HOs/min in Real Measurements	HOs/min in Simulations
~6 (walk)	0.68	–
6	–	0.47
~20 (car #1)	1.1	–
~20 (car #2)	1.57	–
~20 (car #3)	1.45	–
20	–	1.06

impact on the results. The measured mobility statistics from two drive test on the same path are therefore subject to some variations. These variations are especially evident during the campaign by car, therefore suggesting conducting more than one single campaign and then averaging the results. Hence, a total number of four on-site tests are conducted for each of the two measurement routes depicted in Figure C.1: One by walking and 3 by car. The used User Equipment (UE) is a commercial mobile phone Evolved High-Speed Packet Access (HSPA)+ 850MHz/900MHz/2100MHz and Long Term Evolution (LTE) 800MHz/1800MHz/2600MHz capable – Model Samsung Galaxy III. The phone is forced to operate with HSPA+ at 2100MHz. The Wi-Fi is disabled during the measurements. The phone is equipped with proprietary software that enables extraction of information from the modem such as e.g. RRC message data. The phone is programmed to periodically download a 100 MB file, which contains random generated data from a FTP server. When the download finishes, the UE waits 2 seconds to initiate a new download session. The UE location is recorded by the Global Positioning System (GPS) device of the phone. Assisted GPS information is not utilized. Different statistics are extracted by post-processing the measurement files with the software provided by the developer of the measurement software. Serving cell IDs, active set tables, Received Signal Code Power (RSCP), Received Signal Strength Indicator (RSSI), Ec/Io, Layer 3 messages, locations and time stamps constitute the selected extracted data for these studies.

4 Performance Results

Table A.3 shows the average number of handovers per minute occurring in real measurements and in simulations. The main observation is that the number of measured handovers always is higher in the measurement drive tests as compared to statistics from the simulations. The three measurements by car show on average 1.37 handovers per minute, with a standard deviation of 0.24, while the statistics from the simulations show 1.06 handovers per minute.

The differences in the number of handovers can be explained by multiple factors.

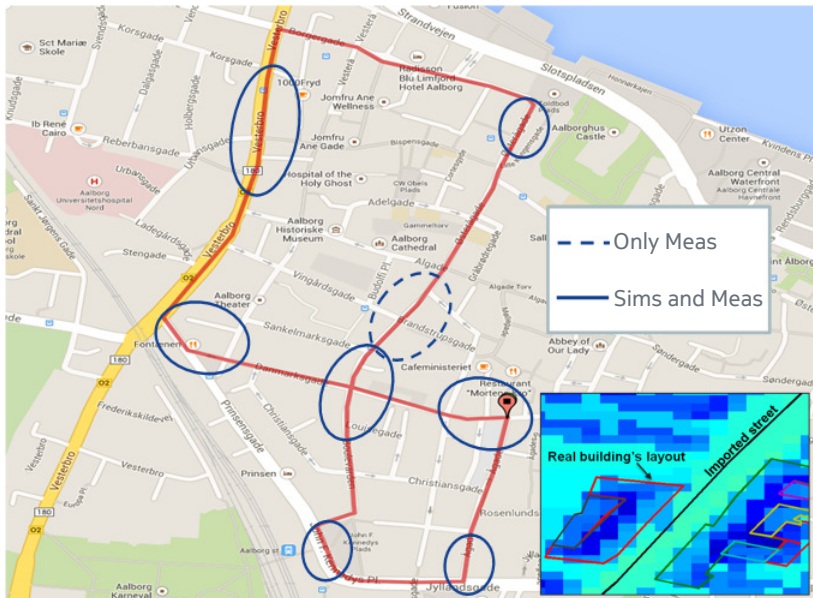


Fig. A.2: Handovers location and zoom of an area where a building's footprint crosses a street due to the 5x5 m map resolution.

First, the measurement campaigns are affected by localized variations in radio propagation conditions caused by e.g. movement of surrounding cars, buses and trucks, which occasionally can cause additional handovers and are not explicitly reproduced in the simulator. Secondly, traffic conditions and traffic lights make it difficult to maintain a constant drive speed during the measurements. Moreover, despite mobility parameterization has been aligned with the deployed network, the UE measurements model of the simulator cannot exactly reproduce the same results. Additionally, few mobility events are missing from the simulations due to the map resolution of 5×5 meters. In order to get a better full understanding of the handover count statistics, Figure A.2 illustrates where the handovers happen in simulations and in the drive tests. The solid circles in Figure A.2 mark the areas where handovers take place in both the simulations and drive test, while the area marked with the dashed circle marks the location of handovers that are only observed in the drive test (i.e. not observed from the simulations). A closer inspection of the area marked with dashed circle in Figure A.2 reveals that the reason for not being able to reproduce the same handover behavior in this area is primarily due to the limited 5x5 meters resolution of the used propagation data. If removing the data from the problematic area in Figure A.2 (i.e. the area marked with the dashed circle), the average numbers of handovers observed from the simulations and drive tests match better, as drive tests at 6kmph and 20kmph then result in 0.6 and 1.29 handovers per minute on average.

Figure A.3 shows the location of RLFs. Here it is worth noticing that the UE typically recovers from the RLF (re-establishment) such that call dropping is seldom experienced. Out of 7 identified areas where RLF are detected, 6 of them are observed

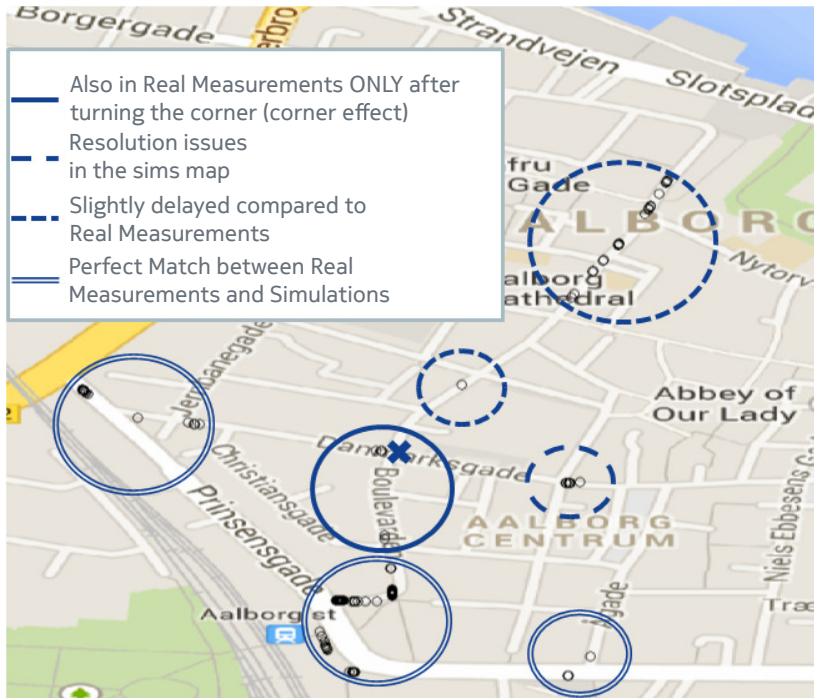


Fig. A.3: Radio Link Failures in simulations, identified by the black dots, and comparison with measurements.

from both simulations and measurements. However, simulations show an additional area where RLFs happen, and this is again primarily due to the limited propagation map resolution used in the simulations. As a second effect, there is a tendency towards having the RLFs occur a bit later in the simulations as compared to the drive tests. However, for most RLF occurrences, the offset in the location of the RLFs from the simulations and drive tests are within the accuracy of the GPS location data.

In addition, it is worth high-lighting the effect of the so-called “corner effect” as also observed in other studies [15]. In short, the corner effect refers to the case where the UE is turning a corner, resulting in a decline of the received signal strength from the serving cell due to the change from Line of Sight (LOS) conditions to non LOS (NLOS). Similarly, the signal strength from the target (interfering) cell has a tendency to increase, resulting in a decrease of the experienced SINR if timely handover is not made at the correct moment. In addition, it may also occur that when turning a corner, the UE enters an area of a new base station that it previously did not discover. If the new base station is too close to the junction, the signal strength at the UE may be too high causing an increase in the interference perceived by the UE. If the handover is not processed fast enough or the interference levels make impossible to exchange handover messages, RLF occurs. An example of the “corner effect” is illustrated in Figure A.4, where the received power from the serving cell and the

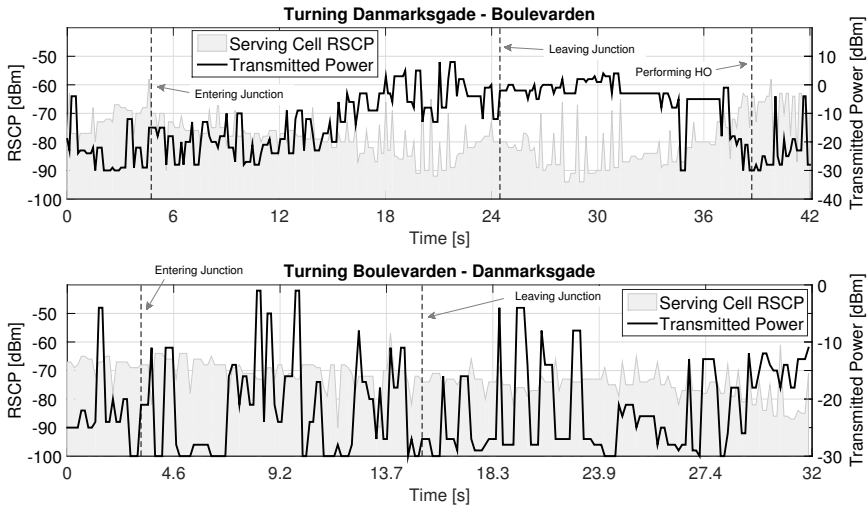


Fig. A.4: Corner effect example: RSCP vs. Transmitted Power.

transmitted power by the UE are shown for two turns following different directions in the same intersection (indicated with an 'x' sign in Figure A.3). The time instants when the UE enters and leaves the junction are marked with a solid and dashed line respectively. The dash-dotted line marks the time instant when a handover towards a new cell is completed. Analyzing the case of turning from east to south in the intersection Danmarksgade – Boulevarden, it can be seen how, some seconds after entering the junction and performing the turn around the corner, the RSCP from the serving cell drops down 20dB. In order to maintain the connection the UE link power control combats this effect by increasing the transmitted power in the uplink with the same amount. This situation continues even after the UE has left the intersection, as both RSCP and transmitted power fluctuates around the same levels. Afterwards, 14 seconds later, the HO towards a new cell is performed and the RSCP and transmitted power levels go back to normality. In this example, the handover is successfully performed. However, in other measurements RLFs have been observed. On the other hand, Figure A.4 depicts as well how, when turning from north to west (direction Boulevarden – Danmarksgade) in the same intersection, this effect is not present and the RSCP softly decays with the travelled distance. During the turning, the serving cell is identical in both directions.

Besides the “corner effect”, RLFs occur primarily due to high interference or low coverage. Figure A.5 shows the critical areas in terms of coverage or interference detected in simulations and in on-site measurements. Solid circles represent the areas where the signal strength from the serving cell is low whereas the dash circles mark the areas with high interference levels. Comparing these results with the ones illustrated in Figure A.3, it can be seen how areas where RLFs occur match with the areas where either low signal strength or high interference is perceived by the UE. The areas pointed by both simulations and measurements are aligned. Hence, only a general overview of these locations is depicted in the figure.

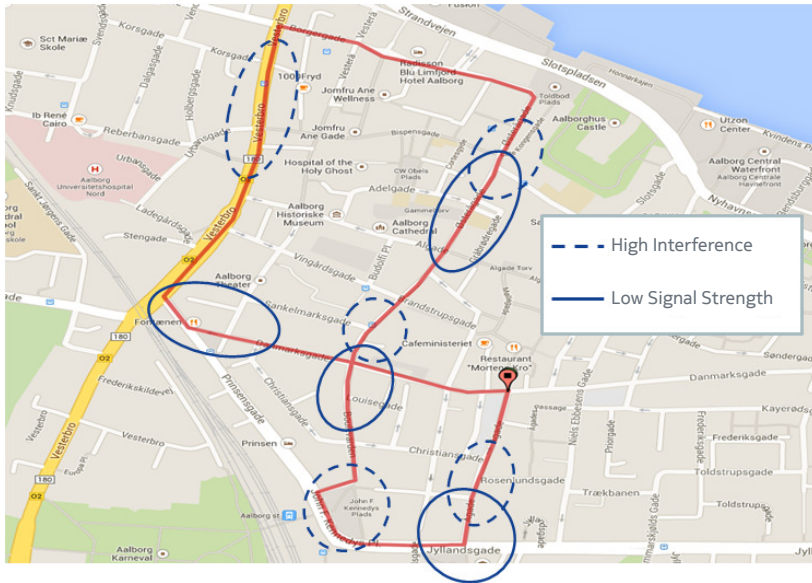


Fig. A.5: Areas with low signal strength or quality.

It is worth noticing that although the presented comparison of mobility simulation results and drive tests are for a 3G setting with HSPA+, the results are also useful for other RATs. The latter is the case because the basic simulation methodology used for 3G in this study is also applied for 4G and 5G investigations. As an example, modeling of propagation characteristics, interference footprint, UE movement and other features are RAT independent. This essentially means that the findings in this paper also give confidence for 4G/5G mobility simulations that are based on the same methodology. The former naturally assumes that the simulator is explicitly modeling the 4G/5G mobility procedures at the same level of details as assumed in this study for 3G.

5 Conclusions

In this paper we have presented a comparison of mobility statistics from advanced dynamic system level simulations of a realistic 3D modeled scenario and field measurement results from drive tests. The study is based on real data from the metropolitan city center area of Aalborg, Denmark. As a general conclusion, good alignment between the measurements and the simulations results are observed. The positions in which handovers and radio link failures take place match quite well. In fact, out of the 7 localized areas where RLFs are detected from the drive tests, the same RLF behavior is observed in 6 of those locations from the simulations. The main reason for having this modest mismatch is due to the limited propagation map resolution of 5x5 meters in the simulations. All in all, the critical areas in terms of coverage or interference are

rather consistent. It is also found that both simulations and measurements confirm the so-called “corner effect” that is particularly challenging for performing handovers at the exact right point. As future work, it is suggested to perform additional measurement vs. simulator comparisons for other scenarios and terrain types, using a finer resolution of the propagation maps.

References

- [1] M. Schinnenburg, I. Forkel, and B. Haverkamp, “Realization and optimization of soft and softer handover in UMTS networks,” in *Personal Mobile Communications Conference, 2003. 5th European (Conf. Publ. No. 492)*, April 2003, pp. 603–607.
- [2] I. Forkel, M. Schinnenburg, and B. Wouters, “Performance evaluation of soft handover in a realistic UMTS network,” in *Vehicular Technology Conference, 2003. VTC 2003-Spring. The 57th IEEE Semiannual*, vol. 3, April 2003, pp. 1979–1983 vol.3.
- [3] P. Legg, G. Hui, and J. Johansson, “A Simulation Study of LTE Intra-Frequency Handover Performance,” in *Vehicular Technology Conference Fall (VTC 2010-Fall), 2010 IEEE 72nd*, Sept 2010, pp. 1–5.
- [4] T. Jansen, I. Balan, J. Turk, I. Moerman, and T. Kurner, “Handover Parameter Optimization in LTE Self-Organizing Networks,” in *Vehicular Technology Conference Fall (VTC 2010-Fall), 2010 IEEE 72nd*, Sept 2010, pp. 1–5.
- [5] J. Lacki, J. Niemelä, and J. Lempäinen, “Optimization of soft handover parameters for UMTS Network in indoor,” in *The 9th International Symposium on Wireless Personal Multimedia Communications (WPMC)*, 2006.
- [6] A. Elnashar and M. El-Saidny, “Looking at LTE in practice: A performance analysis of the LTE system based on field test results,” *Vehicular Technology Magazine, IEEE*, vol. 8, no. 3, pp. 81–92, Sept 2013.
- [7] *3GPP Technical Specification (TS) 25.331. Universal Mobile Telecommunications Systems (UMTS); Radio Resource Control (RRC); Protocol specification*, March 2014, available at www.3gpp.org.
- [8] I. Viering, M. Dottling, and A. Lobinger, “A mathematical perspective of self-optimizing wireless networks,” in *Communications, 2009. ICC '09. IEEE International Conference on*, June 2009, pp. 1–6.
- [9] A. J. Fehske, I. Viering, J. Voigt, C. Sartori, S. Redana, and G. P. Fettweis, “Small-cell self-organizing wireless networks,” *Proceedings of the IEEE*, vol. 102, no. 3, pp. 334–350, March 2014.
- [10] P. Fotiadis, M. Polignano, D. Laselva, B. Vejlggaard, P. Mogensen, R. Irmer, and N. Scully, “Multi-Layer Mobility Load Balancing in a Heterogeneous LTE Network,” in *Vehicular Technology Conference (VTC Fall), 2012 IEEE*, Sept 2012, pp. 1–5.
- [11] S. Barbera, P. Michaelsen *et al.*, “Mobility performance of LTE co-channel deployment of macro and pico cells,” in *Wireless Communications and Networking Conference (WCNC), 2012 IEEE*, April 2012, pp. 2863–2868.

- [12] R. Wahl and G. Wölfle, "Combined urban and indoor network planning using the dominant path propagation model," in *2006 First European Conference on Antennas and Propagation*, Nov 2006, pp. 1–6.
- [13] R. Wahl, G. Wölfle *et al.*, "Dominant path prediction model for urban scenarios," *14th IST Mobile and Wireless Communications Summit, Dresden (Germany)*, 2005.
- [14] I. Rodriguez, H. Nguyen *et al.*, "A geometrical-based vertical gain correction for signal strength prediction of downtilted base station antennas in urban areas," in *Vehicular Technology Conference (VTC Fall), 2012 IEEE*, Sept 2012, pp. 1–5.
- [15] Z. Corporation, *UMTS Handover Performance Optimization Guide. R.1.0*, 2014, available in www.slideshare.net. Accessed August 2014.

Paper B

Mobility Performance in Slow- and High-Speed LTE Real Scenarios

Lucas Chavarría Giménez, Maria Carmerla Cascino, Maria
Stefan, Klaus I. Pedersen, Andrea F. Cattoni

Published in
IEEE 83rd Vehicular Technology Conference (VTC Spring), 2016.

© 2016 IEEE

Reprinted with permission. The layout has been revised.

Abstract

Mobility performance and handover data interruption times in real scenarios are studied by means of field measurements in an operational LTE network. Both slow- and high-speed scenarios are analyzed by collecting results from two different areas: Aalborg downtown and the highway which encircles the same city. Measurements reveal that the terminal is configured by the network with different handover parametrization depending on the serving cell, which indicates the use of mobility robustness optimization. Although the network is dominated by three-sector sites, no intra-site handovers are observed in the city center as cells on the same site often cover different non-crossing street canyons. Moreover, no handover failures are experienced in the measurements which confirms robust LTE mobility performance. The average interruption time, which is at least equal to the handover execution time, lays within a 24-29 ms interval. Nevertheless, examples of delays larger than 100 ms are occasionally observed. The studied scenarios are replicated in a system level simulator to investigate whether simulations are capable of reproducing similar mobility performance.

1 Introduction

Today's Long Term Evolution (LTE) systems implement the so-called *break before make* handover mechanism, where the User Equipment (UE) breaks data exchange with the serving cell after receiving the handover command, resulting in temporary data interruption at every cell change. Some measurements performed in [1] conclude that, in the 95% of the cases the device performs an intra-frequency handover, it experiences a detach time of 50 ms while in [2], times below 40 ms are found. After estimating an interruption time of 55 ms by means of measurements in a lab, [3] proposes synchronous Random Access Channel (RACH)-less handover procedures to reduce this time. Additionally, [4] suggests a stochastic model for estimating handover interruption times supported by field measurements, finding delays out of the usual range provided by the literature.

Although these gaps in the data-link have a minimal impact on the user experience in most of the multimedia and voice applications, the new *Traffic Efficiency and Safety* scenarios for future wireless systems, envisioned in [5], will require higher reliability constrains and lower latencies than the ones the current communications systems are able to provide. As a result, large handover data interruption times may compromise the requirement of providing a reliable exchange of information with less than 5 ms end-to-end latency, especially in scenarios affected by a large amount of handovers like high-speed scenarios.

The present paper analyzes intra-frequency mobility performance by field measurements in an operational 4G network. The experienced handover execution time and its associated data interruption time is observed for low and high mobility. To the best of our knowledge, previous studies do not distinguish between slow- and high-speed scenarios when analyzing handover delays. To this end, two different urban scenarios are considered: the downtown area of the city of Aalborg, Denmark, and the stretch of the highway which encircles the same city.

The experimental mobility results are, furthermore, used to verify the validity of

the performance results obtained from our dynamic system simulations. Hence, the measurement scenarios are reproduced in our simulator including the same drive test routes. Simulation results and field measurements are afterwards compared to check how well the simulator reproduces real-life LTE performance. A similar study for 3G was reported in [6].

The paper is organized as follows: Section 2 describes the considered handover timing and the observed Key Performance Indicators (KPIs), while Section 3 presents the characteristics of each scenario. Section 4 describes how measurements have been conducted, and the experimental results are shown in Section 5. Simulation methodology, as well as a comparison between measurements and simulations results, are discussed in Section 6. Finally, Section 7 summarizes the concluding remarks.

2 Handover Timing and Key Performance Indicators

Figure B.1 shows the handover procedure in LTE. It is a network controlled and UE assisted mechanism, where the UE is configured to send measurement reports to the serving cell according to certain triggering criteria.

Upon receiving the *Measurement Report*, the source cell sends the *Handover Request* to the target cell, which decides whether the UE can be accommodated or not (*Admission Control*). The decision is then communicated to the serving cell by means of the *Handover Request Acknowledgment*. The serving cell furthermore indicates to the UE that the handover can take place by the *Handover Command*, known as the *Radio Resource Control (RRC) Connection Reconfiguration* message. The elapsed time between the moment the UE sends the *Measurement Report* and the moment it receives the *Handover Command* is defined as the handover preparation time. After receiving the *Handover Command*, the UE detaches from the serving cell and initiates the synchronization phase with the target. Data communication is interrupted during this time and is not restored until the UE sends the *Handover Confirmation* or *RRC Connection Reconfiguration Complete* message. The time interval between both RRC messages is referred to as the handover execution time. In these studies it is assumed that the data interruption time is equal to the handover execution time. However, it typically takes around 5 ms from the time when the UE transmits the *RRC Connection Reconfiguration Complete* message until the target eNB starts scheduling data for the UE [3]. Hence, the data interruption time is slightly larger than the handover execution time.

In addition to the handover timing, other KPIs will be also considered in these studies such as: average number of intra- and inter-site handovers, number of Radio Link Failures (RLFs) and rate of Handover Failures (HOFs), as defined in [7]. Coverage is also analyzed by recording the Reference Signal Received Power (RSRP) during the drive tests.

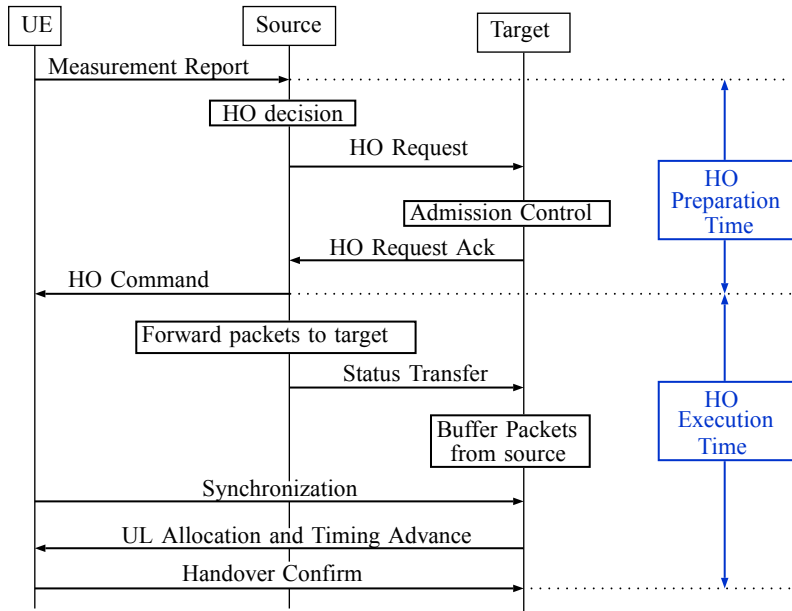


Fig. B.1: Definition of the handover preparation and execution times.

3 Scenario Description

Low and high mobility performance is studied by analyzing two different scenarios of the city of Aalborg: The city center and a stretch of a highway. The analysis is performed under an operational LTE macro network deployed at 1800 MHz with 20 MHz channel bandwidth.

City Center

The network in this area consists of 29 macro sites with an average Inter-Site-Distance (ISD) of 741 m and antenna heights that vary from 15 m to 60 m. Although the majority of the sites have 3 sectors, some of them count with 2 or even 4 sectors. Whereas the entire urban scenario measures 5450 m x 5335 m, the results are collected in a smaller observation area of 800 m x 1200 m. The area is surrounded by buildings of an average height of 4 stories. Some open areas such as parks, squares and a fjord can be also found. The scenario characteristics are summarized in Table B.1.

Highway

High-speed mobility performance is studied by analyzing the 8.5 km stretch of the E-45 highway that encircles the city of Aalborg. Wider open areas than in the city center can be found in this scenario, as well as, an immersed tunnel of 582 m length. The network of this area is characterized by 13 macro sites with 2 or 3 sectors and an

Table B.1: Aalborg city center scenario parameters

Parameter	Value
Total scenario area	5450 m x 5335 m
Number of cells	88
Number of sites	29
Average antenna height	30.8 m
Antenna height std. deviation	13 m
Average antenna tilt	3.9°
Average tilt std. deviation	2.4°
Average ISD	741 m
Minimum ISD	308 m

Table B.2: Aalborg E-45 Highway scenario parameters

Parameter	Value
Stretch length	8.5 km
Number of cells	23
Number of sites	13
Average antenna height	31.3 m
Antenna height std. deviation	13.22 m
Average antenna tilt	2.1°
Average tilt std. deviation	1.6°
Average ISD	1092 m
Minimum ISD	624 m

average ISD of 1092 m. The average antenna height is 31.3 m. Scenario information can be found in Table B.2.

4 Measurements

Drive test campaigns are performed along selected routes on each scenario. For the City Center, four drive tests are conducted at an average speed of 15 kmph whereas, in the Highway scenario, a total of eight drive tests are performed: four at an average speed of 80 kmph and four at 100 kmph. While the drive test in the City Center is defined by a closed path, the measurements in the Highway are taken in both directions:

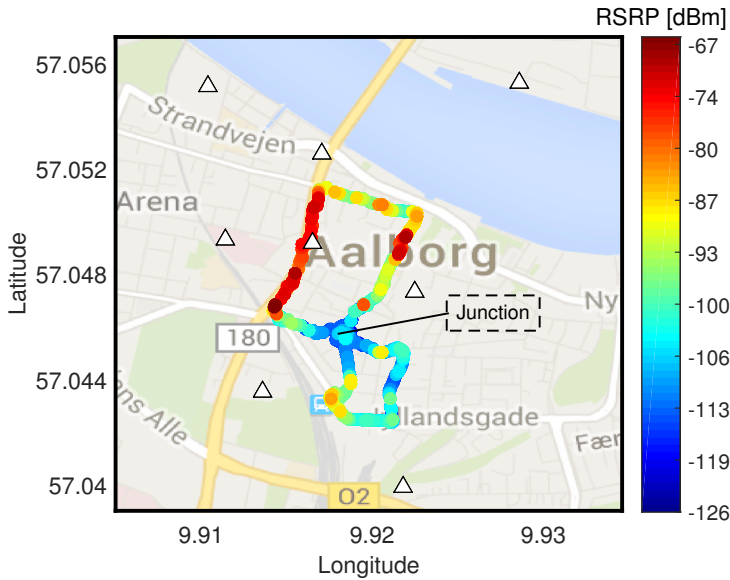


Fig. B.2: Zoom into the observation area of the Aalborg City Center scenario. Base station locations depicted as white triangles. Measured RSRP during drive tests is shown in a color scale. This drive test path has been also analyzed in a 3G study in [6].

from starting point A to an ending point B, and vice-versa. The terminal used in the measurements is a Samsung Galaxy S-III, LTE capable, forced to work at 1800 MHz. The UE is classified as *Category 3*, meaning that it supports a maximum data rate of 100 Mbps in the down-link. The device is programmed to periodically download a 100 MB file from a FTP server. The position of the UE is recorded using the Global Position System (GPS). Proprietary software installed in the phone allows to extract the RRC messages exchanged between the UE and the serving cell, as well as information about the physical cell ID, RSRP, Reference Signal Received Quality (RSRQ), Received Signal Strength Indicator (RSSI) and experienced Physical Downlink Shared Channel (PDSCH) throughput. RRC messages analysis is done to extract the mobility parametrization of the network in both scenarios. This mobility parametrization has been taken into account during the simulation phase.

5 Experimental Results

5.1 Coverage

Figure B.2 and Figure B.3 show the observation area and the network layout of each scenario together with the measured RSRP during the drive tests. As it can be observed in Figure B.2, high RSRP is experienced in areas where the network is more dense whereas low values are found around the highlighted junction (intersection Boulevarden with Danmarksgade), as it was previously concluded in [6]. Neverthe-

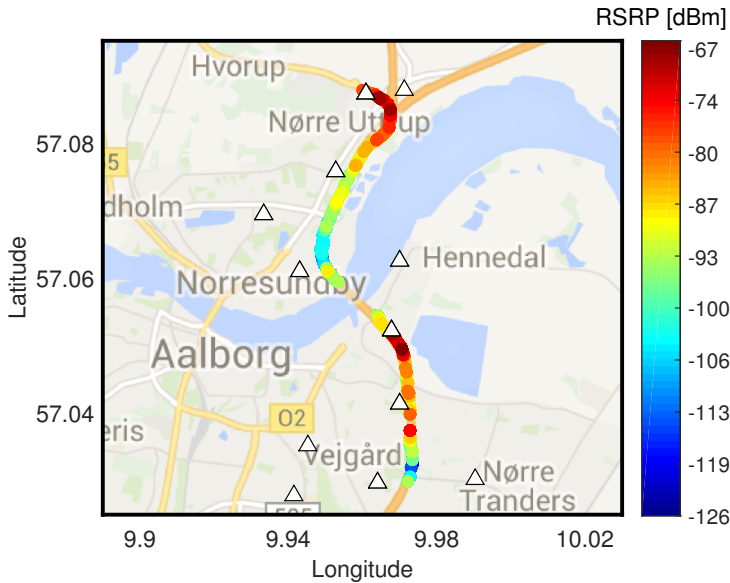


Fig. B.3: Zoom into the observation area of the Highway E-45 scenario. Base station locations depicted as white triangles. Measured RSRP during drive tests is shown in a color scale.

less, levels are sufficiently high to maintain connectivity during the whole drive test. On the other hand, the coverage along the Highway is more uniform as only few locations with low RSRP levels are found. Although no data is recorded while driving through the immense tunnel due to GPS signal loss, the coverage is generally good inside the tunnel and the connection is never lost.

5.2 RRC Messages Analysis

The RRC message analysis shows that the UE is configured by the network to send the *Measurement Report* both periodically and event-triggered. These reports may include a list of neighboring cells, their measured RSRP and RSRQ values, the event used for triggering handovers and the corresponding target cell. The configuration is done through the *Measurement configuration* field included in the *RRC Connection Reconfiguration* message which also contains information about which carriers and Radio Access Technologies (RATs) should be measured. Figure B.4 shows the measurement configuration extracted during the drive tests. By analyzing the *Measurement Report* prior to each Handover Command it can be identified that handovers at 1800 Mhz are triggered by the commonly used A3 event (*measID 1*, *measObjectID 1*, *ReportConfID 1*). The *RRC Connection Reconfiguration* message also provides information about the RRM measurement, which in this case is RSRP, and the values of the handover parameters: time-to-trigger (TTT) and offsets.

From the message analysis, it is discovered that the A3 offset and hysteresis remain constant and equal to 2 dB respectively, while the TTT varies from cell to cell.

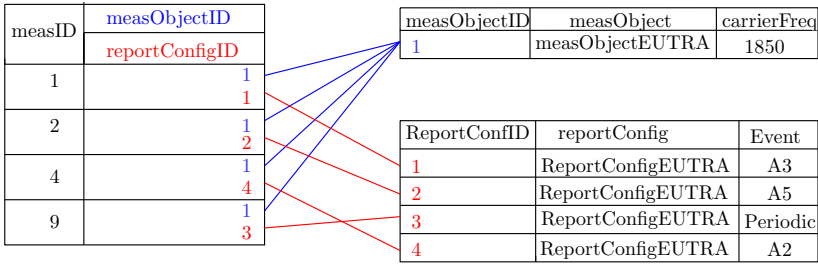


Fig. B.4: UE measurements configuration recorded during the drive tests.

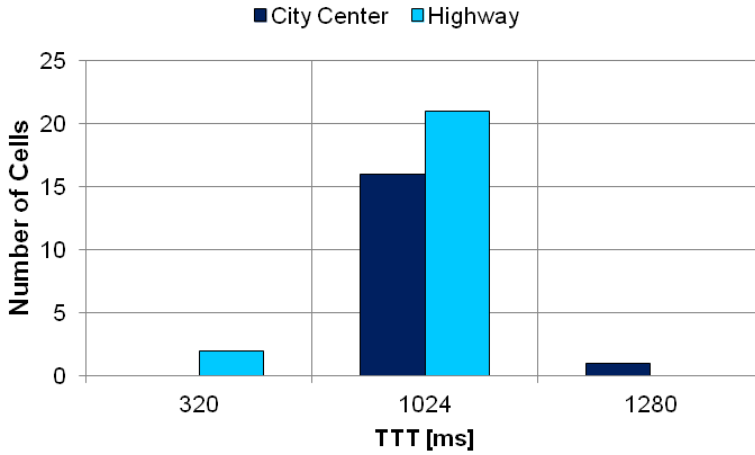


Fig. B.5: TTT distribution among the discovered cells by the phone during the measurements for each scenario.

Three TTT values are found distributed among the cells of each scenario: 320, 1024 and 1280 ms. The use of different handover event configuration for different cells indicates the use of Mobility Robustness Optimization (MRO) at the network. MRO essentially tunes the handover parameters in coherence with the characteristics of different cell boundaries. A larger value of the TTT tends to postpone handovers, while the short TTT results in faster and more aggressive handover. The use of MRO helps eliminating HOFs. Figure B.5 shows the distribution of the TTTs found during the measurements. Notice that, although the City Center scenario consists of 88 cells, only 17 are discovered by the phone. On the other hand, the phone reports measurements from all cells in the Highway. An interesting fact is that the cell in the City Center scenario with a larger TTT is the one located on the other side of the fjord compared to where the drive tests are performed.

5.3 RLFs and HOFs

Upon detection of physical layer problems, the UE starts the timer T_{310} . If better radio conditions are not experienced and T_{310} expires, a RLF is declared. Afterwards, the UE attempts the re-establishment and if it does not succeed in a period of time T_{311} , the UE goes to RRC idle mode. HOF is declared if a RLF occurs during the handover process.

From the RRC messages analysis it is found that the timer T_{310} is parametrized with a value of 2 s. This large value assures that the UE has enough time to get back in synchronization after experiencing bad radio conditions and hence, avoiding RLF declaration. Furthermore, the timer T_{311} is found to be 3 s. Measurements revealed that neither RLFs or HOFs are experienced in any of the scenarios, even though some areas with low RSRP levels are found.

In order to confirm that our method for checking RLFs and HOFs is valid, a simple experiment to force a RLF was conducted before the drive tests. After setting the configuration for performing a download, the phone was wrapped in aluminum foil, replicating a scenario in which the UE experiences a signal drop. Analyzing the RRC messages, it was observed that following the wrapping of the phone, the device sends an *RRC Connection Re-establishment Request* message with the value *OtherFailure* in the cause field. At this point, if the phone is unwrapped before the timer T_{311} expires, the connection is successfully re-established. However, maintaining it wrapped for a longer time, causes the phone to go to idle mode after the T_{311} expiration.

5.4 Handover Events and Timing

Figure B.6 shows the average number of measured handover events per user per minute split into inter- and intra-site handovers. As expected, the number of handover increases with the speed. However, although the UE velocity is a factor 5-7 higher in the highway scenario as compared to the city center, the handover rate is only a factor 1.5-1.6 higher for the highway case. The larger ISD in the highway is the reason for not experiencing higher relative handover rates, as compared to the city center. The chosen drive path and the location of the sites with respect to the streets layout play an important role in these studies. The street canyon effect makes the signal from far sites to dominate over closer sites. Thus, no intra-site handovers have been recorded in any of the measurements in the City Center. In connection to this, it is worthy to highlight that due to Line Of Sight (LOS) conditions, the site located at the other side of the fjord is the main dominant in this observation area. Moreover, the TTT assigned to this particular cell, larger than the one in the neighbors, makes it more difficult for the UE to connect to this server. Although the presence of wider open areas explains the existence of intra-site handovers in the drive tests for the highway, the inter-site events are still dominant in this scenario.

Table B.3 shows the average handover times experienced during the drive tests. As some of the times are found to be in the region of hundreds of milliseconds, the median values are also shown to avoid a possible bias in the results. The recorded latency values in the City Center are generally higher than in the Highway scenario due to presence of inter-site handovers only. Nonetheless, the predominant number of inter-site events in both scenarios makes the median values similar in all the cases.

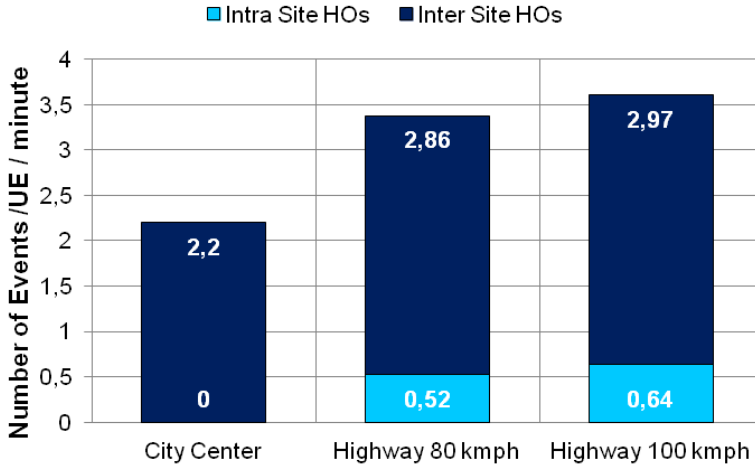


Fig. B.6: Average number of handovers per UE per minute obtained in the measurements for both scenarios.

Table B.3: Measured handover times during the drive tests.

Scenario	Average Times [ms]		Median Times [ms]	
	HO Prep.	HO Exec.	HO Prep.	HO Exec.
City Center	48.2	28.9	39.0	26.0
E-45 80 kmph	39.2	26.1	36.0	26.5
E-45 100 kmph	44.7	24.5	38.0	24.0

On average, it takes a total time of 77 ms to perform a handover in the City Center whereas, in the Highway, it takes 65 and 69 ms when driving at 80 and 100 kmph respectively. The measured average handover execution time –and its associated data interruption time– corresponds to 28.9 ms in the City Center, 26.1 ms in the Highway while driving at 80 kmph and 24.5 ms at 100 kmph. The average number of handovers experienced in the City Center is 16.5, while in the Highway are experienced 24.9 and 21.3 handovers at each speed. From these numbers, and considering that it takes 450 s to travel the observed urban path and 444 s and 354 s to transverse the segment of the E-45 at 80 and 100 kmph respectively, it can be calculated that the phone was able to transmit or receive data the 99.8% of the time.

Figure B.7 depicts the empirical Cumulative Distribution Function (CDF) of the extracted handover preparation and execution times. While the lower tail of the plot reaches a few milliseconds, it can be observed that the 5% of the cases, the handover execution time is higher than 55 ms for the City Center, reaching extreme values of

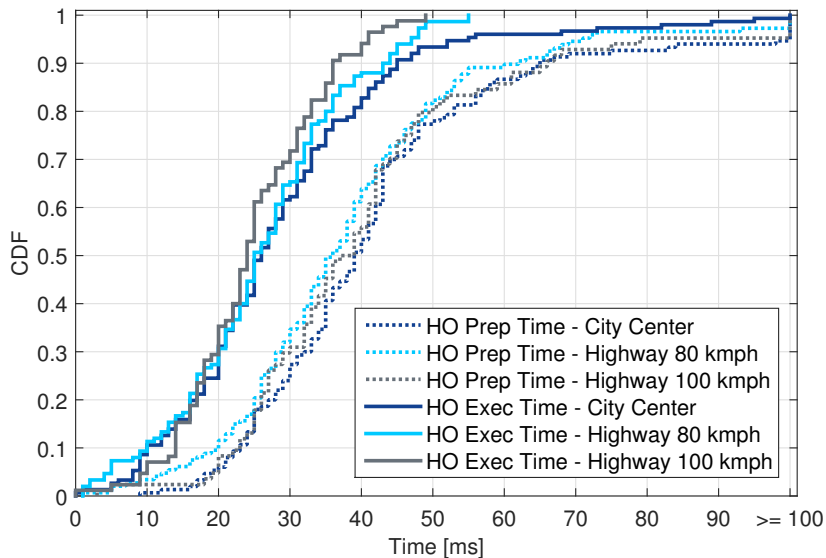


Fig. B.7: CDF of the handover preparation and execution times obtained during the measurements for both scenarios.

more than 100 ms. This can be due to the back-haul latency, load conditions in the target cell, and the Random Access procedures during the *Synchronization* phase. These large values may compromise the requirements, in terms of latency and reliability, for future real-time applications.

6 Measurements and Simulations Comparison

To verify whether our simulator is able to reproduce results in coherence with the measurements, the site-specific scenarios are simulated under a dynamic system level simulator which implements the majority of the RRC connected mode mobility mechanisms defined by the 3rd Generation Partnership Project (3GPP) for LTE, including terminal physical-layer measurements, Layer-3 filtering and reporting events. The simulator has been utilized in several mobility studies, for 3G and 4G, involving 3GPP ([7], [8]) and site-specific scenarios ([6], [9]).

Mobility parametrization discovered by the measurements and the network information provided by the operator are taken into account to align simulations with measurements. Scenarios are modeled by using a three-dimensional map of the city. Signal propagation is predicted by path loss maps computed using state-of-the-art ray-tracing techniques based on the Dominant Path Model (DPM) [10] and calibrated following recommendations from [11]. As each path loss map has a resolution of $5\text{ m} \times 5\text{ m}$, radio propagation conditions are considered constant within a 25 m^2 area. More details on the simulation methodology and scenario modeling can be found in [6]. Each scenario is simulated separately and statistics are only collected within

certain observation areas. All cells outside the observation areas are considered to be fully loaded, generating constant interference. The City Center scenario is simulated at 15 kmph while the Highway is simulated at 80 and 100 kmph.

Initial analysis of the first order statistics from the simulations show a promising match with the measurements. Like in the experimental results, inter-site handovers are found to be dominant, and the probability of experiencing RLFs and HOFs is close to zero in the simulations. Additionally, simulations are able to point out most of the locations where the handovers happen in the field. Nevertheless, the obtained handover rate is slightly larger in the simulations compared to findings from the field trials. The latter is mainly explained by the 5 m x 5 m resolution of the ray-tracing propagation data in the simulator, and the lack of modeling dynamic effects such as e.g. drive-by vehicles that temporarily blocks dominant radio paths to some cells. Despite not experiencing a 100 % match between measurements and simulations, our study indicates that the followed modeling methodology is suitable for reproducing real-life effects to a large extend. Nevertheless, a deeper comparison including more statistics are needed.

7 Conclusions

Mobility performance and handover timing for site-specific scenarios are studied in this paper by means of drive tests measurements and system level simulations. Field measurements are performed in an operational LTE network in the metropolitan area of the city center of Aalborg, Denmark, to study slow mobility at 15 kmph. Additionally, high mobility is analyzed in the highway which encircles the city, at speeds of 80 and 100 kmph. Experimental results show that although the average measured data interruption time is found to be, at least, between 24 and 29 ms, some extreme values higher than 100 ms are found. These high delays may compromise the requirements for future traffic and safety applications. The number of handovers are found slightly higher in the simulations than in measurements. Nevertheless, simulations are able to indicate that the scenarios are affected by a high number of inter-site handover and high handover delays.

As future work, it is recommended to further investigate the handover timing in real networks (e.g., for a given back-haul latency, to study how the load conditions in the target cell may modify the handover delay). Moreover, it is also suggested to explore solutions to decrease the handover interruption time considering latency and reliability requirements for future 5G applications.

References

- [1] A. Helenius, "Performance of handover in long term evolution," Master's thesis, School of Electrical Engineering. Aalto University, Nov 2011.
- [2] A. Elnashar and M. El-Saidny, "Looking at LTE in practice: A performance analysis of the LTE system based on field test results," *Vehicular Technology Magazine, IEEE*, vol. 8, no. 3, pp. 81–92, Sept 2013.

-
- [3] S. Barbera, K. I. Pedersen *et al.*, "Synchronized RACH-less handover solution for LTE heterogeneous networks," in *Twelfth International Symposium on Wireless Communication Systems*, Aug 2015, pp. 1–5.
 - [4] D. Han, S. Shin *et al.*, "Measurement and stochastic modeling of handover delay and interruption time of smartphone real-time applications on LTE networks," *Communications Magazine, IEEE*, vol. 53, no. 3, pp. 173–181, March 2015.
 - [5] A. Osseiran, F. Boccardi *et al.*, "Scenarios for 5G mobile and wireless communications: the vision of the METIS project," *Communications Magazine, IEEE*, vol. 52, no. 5, pp. 26–35, May 2014.
 - [6] L. C. Gimenez, S. Barbera *et al.*, "Validation of mobility simulations via measurement drive tests in an operational network," in *Vehicular Technology Conference (VTC Spring), 2015 IEEE 81st*, May 2015, pp. 1–5.
 - [7] 3GPP Technical Report (TR) 36.839. *Mobility Enhancements in Heterogeneous Networks*, Sept 2012, available at www.3gpp.org.
 - [8] S. Barbera, P. Michaelsen *et al.*, "Mobility performance of LTE co-channel deployment of macro and pico cells," in *Wireless Communications and Networking Conference (WCNC), 2012 IEEE*, April 2012, pp. 2863–2868.
 - [9] S. Barbera, L. C. Gimenez *et al.*, "Mobility sensitivity analysis for LTE-advanced hetnet deployments with dual connectivity," in *Vehicular Technology Conference (VTC Spring), 2015 IEEE 81st*, May 2015, pp. 1–5.
 - [10] R. Wahl, G. Wölfle *et al.*, "Dominant path prediction model for urban scenarios," *14th IST Mobile and Wireless Communications Summit, Dresden (Germany)*, 2005.
 - [11] I. Rodriguez, H. Nguyen *et al.*, "A geometrical-based vertical gain correction for signal strength prediction of downtilted base station antennas in urban areas," in *Vehicular Technology Conference (VTC Fall), 2012 IEEE*, Sept 2012, pp. 1–5.

Part III

Mobility Performance of LTE-A with Dual Connectivity

Mobility Performance of LTE-A with Dual Connectivity

This part of the thesis analyzes the mobility performance under LTE-A with DC, including a sensitivity analysis for different scenarios. Having the challenging highway scenario as a reference, how the selected user-plane architecture for implementing DC impacts the experienced data interruption time is also evaluated. Additionally, it is proposed that the UE autonomous cell management approach for reducing signaling overhead, due to DC mobility events, should be adopted.

1 Motivation

Mobile networks must be capable of supporting an explosive demand of data expected to be 1000 times greater than what current networks are able to support [1]. One possible solution for satisfying the traffic demands (and to increase the capacity of the network) is to complement the existing macro-only layouts with the deployment of small cells, constituting a heterogeneous network (HetNet). When upgrading networks to a HetNet scenario, the mobility becomes more challenging [2]. Mobility events should be performed faster as the coverage areas of the small cells tend to appear and disappear quicker as the UE moves.

Another promising technique for meeting the upcoming requirements in future mobile networks is *multi-connectivity* [3, 4]. This feature allows the UE to be simultaneously connected to multiple radio access points. A flavor of this technology is already included in LTE-A under the name of DC, allowing the UEs to consume radio resources from a macro- and a small-cell at the same time. With this feature, UEs benefit from an increased throughput due to the aggregation of additional links, and from enhanced mobility robustness compared to traditional macro scenarios [5]. However, the implementation of DC comes with the cost of experiencing a higher number of mobility events (associated with a certain data interruption) and an increased signaling overhead [2]. The 3GPP has standardized two different user-plane architectures for implementing DC: secondary cell group (SCG) bearer and split bearer. These

different architectures lead to the formulation of the following hypothesis: *"The experienced mobility data interruption time varies according to the selected user-plane architecture for DC"*.

To understand the benefits of DC, a mobility sensitivity analysis of the DC performance under low- and medium speeds for different scenarios is firstly presented. Due to the unavailability of DC in the field, the studies in this part were conducted using the same system-level simulator that was successfully validated in Part II. Standardized simulations were complemented with the analysis of real-scenarios, comparing the results obtained from simulating generic 3GPP scenarios with those obtained from simulating site-specific urban scenarios.

Mobility performance of DC in the same highway scenario studied in Part II, upgraded with small-cells deployed along the road is also evaluated in this part. This scenario is particularly challenging due to the high-speed of the UEs and therefore, it is used for evaluating the experienced mobility data interruption time with DC and for validating the formulated hypothesis.

Furthermore, it is proposed to deviate from the traditional network-controlled mobility and adopt a UE autonomous approach where UEs are capable of directly selecting and accessing the target cell, for reducing the amount of signaling and the number of mobility decisions that the network must support.

2 Objectives

The objectives of this part of the thesis are:

- Study the mobility performance with DC in 3GPP and real scenarios by means of system-level simulations.
- Evaluate the hypothesis of whether the user-plane architecture for implementing DC has an impact on the experienced data interruption time at mobility events.
- Analyze the signaling overhead that the network must support in scenarios with DC, specially at high-speeds.
- Propose solutions for solving the discovered issues in the mobility performance.

3 Included Articles

The articles that relate to the work included in this part of the thesis are:

Paper C. Mobility Sensitivity Analysis for LTE-Advanced HetNet Deployments with Dual Connectivity.

This paper conducts a sensitivity analysis of the DC mobility performance under slow- and medium-speeds, considering users moving at 3, 30, and 60 km/h. The article presents a comparison between the results obtained when simulating standardized 3GPP scenarios, and the ones obtained when simulating two site-specific urban areas.

The analyzed urban scenarios are a simulation replica of the city of Tokyo, and an European capital. The article analyzes for each scenario the number of mobility events, the rate of ping-pongs and radio-link failures, as well as the time-of-stay (TOS) of the UEs in the cells.

Paper D. Analysis of Data Interruption in an LTE Highway Scenario with Dual Connectivity.

This paper analyzes the DC mobility performance at high-speeds. The same highway scenario analyzed in Paper B is considered, but complemented with small cells deployed along the highway as road-units. The article presents a comparison between the mobility performance with single-connectivity and DC implemented with the two user-plane architectures standardized by 3GPP. The paper evaluates the handover data interruption time experienced by the UEs, and identifies which architecture is the most suitable for reducing it, without compromising any of the benefits of DC.

Paper E. UE Autonomous Cell Management in a High-Speed Scenario with Dual Connectivity.

Considering the same highway scenario presented in Paper D, this article studies the amount of signaling required for the DC mobility events. The paper evaluates the signaling reductions (over the air and in the back-haul) with the implementation of UE autonomous cell changes, compared to the classic network-controlled mobility events for DC. The implementation of UE autonomous mobility requires to prepare the small cells in advance. This article proposes to constitute a window of cells that surrounds the UE and follows its movement. As the UE moves along the highway, the set of prepared cells that constitute the window must be updated. Two different policies are presented. The first approach considers to update the set of cells every time the serving small cell changes. The second proposal modifies the set of cells only if the UE connects to any of the last cells of the window, towards the direction of movement.

4 Main Findings

Mobility Sensitivity Analysis of DC for Generic 3GPP and Site-Specific Scenarios

An initial evaluation of the results obtained in Paper C suggested that the mobility performance of DC in a generic 3GPP scenario follows similar trends compared to the performance in the urban scenarios of Tokyo and the European capital. The simulation results revealed that all the scenarios were affected by a large number of mobility events, indicating a large amount of signaling overhead. In general, it was observed that the overall number of events experienced by the UEs increased with the speed. For instance, the number of handovers increased with the same ratio of 1.41 in all the scenarios as the speed of the UE doubled. The results also indicated that the SeNB change was the dominant mobility event independent of the scenario.

However, a deeper analysis of the statistics revealed several differences in the mobility performance among the different scenarios. The proportion of SeNB changes was observed higher in the Tokyo scenario, indicating that the small cells in this urban area experienced higher coverage overlap compared to the other environments. This is due to the specific propagation characteristics of this particular scenario.

Moreover, higher rates of handover failures were found in the simulation results of the site-specific cases compared to the results obtained from 3GPP simulations. This is explained by the fact that in the urban scenarios the handover failures mainly occurred in the street intersections due to the likelihood of experiencing an increase of the interference levels, whereas the 3GPP scenario lacked of the explicit modeling of streets.

The results of the TOS of the UEs in the small cells were observed orders of magnitude longer in the real environments than in the 3GPP scenarios, due to the modeling of radio-propagation in street canyons. Longer TOS were particularly noticeable in the Tokyo scenario, with a higher density of streets compared to the European capital, as can be seen in Figures 3.1 and 3.2. The street canyon effect also caused differences in the ping-pong statistics between the different scenarios.

From the detailed analysis of the results, it is concluded that simulations of generic 3GPP scenarios are a valuable technique for an initial evaluation and benchmarking of features in a cellular network, providing a generic overview of their performance. However, there are important factors that are not fully modeled in the standardized scenarios. 3GPP scenarios do not include explicit modeling of building and street layouts, lacking of specific radio-propagation conditions such as the street canyon and the corner effect that play an important role in the mobility performance. The presented results indicate that the inclusion of the building and street layouts into the modeling of system-level simulations provide an important information that the 3GPP scenarios are unable to supply. Therefore, it is recommended to supplement the 3GPP studies with the explicit modeling of site-specific scenarios for performing the final characterization of the mobility performance.

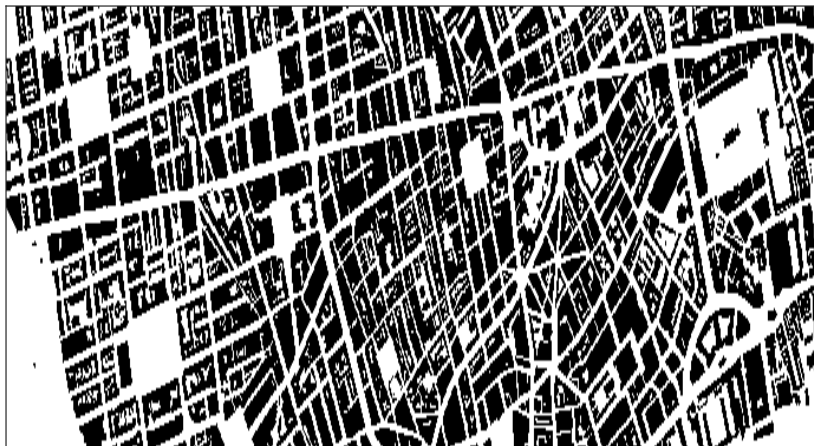


Fig. 3.1: Building and street layouts of the analyzed European capital in Paper C.



Fig. 3.2: Building and street layouts of the Tokyo scenario studied in Paper C.

Reducing the mobility data interruption time with DC

The analysis conducted in Paper D revealed that highway users traveling at high speeds are affected by a large amount of mobility events and consequently, by a large data interruption time. The analysis of the mobility events and the experienced data disruption studied in this paper considered two different connectivity modes: single-node connectivity and DC. For single-node connectivity it was found that a user traveling along the highway stretch suffered from data interruption during approximately 5 % of the duration of the trip. The studies conducted in Paper D also allowed the formulated hypothesis regarding the variability of the data interruption time with the adopted user-plane architecture for implementing DC to be validated. The results showed that with SCG bearer architecture the data interruption increased up to approximately 7 % of the traveling time. However, this time was considerably reduced when selecting split bearer architecture. In this case, the experienced service interruption corresponded to only 0.8 % of the traveling time.

Given these results, it is concluded that split bearer is the most suitable user-plane architecture for implementing DC as it brings the advantages of aggregating additional links while minimizing the data interruption. Nevertheless, the service interruption is not completely eliminated indicating that the enhancements brought by LTE-A with DC are not sufficient for meeting the stringent latency requirements for the next generation of mobile networks.

Reducing the signaling overhead with DC

When implementing DC, the network is affected by a large amount of control signaling and frequent cell management decisions due to the network-controlled nature of the LTE mobility, and the large number of events experienced by the UE. In order to reduce these effects at the network side, Paper E proposes to diverge from the traditional network-controlled mobility, adopting instead UE autonomous cell management procedures. This is a partially UE-controlled mobility mechanism, where the UEs are allowed to directly choose and access the secondary small cell, reducing the amount of signaling and preventing the network from performing frequent mobility decisions. Implementing this feature only in the small cell layer permits the UE to maintain a stable anchor point with the network through the macro-cell that plays the role of the Master eNB (MeNB).

To evaluate this feature under high-mobility conditions, Paper E studied the required signaling overhead for performing each mobility event following traditional DC procedures and UE autonomous cell management. The simulation results demonstrated that with UE autonomous mechanism, the RRC messages were completely eliminated for SeNB additions and SeNB changes, while for SeNB removals, the amount of signaling was reduced by 33 %. The signaling in the back-haul was also considerably reduced. For each SeNB additions, changes and removal, the X2 signaling was diminished by 50 %, 42 % and 33 %, respectively, compared to the traditional network-controlled DC events.

The UE autonomous cell management functionality requires to prepare the small cells in advance with the context of the UEs that can access the cells. To take advantage of the linear nature of the highway scenario, Paper E proposed to create a

window of prepared cells around the UE that followed its movement. The set of cells in the window were updated as the UE moved along the highway according to two different policies. The results showed that this methodology brought significant reductions in the signaling overhead without having to prepare all the cells in the scenario. For example, by preparing only 10 cells around the UE, a reduction in the exchanged messages of 37 % over the air and 4 % between eNBs was achieved with the first proposed updating policy. Furthermore, when the second proposed policy was considered, reductions of 30 % less messages over the air and 82 % less messages in the X2 interface were achieved.

Based on these results, it is concluded that the shift towards UE autonomous cell management mobility is a promising option for reducing the signaling overhead in the network when implementing DC.

References

- [1] J. G. Andrews, S. Buzzi, W. Choi, S. V. Hanly, A. Lozano, A. C. K. Soong, and J. C. Zhang, "What will 5G be?" *IEEE Journal on Selected Areas in Communications*, vol. 32, no. 6, pp. 1065–1082, June 2014.
- [2] K. I. Pedersen, P. H. Michaelsen, C. Rosa, and S. Barbera, "Mobility enhancements for LTE-advanced multilayer networks with inter-site carrier aggregation," *IEEE Communications Magazine*, vol. 51, no. 5, pp. 64–71, May 2013.
- [3] D. S. Michalopoulos, I. Viering, and L. Du, "User-plane multi-connectivity aspects in 5G," in *2016 23rd International Conference on Telecommunications (ICT)*, May 2016, pp. 1–5.
- [4] A. Ravanshid, P. Rost, D. S. Michalopoulos, V. V. Phan, H. Bakker, D. Aziz, S. Tayade, H. D. Schotten, S. Wong, and O. Holland, "Multi-connectivity functional architectures in 5G," in *2016 IEEE International Conference on Communications Workshops (ICC)*, May 2016, pp. 187–192.
- [5] S. C. Jha, K. Sivanesan, R. Vannithamby, and A. T. Koc, "Dual connectivity in LTE small cell networks," in *2014 IEEE Globecom Workshops (GC Wkshps)*, Dec 2014, pp. 1205–1210.

Paper C

Mobility Sensitivity Analysis for LTE-Advanced HetNet Deployments with Dual Connectivity

Simone Barbera, Lucas Chavarría Giménez, Laura Luque
Sánchez, Klaus I. Pedersen, Per Henrik Michaelsen

Published in
IEEE 81st Vehicular Technology Conference (VTC Spring), 2015.

© 2015 IEEE

Reprinted with permission. The layout has been revised.

Abstract

A mobility performance sensitivity analysis is presented for Dual Connectivity cases where the users can be served simultaneously by a macro and a small cell. The performance is assessed for the 3GPP generic simulation scenario and for two site-specific cases, with the aim of comparing the results coming from these different scenarios. The site-specific scenarios are based on detailed three-dimensional topography map data and advanced ray-tracing techniques. It is generally found that the first order statistics and overall conclusions are in good alignment for the considered environments. However, there are also a number of differences in the obtained performance results for the different cases, e.g. in terms of small cell time-of-stay statistics. The explicit modeling of streets and building topology, propagation in street canyons, etc., is found to have an important impact on the mobility performance. Especially the time-of-stay statistics and the location of handover failures differ between generic 3GPP case and the site-specific modeling scenarios. So in conclusion, trends and observations from simulations based on the 3GPP scenario are valuable, but should be supplemented by results from site-specific scenarios, as additional performance-determining effects are more accurately represented for such cases.

1 Introduction

Migration to Heterogeneous Network (HetNet) scenarios with macros and Small Cells (SCs) offers opportunities for use of several variants of multi-cell cooperation techniques [1, 2]. In this study we focus on the case where macros and small cells are deployed at non-overlapping carrier frequencies, and assume usage of Dual Connectivity (DC) [3, 4].

DC is based on broadening the scope of LTE-Advanced Carrier Aggregation (CA) functionality [5] such that a user can simultaneously receive data from a macro and a small cell [6–8]. Among others, DC results in higher end-user throughput, increased network capacity as well as improved mobility robustness, at the cost of more advanced terminals as well as higher signaling overhead from having to manage multiple cells per user. The published studies on mobility performance for DC HetNet cases are relatively few [7–9] and based on performance evaluation only for the generic 3GPP defined HetNet simulation scenario.

Our goal is to present a more extensive HetNet mobility performance sensitivity analysis, where we quantify the performance for different environments. Our starting point is the 3GPP defined HetNet simulation model [10], which relies on a hybrid of static and random deployment models for base station nodes, while using commonly accepted stochastic radio propagation models. The second type of modeling approach is based on site specific use cases. For the site specific cases, a particular urban area is explicitly modeled. Data from 3D topography maps are used together with advanced ray-tracing for determining propagation characteristics, assuming fixed location of base station nodes, movement of users along streets, etc.

We consider two dense metropolitan urban areas for the site specific use cases based on data from a dense urban European capital area and Tokyo in Japan. Given these different modeling approaches, we evaluate the mobility performance charac-

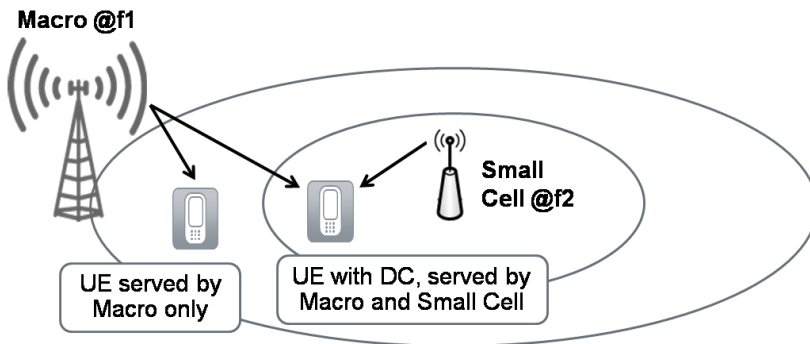


Fig. C.1: Basic scenario: Some UEs are served by a single cell, while Dual Connectivity UEs can be simultaneously served by macro and small cell.

teristics and the sensitivity of these depending on the scenario. The main factors influencing the mobility Key Performance Indicators (KPIs) are identified and discussed with the objective of providing guidance on how strong conclusions can be drawn depending on the underlying modeling assumptions for the network. In order to provide a high degree of realism and statistically reliable results, we have used an advanced dynamic simulator and long simulation runs.

The rest of the paper is organized as follows: In Section 2 the system model is outlined, including the assumed mobility mechanisms. Section 3 contains description of the considered environment modeling. The corresponding performance results are presented and analyzed in Section 4, while concluding remarks appear in Section 5.

2 System Model And Mobility Concept

Let us consider a scenario composed of a set of macro cells and a set of small cells deployed at two non-overlapping carrier frequencies f_1 and f_2 , respectively, assuming $f_1 < f_2$. User Equipments (UEs) are assumed in DC in the form of inter-site CA, which means that they can be simultaneously served by a macro and a small cell as illustrated in Fig. 1.

The macro acts as Master eNB (MeNB), while the small cell acts as Secondary eNB (SeNB). For simplicity, intra-site CA at the MeNB and SeNB is not considered. The focus is on the Radio Resource Control (RRC) Connected mode, where the network decides when handovers are happening based on assistance information from UEs. UE reporting events for mobility assistance are triggered based on measurements of Reference Signal Received Power (RSRP) or Reference Signal Received Quality (RSRQ) from different cells. The RSRP is a measure of the received power of the transmitted reference signal from a cell, while the RSRQ equals the RSRP/RSSI ratio, where RSSI is the Received Signal Strength Indicator (i.e. equivalent to the total wideband received power). It is assumed that UEs have their Primary Cell (PCell) configured on the best macro cell (the MeNB), with the option of also having a small cell configured as a Secondary Cell (SCell) on the SeNB, when feasible. For the sake of simplicity, we

refer to intra-frequency PCell handover as MeNB handover, which is assumed to be based on RSRP A3 (neighbor cell becomes offset better than primary cell). SeNB addition and removal on the small cell layer are based on RSRQ events A4 (neighbor cell becomes better than threshold) and A2 (serving cell becomes worse than threshold) respectively, while intra-frequency SeNB change on the small cell layer is triggered by RSRP A6 (signal level from another SCell candidate becomes offset better than current SCell) [11]. The events need to be fulfilled for duration of Time-To-Trigger (TTT) before triggering reporting to the network. The assumed default mobility settings are summarized in Table C.1 [8].

After the UE triggers the event and the measurement report is received by the network, the MeNB handover (or SeNB management action) is subject to preparation and execution delays. In line with guidelines in [9] the sum of these delays is modeled to equal 90 ms. Similarly, UE physical-layer RSRP measurement imperfections are modeled by adding a zero-mean Gaussian error with 1.2 dB standard deviation to the ideally measured RSRP (expressed in dB). From an end-user perspective, the handover process shall offer a smooth transfer of the users' active connection when moving from one cell to another, while still maintaining the guaranteed quality of service (i.e. without interruptions and errors). The probabilities of Radio Link Failures (RLFs) and Handover Failures (HOFs) are therefore commonly used KPIs for measuring mobility performance. From the network point of view, the mobility performance is also measured by the signaling cost associated with each MeNB handover (or SeNB management action), as well as the probability of having unnecessary cell management Ping-Pong (PP) events. Thus, the objective is to have mobility performance with low probability of experiencing RLF, HOF and PP, as well as low signaling overhead and acceptable time-of-stay. Mobility solutions meeting those objectives are often said to be robust. In this study we adopt the definitions from [9] as follows:

- Ping-Pong (PP) is declared when UE has HO from cell A to B, and back to A within a 1 second time-period; for UEs with DC, PP events are monitored separately for the macro and small cell layer.
- Radio Link Failure (RLF) is declared when the downlink user SINR has been below -8 dB (Q_{out}) and stayed below -6 dB (Q_{in}) for the duration of 1 second.
- HO Failure (HOF) is declared if the RLF occurs after TTT expires, during the HO execution time.

Note that, in line with the current assumption in 3GPP for DC, RLF for triggering re-establishment is based on radio link monitoring on the PCell only (i.e. quality of the MeNB link). Hence, when reporting RLF and HOF statistics, this is based solely on the MeNB link quality.

Table C.1: Default mobility events configuration.

Case	Setting	Remarks
Intra-f MeNB HO	A3 RSRP	For the macro layer it is not that important to have very fast handover decisions, so relatively high values of TTT and Layer-3 filtering (K) are used to avoid unnecessary handovers.
SeNB addition (i.e. SeNB configuration and DC activation)	A4 RSRQ. Thresh.=-12dB, K=1, TTT=160ms	The idea is to enable SeNB on small cell layer as soon as the quality is sufficiently good. Low values of K and TTT are used to have a quick SeNB addition.
SeNB removal (i.e. return to single connectivity)	A2 RSRQ. Thresh.=-17dB, K=1, TTT=160ms	The idea is to disable SeNB when quality on the small layer becomes so poor that scheduling the UE on that layer no longer brings substantial throughput benefits.
Intra-f SeNB change on small cell layer	A6 RSRP. Offset=1dB, K=1, TTT=160ms	Relatively low values of Offset, K, and TTT are used in order to ensure fast SeNB changes between small cell nodes.

3 Scenarios and Related Modeling Assumptions

A realistic HetNet scenario model is desirable. Ideally, it should replicate all important features of the real environment. However, detailed modeling is usually associated with high complexity. Hence, it is a trade-off between accuracy and complexity. In this study we consider two types of models: (i) Generic models based on commonly accepted definitions with certain elements of randomness and (ii) site-specific models with a detailed representation of a specific area with fixed base station installations. Assumptions for the considered environments are summarized in Table C.2.

Table C.2: Modeling assumptions for the considered scenarios

	3GPP	Europe	Tokyo
Macro Sites			
# sites	7x3 sectors Hexagonal grid	15x3 sectors 4x2 sectors 53 cells	90x3 sectors 270 cells
Avg ISD	500 m (Fixed)	293.3 m	227.6 m
Minimum ISD	500 m	94.7 m	177.7 m
ISD std. dev.	-	156 m	18 m
Avg antenna height	30 m (Fixed)	32 m	25 m
Antenna height std. dev.	-	8.2 m	18.5 m
Avg. antenna tilt	14° (Fixed)	1.5°	9.5°
Antenna tilt std. dev	-	2.2°	7.3°
Frequency	1800 MHz	800 MHz	800 MHz
Small Cell Sites			
# sites	42	48	70
Avg. # SCs per macro	2 (Fixed)	2	2.25
Avg SC ISD	120.58 m	138.53 m	64.78 m
SC ISD std. dev.	45.77 m	89.54 m	32.62 m
Avg SC-macro distance	192.64 m	184.35 m	92.77 m
SC-macro dist. std. dev.	55.30 m	77.53 m	30.59 m
Minimum SC-macro distance	94.56 m	47.48 m	41.86 m
Antenna height	5 m	5 m	5 m
Carrier frequency	2600 MHz	2600 MHz	1700 MHz
Scenario Topology			
Area	Not explicitly modeled	3270x930 m	1000x1000 m
Avg. buildings height	Not explicitly modeled	13.8 m	24.45 m
Buildings height std. dev.	Not explicitly modeled	7.84 m	21.95 m
Tallest building height	Not explicitly modeled	113.3 m	150 m

3.1 The Generic 3GPP Scenario

The 3GPP HetNet scenario model [10] is one of the most commonly used baseline references, not only for the 3GPP studies, but also for other studies in academia. The model assumes a static regular hexagonal grid of 3-sector macro base station sites, placed at a fixed Inter-Site Distance (ISD) of 500 meters. Small cells are randomly placed according to a spatial uniform point process, subject to certain minimum distance constraints between base stations. The minimum distance between two SCs is 40 meters, while the minimum distance between a macro and a SC is 75 meters. The radio propagation is modeled according to commonly accepted stochastic models, reproducing typical observations from dense urban environments. It includes a deterministic distance dependent path loss and a random shadow fading component. The shadow fading is modeled with a Log-Normal distributed random variable, using the Gudmundson model [12] for the spatial correlation. From a mobility perspective, it is worth noticing that the shadow fading standard deviation is larger for the small cell links, as well as shorter correlation distance, meaning that small cell links are subject to higher variability as users move. This is also the reason for using mobility settings with shorter time-domain constraints and lower offset margins, for triggering small cell to small cell mobility; see parameters in Table C.1. UEs are uniformly distributed over the simulated area moving at the same constant speed. The direction for each user is randomly selected at the start of each simulation from a uniform distribution with equal probability for all directions.

3.2 Site Specific Scenarios

The site specific scenarios for two local areas in Europe and Tokyo are based on data from detailed three dimensional (3D) topography maps. The maps contain 3D data for buildings, information on streets, open squares, parks, etc. Macro sites are placed in coherence with typical operator installations in the considered areas, meaning that those are deployed to offer wide area coverage, taking the local topology into account. Small cells are placed in street canyons or on open squares to offer additional hotspot improvements. All UEs are outdoors, moving at constant speed along the streets only. When a UE reaches a street intersection, the direction of movement is randomly selected with equal probability for the possible directions. The radio propagation characteristics are obtained by using ray-tracing techniques based on the Dominant Path Model (DPM) [13, 14].

European capital area

The considered dense urban segment measures 3270 x 930 meters, with an average building height of 14 meters, with the tallest building reaching a height of 113 meters. The buildings cover 47 % of the area. The remaining 53 % of the area is a mixture of open areas such as parks and city squares, as well as streets. The locations of the macro sites and their configurations are selected in coherence with typical operators' installations in the considered geographical area [15]. A total of 53 macro cells are deployed, where the majority of those have 3-sectors, while others have 2-sectors. The macro sites are deployed at different heights, taking the local environment into ac-

count in order to have good wide area coverage. A total of 48 small cells are deployed at 5 meters height in street canyons or at open squares. The small cells are deployed to further improve 5 %-ile outage throughput of the network [15]. The former brings to a deployment where the small cells are clustered in certain areas, while other areas contain only few or no small cells. For the areas with small cells, there are on average two small cells per equivalent macro cell coverage area. The small cells are equipped with omni-directional antennas.

Tokyo

buildings in the local area. The orientation of the macro antennas is selected to form good wide area coverage, while minimizing inter-cell interference. The average macro ISD equals 227 meters with a standard deviation of 18 meters. A total of 70 small cells are deployed at 5 meters height. The small cells are mainly placed near the tallest buildings, in order to offload and carry more traffic where the radio signal from macro cells is typically weaker and there is higher traffic.

4 Performance Results

A dynamic system level simulator is used to assess the mobility performance for the three considered scenarios. The simulator follows the LTE specifications with modeling of the major Radio Resource Management (RRM) functionalities in line with the simulation methodology outlined in [9] and [10]. The mobility framework is in coherence with the description in Section II. The simulations are conducted for high offered traffic load close to the system's capacity limit where the inter-cell interference is dominant, and therefore most challenging for achieving good mobility performance.

The simulator has been validated by successfully reproducing mobility performance results reported from various sources in [9]. This gives confidence that the simulator is producing reliable results. In order to ensure statistically reliable performance results, long simulations are conducted to collect a high number of samples (more than 10,000 mobility events) for obtaining confident empirical estimates of the considered mobility KPIs defined in Section 2.

Fig. C.2 shows the statistics for the average number of experienced mobility events per UE per hour. As expected, the number of handover events per UE per hour increases with the UE speed. The increase in the number of handover events is approximately proportional to the square root of the UE speed; i.e. increasing approximately with a factor 1.41 as the UE speed doubles. The former is consistent for all the environments. As also reported in [8], the SeNB management actions are clearly dominant over the MeNB mobility events due to the more frequent small cell related actions, accounting for 50 %-80 % of the events. The proportion of SeNB changes is significantly higher for the Tokyo scenario as compared to the other cases, indicating that this area has higher small cell coverage overlap as compared to the other cases. Note that the former is not due to higher small cell density for the Tokyo case, but rather a result of having a more spatial uniform small cell distribution, as well as differences in the

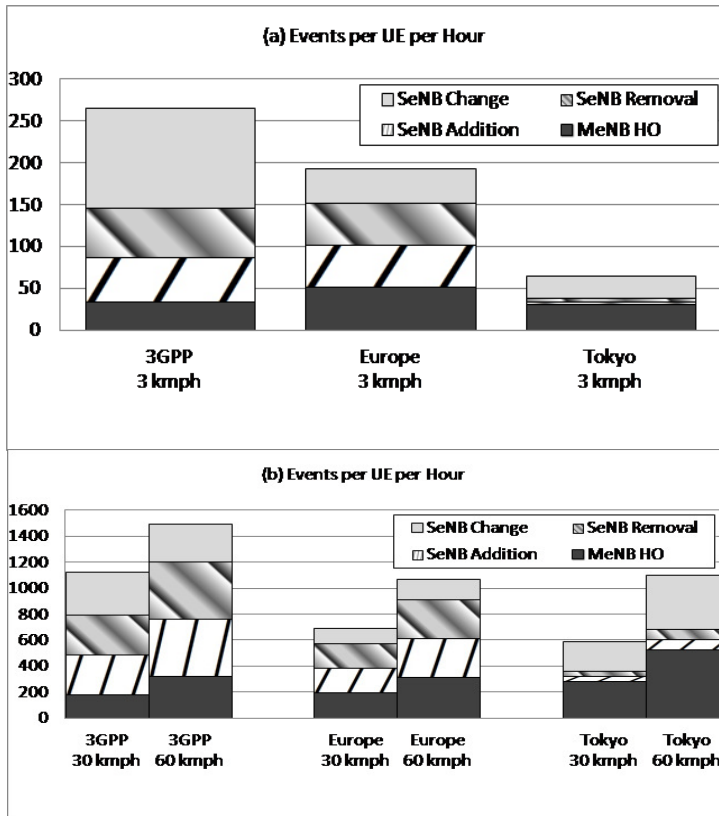


Fig. C.2: Events per UE per hour at 3 kmph (a) and at 30 and 60 kmph (b).

radio propagation characteristics. The percentage of users operating with DC equals 80 % for the Tokyo scenario and 55 % for the European and the 3GPP scenarios.

The empirical cumulative distribution function of the per-cell Time-Of-Stay (TOS) statistics is reported in Fig. C.3 for small cells and in Fig. C.4 for macro cells. It is observed that the TOS per cell is substantially higher for the site-specific cases as compared to the 3GPP case. This is contributed by the following factors: (i) UEs are restricted to move on streets for the site-specific cases, while moving freely for the 3GPP case; (ii) the explicit modeling of radio propagation in street canyons for the site-specific cases is different from the use of generic stochastic propagation models for the 3GPP case. Hence, the sum of (i) and (ii) results in much longer TOS for site-specific cases as compared to what is observed from 3GPP simulations. It is also observed that users are generally experiencing longer TOS in the Tokyo scenario as compared to the European capital area, in particular for small cells. This is mainly a result of having more widespread small cell deployment, lower carrier frequency for small cells, and longer straight street segments. It is observed that the TOS for the Tokyo area is slightly higher for the small cells as compared to macro cells, since

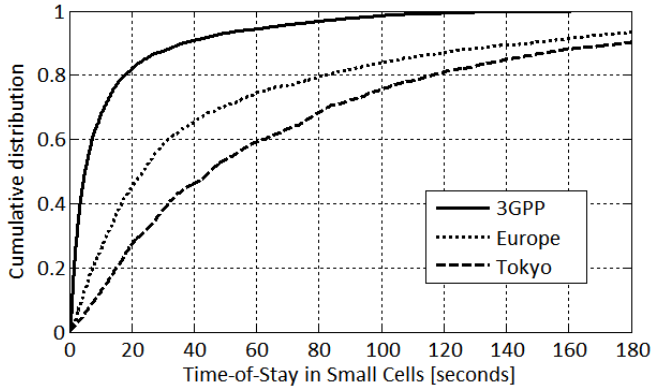


Fig. C.3: Empirical cumulative distribution function of the time-of-stay for UEs in small cells at 3 kmph.

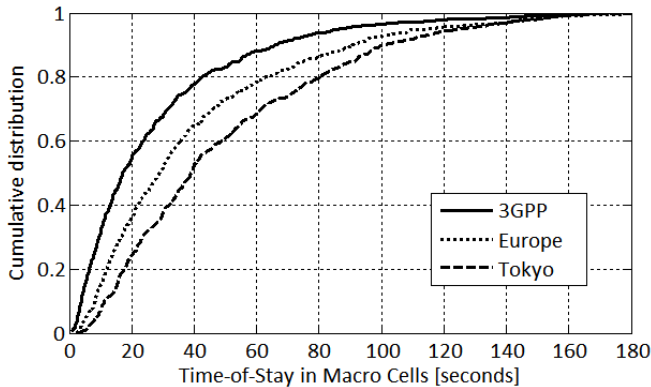


Fig. C.4: Empirical cumulative distribution function of the time-of-stay for UEs in macro cells at 3 kmph.

small cells in many locations offer more favorable signal quality at street level than the macro cells that are deployed above the tall buildings. TOS statistics are also logical and consistent with the results in Fig. C.2a, with the number of mobility events being inversely proportional with the TOS.

Fig. C.5 shows the probability of experiencing HOF events for the considered cases. The low HOF probability is a result of having a reliable MeNB link to the macro layer. For the site-specific scenarios, it is found that the HOFs mainly occur at street inter-sections where the UE is more likely to experience rapid signal strength variations of both the desired and interfering signals. Hence, the higher probability of experiencing abrupt signal fluctuations in the site-specific environments is an important mobility performance-determining factor.

The probability of experiencing SeNB Ping-Pong (PP) events is reported in Fig. C.6.

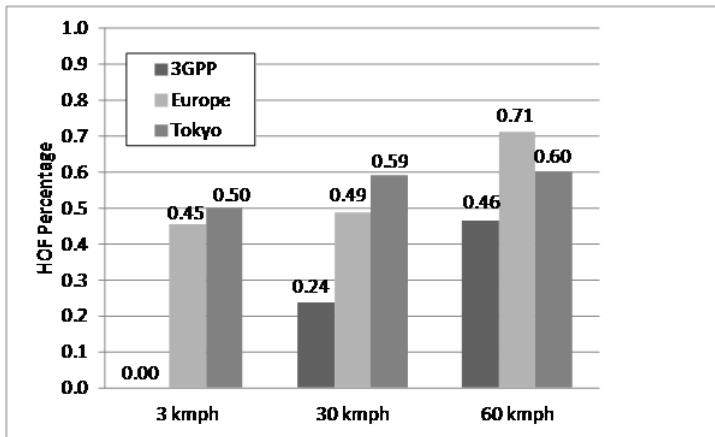


Fig. C.5: Handover failure percentage.

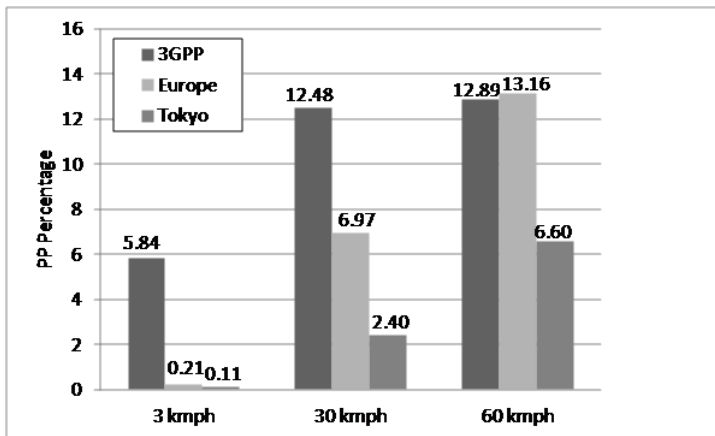


Fig. C.6: SeNBs ping-pong percentage.

Trends and percentages are different between scenarios, with the 3GPP case having the highest values at low speed while higher values are observed for the European area at higher speed. The observed probability of experiencing SeNB PPs is considered acceptable in all cases, as SeNB PPs do not cause any service interruptions, as the UE has anyway the MeNB at the macro layer active. Alternatively, the SeNB PP probability could be reduced by using higher offset margin and longer TTT for the A6 event that triggers SeNB changes [7].

5 Conclusions

In this study, we have presented mobility performance results for LTE HetNet scenarios with Dual Connectivity, given different underlying network modeling methodologies. When comparing the mobility performance for the considered network models, consistent overall conclusions are found. However, when further analyzing the detailed statistics, several differences are observed. For the site specific cases, the handover failures are mainly found to occur for terminals in street inter-sections where high gradients of the desired and the interference signal powers are more likely to happen. For the generic 3GPP case, such details are not explicitly modeled, and hence it is observed that the handover failure probability is slightly higher for the site specific cases, although acceptable in all cases. The small cell time-of-stay statistics are found to be orders of magnitude higher for the site specific environments as compared to the 3GPP scenario. This is primarily due to the explicit modeling of radio propagation in street canyons, causing also differences in Ping-Pong statistics between the different scenarios. We conclude that the generic 3GPP scenario brings valuable first results, although not all mobility performance-determining factors are fully represented. However, for the final performance assessment, it is recommended to supplement the 3GPP mobility performance studies with results from scenarios with explicit modeling of building structures, associated radio propagation effects and terminal movement in streets.

References

- [1] B. Soret, H. Wang, K. I. Pedersen, and C. Rosa, "Multicell cooperation for LTE-advanced heterogeneous network scenarios," *IEEE Wireless Communications*, vol. 20, no. 1, pp. 27–34, February 2013.
- [2] T. Nakamura, S. Nagata, A. Benjebbour, Y. Kishiyama, T. Hai, S. Xiaodong, Y. Ning, and L. Nan, "Trends in small cell enhancements in LTE advanced," *IEEE Communications Magazine*, vol. 51, no. 2, pp. 98–105, February 2013.
- [3] *3GPP Technical Report (TR) 36.872. Small cell enhancements for E-UTRA and E-UTRAN. Physical layer aspects.*, Dec 2013, available at www.3gpp.org.
- [4] *3GPP Technical Report (TR) 36.842. Study on small cell enhancements for E-UTRA and E-UTRAN. Higher layer aspects.*, July 2014, available at www.3gpp.org.
- [5] K. I. Pedersen, F. Frederiksen, C. Rosa, H. Nguyen, L. G. U. Garcia, and Y. Wang, "Carrier aggregation for LTE-advanced: functionality and performance aspects," *IEEE Communications Magazine*, vol. 49, no. 6, pp. 89–95, June 2011.
- [6] H. Wang, C. Rosa, and K. I. Pedersen, "Dedicated carrier deployment in heterogeneous networks with inter-site carrier aggregation," in *2013 IEEE Wireless Communications and Networking Conference (WCNC)*, April 2013, pp. 756–760.
- [7] K. I. Pedersen, P. H. Michaelsen, C. Rosa, and S. Barbera, "Mobility enhancements for LTE-advanced multilayer networks with inter-site carrier aggregation," *IEEE Communications Magazine*, vol. 51, no. 5, pp. 64–71, May 2013.

- [8] S. Barbera, K. Pedersen, P. H. Michaelsen, and C. Rosa, "Mobility Analysis for Inter-Site Carrier Aggregation in LTE Heterogeneous Networks," in *2013 IEEE 78th Vehicular Technology Conference (VTC Fall)*, Sept 2013, pp. 1–5.
- [9] *3GPP Technical Report (TR) 36.839. Mobility enhancements in heterogeneous networks.*, Sept 2012, available at www.3gpp.org.
- [10] *3GPP Technical Report (TR) 36.814. Further advancements for E-UTRA physical layer aspects.*, March 2010, available at www.3gpp.org.
- [11] *3GPP Technical Specification (TS) 36.331. Radio Resource Control (RRC) protocol specification.*, June 2012, available at www.3gpp.org.
- [12] M. Gudmundson, "Correlation model for shadow fading in mobile radio systems," *Electronics Letters*, vol. 27, no. 23, pp. 2145–2146, Nov 1991.
- [13] R. Wahl and G. Wolfle, "Combined urban and indoor network planning using the dominant path propagation model," in *2006 First European Conference on Antennas and Propagation*, Nov 2006, pp. 1–6.
- [14] R. Wahl, G. Wolfle, P. Wertz, P. Wildbolz, and F. Landstorfer, "Dominant path prediction model for urban scenarios." in *14th IST Mobile and Wireless Communications Summit, Dresden, Germany*, 2005.
- [15] C. Coletti, L. Hu, N. Huan, I. Z. Kovács, B. Vejlgaard, R. Irmer, and N. Scully, "Heterogeneous Deployment to Meet Traffic Demand in a Realistic LTE Urban Scenario," in *2012 IEEE Vehicular Technology Conference (VTC Fall)*, Sept 2012, pp. 1–5.

Paper D

Analysis of Data Interruption in an LTE Highway Scenario with Dual Connectivity

Lucas Chavarría Giménez, Per Henrik Michaelsen, Klaus I.
Pedersen

Published in
IEEE 83rd Vehicular Technology Conference (VTC Spring), 2016.

© 2016 IEEE

Reprinted with permission. The layout has been revised.

Abstract

This study evaluates whether last versions of Long Term Evolution with dual connectivity are able to support the latency and reliability requirements for the upcoming vehicular use-cases and time-critical applications. Data interruption times during handovers and cell management operations are evaluated by means of system level simulations for a high-speed scenario. The scenario models a highway covered by a macro layer and an ultra dense network of small cells distributed on both sides of the road. Results reveal that for single connectivity, and due to the large amount of handovers, terminals are unable to exchange data with the network about 5 % of the time. This time is considerably reduced if dual connectivity with split bearer architecture is adopted, with less than 1 % of time in data interruption. However, when adopting secondary cell group architecture, the relative data interruption time increases up to 6.9 %.

1 Introduction

Nowadays, passengers in vehicles tend to consume large amounts of entertainment and media content while commuting [1]. A possible solution to deal with the increasing number of active users along roads, and to increase the capacity, may be the deployment of small cells. This offers several advantages; however, the addition of small cells also comes with some challenges related to efficient mobility management, especially, for users traveling at high speeds [2].

Dual connectivity (DC) is a recently developed feature for Long Term Evolution (LTE) Release-12 [3], which significantly increases the end-user throughput and achieves enhanced mobility robustness [4]. Examples of DC studies include assessments of throughput gains [4–6], as well as mobility performance results [2, 7]. The majority of these former studies are conducted for urban scenarios, with the users moving at moderate velocities, and do not study the effects at handovers and cell management events as, for example, data interruption times.

Field measurements of LTE mobility reported in [8], show that each handover results in an average data interruption time of 50 ms. Nevertheless, delays can be larger than 80 ms 5 % of the time. As a result, data interruption times caused by mobility events are becoming an increasing problem that needs special attention, especially, in the highway scenario as handovers and cell management events rates increase with the speed. The majority of broadband applications may be supported by the use of small cells and DC; however, data interruption becomes a potential issue when considering the stringent latency and reliability requirements of the upcoming vehicular use-cases, traffic safety applications and the eventually migration towards higher degree of autonomous driving [9, 10].

The focus of this paper is, therefore, on the data interruption time caused by handovers and cell management events in a highway scenario. A network topology with an overlay macro layer is assumed, supplemented by small cells along the highway to boost the capacity. Macro and small cells are deployed at separated carrier frequencies using LTE. Cases with and without DC are studied. For DC operations, the performance is analyzed including the two user-plane architectures that the 3rd Generation Partnership Project (3GPP) has defined [11]. As our objective is to present

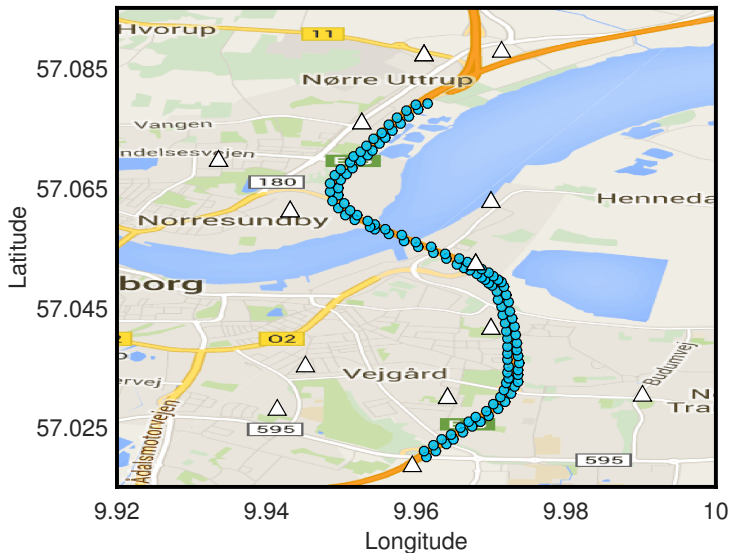


Fig. D.1: Illustration of the analyzed highway scenario. Macro sites are depicted as white triangles while small cells are illustrated as blue circles.

results of high practical relevance, we conduct the analysis for a specific real-life highway segment, which is reproduced in a system level simulator. In addition, latency measurements of the various steps of the handover procedures and cell management actions conducted in [12], are fed into the simulations to have high realism on the assumed parameters.

The rest of the paper is structured as follows: Section 2 describes the scenario that will be analyzed and the mobility framework. Section 3 explains the adopted simulation methodology, and Section 4 presents the performance results. Finally, Section 5 concludes with the final remarks and the proposed future work.

2 Scenario Description and Mobility Framework

The studied scenario is a 7.5 km section of the E-45 highway that encircles the city of Aalborg, Denmark. As illustrated in Figure D.1, the scenario is characterized by two network layers operating at separate frequency bands (non co-channel). The LTE macro layer represents the actual network deployment of one of the Danish operators. The small cells layer, on the other hand, is a fictitious Ultra Dense Network (UDN) distributed along the highway.

The macro network is deployed at 1800 MHz and consists of 23 cells, distributed on 13 base station sites, with an average Inter-Site-Distance (ISD) of 1092 m, an average antenna height of 31.3 m and an average tilt (mechanical and electrical) of 2.1° . The small cells layer operates at 3400 MHz with a minimum ISD of 100 m. The small cells are deployed on both sides of the highway to ensure good coverage along the road.

Table D.1: Network parameters

Macro Layer	
Carrier frequency	1800 MHz
Channel bandwidth	20 MHz
Number of cells	23
Number of sites	13
Average antenna height	31.3 m
Antenna height std. deviation	13.22 m
Average antenna tilt	2.1°
Average tilt std. deviation	1.6°
Average ISD	1092 m
Minimum ISD	624 m
Small Cells Layer	
Carrier frequency	3400 MHz
Channel bandwidth	20 MHz
Number of cells	119
Antenna height	5 m (Fixed)
Antenna pattern	Omni-directional
Average ISD	100 m

In total, there are 119 small cells in the scenario. Table D.1 summarizes additional information about the characteristics of the network.

This study considers a case with single connectivity User Equipments (UEs) used as a baseline, and another one with all UEs capable of performing DC operations.

2.1 Mobility with Single Connectivity

In this mode, the UE consumes radio resources from one cell at a time. Following the parametrization in [7], intra- and inter-frequency handovers are triggered by the A3 event (neighboring cell becomes offset better than the serving cell). Intra-frequency events (macro-to-macro and pico-to-pico) are based on the Reference Signal Received Power (RSRP) Radio Resource Management (RRM) measurement while inter-frequency handovers (macro-to-pico or vice-versa) are based on Reference Signal Received Quality (RSRQ).

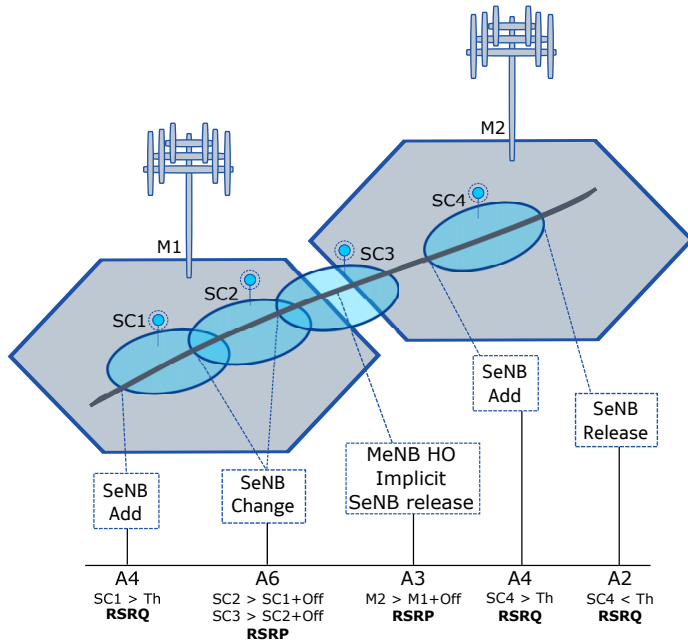


Fig. D.2: Mobility events with dual connectivity.

2.2 Mobility with Dual Connectivity

In this case, the UE is able to consume radio resources provided by, at least, two different network points [3]. The eNodeB (eNB) that terminates the S1-Mobility Management Entity (MME) interface, acts as the mobility anchor towards the Core Network (CN), and manages the Radio Resource Control (RRC) signaling, is named the Master-eNB (MeNB). The eNB which provides additional radio resources for the UE is defined as Secondary-eNB (SeNB). In this study, it is assumed that a macro cell acts as the MeNB while a small cell plays the role of the SeNB. Moreover, it is also assumed that each UE can be configured with only one SeNB. As recommended in [7], mobility at the macro layer (MeNB handover) is governed by the A3 event, based on the RSRP. A second data link from the small cell layer is added (SeNB addition) if a neighbor small cell becomes better than a certain threshold as the event A4 dictates, based on the RSRQ. The small cell serving the second data link is changed (SeNB change) according to the RSRP A6 event (neighbor small cell becomes offset better than serving small cell). Finally, if the measured RSRQ from the SeNB becomes worse than a certain threshold, as the event A2 states, the additional link is removed (SeNB removal). The use of these mobility events is shown in Figure D.2. Notice that in LTE Release-12 any aggregated SeNB should be released before a MeNB handover.

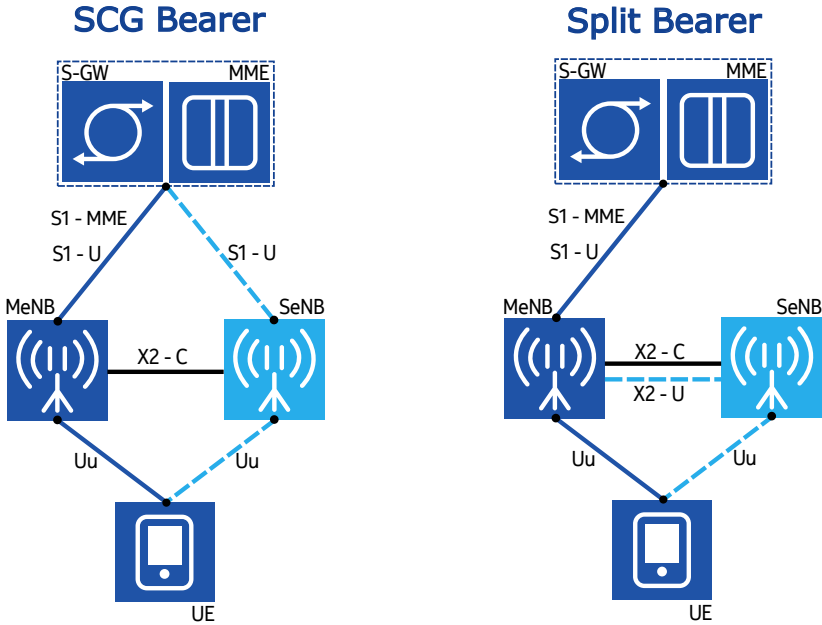


Fig. D.3: User-plane architectures for dual connectivity.

2.3 User-Plane Architectures for Dual Connectivity

This study considers the two user-plane architectures defined by the 3GPP in [11]. Both architectures are depicted in Figure D.3. A detailed comparison between architectures can be found in [3].

- SCG Bearer Architecture:* In Secondary Cell Group (SCG) bearer the SeNB is connected directly to the CN via S1, allowing the S1-U termination not only at the MeNB, but also at the SeNB. In this architecture, the two eNBs carry different data bearers. Independent Packet Data Convergence Protocol (PDCP) entities are considered at both nodes, and low requirements in the back-haul interface between the MeNB and the SeNB are needed. Regarding mobility, SeNB cell management is visible to the CN.
- Split Bearer Architecture:* In split bearer architecture the data bearer is split into multiple eNBs. In this alternative, the S1-U is terminated at the MeNB, where the PDCP layer resides. All DC traffic should hence be routed, processed and buffered at the MeNB, requiring flow-control and efficient back-haul connection between the MeNB and the SeNB. Unlike the SCG bearer architecture, the SeNB mobility is hidden to the CN and it is not necessary to forward data between SeNBs or to perform a S1 path switch at each SeNB change.

Table D.2: Mobility events duration and interruption times.

	SCG Bearer	Split bearer
Total time - Handover	164 ms	164 ms
Total time - SeNB addition	144 ms	79 ms
Total time - SeNB change	154 ms	89 ms
Total time - SeNB release	117 ms	52 ms
Data interruption time - Handover	42 ms	42 ms
Data interruption time - SeNB addition	37 ms	0 ms
Data interruption time - SeNB change	37 ms	0 ms
Data interruption time - SeNB release	37 ms	0 ms

2.4 Data Interruption Time

During the handover execution phase, the UE interrupts data exchange with the network. Communication is not restored until the handover is completed and the UE receives the first data package from the target cell. Data interruption is experienced at each cell change for single connectivity and at each MeNB handover for DC.

For DC, the interruption of the second link due to SeNB management events depends on the chosen user plane architecture. In SCG bearer architecture, the bearer terminated at the SeNB experiences an interruption at every SeNB change because the path at the Serving Gateway (S-GW) has to be updated. This interruption time can be decreased by allowing data forwarding between the serving and target SeNBs. Nevertheless, it cannot be totally eliminated because of the time it takes to reconfigure the UE. For split bearer architecture, the bearer terminates at the MeNB. As a result, and assuming that there are enough available resources, the MeNB can adapt the scheduled resources to the UE while it performs an SeNB operation hence, compensating the effects of the data interruption. Thus, SeNB management interruption time can be considered close to zero for split bearer.

Measurements reported in [12] characterized the time it takes to exchange signaling messages between nodes, including the needed time to process each message and the time it takes to perform a data path update. Using these times and following the signaling flows described in [3] for each mobility event, the interruption times shown in Table D.2 are used. Notice that these are typical average values, and different factors at the network side, e.g. load conditions at the target cell, may increase the interruption times. Additional back-haul delays are not included.

3 Simulation Methodology

Connected-mode mobility performance is evaluated by means of advanced simulations. The system level simulator implements the mobility mechanisms defined by the

3GPP for LTE, including physical-layer measurements, Layer-3 filtering and reporting events. The RSRP, RSRQ and Signal to Interference plus Noise Ratio (SINR) for each user are calculated on each time-step, followed by the SINR to throughput mapping estimation. Effects of scheduling, link adaptation, Hybrid-Automatic-Repeat-Request (HARQ) and Multiple-Input and Multiple-Output (MIMO) are included. The tool has been used in several standardization and research studies, such as [7, 12, 13]. More details on the simulator can be found in [14].

A total of 630 users are dropped in the simulations, divided into slow- and high-speed users. Ten slow-speed users per macro area are considered, moving at 3 kmph. Each of the users follow random directions thorough the whole scenario, shown in Figure D.1. The purpose of these slow-users is to generate background interference. Additionally, 400 users moving at 130 kmph are dropped along the highway. The stretch of the highway is modeled with two lanes per direction, and each high-speed user is randomly assigned to one lane. Among all simulated users, statistics are only collected from the highway users. All users in the network generate traffic according to a Poisson process.

For the baseline case, a fast transition between small cells is favored by setting a Time-To-Trigger (TTT) of 40 ms. Macro-to-pico handovers are set to a larger TTT to ensure that the signal from the small cells is stable for a longer time, thus avoiding Radio Link Failures (RLFs). For DC simulations, the SeNB events are also set to 40 ms of TTT so that, results can be compared with the baseline case. Moreover, a fast transition between small cells is guaranteed by setting the SeNB change offset to 1 dB. Poor secondary links are avoided by setting the SeNB release threshold to -17 dB of RSRQ. Furthermore, a Range Extension (RE) of 6 dB is applied to increase the utilization of the small cells in the highway. To ensure that the users are able to traverse the whole highway stretch, the simulation time is set to 210 s. Simulation parameters are summarized in Table D.3.

The main Key Performance Indicators (KPIs) collected from the simulations are: the number of mobility events, the rate of RLFs, the number of Handover Failures (HOFs) and the data interruption times. The definition of RLF and HOF can be found in [17]. Moreover, the user throughput is also analyzed.

4 Performance Results

Figure D.4 shows the number of events and the connectivity distribution that a UE experiences. As can be seen, this scenario is especially challenging due to the large number of mobility events. When using single connectivity, a UE at 130 kmph experiences an average of 4176 handovers per hour, corresponding to 1.16 events per second. The device is connected to the small cells 96.6% of the time, where intra-frequency handovers between the small cells dominate the statistics. For DC, the total number of events increases because each UE maintains two active links. However, MeNB handovers are reduced by 83%, with a total number of 0.2 events per second. In this case, SeNB changes are dominant with 1.3 events per second. The latter is expected because the mobility parametrization of 1 dB offset favors it. On average, a UE is operating in DC 95.7% of the time. No RLFs or HOFs are observed in the simulations for single and dual connectivity.

Table D.3: Simulation Parameters.

Transmitted power	Macro: 46 dBm. Pico: 30 dBm
Path loss	Macro: Vehicular test environment [15] Small Cells: Urban Micro (UMi) [16]
Number of UEs	230 free users + 400 highway users
Users speed	Background: 3 kmph. Highway: 130 kmph
Packet call size	Negative exponential distributed. Average: 1 Mbit
Inter-arrival time	Average: 2 s
Sim. Time	210 s
RLF [17]	Qin: -6 dB. Qout: -8 dB. T310: 2 s
Handover / MeNB Changes - A3 event	
Macro-Macro	Offset: 3 dB. RSRP based. TTT: 256 ms
Macro-Pico	Offset: 3 dB. RSRQ based. TTT: 128 ms
Pico-Pico	Offset: 3 dB. RSRP based. TTT: 40 ms
Pico-Macro	Offset: 3 dB. RSRQ based. TTT: 40 ms
Pico RE	6 dB
SeNB Management Events	
SeNB Addition	A4 event. Threshold: -12 dB-RSRQ. TTT: 40 ms
SeNB Change	A6 event. Threshold: 1 dB-RSRP. TTT: 40 ms
SeNB Release	A2 event. Threshold: -17 dB-RSRQ. TTT: 40 ms

Figure D.5 depicts the data interruption time experienced per UE. For single connectivity, each UE performs an average of 1.16 handovers per second. Considering 42 ms of interruption time per event and a driving time of 210 s, it can be calculated that each UE experiences a total interruption time of 10.2 s. This means that a single connectivity device is not able to transmit or receive any data 4.8% of the driving time. Notice that when considering 80 ms of interruption time per event, as found in [8], the total data interruption time increases up to 9.3%, and 11.6% when considering 100 ms.

For DC, 0.2 MeNB handovers per second occur, resulting in an interruption time of

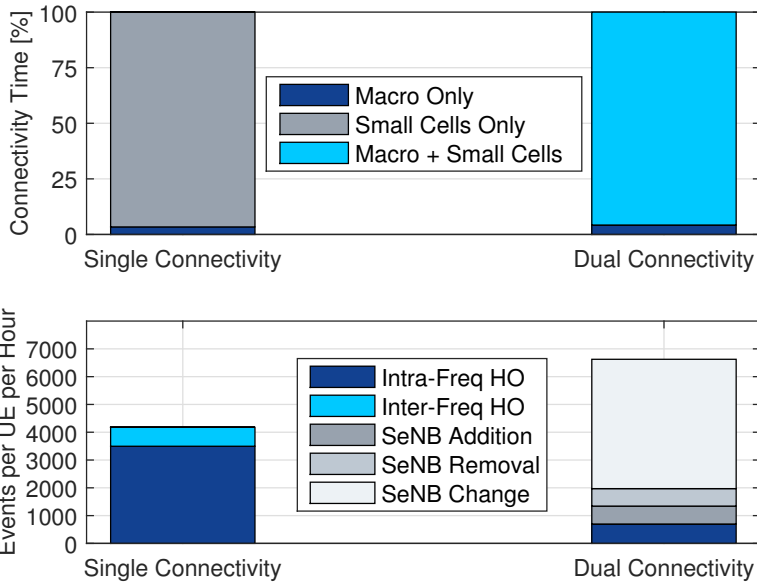


Fig. D.4: Connectivity distribution and mobility events for single and dual connectivity modes.

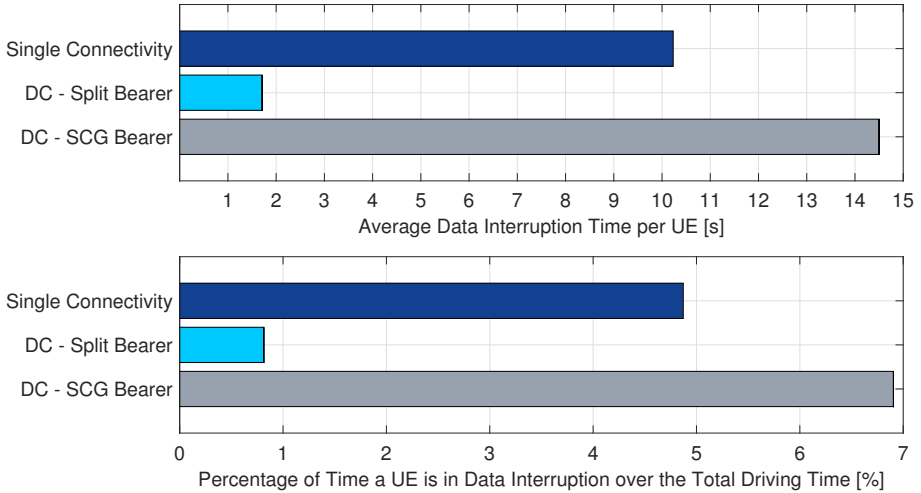


Fig. D.5: Data interruption time per UE with single and dual connectivity.

1.7s. When SCG bearer architecture is used, the delays at the small cells layer should be added. Since the data bearer terminates at the SeNB, each SeNB management event is affected by the E-UTRAN Radio Access Bearer (E-RAB) modification and the possible delays when the S-GW forwards the data packets towards the eNBs involved. Moreover, due to the large number of SeNB events, SCG bearer adds 12.8s to the total

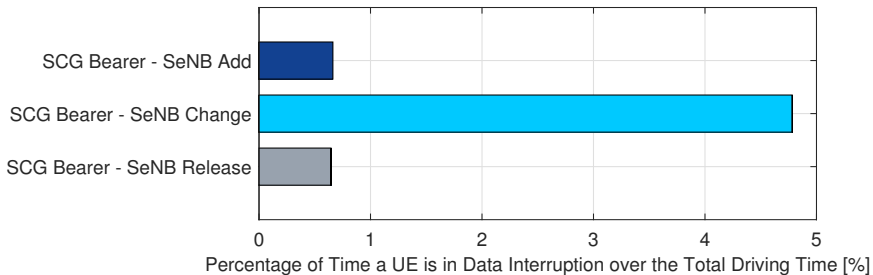


Fig. D.6: Percentage of time in data interruption at the small cells layer with SCG bearer architecture for each SeNB management event.

Table D.4: Highway users throughput for single and dual connectivity.

	Single connectivity	Dual connectivity	Gain
Average	15.6 Mbps	17.3 Mbps	+ 10.9 %
5-percentile	617 Kbps	717 Kbps	+ 16.2 %
50-percentile	10.7 Mbps	11.9 Mbps	+ 11.8 %
95-percentile	46.9 Mbps	51.8 Mbps	+ 10.5 %

interruption time. Considering the interruption time due to MeNB handovers and due to SeNB management events, it can be calculated that the UEs are in data interruption for 6.9% of the time. The contribution of each SeNB event to the interruption time for SCG bearer is depicted in Figure D.6. On the other hand, for the split bearer, the delays at each SeNB management event can be neglected and the main contribution to the data interruption time is given by the MeNB handovers, reducing the latency. In other words, for the split bearer, the UEs are in data interruption only 0.81% of the total time.

Table D.4 shows one of the main benefits of DC: to improve the per-user throughput. As it can be observed, maintaining two data links increases the average user throughput by 10%. The major improvement is obtained in the 5-percentile with a gain larger than 16%. This shows that users experiencing bad radio conditions in a link, can mitigate the effects by aggregating an SeNB hence, increasing their throughput. The average Physical Resource Block (PRB) utilization of the macro cells close to the highway is larger than 70%, indicating high load conditions. Previous DC studies reported that the achievable throughput gain varies with the load of the network [5, 18]; therefore, under lower offered load, users will perceive larger throughput gains with DC.

In general, results show how DC is able to reduce the overall experienced data interruption time. In real implementations, the interruption times will lay in between the presented numbers. For example, data forwarding between nodes may not always be available, resulting in larger delays for split bearer. On the other hand, results for SCG can be improved with some mobility enhancement techniques –like preparing

cells as the UE moves along the highway to anticipate the mobility events and forward data towards the target cells—reducing the interruption times. Nonetheless, the presented numbers show that the improvement provided by split bearer may not be sufficient to deal with the 5 ms end-to-end latency required by the vehicular use-cases envisioned for the next generation of mobile networks [10]. Additionally, the cost in terms of signaling is also becoming a potential issue as the users experience a large number of mobility events.

5 Conclusions

Mobility performance in a LTE highway scenario with and without dual connectivity is studied by means of extensive system level simulations. Results reveal how, with single connectivity, the UEs are unable to receive or transmit any data about the 5% of the time due to handovers. Dual connectivity significantly reduces the interruption time depending on the chosen architecture. By adopting the split bearer user-plane architecture, the devices experience data interruption only 0.81% of the time. Nevertheless, results show that the improvement is not sufficient to deal with the latency requirements demanded by the new vehicular use-cases.

As future work, it is recommended to investigate solutions to reduce the interruption time and the signaling load towards fulfilling the requirements imposed by the envisioned use-cases for the next generation of mobile networks.

References

- [1] *Liberation from Location. Consumers developing place-agnostic internet habits.*, Oct 2014, available at www.ericsson.com.
- [2] K. Pedersen, P. Michaelsen *et al.*, “Mobility enhancements for LTE-advanced multilayer networks with inter-site carrier aggregation,” *Communications Magazine, IEEE*, vol. 51, no. 5, pp. 64–71, May 2013.
- [3] *3GPP Technical Report (TR) 36.842. Study on Small Cells enhancements for E-UTRA and E-UTRAN. Higher layer aspects*, Dec 2013, available at www.3gpp.org.
- [4] S. Jha, K. Sivanesan *et al.*, “Dual connectivity in LTE small cell networks,” in *Globecom Workshops*, Dec 2014, pp. 1205–1210.
- [5] B. Soret, H. Wang *et al.*, “Multicell cooperation for LTE-advanced heterogeneous network scenarios,” *Wireless Communications, IEEE*, vol. 20, no. 1, pp. 27–34, February 2013.
- [6] G. Poci, S. Barcos *et al.*, “Analysis of heterogeneous networks with dual connectivity in a realistic urban deployment,” in *81st Vehicular Technology Conference (VTC), IEEE*, May 2015, pp. 1–5.
- [7] S. Barbera, L. Gimenez *et al.*, “Mobility sensitivity analysis for LTE-advanced het-net deployments with dual connectivity,” in *81st Vehicular Technology Conference (VTC), IEEE*, May 2015, pp. 1–5.

-
- [8] A. Elnashar and M. El-Saidny, "Looking at LTE in practice: A performance analysis of the LTE system based on field test results," *Vehicular Technology Magazine, IEEE*, vol. 8, no. 3, pp. 81–92, Sept 2013.
- [9] A. Osseiran, F. Boccardi *et al.*, "Scenarios for 5g mobile and wireless communications: the vision of the METIS project," *Communications Magazine, IEEE*, vol. 52, no. 5, pp. 26–35, May 2014.
- [10] G. Pocovi, M. Lauridsen *et al.*, "Automation for on-road vehicles: Use cases and requirements for radio design," in *IEEE 82nd Vehicular Technology Conference*, Sept 2015, pp. 1–5.
- [11] *3GPP Technical Specification (TS) 36.300. Evolved Universal Terrestrial Radio Access (E-UTRA) and Evolved Universal Terrestrial Radio Access Network (E-UTRAN). Overall Description*, Sept 2015, available at www.3gpp.org.
- [12] S. Barbera, K. I. Pedersen *et al.*, "Synchronized RACH-less handover solution for LTE heterogeneous networks," in *Twelfth International Symposium on Wireless Communication Systems*, Aug 2015.
- [13] S. Barbera, P. Michaelsen *et al.*, "Mobility performance of LTE co-channel deployment of macro and pico cells," in *Wireless Communications and Networking Conference (WCNC), IEEE*, April 2012, pp. 2863–2868.
- [14] I. Viering, M. Döttling *et al.*, "A mathematical perspective of self-optimizing wireless networks," in *International Conference on Communications (ICC), IEEE*, June 2009, pp. 1–6.
- [15] *ETSI Technical Report (TR) 101 112. Selection procedures for the choice of radio transmission technologies of the UMTS*, Apr 1998, available at www.etsi.org.
- [16] *3GPP Technical Report (TR) 36.814. Further advancements for E-UTRA physical layer aspects*, Mar 2010, available at www.3gpp.org.
- [17] *3GPP Technical Report (TR) 36.839. Mobility Enhancements in Heterogeneous Networks*, Dec 2012, available at www.3gpp.org.
- [18] H. Wang, C. Rosa *et al.*, "Dedicated carrier deployment in heterogeneous networks with inter-site carrier aggregation," in *Wireless Communications and Networking Conference (WCNC), IEEE*, April 2013, pp. 756–760.

Paper E

UE Autonomous Cell Management in a High-Speed Scenario with Dual Connectivity

Lucas Chavarría Giménez, Per Henrik Michaelsen, Klaus I.
Pedersen

Published in
*27th Annual IEEE International Symposium on Personal, Indoor and Mobile Radio
Communications (PIMRC). September 2016.*

© 2016 IEEE

Reprinted with permission. The layout has been revised.

Abstract

This study compares the amount of control signaling required by traditional network-controlled mobility management with the one required by user equipment autonomous cell management operations in a real-life highway scenario. The scenario is covered by macros and densely-deployed small cells. Different strategies for preparing the small cells for autonomous operations are studied. Our results show that traditional dual connectivity requires an average of 4.9 messages, per user per second, to be exchanged between the user equipment and the network, and 11.6 messages between e-NodeBs. On the other hand, autonomous cell management operations considerably decrease the amount of signaling. The highest reductions can be achieved by preparing all cells along the highway, cutting the signaling overhead by 92 % over the air, and 39 % between e-NodeBs. Furthermore, the approach of applying a newly developed window-based feature for preparing the cells brings significant benefits.

1 Introduction

Nowadays, travelers demand uninterrupted connectivity, and consume large amounts of media content while commuting [1]. The deployment of small cells along roads is a possible solution to quench the users' thirst of data, supplementing the capacity provided by the macro cells. In this regard, dual connectivity (DC) is an operational mode, developed for long term evolution (LTE) Release 12, that favors the macro and small cells integration by allowing an UE to consume radio resources provided by more than one network point [2].

Previous studies on mobility performance show that scenarios with DC are affected by high rates of mobility (or cell management) events [3, 4]; therefore, challenging the mobility management, specially in scenarios with users traveling at high-speeds. The mobility management in current cellular networks relies on a network-controlled mechanism, assisted by the user equipment (UE), in which the network decides when mobility events should take place based on radio resource management (RRM) measurements reported by the UE. The result of the decision, is afterwards communicated to the UE via dedicated radio resource control (RRC) signaling. This process, repeated at each mobility event, is becoming a critical issue in ultra dense networks (UDNs), due to the high signaling overhead and the frequent mobility decisions performed by the network.

Therefore, we study the performance of UE autonomous cell management; a partially UE-controlled mobility mechanism that prevents the network from performing frequent cell management decisions, and reduces the amount of signaling required for DC operations [4–6]. In this mode, the UE is not required to forward measurements reports at each small cell mobility event. Moreover, the devices are allowed to directly access the small cells that have been prepared in advance.

Mobility management between primary and secondary cells, and corresponding signaling overhead have been studied in [7] and [8]; however, to the best of our knowledge, existing DC studies do not evaluate the reduction in the signaling overhead with UE autonomous cell management. Therefore, our main focus is to study UE autonomous cell management for DC operations in a highway scenario. Furthermore,

this study analyzes strategies for preparing the cells of the network for autonomous cell management operations. To produce results of high practical relevance, the analysis is performed by simulating a real-life highway segment, reproduced in a system level simulator. The scenario replicates an operational macro layer, supplemented by an UDN of small cells deployed along the highway to boost the capacity. UE autonomous cell management is applied only to the small cells layer whereas, due to the low rate of macro handovers, traditional network-controlled macro mobility is preserved thus, maintaining a stable anchor point for the UEs.

The paper is structured as follows: Section 2 describes the network-controlled mobility mechanisms. Section 3 presents the UE autonomous cell management scheme. Section 4 describes the analyzed scenario and the simulation methodology, while Section 5 presents the obtained performance results. Finally, Section 6 concludes with the final remarks.

2 Network-Controlled and UE-assisted mobility

In network-controlled and UE-assisted mobility procedures, the network decides whether mobility events should take place based on radio measurements reported by the UE. The UE is configured by the network to periodically measure the reference signal received power (RSRP) or the reference signal received quality (RSRQ) from the neighboring cells. After filtering and processing the measurements, and if a certain triggering condition is met, the UE sends to the network information about the measurements through a measurement report. Then, serving and target cells exchange the necessary information, via X2 signaling, to prepare the mobility event, and dedicated RRC signaling is used for commanding the UE to perform the mobility event.

In DC, the e-NodeBs (eNBs) can play two different roles. The master-eNB (MeNB) role is assigned to the eNB that terminates the S1-mobility management entity (MME) interface, manages the RRC signaling, and acts as mobility anchor towards the core network (CN). On the other hand, the title of secondary-eNB (SeNB) is given to the eNBs that provide additional radio resources to the UE. In this study, it is assumed that a macro cell acts as a MeNB and a small cell plays the role of the SeNB. Additionally, it is assumed that each UE can aggregate one SeNB at a time. Among the different network architectures defined in [2], this study considers the split bearer architecture for the user-plane, as suggested in [9].

The most common triggering conditions used for initiating the cell management events, are shown in Figure E.1. MeNB handovers are typically triggered by the A3 event (neighboring cell becomes an offset better than the serving cell), based on the RSRP [3]. Moreover, the addition of a secondary data link, or SeNB addition, is normally triggered by the A4 event (a neighbor small cell becomes better than a certain threshold), based on the RSRQ. The small cell that serves the secondary link may be substituted (SeNB change) if the A6 event is triggered (neighboring small cell becomes an offset better than serving small cell). This trigger is typically based on the RSRP. Furthermore, the secondary link is removed (SeNB removal) if the event A2 is triggered (serving small cell becomes worse than a certain threshold). This trigger is based on the RSRQ.

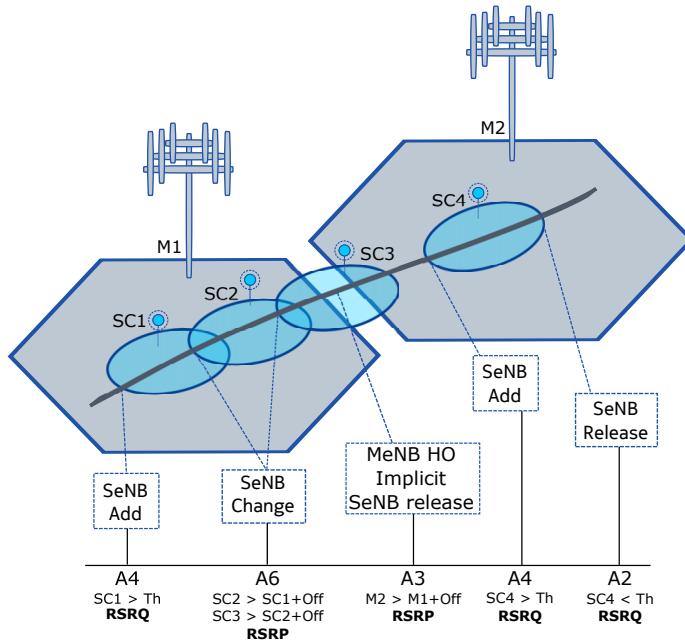


Fig. E.1: Illustration of the mobility events with DC.

Table E.1: Number of messages required by SeNB mobility events with DC

Protocol	SeNB Addition	SeNB Change	SeNB Release
RRC	3	3	3
X2	4	7	3

The signaling charts for DC operations presented in [2], show that each cell management event requires to exchange a considerably amount of messages between the network nodes. Table E.1 summarizes the number of messages per event, split into RRC and X2 signaling. Notice that the SeNB change is the event that requires the highest amount of signaling. This constitutes a challenge in terms of signaling overhead in scenarios with a high density of small cells, or with high-speed users, as terminals are constantly performing SeNB changes.

3 UE Autonomous Cell Management

UE autonomous cell management is an operational mode where the small cell management is partly left for the terminals [4]. In this partially UE-controlled mobility scheme, the devices have the autonomy of deciding the target cell and when to perform the mobility event, preventing the network from taking frequent small cell

management decisions.

The network configures the UEs to perform radio measurements of the neighboring cells. However, as the UEs have the liberty of deciding SeNB additions, changes or releases, they do not report the measurements to the network when a cell management triggering condition is met. Moreover, interaction with the network is reduced by letting the UEs to directly access the target cells via the random access channel (RACH), reducing considerably the amount of signaling for each event.

Macro handovers are not as frequent as the small cells events hence, UE autonomous is only applied to the SeNB layer, letting the network to be in full control of the macro mobility. Therefore, the UEs have a stable anchor point with the network and some policies, such as load balancing and mobility robustness optimization can be applied.

To carry out such operations, UEs and small cells should be prepared in advance. First of all, the small cells should be configured beforehand with the UE context, so they are aware of the identity of the potential UEs that may request the access. At the terminal side, the UEs should be configured with the list of cells that are prepared for autonomous mode. Moreover, terminals should be provided with the system information, cell specific parameters and the RACH preamble to be used with the prepared cells. Thus, as these cells are aware of the identity of the autonomous devices, the UEs are allowed to select the target cell and directly request the access.

Notice that the UE is not completely autonomous. For instance, the network decides if a UE should use autonomous mode. Moreover, like in current LTE specifications, radio measurements and triggering criteria, at the UE side, are configured by the network. Additionally, the network can block the access to a cell that has been previously prepared by reconfiguring the UE and deleting that cell from its list.

Figure E.2 shows the signaling charts of each SeNB event with UE autonomous operations [4]. As can be seen, the signaling has been reduced compared to traditional DC cell management and, messages like the sequence number (SN) status transfer, are assumed to be encapsulated in the *SeNB_Addition_Response*. Hence, UE autonomous cell management reduces the amount of signaling and provides a faster execution of SeNB events. These enhancements are performed without degrading signal quality or introducing additional SeNB ping-pongs.

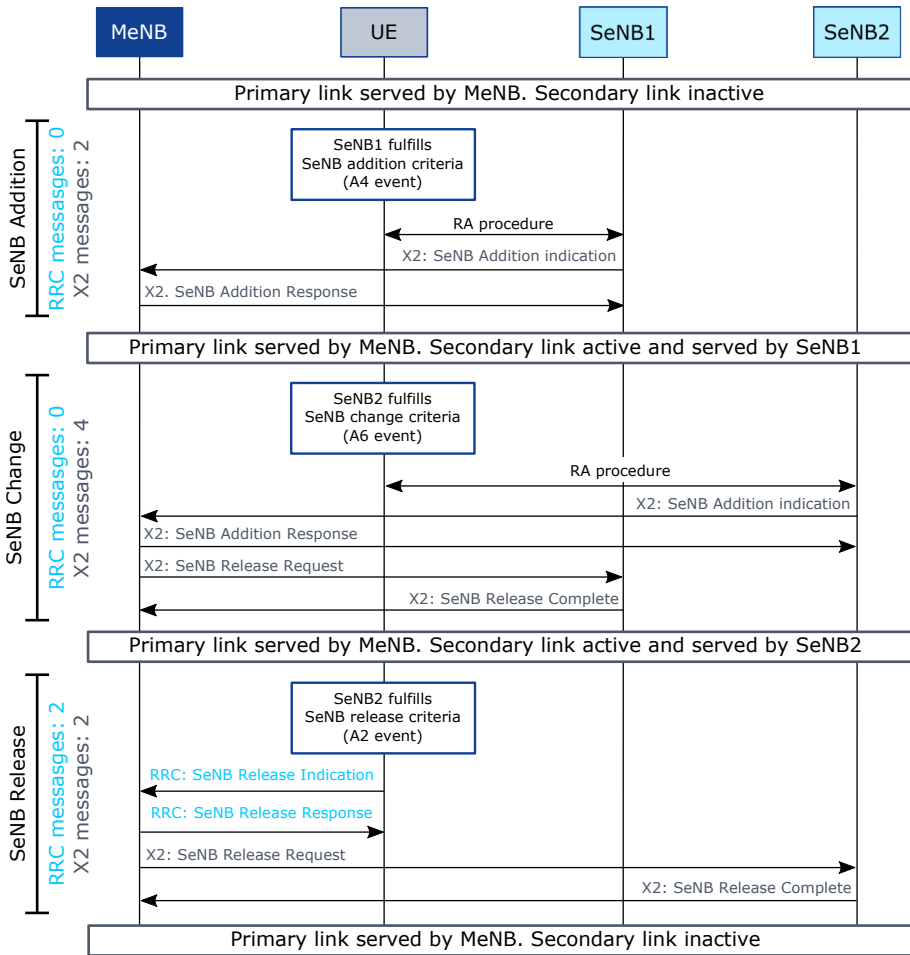


Fig. E.2: Signaling charts of SeNB addition, change and release with UE autonomous cell management.

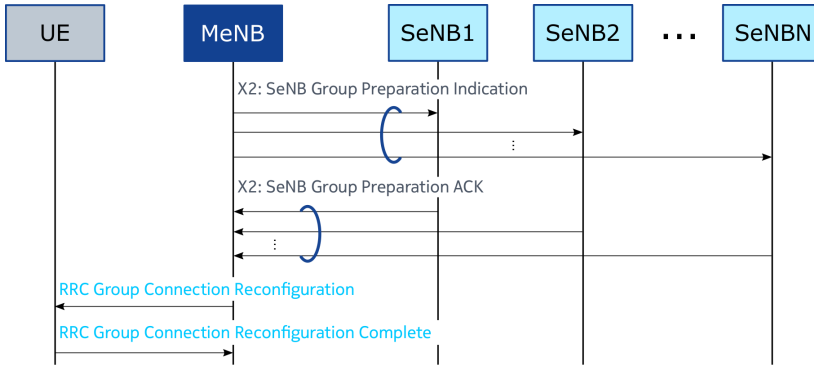


Fig. E.3: Signaling chart of SeNB group-preparation for UE autonomous.

Figure E.3 shows the procedure for group-based preparation of small cells for UE autonomous operations. The figure has been created following the descriptions in [4–6]. The process is similar to the handover preparation procedure described in [10]. To save signaling, a group of cells are simultaneously prepared and the UE is informed with a unique list of cells. The MeNB sends to the SeNBs, via X2 signaling, the UE context of those that may perform autonomous operations. Upon storing the UE IDs, each SeNB acknowledges the preparation to the MeNB. Afterwards, the MeNB configures the UE, through RRC signaling, providing the list of prepared cells and the RACH preambles. Preparing cells produces additional signaling: assuming that a group of N cells are simultaneously prepared, $2N$ -X2 and 2-RRC messages are needed for preparing the SeNBs and for configuring the UE, respectively. This process should be repeated every time the list of prepared cell changes; therefore, it is necessary to find preparation strategies that avoid excessive signaling.

3.1 Preparation strategy

The strategy for preparing the small cells depends on the network topology and the type of scenario. In the scenario of our focus, the MeNB may prepare all cells as soon as the UE enters the highway. However, the network does not know when the UE will leave the highway and many cells may be prepared in vain. Another approach is to prepare the small cells on demand, following the movement of the UE. Assuming that the network knows which small cell serves a certain link and the geographical location of each SeNB, the movement of the UE can be tracked. In this regard, a possible strategy is to prepare the cells ahead of the UE direction of movement. However, to implement this approach, the network needs to detect a few SeNB changes to estimate the UE movement. Moreover, due to changes in line-of-sight (LOS) conditions and signal fluctuations due to the shadowing, the UE may connect to a small cell located opposite to the direction of motion.

Hence, this study proposes the strategy of preparing the nearest set of small cells located around the UE. By knowing the current serving SeNB and its geographical location, the network can prepare the nearest N cells, conforming a window of cells

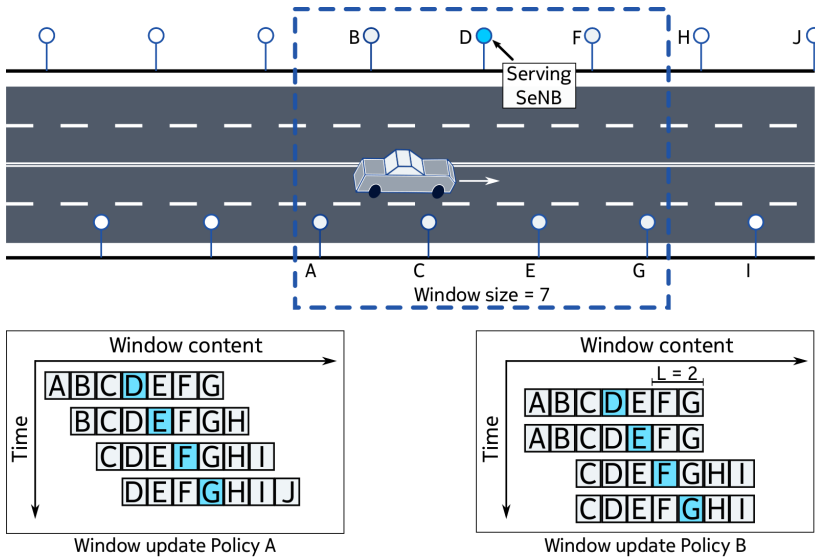


Fig. E.4: Illustration of the window of prepared cells and the considered updating policies. The serving SeNB is depicted in blue.

that moves together with the UE as it advances along the highway. Figure E.4 depicts an example of the window with seven prepared cells around the UE.

Assuming that the network is capable of sorting the cells (for instance, sorted by cell ID), two different policies for updating the window are considered:

- **Policy A:** Update the window at each SeNB change. The network creates a new set of prepared cells every time the serving SeNB changes.
- **Policy B:** The window is updated only if the UE connects to any of the last L cells in the window. Let's assume that cell N is the last cell in the window and $L = 2$. Then, the window is updated if the UE connects to a cell within the range $[N - 1, N]$. Otherwise, the window remains unchanged although an SeNB change is performed.

The size of the window constitutes the maximum amount of small cells that can be simultaneous prepared for a certain UE. Hence, every time a new cell enters the window, a previous prepared cell should leave, and the UE should be reconfigured with the new list of cells.

As the UE moves, it may happen that it finds a cell that is not prepared for autonomous operations. The probability of this happening is closely related to the size of the window. Thus, if the window is too small, the probability of accessing an unprepared cell increases. Moreover, to minimize the probability of finding an unprepared cell due to the shadowing and changes in the LOS conditions, it is proposed to use a symmetric window that, at each update, is centered at the serving SeNB. If the UE finds an unprepared cell, it is assumed that it will perform a traditional DC SeNB event, and the network will proceed to prepare the nearest N cells.

Table E.2: Network parameters

Macro Layer	
Carrier frequency	1800 MHz
Channel bandwidth	20 MHz
Number of cells	23
Number of sites	13
Average antenna height	31.3 m
Antenna height std. deviation	13.22 m
Average antenna tilt	2.1° (mechanical + electrical)
Average tilt std. deviation	1.6°
Average ISD	1092 m
Minimum ISD	624 m
Small Cells Layer	
Carrier frequency	3400 MHz
Channel bandwidth	20 MHz
Number of cells	119
Antenna height	5 m (Fixed)
Antenna pattern	Omni-directional
Average ISD	100 m

4 Scenario and Simulation Methodology

The studied scenario, the same as the one used in [9], is a 7.5 km section of the highway that encircles the city of Aalborg, Denmark. The scenario is characterized by two network layers operating at dedicated frequency bands. The first one is an LTE macro layer that represents the current network deployment of one of the Danish operators. Additionally, a fictitious UDN of small cells is distributed along the highway.

The macro network is deployed at 1800 MHz and consists of 23 cells, distributed on 13 base station sites, with an average inter-site-distance (ISD) of 1092 m. The small cells layer operates at 3400 MHz with an average ISD of 100 m. The small cells are deployed on both sides of the highway to ensure good coverage along the road. In total, the whole scenario is covered by 119 small cells. More details about the characteristics of the network are summarized in Table E.2.

The simulator utilized in this study implements the majority of the mobility mechanisms defined by the 3rd generation partnership project (3GPP) for LTE, including physical-layer measurements, Layer-3 filtering and reporting events. On each time-

step the RSRP, RSRQ and signal-to-interference-plus-noise-ratio (SINR) for each user are calculated, followed by the SINR to throughput mapping estimation. The tool has been used in several standardization and research studies, such as [3, 11]. Additional simulator modeling can be found in [12].

A total of 630 users are dropped in the scenario, split into slow- and high-speed users. Ten slow-speed users per macro area are considered, that move at 3 kmph and follow random directions thorough the whole scenario. The purpose of these slow-speed users is to generate background traffic. Moreover, 400 users are dropped along the highway, moving at 130 kmph. All type of users generate traffic according to a Poisson process. The stretch of the highway is modeled with two lanes per direction, and each user is randomly assigned to one lane. Anytime a user arrives to the end of the highway, it performs an u-turn. Moreover, when arriving to any of the ends of the highway, the number of prepared cells in the window decreases because there are no more cells in the area. When turning back, the number of prepared cells starts growing at the same rate as the UE advances through the highway. As a result, the number of cells in the window is minimum at the ends of the highway, and maximum in the middle point. This models the effect of users entering and leaving the small cells area, while keeping a certain traffic density along the road. Statistics are only collected among the highway users.

A fast transition between small cells is guaranteed by setting the SeNB change offset to 1 dB and 40 ms of time-to-trigger (TTT). Poor secondary links are avoided by setting the SeNB release event with a threshold of -17 dB of RSRQ. To ensure that the users are able to traverse the whole highway stretch, the simulation time is set to 210 s. Additional simulation parameters are summarized in Table E.3.

Two sets of simulations are considered. One where all highway users perform traditional DC operations, and another one where all users and small cells support autonomous cell management. For autonomous operations, the maximum size of the window (N) varies from 3 to 119 cells. Furthermore, both aforementioned window updating policies are adopted. For Policy B, the threshold L is set to a half, a third and a quarter of the maximum window size. If L results in an odd number, the value is rounded to the next integer.

The key performance indicators (KPIs) considered in this study are: the number of cell management events, the number of RRC and X2 messages exchanged between eNBs and UEs, and the number of times an UE access an unprepared cell. All KPIs are counted per UE per second.

Table E.3: Simulation Parameters

Transmitted power	Macro: 46 dBm. Pico: 30 dBm
Path loss model	Macro: Vehicular test environment [13] Small Cells: Urban Micro (UMi) [14]
Number of UEs	230 slow users + 400 highway users
Users speed	Background: 3 kmph. Highway: 130 kmph
Packet call size	Negative exponential distributed. Average: 1 Mbit
Inter-arrival time	Average: 2 s
Sim. Time	210 s
RLF	$Q_{in} = -6\text{dB}$. $Q_{out} = -8\text{dB}$. $T_{310}+T_{311} = 2\text{ s}$
MeNB Handover - A3 event	
Offset: 3 dB. RSRP based. TTT: 256 ms	
SeNB Management	
SeNB Addition	A4 event - RSRQ. Threshold: -12 dB. TTT: 40 ms
SeNB Change	A6 event - RSRP. Threshold: 1 dB. TTT: 40 ms
SeNB Release	A2 event - RSRQ. Threshold: -17 dB. TTT: 40 ms
Window Size (N)	From 3 to 119
Threshold L	$N/2$, $N/3$ and $N/4$

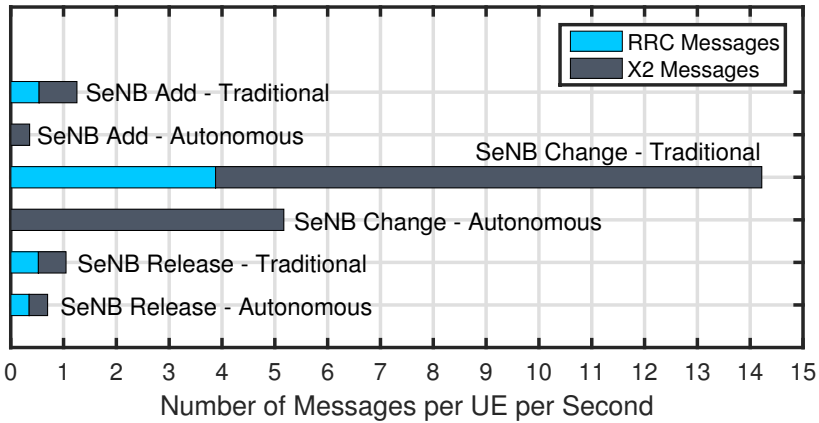


Fig. E.5: Number of required messages per UE per second for each SeNB event with traditional dual connectivity and UE autonomous operations.

5 Performance Results

Simulation results indicate that an UE, traveling at 130 kmph, experiences an average of 0.17 SeNB additions, 1.3 SeNB changes, and 0.16 SeNB releases per second. As expected, the SeNB change dominates the statistics. Figure E.5 shows the average number of messages necessary for performing each cell management event, with traditional DC and UE autonomous operations. The amount of signaling is calculated by scaling the number of events with the counting of RRC and X2 messages presented in Table E.1 and Figure E.2. Focusing the attention in the most dominant event, SeNB change, traditional DC operations require a total of 14.2 messages per UE per second. Concretely, 3.9 RRC and 10.3 X2 messages per UE per second. Autonomous cell management reduces considerably the signaling overhead for this event, as all RRC messages are eliminated, and the X2 signaling decreases to 5.2 messages per UE per second. Summing up the overall signaling required for all the events, traditional DC operations require a total of 4.9 RRC and 11.6 X2 messages per UE per second; while UE autonomous requires only 0.35 RRC and 5.9 X2 messages per UE per second.

Nonetheless, UE autonomous also adds new signaling, as the small cells have to be prepared in advance. Figure E.6 shows the amount of RRC and X2 signaling required for preparing the small cells depending on the maximum size of the window. In these simulations, the size of the window slowly increases as the UE enters the highway, and shrinks as the UE arrives to any of the ends of the small cells area. As a result, the number of cells preparations, at the extremes of the highway, are reduced compared to the number of preparations in the center hence, producing the shape of a decreasing curve for the overall results. The minimum amount of required signaling can be achieved by simultaneously preparing (only once) all the cells in the highway. However, many cells may be prepared in vain. Significant reductions can also be achieved by adopting the moving window approach with the benefit of preparing less amount of cells. Concretely, Policy B requires the smallest widow size to achieve

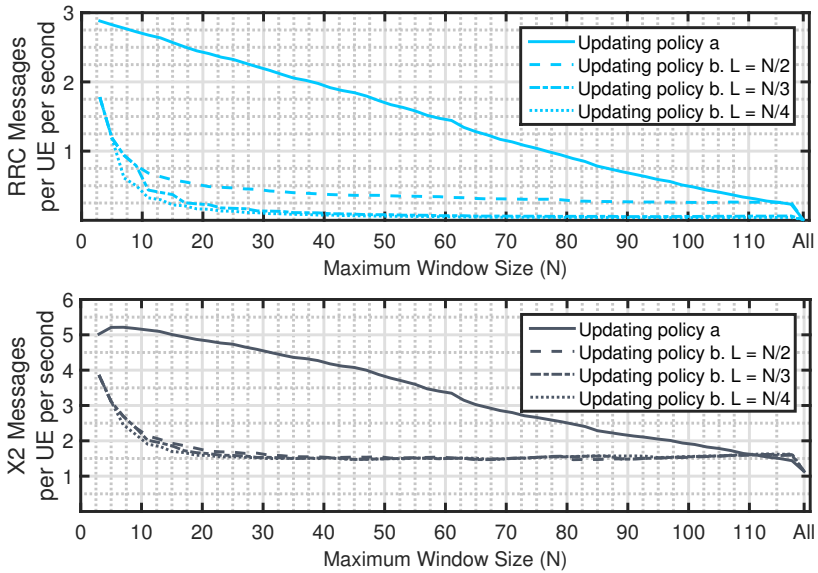


Fig. E.6: Number of RRC and X2 messages, per UE per second, required for SeNB group-preparation in UE autonomous operations.

the reduction in signaling that UE autonomous can provide.

Figure E.7 depicts the total contribution to signaling made by the combination of all the SeNB events and the SeNB group-preparations. As a reference, the amount of signaling that traditional DC operations require is also depicted. UE autonomous eliminates completely the RRC signaling for the most predominant event, SeNB change; therefore, even when adding the SeNB group-preparation, the overall RRC signaling remains below the required amount for traditional DC. Analyzing the X2 signaling, it can be seen that for small window sizes, the amount of required signaling for UE autonomous is higher or equal that the amount required for traditional DC. This is due to two effects: the first one is that the smaller the window is, the more group-preparations have to be performed, specially if the window is updated at each SeNB change (Policy A). The second reason is that for small window sizes, the probability of finding an unprepared cell increases. Each time that this happens, the UE performs a traditional DC operation, increasing the overall signaling.

Figure E.8 shows the overall achieved signaling reduction and the number of times an autonomous UE finds an unprepared cell. As can be seen, the maximum achievable reduction in signaling can be obtained by preparing all cells simultaneously. In this case, the RRC and X2 messages are reduced by 92 % and 39 %, respectively. Significant reductions in signaling can be also achieved by adopting the moving window approach; however, small window sizes have a negative impact due to the probability of the UE finding an unprepared cell along the way. The policy of updating the window at each SeNB change gives the lowest signaling reduction, due to the too frequent window updating rate. Nevertheless, this policy achieves the minimum probability

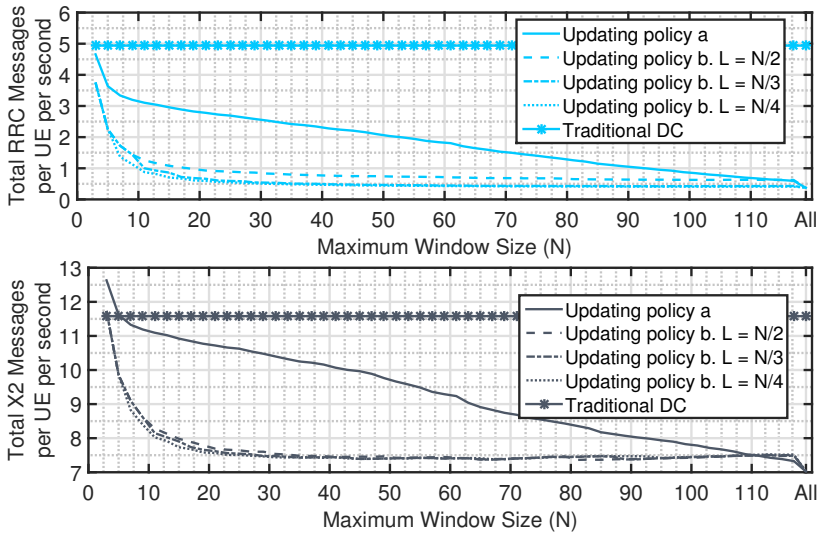


Fig. E.7: Total amount of RRC and X2 messages required for traditional DC and UE autonomous cell management operations.

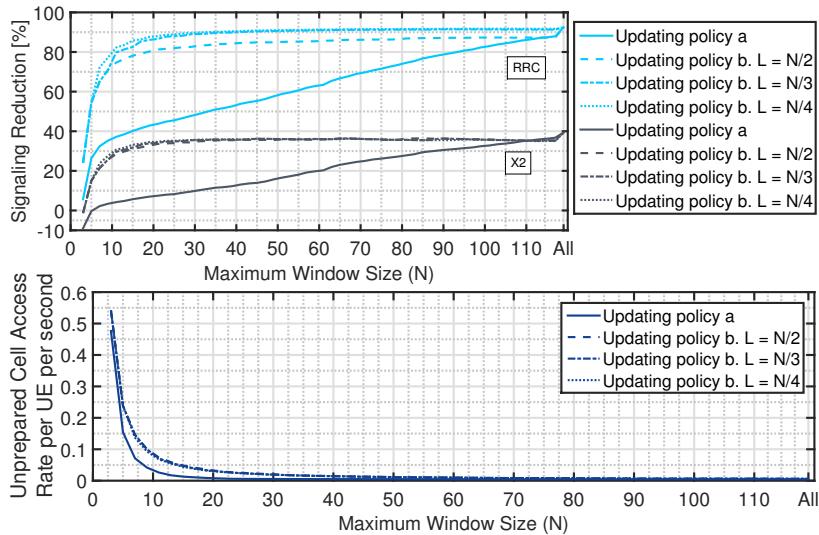


Fig. E.8: Achieved signaling reduction with UE autonomous and number of times an UE finds an unprepared cell.

of the UE finding an unprepared cell.

The presented results manifest that it is not necessary to prepare a big amount of small cells to achieve a significant signaling reduction, with a low probability of accessing an unprepared cell. For instance, preparing only 10 cells (5 at each side of

the highway), gives a signaling reduction of 37% over the air and 4% between eNBs, when updating the window at each SeNB change. On the other hand, by adopting the updating Policy B, with $N = 10$ and $L = N/4$, the RRC and X2 signaling are reduced by 30% and 82%, respectively.

6 Conclusions

Control signaling overhead in a highway scenario with traditional LTE DC operations and with UE autonomous cell management is studied by means of system level simulations. The results reveal that traditional DC operations require an exchange of 4.9 RRC and 11.6 X2 messages per UE per second, due to the large amount of mobility events. UE autonomous cell management significantly reduces the amount of signaling, although it requires preparing the cells in advance. The maximum reduction can be achieved by simultaneously prepare all cells in the highway; however, many cells may be prepared in vain. The approach of a window that follows the movement of the UE brings significant reductions with the benefit of preparing less number of cells. By preparing only 10 cells around the UE, a reduction in the exchanged messages of 37% over the air, and 4% between eNBs, can be obtained.

As future work, it is proposed to further study other strategies for preparing the small cells as well as the impact on the end-user throughput. Furthermore, it is also recommended to explore the benefits of implementing improved mobility mechanism where, for instance, cell management decisions are supported by uplink measurements. Moreover, the learnings from these studies can be used as an inspiration for reducing the signaling when designing the mobility procedures for the upcoming fifth-generation (5G) of mobile networks.

7 Acknowledgments

Part of this work has been performed in the framework of the Horizon 2020 FANTASTIC-5G project (ICT-671660), receiving funds from the European Union. The authors would like to acknowledge the contributions of their colleagues in the project, although the views expressed in this contribution are those of the authors, and do not necessarily represent those of the project.

References

- [1] Ericsson Consumerlab. *Commuters Expect More. An Ericsson Consumer Insight Summary Report*, June 2015.
- [2] 3GPP Technical Report (TR) 36.842. *Study on Small Cells enhancements for E-UTRA and E-UTRAN. Higher layer aspects*, Dec 2013.
- [3] S. Barbera, L. Gimenez *et al.*, "Mobility sensitivity analysis for LTE-Advanced HetNet deployments with dual connectivity," in *IEEE 81st Vehicular Technology Conference (VTC)*, May 2015, pp. 1–5.

- [4] K. Pedersen, P. Michaelsen *et al.*, "Mobility enhancements for LTE-Advanced multilayer networks with inter-site carrier aggregation," *IEEE Communications Magazine*, vol. 51, no. 5, pp. 64–71, May 2013.
- [5] 3GPP draft R2-132339. *Autonomous SCell management for dual connectivity cases*, Dec 2013.
- [6] L. Haitao, L. Dalsgaard *et al.*, "Method, apparatus and computer program product for autonomous cell change by UE in network," Patent US2015/0 133 121A1, May, 2015.
- [7] K. Yagyu, T. Nakamori, H. Ishii, M. Iwamura, N. Miki, T. Asai, and J. Hagiwara, "Investigation on mobility management for carrier aggregation in LTE-Advanced," in *IEEE 74th Vehicular Technology Conference (VTC)*, Sept 2011, pp. 1–5.
- [8] X. Cao, D. Xiao, and C. Xiu, "Handover performance of relaxing SCell measurement period in LTE-A with carrier aggregation," in *International Conference on Electric Information and Control Engineering (ICEICE)*, April 2011, pp. 438–441.
- [9] L. Gimenez, P. Michaelsen *et al.*, "Analysis of data interruption in an LTE highway scenario with dual connectivity," in *IEEE 83rd Vehicular Technology Conference (VTC)*, May 2016, pp. 1–5.
- [10] 3GPP Technical Specification (TS) 36.300. *Evolved universal terrestrial radio access (E-UTRA) and evolved universal terrestrial radio access network (E-UTRAN). Overall description*, Sept 2015.
- [11] S. Barbera, P. Michaelsen *et al.*, "Mobility performance of LTE co-channel deployment of macro and pico cells," in *IEEE Wireless Communications and Networking Conference (WCNC)*, April 2012, pp. 2863–2868.
- [12] I. Viering, M. Dottling *et al.*, "A mathematical perspective of self-optimizing wireless networks," in *IEEE International Conference on Communications (ICC)*, June 2009, pp. 1–6.
- [13] ETSI Technical Report (TR) 101 112. *Selection procedures for the choice of radio transmission technologies of the UMTS*, Apr 1998.
- [14] 3GPP Technical Report (TR) 36.814. *Further advancements for E-UTRA physical layer aspects*, Mar 2010.

Part IV

**Mobility Performance
Towards 5G**

Mobility Performance Towards 5G

This part of the thesis sets out to solve the most critical limitation for low-latency applications: the handover data interruption time. As a reference, the solutions that are currently under investigation by the 3GPP for LTE-A Pro are taken as a starting point. Different enhancements are later proposed in order to eliminate the data disruption at handovers.

Moreover, this part also proposes other mobility management enhancements, where the handover decision algorithms select the most suitable target cell in terms of user throughput, improving the user experience for media-content applications.

1 Motivation

To date, the handover data interruption time has not been considered a critical issue, as the majority of multi-media and voice applications are able to support the typical handover latencies, minimizing the impact on the end-user experience. However, the envisioned applications for 5G with more stringent specifications calls for new scenarios where latencies in the order of milliseconds must be complemented with zero mobility interruption gaps, not only in ultra-reliable scenarios such as mobile service robots in factories, but also in high-mobility scenarios with connected cars in highways [1].

Therefore, and due to the high importance of meeting these mobility requirements, two techniques are considered in this part of the thesis for reducing mobility interruption time. The random access (RA)-less handover (RA-less handover) and the make-before-break handover type. The first technique takes advantage of having time-synchronized base stations, where the RA and synchronization phase during the handover can be eliminated, reducing the overall handover latency and the data interruption time. The second one allows the UE to maintain the connectivity towards the source cell during the entire handover process. As a result, the UE still receives data while the handover procedure is carried out, thereby reducing the service interruption.

Firstly, this part of the thesis evaluates the suitability of these solutions for fulfilling the zero-data interruption at handovers. The overall latency of the legacy LTE

and the new RA-less handover is analyzed. After identifying the main challenges, enhancements for further reducing the data interruption in the RA-less handover are proposed. These proposals include an integration of the synchronous handover and the make-before-break functionality, with an enhanced data forwarding mechanism between eNBs.

Furthermore, this part of the thesis proposes additional mobility enhancements. For ultra-reliable low latency applications, the handover data interruption time must be eliminated. However, for media-content applications it is required to provide the best user experience in terms of throughput. To this end, and from the point of view of mobility management, handover decision algorithms must assure that the users are connected to the most suitable cells. Therefore, a user association and traffic-steering algorithm that selects the best target cell based on end-user throughput estimates is also presented.

2 Objectives

The objectives pursued in this part of the thesis are:

- Evaluate the suitability of the synchronous RA-less handover and the make-before-break techniques for meeting the zero-data interruption time at handovers required for the ultra-reliable low latency applications. The evaluation must be done by performing a detailed latency analysis of the handover procedures.
- Based on the previous evaluation, identify the weaknesses and issues of those solutions and propose enhancements for further reducing the interruption time.
- Analyze the possibilities for realizing real make-before-break handovers where the data interruption is eliminated, without increasing the overall handover latency.
- Propose additional mobility enhancements and user association techniques in HetNet scenarios that increase the end-user throughput, hence improving the user experience for media-content applications.

3 Included Articles

The work related to this part of the thesis is collected in the following papers:

Paper F. Towards Zero Data Interruption Time with Enhanced Synchronous Handover

This article presents an extensive analysis of the overall handover latency considering UE and eNBs processing delays, UE reconfiguration times, and X2 interface latencies. Having the current LTE-A Pro solutions as a reference, this paper proposes enhancements of the handover procedure for reducing and eliminating the data interruption time. An enhanced handover mechanism is presented, integrating both, the RA-less

and the make-before-break procedures, for eliminating the data interruption without increasing the overall handover latency. Moreover, a promising procedure for managing and synchronizing the buffers at the source and target cells is proposed, which reduces the data transmission interruption time.

Paper G. Mobility Enhancements from LTE towards 5G for High-Speed Scenarios

This magazine provides an overview of the presented results and the proposed mobility enhancements from papers B, D, E and F, showing how each publication relates to each other. Furthermore, the magazine discuss some of the disruptive ideas in the design of mobile networks such us the uplink and downlink decoupling, and the user-centric and cell-less concept [2–4] in relation to mobility procedures.

Paper H. Throughput-based Traffic Steering in LTE-Advanced HetNet Deployments

This paper proposes traffic steering algorithms on which the network utilizes the user experienced SINR and the number of users connected to each cell, to estimate the target cell where the users will achieve the highest throughput. Two algorithms are proposed. In the first implementation, the network blindly handover the users to the cell that offers the highest throughput. In the second implementation, the handover is forced if, and only if the network estimates that the sum of the overall user throughput in the system augments. As an initial evaluation, the performance of these features is analyzed by means of system level simulations of a dual-layer HetNet 3GPP scenario with users moving at low and medium-speeds. Results are presented comparing a baseline case (where none of the traffic steering solutions are enabled), with those cases where the proposed algorithms are activated in the network.

4 Main Findings

Eliminating the data interruption time with RA-less handovers and make-before-break techniques

The synchronous handover reduces the overall latency by avoiding the RA at each mobility event. The results showed in Paper F demonstrate that even though the RA-less handover potentially reduces the service interruption, the 0 ms required for the upcoming 5G applications is not fulfilled. This is due to the fact that there are several non-ideal factors to consider in the handover latency.

First, the processing times at the UE and eNB cannot be neglected. At the UE side, the processing time increases when the UE needs to reconfigure towards a new frequency band (in case of an inter-frequency handover), as the radio-frequency retuning is not instantaneous. Second, to carry out the handover process, the cells involved need to exchange signaling messages, and the source cell must forward the content of its buffer to the target. These procedures result in additional delays due to the non-zero eNB processing times and the latencies of the X2 interface that implements

the back-haul. As a result, the processing delays, the UE reconfiguration times, and the X2 interface latency should be simultaneously reduced to minimize the handover data interruption time.

The RA-less handover implements the data forwarding during the handover execution. This means that the source cell forwards the content of its buffer to the target after commanding the handover to the UE. Right after receiving the handover command, the UE proceeds to reconfigure its receiver chain towards the target cell. The data forwarding between cells is a process that is highly sensitive to the X2 latency. Therefore, the UE may complete the reconfiguration towards the target cell before the source finishes forwarding the content of its buffer, not allowing the target cell to resume the data exchange at the instant of the handover, and increasing the data interruption. To reduce these effects, Paper F proposes a buffer management procedure for synchronous handovers during the handover preparation stage, where the serving cell estimates the amount of data that should be forwarded to the target based on CQI reports, QoS and other parameters. The evaluation of this technique performed in Paper F revealed that this feature reduces the data interruption by 18 % (8 ms) compared to the basic RA-less implementation.

Paper F also evaluates the handover latency for a 5G scenario where the UE and eNB processing times are reduced by a factor of 10 and the latency of the interfaces that interconnects the eNBs is reduced by a factor of 5. The results concluded that although the data interruption is considerably reduced, the data disruption still persists in the RA-less handover procedure.

However, the studies conducted in Paper F also showed that the data interruption time can be completely eliminated with the make-before-break technique. The solution presented proposes the integration of the make-before-break with the RA-less handover. Thereby, making it possible to use the proposed buffer management procedure for synchronous handovers. It is also suggested that a duplicated receiver chain at the UE side should be implemented, so the reconfiguration towards a new frequency band can be performed while the UE still receives data from the source cell.

The results obtained in the evaluation of this method conclude that the proposed synchronous make-before-break handover achieves zero-service interruption without increasing the overall handover latency.

Improving the user experience by selecting the most suitable target cell, based on estimates of the achievable user throughput

It is expected that future 5G networks will evolve towards even more heterogeneous systems. Therefore, it is necessary to develop fast and efficient user association techniques for HetNet scenarios capable of tracking the dynamics of the network. To this end, instead of relying on traditional power measurements for triggering handovers, paper H proposed two traffic steering algorithms that monitor the instantaneous user throughput. In the presented algorithms the achievable throughput on each of the neighboring cells was estimated. Afterwards, the set of candidate cells that could provide the highest throughput was selected.

The simulation results showed that the first of the proposed algorithms brought the best performance in terms of average user session throughput, and in terms of the efficient used of the available resources. Using this method, the network forced the

handover of the active users towards the cell where it is predicted the highest achievable instantaneous throughput. As a result, the fast traffic fluctuations in the system were tracked, achieving an average session throughput gain of 32 % at low-load network conditions. However, this was accompanied by an increase in the number of handovers, reaching as high as 3 handovers per user per second.

The second algorithm forced the handovers only when an increase in the sum of the overall user throughput was estimated, producing more promising results. This technique reduced the number of handovers without degrading the performance significantly. For instance, at medium-load network conditions, the number of handovers were reduced by 41 % while still offering session throughput gains of 19 %.

As both, low- and medium-speed cases were simulated under the same handover parametrization, the performance of the baseline case (with no traffic steering solutions enabled) dropped when the users in the system moved at 50 kmph compared with 3 kmph. However, the results revealed that the first suggested traffic steering algorithm tended to overcome this issue, bringing the average session throughput curves for 3 and 50 kmph together. Moreover, the RLFs observed at 50 kmph in the baseline case were eliminated whenever any of the traffic steering implementations were switched-on.

References

- [1] 3GPP Technical Report (TR) 38.913. *Study on Scenarios and Requirements for Next Generation Access Technologies. V.0.4.0*, June 2016.
- [2] F. Boccardi, J. Andrews, H. Elshaer, M. Dohler, S. Parkvall, P. Popovski, and S. Singh, "Why to decouple the uplink and downlink in cellular networks and how to do it," *IEEE Communications Magazine*, vol. 54, no. 3, pp. 110–117, March 2016.
- [3] S. Chen, F. Qin, B. Hu, X. Li, and Z. Chen, "User-centric ultra-dense networks for 5G: challenges, methodologies, and directions," *IEEE Wireless Communications*, vol. 23, no. 2, pp. 78–85, April 2016.
- [4] C. L. I, C. Rowell, S. Han, Z. Xu, G. Li, and Z. Pan, "Toward green and soft: a 5G perspective," *IEEE Communications Magazine*, vol. 52, no. 2, pp. 66–73, February 2014.

Paper F

Towards Zero Data Interruption Time with Enhanced Synchronous Handover

Lucas Chavarría Giménez, Per Henrik Michaelsen, Klaus I.
Pedersen, Troels E. Kolding

Submitted for publication to
IEEE 85th Vehicular Technology Conference (VTC Spring), 2017.

© 2017 IEEE

Reprinted with permission. The layout has been revised.

Abstract

This paper presents enhancements for lowering the handover data interruption time in future wireless networks. We propose a selective data forwarding for the handover preparation phase, and the integration of the make-before-break procedure with the synchronous random access-less handover. To evaluate our proposals, we analyze the handover timing for typical and variable values of the user equipment and e-NodeB processing times, and X2 interface latencies. Our results show that the processing delays, reconfiguration times, and the X2 latency should be simultaneously reduced to minimize the data interruption time. Selective data forwarding during the handover preparation reduces the data interruption time by 18 % compared to the basic random access-less handover with typical network delays. Make-before-break is the most suitable handover type for future low-latency applications, as it achieves zero data interruption independent of the latency of the handover steps.

1 Introduction

The long term evolution (LTE) handover (HO) is of the *break-before-make* type, meaning that there is a data interruption at each HO. Measurements in operational LTE networks have reported typical interruption times of 17-50 ms ([1–3]). These values are in line with the average target requirements of 27-60 ms set in [4]. However, the measurements in [1, 3] also revealed that interruption times of hundreds of milliseconds are sometimes experienced.

To date, the service interruption has not been considered a critical issue as it has been tolerated by the majority of current LTE use cases. Nonetheless, nowadays it is becoming more and more relevant. Thus, the 3rd Generation Partnership Project (3GPP) is investigating options for reducing the HO latency in LTE-Advanced Pro (LTE-A Pro), where a typical data interruption time of 49.5 ms is assumed as a baseline [5].

One considered solution is the time-synchronous random access (RA)-less HO [6]. This option reduces the HO latency by avoiding the RA procedure. Nevertheless, the data interruption is not eliminated as the target cell must wait for the UE reconfiguration before resuming the data transmission. The second solution that 3GPP considers is the *make-before-break* HO, where the user equipment (UE) is able to receive data from the source and target cell during the HO process [5].

For the future fifth generation (5G) of mobile networks the target data interruption time is 0 ms for intra- and inter-frequency HOs [7]. To achieve this goal, this paper proposes enhancements for reducing the HO time and the data interruption in the synchronous RA-less HO.

Firstly, we propose a selective data forwarding between cells during the HO preparation phase. In a RA-less HO the UE receives data from the source cell during this HO stage. Therefore, this solution requires an efficient flow-control mechanism to keep the buffers of the source and target in-sync. Given this, [8] proposes a scheme where the same data is available at both access points. Buffer synchronization is done by means of messages exchanged between the access points to notify the successful delivery of the packets to the UE, increasing the amount of signaling overhead. In-

instead of the source cell forwarding a full copy of its buffer to the target, we propose a method for predicting a selected amount of data that the source should forward to the target so data transmission can be resumed from the first non-delivered packet. This prediction is based on channel quality indicator (CQI) reports from the UE. Secondly, we propose a synchronous make-before-break technique for intra- and inter-frequency handovers, in-line with the HO procedure currently considered by 3GPP.

Our proposals are evaluated by an exhaustive analysis of the HO timing and the data interruption. We include the delays of each of the HO steps such as the UE and e-NodeB (eNB) processing times, the X2 interface latency, and the transmission times of each exchanged message. We not only consider the typical delays measured and reported in [5] and [6], but also variable X2 interface delays, and variable UE reconfiguration times.

The paper is structured as follows: Section 2 explains the HO procedure in LTE and the typical HO delays. Section 3 presents the synchronous RA-less HO, while Section 4 describes the proposed enhancements. Section 5 presents the results in terms of latency reductions and Section 6 concludes the paper with the final remarks.

2 The LTE Baseline Handover

Fig. F.1 depicts the flow chart of the LTE HO, which is divided into three phases: *HO preparation*, *HO execution* and *HO completion* [9]. Measured at the UE, the HO preparation starts when the UE sends the measurements report to the network, and finishes when the UE receives (and processes) the HO command. This phase is dominated by the time the network takes to decide whether the HO should take place.

Once the UE receives the HO command, the HO execution phase starts. Then, the UE terminates the data exchange with the source cell, and proceeds to reconfigure towards the target. In parallel, the source cell starts forwarding the content of its buffer to the target. In case of an inter-frequency HO, the UE reconfiguration includes the radio-frequency (RF) retuning. Afterwards, the UE proceeds to access the target cell via the RA channel (RACH). The HO execution finishes when the UE sends the *Radio Resource Control (RRC) Connection Reconfiguration Complete* message, confirming that it is ready to receive data, and the target cell resumes the data transmission. The data interruption equals approximately the HO execution. However, additional time for the UE to receive and decode the first data from the target cell is required because of scheduling delays, hardware processing times and propagation delays.

The HO completion phase concludes the whole procedure with the user plane update at the mobility management entity (MME) and the serving gateway (SGW). More details of the LTE HO procedure can be found in [10]. The typical latency values considered for the computation of the HO timing are shown in Table F.1, and also correspond to the numbers in brackets in Fig. F.1.

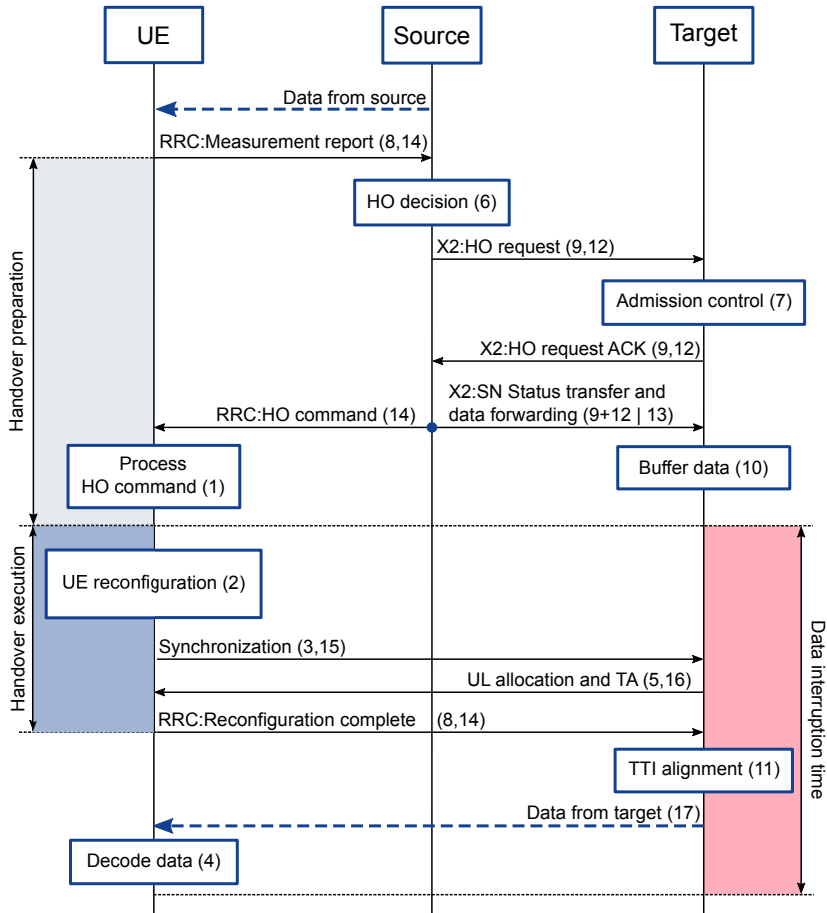


Fig. F.1: The baseline LTE HO. The number on brackets correspond to the latency components from Table F.1. The sign | indicates parallel events.

Table F.1: Typical Latency Values in the LTE Handover

UE Processing Times	
(1) Processing HO command	15 ms [5]
(2) UE reconfiguration including RF retuning	20 ms [5]
(3) Acquiring first available RACH in target cell	2.5 ms [5]
(4) DL Data decoding	3 ms [5, 9]
(5) Processing UL allocation message	3 ms
eNB Processing Times	
(6) HO decision	15 ms
(7) Admission control	22 ms [6]
(8) Processing RRC message	5 ms [6]
(9) Processing X2 message	5 ms [6]
(10) Buffering incoming data	3 ms
(11) TTI alignment	0.5 ms [5]
eNB-eNB Messages	
(12) X2 message encapsulation and transmission	5 ms [6]
(13) Data forwarding preparation and transmission	5 ms [6]
Air Interface Messages	
(14) RRC message encapsulation and transmission	6 ms [5, 6]
(15) PRACH preamble transmission	1 ms [5]
(16) UL allocation and TA transmission	5 ms [5]
(17) Data transmission	1 ms [5]

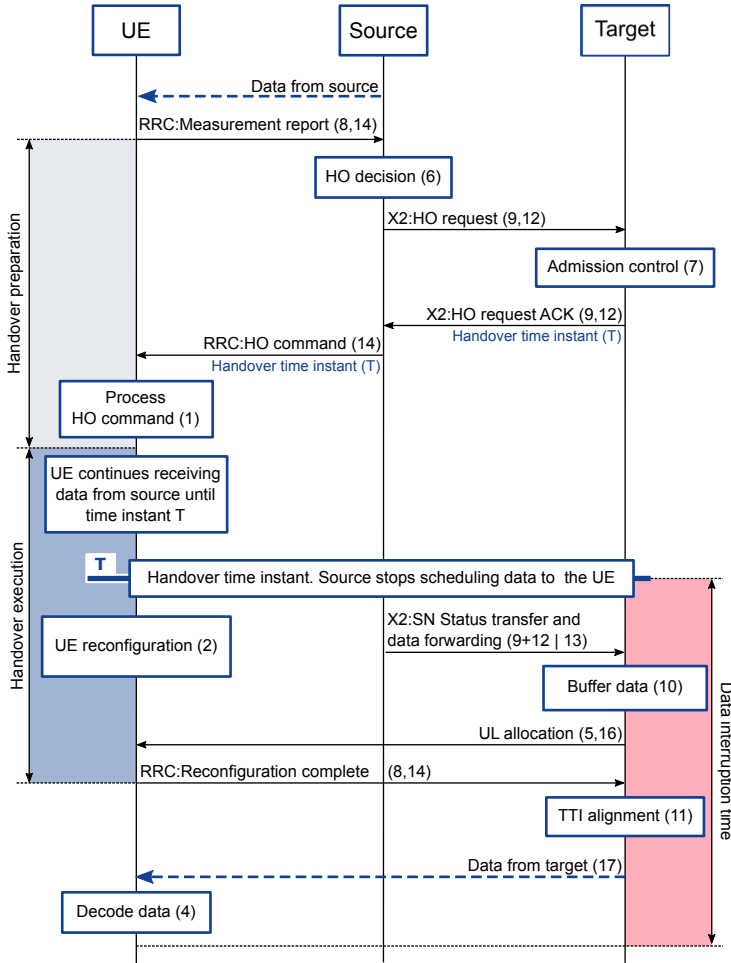


Fig. F.2: The basic RA-less HO [6]. The number on brackets correspond to the latency components from Table F.1. The sign | indicates events that happen in parallel.

3 The Basic Synchronous RA-less Handover

Fig. F.2, illustrates the synchronous RA-less HO. Assuming a time-synchronized network, the source and target cells agree on the time instant (T) for the HO, which is then communicated to the UE in the HO command. The source cell schedules data to the UE until the HO time instant (T). Thereafter, the target starts sending data to the UE. The selection of time instant T is critical. A large value would unnecessarily increase the HO time, whereas a small value would not be sufficient for the UE and the network to be ready before the HO takes place. As can be seen in Fig. F.2, the instant T must be selected for allowing the UE to process the HO command with a certain margin, but as small as possible to avoid a radio-link failure (RLF) on the degrading

link with the source cell.

Given that the source and target cells are time-synchronized, the UE is capable of computing the time advance (TA) at the target cell by measuring the time difference between the received signals from the source and the target. This procedure can be done while the UE performs the measurements of the reference signals transmitted by the cells [6]. Therefore, the RA is no longer required, avoiding the latency components 3 and 15 from Table F.1 and reducing the data interruption time.

Although the RA is avoided, the data interruption persists due to several factors. The target cell has to wait for the UE to send the *RRC Connection Reconfiguration Complete* before resuming the data transmission. This RRC message cannot be sent until the UE receives the up-link (UL) allocation at the target cell. Moreover, the target cell cannot send data to the UE until the source forwards the content of its buffer, a process that is highly sensitive to the latency of the X2 interface.

The UL allocation can be included in the HO command, eliminating the latency components 5 and 16 from the HO execution, and further reducing the data interruption time [5].

4 Enhancements of the RA-less Handover

4.1 Early Data Forwarding During the Handover Preparation

In the basic RA-less HO, the source cell forwards the content of its buffer to the target (via X2 interface) while the UE performs the reconfiguration. In real networks the X2 latency may vary from a few to tens of milliseconds. Therefore, the UE could complete the reconfiguration and send the *RRC Connection Reconfiguration Complete* before the forwarded data is available at the target cell. If the target has no data to transmit this situation leads to additional data interruption time.

To avoid having an empty buffer in the target at the HO time instant we propose to move the data forwarding to the HO preparation. Specifically, the early data forwarding can be initiated at the same time the HO is commanded to the UE. However, as the source cell continues transmitting data during the HO preparation it is necessary to implement a mechanism that keeps the buffers of both cells in-sync without interrupting the ongoing communication. As shown in Fig. F.3, we propose that the source cell predicts the fraction of its buffer that should be available at the target. This prediction should minimize the probability of running out of data before the HO instant, and minimize the probability of a buffer overrun at the target.

The CQI, periodically reported by the UE, indicates the highest modulation scheme and code rate to be used during data transmission. The source cell can combine this information with the amount of physical resource blocks (PRBs) scheduled to the UE, the quality of service (QoS), and the transmission error rate, to estimate the data rate (R) for transmitting data to the UE between the reception of the *HO request acknowledgment (ACK)* (T_{HO_ACK}), and the HO time instant (T). Then, the estimated amount of data to be transferred to the UE between T_{HO_ACK} and T , is calculated as $M_{Source \rightarrow UE} = R \cdot (T - T_{HO_ACK})$. If M is the total amount of data stored in the buffer of the source cell then, the amount of data to be transferred to the target can be calculated as $M_{Source \rightarrow Target} = M - M_{Source \rightarrow UE}$.

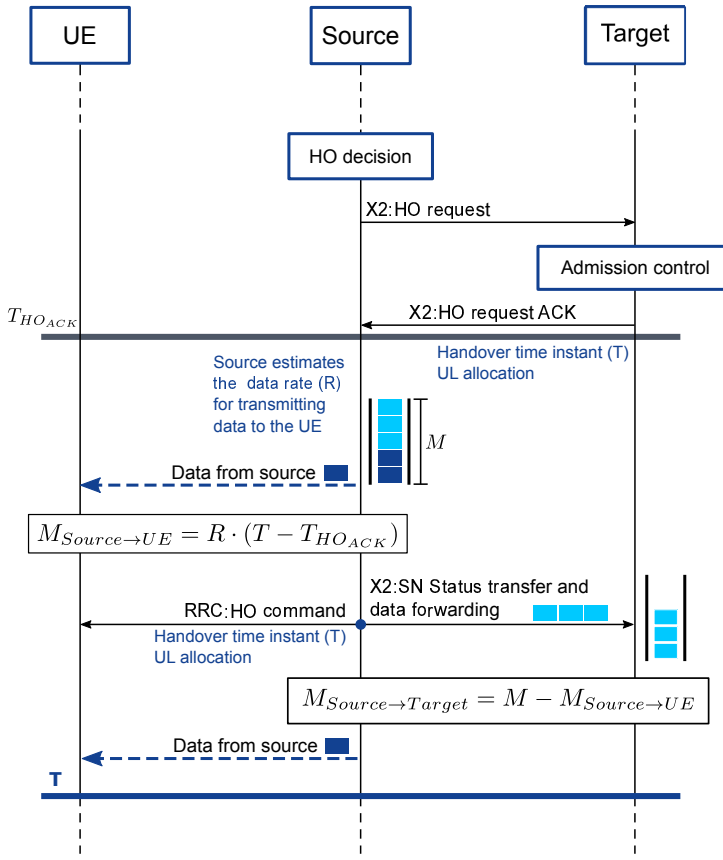


Fig. F.3: Proposed data forwarding during the HO preparation.

4.2 Synchronous Make-Before-Break Handover

The make-before-break HO consists of keeping the connection to the source cell until the access towards the target has been completed [5]. Therefore, the UE receives data during the entire HO process, eliminating the service interruption.

Fig. F.4 illustrates our proposed implementation of this type of HO in a time-synchronous network. The UL allocation is sent together with the HO command, eliminating the need of a specific message during the HO execution. Assuming the adoption of the previously discussed technique, the data forwarding between cells is moved to the HO preparation. For inter-frequency HOs, where the UE is unable to receive data while performing the RF tuning towards a different frequency band, this solution requires the use of a duplicated receiver (Rx) chain at the UE. In this way, the UE can still receive data from the source in one of the chains while it reconfigures the second one towards the target cell. The cost of this benefit is a higher UE complexity, as it is required for implementing today's LTE dual connectivity solutions [11].

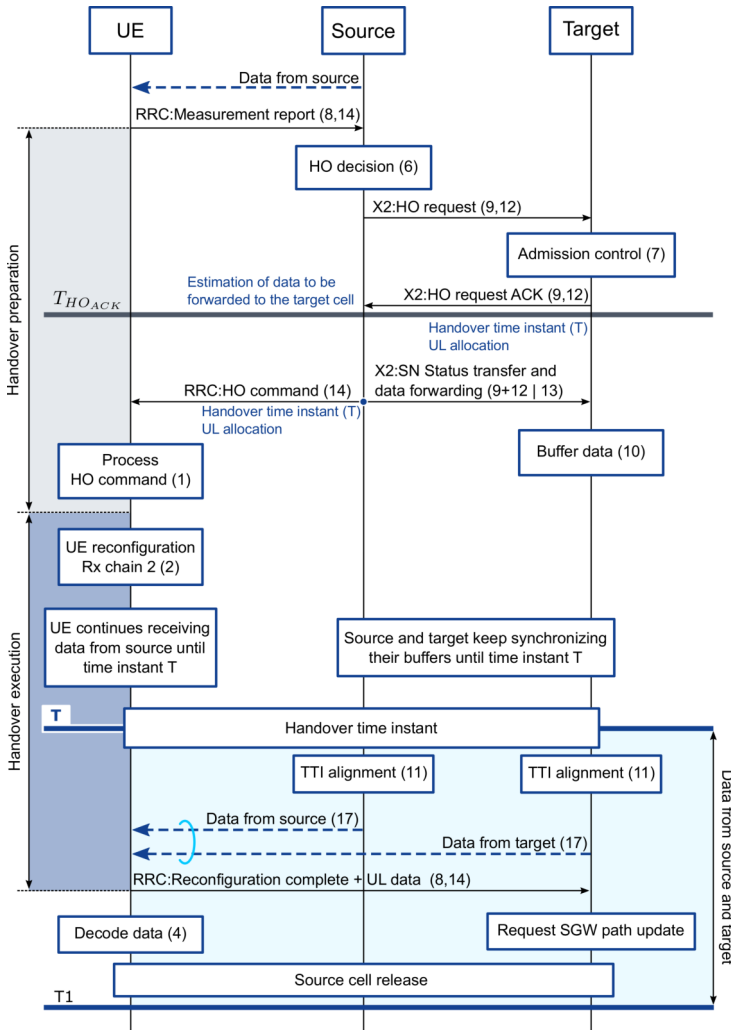


Fig. F.4: The proposed synchronous break-before-make HO. The number on brackets correspond to the latency components from Table F.1. The sign | indicates events that happen in parallel.

To ensure that the UE is ready to receive data from the target at the HO time, it is proposed that the UE performs the reconfiguration right after receiving the HO command. Thus, in this study, the HO time instant (T) coincides with the instant the UE completes the reconfiguration.

Immediately the time instant T the target cell starts sending data to the UE, together with the source cell. In parallel, the UE simultaneously transmits the *RRC Reconfiguration Complete* message and data to the target in the UL allocation indicated in the HO command. This RRC message is used for triggering the network path switch update and initiate the release of the source cell. However, if radio conditions

are favorable, the source cell can be kept for a longer time. As depicted in Fig. F.4, the UE receives data from the source and target cells simultaneously, during the time interval $[T, T_1]$. As the connection to both cells are overlapping in time, this HO scheme is more robust towards inaccuracies in the estimation of T , and in the prediction of the amount of data to be forwarded to the target cell. Therefore, a larger margin for the time instant T is allowed. Nonetheless, as the likelihood of experiencing an RLF on the source link increases with the HO time instant, a large value of T is not recommended.

5 Evaluation of the Proposed Enhancements

The proposed enhancements are evaluated by comparing the HO timing of the legacy LTE HO, the basic RA-less HO, the RA-less HO with early data forwarding, and the synchronous make-before-break HO. For computing the timing of the RA-less HO with early data forwarding we follow the chart in Fig. F.2, but with the UL allocation included in the HO command, and the data forwarding starting in the HO preparation.

We assume that it takes 4 ms for the source cell to predict the fraction of the buffer that should be forwarded. For the sake of simplicity, we consider that there are no errors in the prediction. However, if the source cell overestimates the fraction of the buffer to be forwarded, it may then run out of data before the handover time instant. On the contrary, if the source cells underestimates the amount of data, it may have to forward the remaining content of its buffer to the target after the handover time instant. All the received packets from the target cell must then be reordered at the UE. In any case, the impact of these issues are diminished by the make-before-break. Moreover, we assume no data loss during the forwarding and that the source cell can always transmit data to the UE during the HO preparation. For each HO implementation, we analyze the preparation time, the execution time, and the data interruption time. Furthermore, the overall HO latency is evaluated by computing the elapsed time from the UE sending the measurement report that triggers the HO, until it receives the first data from the target cell.

5.1 Handover Timing with Typical Delays

Fig. F.5 shows the HO timing for each of the solutions with the typical delays from Table F.1. As can be seen, all HO types result in the same preparation time. Although early forwarding and make-before-break implement the data forwarding between cells within the HO preparation, the required time for this phase does not increase. This is because the typical time that it takes for the UE to process the HO command (15 ms) is larger than the typical time it takes for the source cell to send the first set of data to the target (5 ms), and the time it takes for the target cell to buffer it (3 ms).

The RA-less HO reduces the HO execution time (and the data interruption) by 3.5 ms compared to legacy LTE. Moving the data forwarding between cells to the HO preparation, reduces the HO execution time by 8 ms more. Nonetheless, 35.5 ms of data interruption time still persists because the target cell has to wait for the UE to

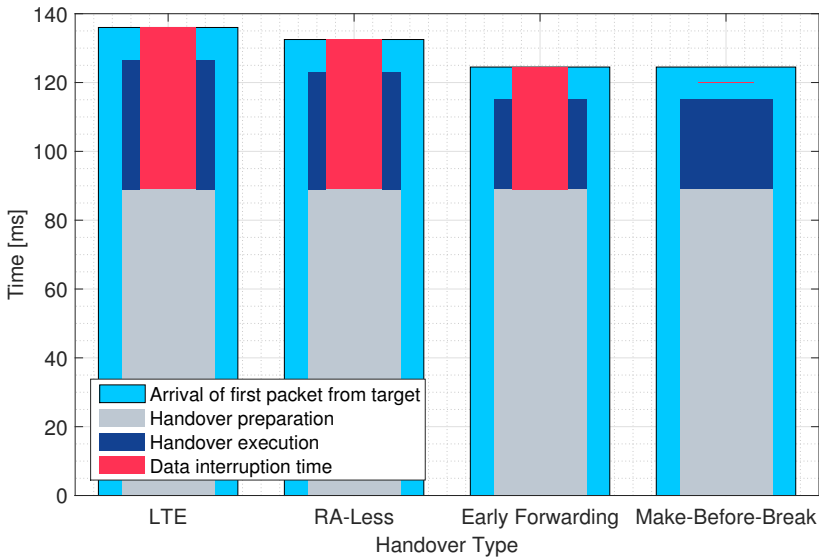


Fig. F.5: Timing for the different HO types with typical latency values.

complete the reconfiguration. Make-before-break achieves the best performance as it is the only HO implementation that completely eliminates the data disruption, while achieving the lowest HO execution time.

This is the performance considering typical delays. However, each UE, eNB and X2 interface may have different latency profiles, producing other HO timing.

5.2 UE and X2 Latency Sensitivity Analysis

Fig. F.6 illustrates the data interruption time for each HO considering variable UE reconfiguration times and X2 latencies. The UE reconfiguration time is set to 0, 5, 10, 15 and 20 ms while the X2 latency is swept from 0 to 20 ms. An X2 latency close to 0 ms can be achieved by interconnecting the eNBs with optical fiber. The rest of delays are as shown in Table F.1.

Figs. F.6 (a) and (b) show that for UEs with a low reconfiguration time the performance of the legacy LTE is similar to RA-less. However, as the UE reconfiguration time increases the reductions in the HO execution and data interruption time brought by the RA-less HO becomes significant.

The figures also show the trade-off between the X2 latency and the UE reconfiguration time in the legacy LTE and RA-less HO. The source and target cells need to exchange some X2 messages for the status transfer and the data forwarding. If the time that it takes to exchange these messages is larger than the UE reconfiguration time, the X2 latency dominates the overall delay. As a result, the plots show an increasing linear tendency with the X2 latency. On the other hand, there is no benefit from having a super fast X2 interface as the network has to wait for the UE to complete the reconfiguration.

Fig. F.6 (c) shows that forwarding data between cells during the HO preparation eliminates the dependency of the data interruption time with the X2 latency. Nevertheless, the UE reconfiguration time should be reduced to keep a minimum data interruption. Additionally, as can be observed in Figs. F.6 (a), (b) and (c), short UE reconfiguration times and low latency X2 interfaces do not eliminate completely the data interruption, due to other delays such as the UE and eNB processing times and the exchange of RRC messages.

These results show that it is necessary to simultaneously lower the UE and eNB processing times, and the X2 latency to minimize the data interruption time. Nonetheless, the make-before-break HO eliminates the data interruption independent of the latency of HO steps.

5.3 Handover Timing Towards 5G

Next, we consider 10x lower HO UE processing times, 10x lower HO eNB processing times, and 5x lower delays for encapsulating and transmitting a message via the X2 interface, compared to the typical values from Table F.1. These factors correspond to our estimations for 5G. We also assume 1 ms for transmitting any message over the air and 125 μ s for the TTI alignment at the eNB.

Table F.2 shows a comparison between the HO timing assuming typical delays, and the timing with lower latencies. 10x faster UEs and eNBs, and 5x faster X2 interfaces, reduces the interruption time by a factor of 5.9 for legacy LTE HO, and 6.5 for RA-less HO. Similar reductions can be achieved with early data forwarding. However, even with all latencies reduced, the data interruption persists. The make-before-break is the only HO type that achieves zero data interruption time, being the only implementation that fulfills the new stringent requirements for the next generation of mobile networks.

6 Conclusions

To reduce the data interruption time in the RA-less HO we propose a selective data forwarding mechanism during the HO preparation phase, where the source cell estimates the amount of data that should forward to the target based on CQI reports, QoS and other parameters. Moreover, we also propose the make-before-break procedure in the synchronous RA-less HO. To evaluate the performance of the proposals, an analysis of the HO timing is performed, including the UE and eNB processing times, and the X2 latencies. Our results reveal that selective data forwarding reduces the data interruption by 8 ms compared to the basic RA-less HO with typical delays. Make-before-break eliminates the data interruption, fulfilling the latency requirements imposed by the design specifications of the next generation of mobile networks.

For future work, it is recommended to further assess the performance of these proposals in various scenarios via system level and protocol simulations, including packet loss and cases where the source cell cannot transmit the estimated amount of data to the UE due to poor radio-link conditions. Moreover, it is proposed to study

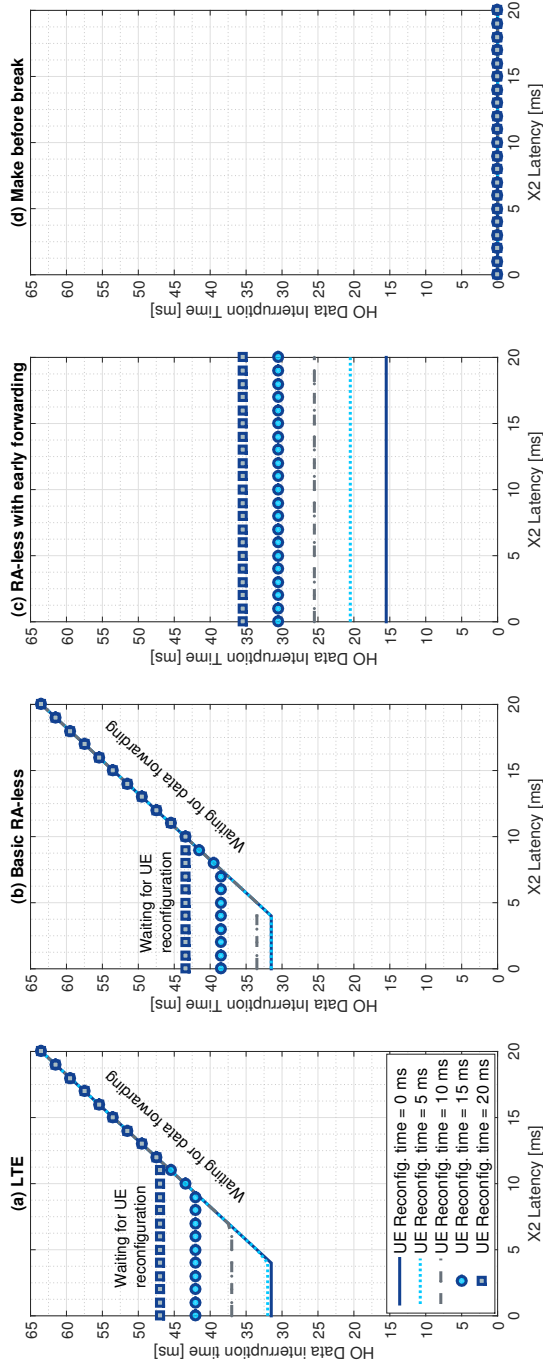


Fig. F.6: Data interruption time for the different HO implementations considering variable UE reconfiguration time and X2 interface latency.

Table F2: Comparison of the handover timing with typical and low latency values.

HO Phase	Legacy LTE		Basic RA-less		RA-less with early forwarding		Make-Before-Break	
	Typical	Low	Typical	Low	Typical	Low	Typical	Low
HO preparation	89 ms	11.7 ms	89 ms	11.7 ms	89 ms	11.7 ms	89 ms	11.7 ms
HO execution	37.5 ms	6 ms	34 ms	4.8 ms	26 ms	3.5 ms	26 ms	3.5 ms
Data interruption	47 ms	8 ms	43.5 ms	6.7 ms	35.5 ms	5.4 ms	0 ms	0 ms

procedures in order to detect and handle failures during a make-before-break HO, and to evaluate the presented solutions under different network topologies.

References

- [1] A. Elnashar and M. A. El-Saidny, "Looking at LTE in practice: A performance analysis of the LTE system based on field test results," *IEEE Vehicular Technology Magazine*, vol. 8, no. 3, pp. 81–92, Sept 2013.
- [2] D. Han, S. Shin, H. Cho, J. m. Chung, D. Ok, and I. Hwang, "Measurement and stochastic modeling of handover delay and interruption time of smartphone real-time applications on LTE networks," *IEEE Communications Magazine*, vol. 53, no. 3, pp. 173–181, March 2015.
- [3] L. C. Gimenez, M. C. Cascino, M. Stefan, K. I. Pedersen, and A. F. Cattoni, "Mobility performance in slow- and high-speed LTE real scenarios," in *IEEE 83rd Vehicular Technology Conference (VTC Spring)*, May 2016, pp. 1–5.
- [4] *Report ITU-R M.2134. Requirements related to technical performance for IMT-Advanced radio interface(s)*, 2008.
- [5] *3GPP Technical Report (TR) 36.881. Study on latency reduction techniques for LTE. V.14.0.0*, June 2016.
- [6] S. Barbera, K. I. Pedersen, C. Rosa, P. H. Michaelsen, F. Frederiksen, E. Shah, and A. Baumgartner, "Synchronized RACH-less handover solution for LTE heterogeneous networks," in *International Symposium on Wireless Communication Systems (ISWCS)*, Aug 2015, pp. 755–759.
- [7] *3GPP Technical Report (TR) 38.913. Study on Scenarios and Requirements for Next Generation Access Technologies. V.0.4.0*, June 2016.
- [8] D. S. Michalopoulos, I. Viering, and L. Du, "User-plane multi-connectivity aspects in 5G," in *23rd International Conference on Telecommunications (ICT)*, May 2016, pp. 1–5.
- [9] H. Holma and A. Toskala, *LTE for UMTS. Evolution to LTE-Advance*. John Wiley & Sons, 2011.
- [10] *3GPP Technical Specification (TS) 36.300. E-UTRA and E-UTRAN Overall Description. Stage 2. V.13.3.0*, April 2016.
- [11] C. Rosa, K. Pedersen, H. Wang, P. H. Michaelsen, S. Barbera, E. Malkamaki, T. Henttonen, and B. Sebire, "Dual connectivity for LTE small cell evolution: functionality and performance aspects," *IEEE Communications Magazine*, vol. 54, no. 6, pp. 137–143, June 2016.

Paper G

Mobility Enhancements from LTE towards 5G for High-Speed Scenarios

Lucas Chavarría Giménez, Klaus I. Pedersen, Per Henrik
Michaelsen, Preben E. Mogensen

Submitted for publication to
IEEE Wireless Communications Magazine. 2017.

© 2017 IEEE

Reprinted with permission. The layout has been revised.

Abstract

Field measurements are analyzed to identify the most critical limitation of today's LTE networks, namely the handover data interruption time. Typically, it varies from 24 to 50 ms, sometimes reaching values greater than 100 ms. The analysis of the measurements is followed by a study of potential solutions to reduce the interruption time. Our results reveal that when upgrading the network to a heterogeneous network topology with dual connectivity, the architectural option of split bearer offers a promising solution for reducing the data interruption. Additional mobility solutions in the form of synchronized handovers, make-before-break techniques and partial user equipment autonomous cell management schemes are explored. These solutions are equally relevant for the evolution of LTE and for 5G. An optimized data forwarding scheme that reduces the interruption time for synchronous handovers is proposed. Finally, we discuss further disruptive mobility research directions, including migration towards cell-less designs, and decoupled downlink and uplink network associations for cases with centralized radio network architectures.

1 Introduction

In December 1947, two engineers at Bell Labs, Douglas H. Ring and W. Rae Young, proposed the concept of cells for mobile networks. Later, in 1960, R.H. Frenkiel and P.T. Porter described the first ideas of handover, or changes between cells. Today, the design of modern mobile communication systems continues to build on those pioneering cell-centric principles. Accordingly, the fourth-generation Long Term Evolution (LTE) also inherits the fundamental paradigms of cells (and handovers between cells) to maintain a continuous data connection for users in motion, ranging from pedestrian mobility to users in fast vehicles.

The LTE handover is network-controlled and user equipment (UE)-assisted for active mode users, where the network is in charge of the handover decisions, based on radio measurements performed by the UEs. The handover procedure is of the break-before-make type, which means that during every handover there is a short data interruption, as the connection to the source cell is “broken” before “making” the connection to the target cell. Since the first LTE release, the standard has evolved into LTE-Advanced (LTE-A), and recently into LTE-A Professional (Pro), the new branding name used for the 3rd generation partnership project (3GPP) Release-13, and onwards. Whereas the data interruption has not been considered a critical issue in the past, it has recently attracted attention as part of the design of the fifth-generation (5G) new radio (NR), targeting zero-data interruption at handovers [1].

In this article, we study the handover performance in a high-speed scenario covered by a network that evolves from traditional macro LTE towards LTE-A Pro and 5G NR, with special emphasis on the associated service interruption, the signaling overhead and other commonly accepted counters of mobility performance. Such a scenario is particularly challenging due to the large number of handovers experienced by the UEs.

As understanding the mobility performance and the associated challenges for legacy LTE in the scenario is a prerequisite, we start by presenting drive-test mea-

measurements for an operational macro-cellular LTE network in a highway. These field measurements supplement earlier LTE measurement results reported in [2] and [3].

Secondly, we extend the analysis to the case where the network topology is upgraded to a heterogeneous network (HetNet) layout by deploying small cells along the highway, offering higher capacity in line with the growing traffic demands. The mobility challenges that emerge in such a HetNet scenario are presented (see also [4]), together with the opportunities for improving the mobility performance when combined with the proper use of LTE-A Dual Connectivity (DC) ([5, 6]). For the latter, we analyze the dependency on the mobility performance from using different network architectures. In fact, depending on the DC architecture an element of make-before-break can be achieved, as the small cell connectivity can be changed while still maintaining a stable data connection through the macro-layer.

Afterwards, we focus our attention on future candidate solutions such as synchronous handovers, and make-before-break procedures [7]. Such solutions have equal relevance for LTE-A Pro and the NR, both considered part of the 5G umbrella of radio technologies. We evaluate the possibilities of these techniques for improving the mobility performance, and provide recommendations for realizing real make-before-break handovers. Our proposals include an enhanced data forwarding for synchronous handovers, a realization of a synchronous make-before-break technique and UE autonomous cell management actions [4, 8], for reducing the signaling overhead.

Finally, we conclude the article by presenting an evolution of the mobility innovations from the early releases of LTE and LTE-A, towards LTE-A Pro, and providing our visions for the 5G NR. In line with the studies in [9] and [10], we also discuss options for moving beyond the original cellular mobile communications design paradigm from 1947, and aim for a cell-less/user-centric design to further improve the mobility performance. In order to ensure a high degree of realism, the presented performance results in this article are based on the analysis of field measurements, findings from laboratory measurements, and advanced system level simulations results.

2 Mobility performance in current LTE networks

Analysis of an LTE Macro-Network

The LTE handover is triggered by the UE reporting to the network the reference signal received power (RSRP) or the reference signal received quality (RSRQ) measured from the neighboring cells. After processing the measurements report, the network commands the handover to the UE via the *RRC Connection Reconfiguration* message, including the mobility control information. At this point, the UE stops data exchange with the serving cell, originating the data interruption time. Thereupon, the UE initiates the random access (RA) towards the target cell. Once completed, the UE sends the *RRC Connection Reconfiguration Complete* message, restoring the data exchange with the network. At the UE side, the elapsed time from the instant the UE sends the measurements report until it receives the handover command is called handover preparation time. The elapsed time between the handover command and the *RRC Connection Reconfiguration Complete* message is called handover execution time. Ide-

ally, the data interruption time equals the handover execution time. However, other factors such as scheduling delays and air-interface transmission times add further service interruption to the end-user experience.

To characterize the data interruption time in a high-speed scenario, we performed field-measurements in an operational LTE macro-network deployed by a major Danish operator along a highway stretch. The scenario is a 7.5 km section of the European route E-45 that passes through the city of Aalborg in Denmark. By the time the measurements were performed, the whole segment was covered by 23 macro-cells, operating at 1800 MHz. Four sets of drive tests were performed, traversing the highway from north to south and back, at an average speed of 100 km/h. Measurements samples were collected through a Samsung Galaxy S-III with a proprietary software, that allowed us to extract the radio resource control (RRC) signaling, among other statistics. The handover timing at Layer-3 is calculated by analyzing the time-stamp of the RRC messages at each handover. Further details on the measurement setup can be found in [3].

There was no record of radio link failures (RLFs) or handover failures (HOF) during the measurements. So the 3.6 handovers per minute experienced by the phone (on average) were all successfully completed. The observed median handover preparation time was 38 ms (with an extreme value of 130 ms), whereas the measured median handover execution time was 24 ms. However, in 5 % of the cases, the data interruption time was larger than 42 ms. On average, the phone was unable to receive or transmit any data for 0.15 % of the traveling time. These results represent the performance of a well-optimized macro-network. However, depending on the specific network implementation, the experienced interruption time can be larger. For instance, the field measurements in [2], reported typical interruption times of 50 ms.

Analysis of LTE-Advance with Dual Connectivity

We next consider the case where the network is upgraded with small cells distributed along the roadsides of the highway, operating at the dedicated frequency of 3.4 GHz, using the DC feature. A UE that is configured with DC consumes radio resources from more than one cell, benefiting from the aggregation of multiple radio links. In this operational mode, a macro-cell typically plays the role of the master e-NodeB (MeNB), acting as the mobility anchor and managing the RRC signaling. The role of the secondary eNB (SeNB) is played by a small-cell, providing additional radio resources. While the connectivity in the primary link is governed by traditional handovers (denominated MeNB handovers), the secondary link is managed by additional mobility events: SeNB additions for aggregating the link, SeNB changes for changing the serving cell, and SeNB removals for removing the aggregated link. Therefore, with DC, the total number of mobility events increases compared to single connectivity.

In single-node connectivity, the radio bearers that carry the user-plane data experience a disruption every time a handover occurs, as the bearers must be moved from the source to the target cell. However, in DC the data interruption depends on the adopted network architecture. Two different user-plane architectures can be used for implementing DC [6]: Secondary cell group (SCG) bearer and split bearer. Both architectures are illustrated in Figure G.1.

In the SCG bearer architecture, the SeNB is connected directly to the core network

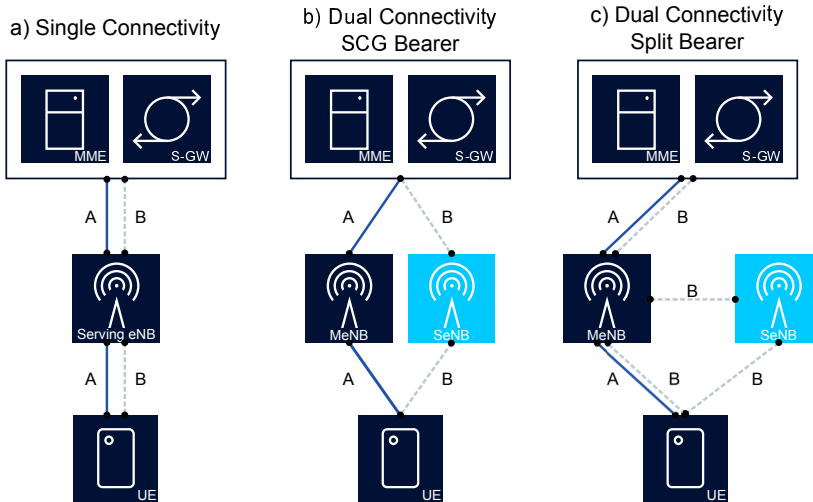


Fig. G.1: Flow of two data bearers (A and B) considering different network architectures. a) Single-node connectivity. b) DC with SCG architecture. c) DC with split bearer architecture.

(CN) and the user-plane data is split between eNBs at the serving gateway (S-GW). The MeNB and the SeNB carry different data bearers (A and B in Figure G.1). Every time an SeNB mobility event occurs, the serving gateway (S-GW) should transfer bearer B from the MeNB to the added SeNB (in case of an SeNB addition), or from the serving SeNB to the target SeNB (in case of an SeNB change), disrupting the data bearer. Similarly, bearer A is interrupted every time a MeNB handover occurs. These effects can be partially mitigated by forwarding data between eNBs. However, the data interruption is inevitable, as the UE should perform the synchronization towards the new cells, disrupting the data exchange.

In the split bearer architecture, the MeNB is the only one connected to the CN, therefore in charge of splitting the user-plane data. As all bearers are terminated at the macro-cell, data from bearer B can be transmitted via the MeNB and the SeNB. Thus, during a SeNB operation such as SeNB change, bearer B is still scheduled from the MeNB, eliminating the data interruption at SeNB events. However, the UE is still subject to data interruption at each MeNB handover. Nevertheless, the overall interruption time is reduced as the number of macro handovers is significantly smaller than the number of small cells events.

To quantify the performance with DC, we consider 119 small cells deployed every 100 meters along the high-way. Both connectivity options with single-node LTE connectivity and LTE-A DC are evaluated. The performance is studied by means of a dynamic system level simulator that reproduces the highway scenario. The study in [3] confirms that the simulator produces accurate mobility results comparable with real-life. Users traveling at a speed of 130 km/h are simulated. In line with our measurements and the values reported in [7] and [11], 42 ms of data interruption time is modeled for each handover. Additional details on the simulation methodology are available in [12].

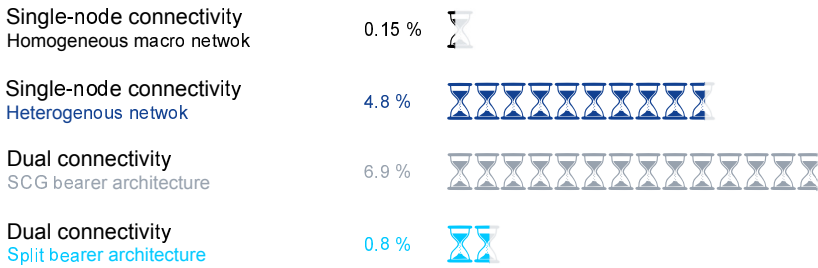


Fig. G.2: Percentage of time an UE is unable to exchange any data with the network over the total driving time in the highway for each connectivity mode and different user-plane architectures.

Our results reveal that the number of handovers increases from 3.6 to 69.6 events per UE per minute, when upgrading the network to the considered HetNet layout with single-node connectivity. Consequently, the UE is now unable to exchange any data for approximately 5 % of the driving time. When adopting DC, the number of handovers is reduced to 12 events per UE per minute, as those only happen at the macro-layer. However, the number of secondary cell management events at the small cell layer is high, as the UEs experience 98 SeNB events per minute.

The impact of these events on the data interruption varies significantly with the adopted user-plane architecture. As shown in Figure G.2, with the SCG bearer architecture the interruption time increases up to 7 % of the driving time, due to the frequent SeNB changes. However, with split bearer architecture data gaps occur only at the MeNB handovers, reducing the total service interruption to 0.8 % of the traveling time, despite of the large number mobility events in the scenario. The interruption time is higher than in the macro-only case due to the slightly larger number of handovers produced by the more aggressive handover parametrization required when deploying the small cell layer. More details can be found in [12].

Although the service interruption is not eliminated, split-bearer is the most suitable architecture for implementing DC as it brings the advantages of aggregating additional links, while minimizing the data interruption. Nevertheless, DC comes at the cost of higher signaling overhead and higher number of mobility decisions processed by the network, due to the frequent mobility events.

3 Mobility enhancements towards 5G

Next, we present and analyze some of the candidate techniques for further reducing the data interruption time [7], and for reducing the signaling overhead at mobility events. These techniques are equally relevant for the continuous evolution of LTE (LTE-A Pro) and the NR, which is currently under standardization.

Synchronous RA-less and make-before-break handover

Nowadays, there is a clear trend towards having time-synchronized base stations in the field, offering possibilities for improved mobility performance. The time synchro-

nized RA-less handover is one example that reduces the interruption time at each handover [11]. The principle of this technique is as follows: During the handover preparation phase, the serving and target cells negotiate the time instant where the handover should take place. Afterwards, the serving eNB informs the UE about the handover switching instant through the handover command. As the three entities involved in the process are fully synchronized, the device can switch from the source to the target cell at the negotiated instant. Given the time-synchronization of the cells, and that the UE knows the current value of the time advance (TA) for the source cell, the UE is hence capable of computing the TA at the target as outlined in [11]. This means that the RA procedure is no longer required for acquiring the TA information when accessing the target cell. Avoiding the RA, reduces the overall handover latency and the data interruption time, resulting also in additional mobility robustness with even lower probability of experiencing HOFs.

Figure G.3(a) illustrates the scheduled downlink data from the source and the target cell versus time. Before the handover time, the UE is listening to the source cell. At the handover time, the source cell stops transmission to the UE and the target starts scheduling packets to the UE. At this point, the UE switches to the target cell. Ideally, this transition could be done quasi-instantaneous at lower layers, reducing the interruption time to fractions of a transmission-time-interval (TTI). Nonetheless, at the RRC layer, the required exchange of signaling messages, and the eNB and UE processing times make the service interruption time unneglectable. Moreover, in case of an inter-frequency handover this transition may take longer, as the UE should perform the radio-frequency retuning towards a different frequency. Additionally, the data forwarding between cells occurs while the UE switches from the source to the target cell [11]. Due to eNB processing delays and the latency of the X2 interface, this procedure is not instantaneous, producing additional data interruption during the handover.

Figure G.3(b) depicts an option for further reducing the interruption time in the synchronous handover. In this case, data duplication from the source and target cell is allowed, and the UE listens to both cells while performing the handover for a short hysteresis time. However, it should be noted that for achieving the zero-data interruption the network should support fast data forwarding between the cells involved in the handover process, and an efficient flow-control mechanism to keep the buffers at both cells in sync. Furthermore, the probability of an empty buffer at the target cell and the probability of running out of data at the source before the handover takes place should be minimized.

Figure G.4 illustrates a proposed buffer management for synchronous handovers. In this procedure, the source cell derives the data-rate towards the UE, from the moment it commands the handover until the handover time instant. The source cell thereby predicts the amount of buffered data that it can deliver to the UE, and immediately starts forwarding the remaining data to the target cell. Estimation of the data-rate is based on a combination of different parameters such as the periodical channel quality indicator reported by the UE, the number of resources allocated to the UE, the required quality of service, and the air interface transmission error rate.

The enhancements in Figures G.3(b) and G.4 present a synchronous make-before-break handover, where the connection to the source cell is maintained until the ac-

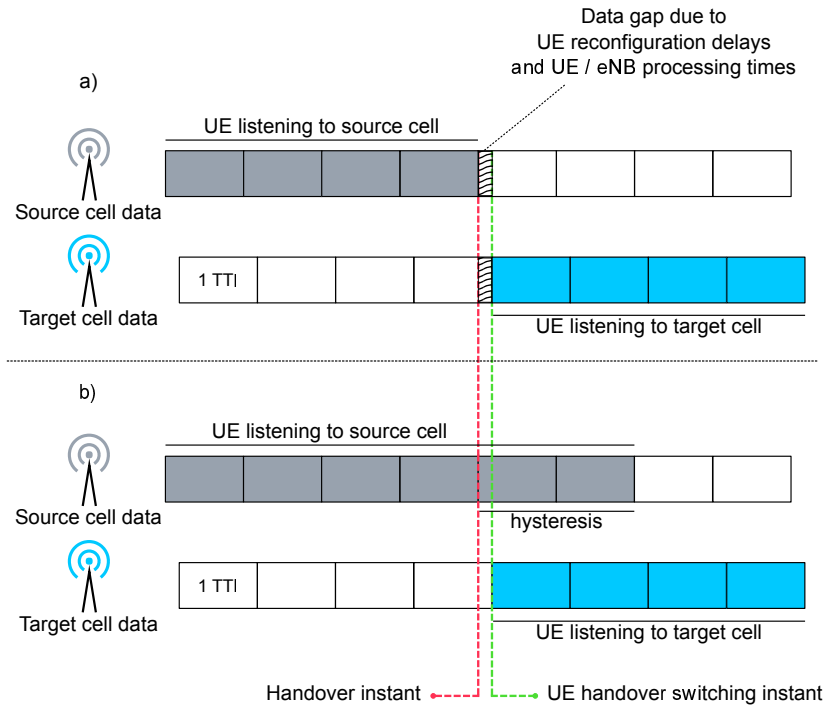


Fig. G.3: Synchronous RA-less handover. a) The UE experiences a data interruption while switching from the source to the target cell. b) The interruption can be potentially reduced by allowing data duplication from both, source and target cell during the handover switching.

cess towards the target cell has been established. Consequently, the UE can receive data from the source cell during the entire handover execution, hence eliminating the data disruption. As the UE needs to be able to receive data from both cells at the same time, this solution requires to increase the UE complexity by duplicating the radio-frequency (RF) chains, similarly to the implementation of those terminals that currently support LTE-A with DC [6]. In an inter-frequency handover, the UE can use one chain to perform the RF-retuning towards a new frequency, while still receive data from the source at the other one.

Moreover, we propose to perform the UE reconfiguration during the preparation stage, before the handover takes place. Thereby, the target cell can initiate the data transmission immediately after the handover instant. In this case, the target does not wait for the UE to send the *RRC Connection Reconfiguration Complete*, and the reception of this message by the target is left for initiating the source cell release. However, if radio conditions favor it, the link with the source cell can be maintained over a longer time.

To benchmark each of the presented enhancements, we calculate the typical handover latencies for each of the described procedures: legacy LTE, RA-less handover, RA-less handover with our proposed data forwarding mechanism, and the synchronous make-before-break. We assume that the UE takes 15 ms to process the handover com-

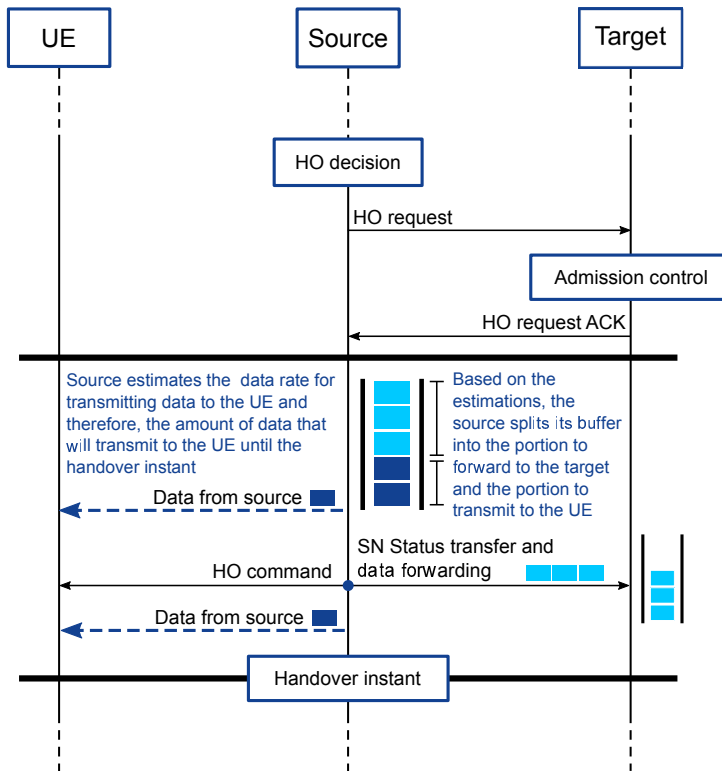


Fig. G.4: Proposed enhanced data forwarding during the handover preparation phase for synchronous handovers.

mand, an X2 interface latency of 5 ms, and a UE reconfiguration time of 20 ms that includes the radio-frequency retuning. Other latency values such as encapsulation and transmission times of each message over the air, and additional UE and eNB processing times are extracted from the lab measurements reported in [11] and the values used by 3GPP in [7].

Considering the different latencies of the handover steps, it can be calculated that the typical data interruption time for an inter-frequency LTE handover is 47 ms. For a RA-less handover, this interruption time is reduced to 43.5 ms. If the synchronous handover is complemented with the proposed optimized buffer management, the interruption time is further reduced to 35.5 ms. Nevertheless, due to signaling exchange, hardware processing times, frequency retuning, and the exchange of the necessary signaling, the data interruption persists. The calculation of these values can be replicated by combining the latency values reported in [7] and [11], and the flow-charts from [7] and Figure G.4.

Nonetheless, the make-before-break is the only solution that achieves zero-data interruption. As the connection to the source and target cell is maintained during the entire process, the handover data interruption is eliminated, with independence of

the handover steps, the back-haul latency, and the time the different entities need to perform the required operations for executing a successful serving cell change.

UE autonomous cell management

The work conducted in [13] presented different network-controlled mobility management policies for LTE-A and their associated amount of signaling. To further decrease the signaling overhead for scenarios with DC, we propose to move from the traditional design paradigm of network-controlled cell management towards UE autonomous cell management procedures for the small cell layer [4]. The basic idea is that the devices have the autonomy of deciding the mobility events at the small cell layer, whereas the mobility at the macro layer is still governed by the network, providing the UEs a stable anchor point. By letting the devices decide on SeNB additions, changes, and removals, the network is offloaded from the burden of taking frequent mobility decisions. This feature lets the UEs to access directly the target cell via the RA channel (RACH), reducing interaction with the network. Additionally, with this level of autonomy, the UEs do not need to send measurement reports at each small cell mobility event, considerably reducing the amount of signaling overhead.

The scheme requires preparing the involved cells in advance, as they should be aware of the context of the devices that may request the access. Moreover, the UEs should be configured with the list of prepared cells, their cell-specific parameters and the set of RACH preambles to use when accessing the target cells. Preparing all the roadside small cells for UE autonomous mobility would be the brute force solution. However, this would mean preparing many small cells in vain. Therefore, we propose a method for such a linear scenario, where a window of prepared cells surrounds the UE, following its movement. As the UE moves along the highway the set of prepared small cells that makes up the window should be updated. Two policies for modifying the set of prepared small cells are proposed. The first one updates the cells every time the serving SeNB changes. The second proposal modifies the set of prepared cells only if the UE connects to the last cells of the window towards the direction of movement. More details on these strategies can be found in [8].

Figure G.5 shows a comparison between the amount of RRC and X2 messages per UE per second generated by traditional DC operations, and the amount of signaling that UE autonomous cell management requires. The results are obtained by scaling the number of cell management events obtained in the system-level simulations with the number of signaling messages required by each event. As can be observed, autonomous operations eliminate the RRC signaling for SeNB addition and change, and considerably reduces the amount of signaling exchanged between eNBs through the X2 interface at each SeNB event. Moreover, with this feature, the UE does not need to wait for network cell management decisions. Therefore, the faster UE reactions at each SeNB mobility event, helps to reduce the probability of RLFs at the secondary links. This feature applies only to the small cell layer. Hence, the amount of MeNB handovers and traditional RLFs in the primary link remain unaltered. Furthermore, this solution can be complemented with our proposed synchronous make-before-break handover at the MeNBs, avoiding the service interruption.

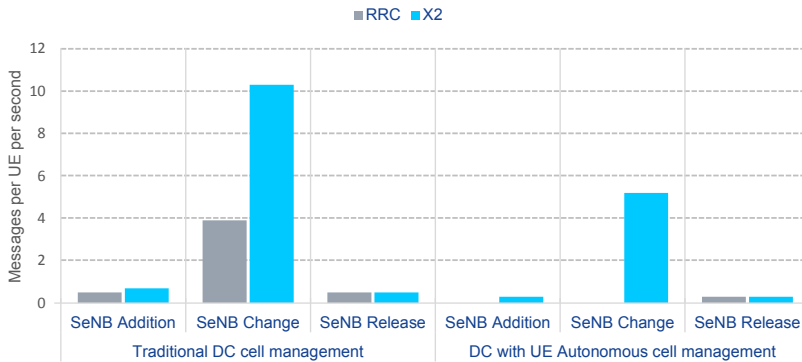


Fig. G.5: Number of RRC and X2 messages per UE per second necessary for traditional dual connectivity and UE autonomous operations.

4 Overview of mobility enhancements

Table G.1 gives an overview of the mobility techniques and benefits from legacy LTE to LTE-A Pro and 5G; evolving from single-node connectivity, to DC, and towards a more generalized multi-node connectivity [14]. It also presents the paradigm shift from a fully network-controlled towards a partly UE autonomous cell management scheme, offering attractive benefits in terms of reduced signaling overhead, and a reduced burden for the network to constantly orchestrate cell management actions.

For the 5G-era, two possible disruptions of the traditional cellular design are already being discussed in the literature. Firstly, 5G could be the first standard that deviates from the basic cellular design paradigm from 1947 [10]. Rather than managing resources per cell, a possible direction for 5G is to move towards a cell-less design, applying a user-centric approach with resources per user. The realization of the former will require a centralized radio access network (C-RAN) architecture, as studied in [9]. For such cases, the radio nodes will be considered as antenna groups, where transferring user transmissions from one radio-node to another would correspond to antenna switching. Likely, this feature will be controlled by physical-layer signaling as opposed to the utilization of RRC signaling in current LTE mobility procedures. However, although appearing as a promising disruption, there are still several open research questions that need careful attention before concluding if a fully cell-less design is a strong candidate solution for 5G C-RAN scenarios.

Secondly, since the very first cellular design, it has been assumed that a UE should have the same cell association for the downlink and uplink communication links, also known as a fully coupled link design. However, for HetNet topologies, recent studies have shown that there are attractive performance benefits from allowing a decoupled design, where a UE could be served in the downlink from one node, while having its uplink transmission towards a different node [15]. Decoupling the links generally requires strict synchronization and data connectivity between the involved nodes, hence being relevant for centralized RAN architectures. However, it could be realizable for other RAN architectures. For the 5G-era, with large diversity of used

carrier frequencies (ranging from below 6 GHz operation up to cm-Wave and mm-Wave band [1]), the benefits of pursuing a decoupled link design are anticipated to be even more attractive. In terms of mobility management, a decoupled link design calls for partly-independent handover actions for the two link directions, and the necessity for deriving new procedures to facilitate that.

Although the enhancements listed in Table 1 are indicated per technology, there are no solid restrictions on which enhancements are applicable to which standard. This is mainly because standards such as LTE-A Pro are in constant development to include more sophisticated enhancements.

Table G.1: Comparison of the handover timing with typical and low latency values.

Technology	Scenario	Characteristics	Challenges & Benefits
Legacy LTE LTE-A	Macro-only	Fully network-controlled and UE-assisted asynchronous break-before-make handover	Typical data interruption time of 24-50 ms at each handover, with extreme values larger than 100 ms
	HetNet	Single node connectivity option: Fully network-controlled and UE-assisted asynchronous break-before-make handover	Higher percentage of time in data interruption. Throughput benefits from DC.
		DC with SCG bearer: Two separate bearers to the UE from the eNBs involved in DC	High percentage of time in data interruption. High signaling overhead from SeNB management. Throughput benefits from DC.
		DC with split bearer: Data flow is split in the MeNB between the eNBs involved in DC	Reduced interruption time. High signaling overhead from SeNB management. Throughput benefits from DC.

<p>LTE-A Pro 5G NR</p>	<p>Macro-only Hetnet</p>	<p><u>Single node connectivity:</u> Synchronous RA-less cell change. Advanced buffer management. Make-before-break handover</p>	<p>Possibilities of achieving zero handover data interruption time</p>
<p>HetNet</p>		<p><u>Enhanced multi-node connectivity:</u> Allowing connection to more than two eNBs. Cases with data duplication from multiple cells with advanced buffer management. UE autonomous SeNB management</p>	<p>Enhanced robustness and data rate from being connected to more than two eNBs. Increased reliability from data duplication. Possibilities of achieving zero-data interruption time, and reduced signaling overhead from UE autonomous SeNB actions.</p>
<p>5G NR</p>	<p>Hetnet with centralized RAN</p>	<p><u>Decoupled uplink and downlink cell association:</u> Allow a user to have different serving cells in the uplink and downlink</p>	<p>Enhanced joint uplink/downlink performance optimization. Especially gains in terms of enhanced uplink performance</p>
		<p><u>No more cells:</u> User-centric design where resources are per user, rather than per cell. Handover between radio nodes via fast antenna switching rather than RRC signaling procedures</p>	<p>Greater flexibility and, therefore, higher end-user performance.</p>

5 Conclusions

In this article, we analyze the evolution of the mobility performance in a high-speed scenario for different technologies. Field measurements, extensive system-level simulations, and simple analytics are used to illustrate both the strengths and challenges of today's standardized solutions, as well as proposals of how to improve the mobility performance in future releases. A challenging highway scenario is used as a case study. Measurements reveal that the UE suffers from service interruptions of typically 24-50 ms during every handover with extreme values larger than 100 ms. When upgrading the network with small cells, the use of DC with the split bearer architecture is a promising solution for reducing the interruption time. Nevertheless, LTE-A DC comes at the cost of higher signaling overhead due to the large number of mobility events at the small cell-layer. Innovations such as synchronous handovers, an enhanced mechanism for forwarding data between cells, and UE autonomous small cell management to reduce the signaling overhead, are evaluated as potential mobility solutions for LTE-A Pro and 5G. Our analysis conclude that make-before-break is a promising type of handover for eliminating the data interruption time.

We recommend further research on disruptive solutions with a cell-less design, without RRC controlled handovers, and a fully decoupled downlink/uplink network association for centralized radio network implementations. The latter present another paradigm shift for the functionality of handovers and cell management actions.

References

- [1] 3GPP Technical Report (TR) 38.913. *Study on Scenarios and Requirements for Next Generation Access Technologies. V.0.4.0*, June 2016.
- [2] A. Elnashar and M. A. El-Saidny, "Looking at LTE in practice: A performance analysis of the LTE system based on field test results," *IEEE Vehicular Technology Magazine*, vol. 8, no. 3, pp. 81–92, Sept 2013.
- [3] L. C. Gimenez, M. C. Cascino, M. Stefan, K. I. Pedersen, and A. F. Cattoni, "Mobility performance in slow- and high-speed LTE real scenarios," in *IEEE 83rd Vehicular Technology Conference (VTC Spring)*, May 2016, pp. 1–5.
- [4] K. I. Pedersen, P. H. Michaelsen, C. Rosa, and S. Barbera, "Mobility enhancements for lte-advanced multilayer networks with inter-site carrier aggregation," *IEEE Communications Magazine*, vol. 51, no. 5, pp. 64–71, May 2013.
- [5] H. Holma, A. Toskala, and J. Reunanen, *LTE Small Cell Optimization: 3GPP Evolution to Release 13*. Wiley, 2016.
- [6] C. Rosa, K. Pedersen, H. Wang, P. H. Michaelsen, S. Barbera, E. Malkamaki, T. Henttonen, and B. Sebire, "Dual connectivity for lte small cell evolution: functionality and performance aspects," *IEEE Communications Magazine*, vol. 54, no. 6, pp. 137–143, June 2016.
- [7] 3GPP Technical Report (TR) 36.881. *Study on latency reduction techniques for LTE. V.14.0.0*, June 2016.

- [8] L. C. Gimenez, P. H. Michaelsen, and K. I. Pedersen, "User autonomous cell management in a high-speed scenario with dual connectivity," in *27th Annual IEEE International Symposium on Personal, Indoor and Mobile Radio Communications (PIMRC)*, Sept 2016, pp. 1–5.
- [9] C. L. I, C. Rowell, S. Han, Z. Xu, G. Li, and Z. Pan, "Toward green and soft: a 5g perspective," *IEEE Communications Magazine*, vol. 52, no. 2, pp. 66–73, February 2014.
- [10] S. Chen, F. Qin, B. Hu, X. Li, and Z. Chen, "User-centric ultra-dense networks for 5g: challenges, methodologies, and directions," *IEEE Wireless Communications*, vol. 23, no. 2, pp. 78–85, April 2016.
- [11] S. Barbera, K. I. Pedersen, C. Rosa, P. H. Michaelsen, F. Frederiksen, E. Shah, and A. Baumgartner, "Synchronized RACH-less handover solution for LTE heterogeneous networks," in *International Symposium on Wireless Communication Systems (ISWCS)*, Aug 2015, pp. 755–759.
- [12] L. C. Gimenez, P. H. Michaelsen, and K. I. Pedersen, "Analysis of data interruption in an lte highway scenario with dual connectivity," in *2016 IEEE 83rd Vehicular Technology Conference (VTC Spring)*, May 2016, pp. 1–5.
- [13] K. Yagyu, T. Nakamori, H. Ishii, M. Iwamura, N. Miki, T. Asai, and J. Hagiwara, "Investigation on mobility management for carrier aggregation in lte-advanced," in *Vehicular Technology Conference (VTC Fall), 2011 IEEE*, Sept 2011, pp. 1–5.
- [14] A. Ravanshid, P. Rost, D. S. Michalopoulos, V. V. Phan, H. Bakker, D. Aziz, S. Tayade, H. D. Schotten, S. Wong, and O. Holland, "Multi-connectivity functional architectures in 5g," in *2016 IEEE International Conference on Communications Workshops (ICC)*, May 2016, pp. 187–192.
- [15] F. Boccardi, J. Andrews, H. Elshaer, M. Dohler, S. Parkvall, P. Popovski, and S. Singh, "Why to decouple the uplink and downlink in cellular networks and how to do it," *IEEE Communications Magazine*, vol. 54, no. 3, pp. 110–117, March 2016.

Paper H

Throughput-Based Traffic Steering in LTE-Advanced HetNet Deployments

Lucas Chavarría Giménez, István Z. Kovács, Jeroen Wigard,
Klaus I. Pedersen

Published in
IEEE 82nd Vehicular Technology Conference (VTC Fall), 2015.

© 2015 IEEE

Reprinted with permission. The layout has been revised.

Abstract

The objective of this paper is to propose traffic steering solutions that aim at optimizing the end-user throughput. Two different implementations of an active mode throughput-based traffic steering algorithm for Heterogeneous Networks (HetNet) are introduced. One that always forces handover of the active users towards the cell offering the highest throughput, and a second scheme that aims at maximizing the systems sum throughput. Results show that the first option brings the best performance at the cost of more than three handovers per user per second for high-load cases. The second option offers slightly lower traffic steering gains at a considerably lower cost in terms of number of handovers. The gain in terms of increased average session throughput for the second option equals 32 % at low-load, 18 % at medium-load, and 7 % at high-load conditions. The gain in the fifth percentile user session throughput is generally higher, reaching values of 36 % and 18 % for the medium- and high-load conditions.

1 Introduction

The extensive deployment of Heterogeneous Networks (HetNets) calls for reliable user association strategies [1], as well as optimized traffic steering and load balancing solutions. Radio handovers based on Reference Signal Received Quality (RSRQ) already constitute a passive traffic steering solution in inter-frequency scenarios due to the sensitivity of the metric to load fluctuations [2]. However, this feature not always results in an efficient approach making it necessary to develop specific algorithms. Current traffic steering solutions modify the user distribution between layers by adjusting handover boundaries or forcing handovers and cell re-selections according to a certain Key Performance Indicator (KPI). A survey of inter-frequency and inter-Radio Access Technology (RAT) traffic steering techniques for idle and connected mode, as well as a fuzzy-logic algorithm for self-tuning handovers parametrization is presented in [3]. Cell load or Physical Resource Block (PRB) utilization are common KPIs utilized in several studies. For instance, [4] defines a version of a Mobility Load Balancing (MLB) scheme where a centralized server decides the optimal values of handover margins. [5] examines an admission control algorithm for performing cell load balancing in HetNets. On the other hand, [6] proposes traffic steering procedures based on the load-based metric Composite Available Capacity (CAC) [7]. Nevertheless, the process of reacting to a change in a certain KPI by adjusting handover parameters leads to slow algorithms based on time scales of several minutes or hours. An exhaustive overview of current load balancing and user association techniques is presented in [8]. It is predicted that future 5G networks will evolve towards ever more heterogeneous systems [9], favoring the exploration of new user association solutions.

Therefore, this article proposes fast traffic steering schemes in connected mode for Long-Term Evolution (LTE) Heterogeneous Networks (HetNet) scenarios which track the dynamics of the network by explicitly monitoring the instantaneous user throughput. For each user, the throughput that could be achieved on each of the neighboring cells is estimated. Afterwards, it is selected a set of candidate cells where the highest throughput is achieved. Furthermore, traffic steering decisions may be evaluated by predicting whether forcing the handover of the users may be beneficial

or not. Performance is evaluated by means of system level simulations.

The paper is organized as follows: Section 2 presents the scenario. Section 3 describes the proposed throughput-based traffic steering algorithms. Section 4 explains the simulation setup while Section 5 details the obtained results. Finally, Section 6 summarizes the concluding remarks.

2 System Model and Performance Indicators

2.1 Scenario Modeling

The studies are conducted under a LTE HetNet scenario characterized by a set of small cells distributed under the coverage of a macro layer. Macro and small cells layers are deployed on dedicated carrier frequencies. Both, free moving users and hot-spot users, are dropped randomly and move following random linear trajectories. Hot-spot model replicates areas with high traffic density by confining the users within a circular area around each small cell. More details on the user modeling can be found in [10]. Data traffic is generated following a Poisson arrival process with a packet call size modeled by a negative exponential distribution. To generate different load conditions in the system, the average inter arrival time is swept while the number of users remains constant. Radio Resource Control (RRC) idle mode is not considered and users are associated to only one cell at a time. A baseline case is defined with mobility parameters according to [10]. Thus, intra-frequency handovers are triggered by the A3 event and based on the Reference Signal Received Power (RSRP) metric. Inter-frequency handovers are also triggered by the A3 event but based on RSRQ. Inter-frequency measurements are triggered by the A2 event based on RSRQ.

2.2 Objectives and Performance Indicators

This paper is focused on proposing dynamic traffic steering solutions which try to improve the user throughput by modifying the user-cell association. Optimized performance with a minimum number of necessary traffic steering handovers is desirable due to their impact in signaling. Low rate of Radio Link Failures (RLF) is also preferred. The set of KPIs utilized in the evaluation is constituted by: five percentile and average session throughputs, number of traffic steering handovers and RLFs rate.

3 Throughput-Based Traffic Steering Algorithm

In order to develop a User Equipment (UE) throughput-based traffic steering algorithm it is necessary to estimate the throughput that each user could get on each of the cells of the system. In this section the mathematical framework of the throughput estimation and the methodology for extracting the target cells are presented. Afterwards, a simplified analysis of the gain that throughput-based traffic steering could achieve is detailed. The section concludes with a description of the algorithm implementation.

3.1 Signal-to-Interference and Noise Ratio Estimation

The Signal-to-Interference and Noise Ratio (SINR) for a user u connected to a certain serving cell $c_s \in C$, Γ_{u,c_s} , can be written as [11]:

$$\Gamma_{u,c_s} = \frac{P_{RX_{u,c_s}}}{\sum_{k=1, k \neq c_s}^C \rho_k P_{RX_{u,k}} + N} \quad (\text{H.1})$$

Where C is the number of cells in the network, $P_{RX_{u,c_s}}$ is the wide-band received power — assuming full transmitted power — by the user u from the serving cell c_s , N is the noise power and $\rho_k \in [0, 1]$ models the resource utilization of each interfering cell. In this model, ρ_k scales the interference depending on the traffic conditions: as soon as there is one or more active users in a cell, all available Physical Resource Blocks (PRBs) are assumed to be scheduled and full interference is considered with $\rho_k = 1$. On the contrary, an empty cell generates no interference with $\rho_k = 0$. By utilizing the physical layer measurements performed at the UE, this formula can be also used to estimate the SINR of all cells discovered by each user even if it is not the current serving cell.

3.2 Throughput Estimation

The mapping of the estimated achievable throughput of a user u in a cell c ($\hat{r}_{u,c}$) in terms of the estimated SINR ($\hat{\Gamma}_{u,c}$) can be done by means of an adjusted Shannon formula for the capacity. Assuming equal sharing of resources between all users, the equation can be written as follows:

$$\hat{r}_{u,c} = W_c \log_2 \left(1 + \hat{\Gamma}_{u,c} \right) \cdot \frac{1}{N_c + 1} \quad [bps] \quad (\text{H.2})$$

Where W_c is the cell bandwidth and N_c is the number of active users in the cell. The term $N_c + 1$ predicts how the long-term averaged UE throughput varies when adding a new user to the current number of active users in the cell. In a system with a total number of N active users, the estimation of the throughput for all UEs and all cells can be grouped in a matrix, \mathbf{R} , of dimensions $N \times C$:

$$\mathbf{R} = \begin{bmatrix} \hat{r}_{1,1} & r_{1,2} & \hat{r}_{1,3} & \dots & \hat{r}_{1,C} \\ \hat{r}_{2,1} & 0 & r_{2,3} & \dots & \hat{r}_{2,C} \\ \hat{r}_{3,1} & \hat{r}_{3,2} & r_{3,3} & \dots & \hat{r}_{3,C} \\ \dots & \dots & \dots & \dots & \dots \\ r_{N,1} & \hat{r}_{N,2} & 0 & \dots & \hat{r}_{N,C} \end{bmatrix} \quad (\text{H.3})$$

Where non hatted elements refer to the experienced throughput in the current serving cell. If the UE is not able to measure a certain cell, the correspondent element is marked with a zero.

3.3 Target Cells Selection

Once the matrix \mathbf{R} has been created, the candidate target cells can be extracted. In order to reduce the algorithm's complexity and possible delays when selecting the final target cell for each user in practical networks, the set of candidates is limited.

Hence, for each active user all cells are ranked and the 2 best cells in terms of estimated throughput are identified: the cell where the user u achieves the maximum estimated throughput, $t_{u,1}$, and the cell where the user u achieves the second maximum throughput, $t_{u,2}$. This can be expressed as:

$$\begin{aligned} t_{u,1} &= \arg \max_j \{\hat{r}_{u,j}\} \\ t_{u,2} &= \arg \max_{k \neq j} \{\hat{r}_{u,k}\} \end{aligned} \quad (\text{H.4})$$

All candidate cells for all active users can be grouped in a new matrix \mathbf{T} of size $N \times 2$, expressed as:

$$\mathbf{T} = \begin{bmatrix} t_{1,1} & t_{1,2} \\ t_{2,1} & t_{2,2} \\ t_{3,1} & t_{3,2} \\ \dots & \dots \\ t_{N,1} & t_{N,2} \end{bmatrix} \quad (\text{H.5})$$

In case a UE is not able to measure any other cell but the current server, the second target cell is marked with 0.

3.4 Theoretical Analysis of the Gain

A simplified single-user traffic steering decision is analyzed to investigate the potential gain that can be obtained when a user is served by cell A and it is steered towards cell B . Both, serving and target cells, operate with the same bandwidth. Full interference ($\rho_k = 1$) is assumed. According to (H.1), the SINR in the serving cell and the estimated SINR in the target can be calculated as:

$$\Gamma_{u,A} = \frac{P_{RX_{u,A}}}{\sum_{k=1, k \neq A}^C P_{RX_{u,k}} + N} \quad (\text{H.6})$$

$$\hat{\Gamma}_{u,B} = \frac{P_{RX_{u,B}}}{\sum_{k=1, k \neq B}^C P_{RX_{u,k}} + N} \quad (\text{H.7})$$

Let N_A and N_B be the number of active users in cell A and B respectively before the traffic steering action. Following (H.2), the throughput in both, serving and target cell follows:

$$r_{u,A} = W_c \cdot \log_2(1 + \Gamma_{u,A}) \cdot \frac{1}{N_A} \quad (\text{H.8})$$

$$\hat{r}_{u,B} = W_c \cdot \log_2(1 + \hat{\Gamma}_{u,B}) \cdot \frac{1}{N_B + 1} \quad (\text{H.9})$$

The ratio of these two estimates the throughput gain when steering the user:

$$\frac{\hat{r}_{u,B}}{r_{u,A}} = \frac{N_A}{N_B + 1} \cdot \frac{\log_2\left(1 - \frac{P_{RX_{u,B}}}{\sum_{k=1}^C P_k + N}\right)}{\log_2\left(1 - \frac{P_{RX_{u,A}}}{\sum_{k=1}^C P_k + N}\right)} \quad (\text{H.10})$$

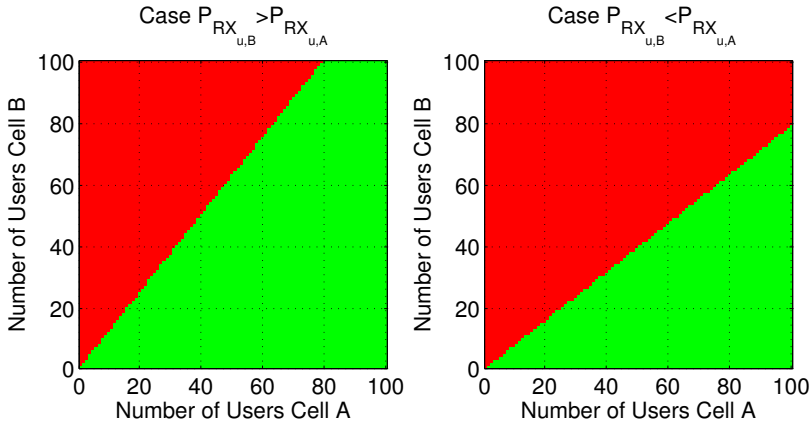


Fig. H.1: Potential gain regions when moving one user from cell A to cell B as a function of the number of active users in both cells. The red and green colors refer to the regions of losses and gain respectively.

From (H.10) it can be seen that the achievable gain depends on the ratio between the number of active UEs in the serving and target, and the received power by the user from both cells. Figure H.1 shows the different regions of gain for the cases when the received power from the target is higher than the serving and vice-versa. The red area points out the region where the quotient $\frac{\hat{r}_{u,B}}{\hat{r}_{u,A}} < 1$, whereas the green color refers to the cases where $\frac{\hat{r}_{u,B}}{\hat{r}_{u,A}} > 1$. When the received power from serving and target cells is the same, the gain and loss regions are symmetric. In such a case, to obtain any gain the number of users in the target cell should be lower than the number of users in the serving. If the received power from the target cell is lower than the one from the current serving, the gain region shrinks. However, the opposite effect occurs when the target cell is stronger than the current serving, e.g. when handover a user from the serving macro to a pico cell on the vicinity. In this case, a gain is obtained even if there are more users in the target cell than in the serving. This simplified analysis does not take into account that a third cell C may simultaneously steer users towards cell B possibly reducing the gain.

3.5 Traffic Steering – Option 1

Traffic Steering – Option 1 is an aggressive method which consists of forcing the handover of the active users towards the cell where the estimated throughput is higher — i.e. towards the first target t_1 — each time the algorithm is triggered. This approach does not take into account how existing users in the target cell may be influenced. If many active users select the same target cell at a given time, the obtained throughput may differ from the estimated by (H.2) since only one additional user is taken into account in the equation. Therefore, this one can be considered as a partially-blind option where the consequences of the traffic steering process are not explicitly taken into account.

3.6 Traffic Steering – Option 2

In the second approach, the users are steered if, and only if, it is predicted that the sum of the estimated throughput of all active users of the entire system increases after the offloading process. With this condition, the method tries to reduce unnecessary traffic steering handovers. This task can be addressed by solving an optimization problem where the sum of all instantaneous user throughputs is maximized according to the following objective function:

$$r_{max} = \max \left\{ \sum_{u=1}^N r_{u,c_i} \right\} \quad (\text{H.11})$$

Where $c_i \in \mathcal{C}$. r_{u,c_i} is the instantaneous achievable throughput by the user u when connected to cell c_i . r_{max} constitutes the observed metric. The matrix \mathbf{T} previously defined offers to each user two different candidate cells where to be steered. As a result, three possible disjoint decisions for this implementation are proposed: 1) to steer all active users to the first target, 2) to steer the users to a specific combination of first and second targets, or 3) to not steer any user at all. One, and only one of these three options is selected depending on which one maximizes Equation H.11. In order to select the best option, it is necessary to predict what is the impact of each decision by an iterative process where different versions of the matrix \mathbf{R} and the metric r_{max} are calculated taking into account the user association of each possible case. In total, three iterations are needed. A full step by step description of this implementation can be seen in Algorithm 1.

Algorithm 1 Traffic Steering – Option 2

```

Calculate initial metric  $r_{max_0}$ 
For each active user estimate  $\hat{\Gamma}_{u,c}$  and  $\hat{r}_{u,c}$ 
Create initial  $\mathbf{R}_0$  matrix
Extract target cells matrix  $\mathbf{T}$ 
Calculate  $\mathbf{R}_1$  having each user connected to its first target cell,  $t_1$ 
Update metric  $r_{max_1} = \max \left\{ \sum_{n=1}^N \hat{r}_{n,t_1} \right\}$ 
if  $r_{max_1} > r_{max_0}$  then
    Handover each user to its  $t_1$ 
else
     $M_1 =$  Users which get better throughput in  $t_1$ 
     $M_2 =$  Users which do not get better throughput in  $t_1$ 
    Calculate  $\mathbf{R}_2$  with  $M_1$  users in its  $t_1$  and  $M_2$  users in its  $t_2$ 
    Update metric  $r_{max_2} = \max \left\{ \sum_{i=1}^{M_1} \hat{r}_{i,t_1} + \sum_{j=1}^{M_2} \hat{r}_{j,t_2} \right\}$ 
    if  $(r_{max_2} > r_{max_1})$  and  $(r_{max_2} > r_{max_0})$  then
        Connect  $M_1$  users to first target
        Connect  $M_2$  users to second target
    end if
end if

```

The initial state is given by the calculation of the observed metric with all the active users connected to their current serving cell and the creation of the matrix which contains the estimation of the achievable user throughput in the neighboring cells. From this matrix, the sets of candidate target cells per user are extracted. Subsequently, an evaluation phase starts and, considering all users connected to their first target cell,

an updated version of the estimated user throughput matrix and the observed metric are calculated. If the updated version of the metric results in bigger value than the initial one, the algorithm finishes by steering all active users to their first candidate cell. Otherwise, the algorithm selects which users perceive a loss in their throughput when connected to the first target cell. Let's assume that over N active users M_1 get better throughput and M_2 users do not get any improvement being connected to the first candidate. The algorithm creates a new estimated user throughput matrix with the M_1 users steered to their first target, and the M_2 users to their second one. With this information, a new value of the metric is calculated. If, in this case, the metric is bigger than the last two, this user association is selected. Otherwise, since connecting all users to the first target or to a specific combination of first and second target does not bring any benefit, the algorithm cancels any attempt of steering them.

4 Performance Evaluation

The performance of the proposed traffic steering algorithms are evaluated by means of extensive dynamic system level simulations in the HetNet scenario 2a defined by the 3rd Generation Partnership Project (3GPP) in [12]. The hexagonal network is characterized by 21 macro cells and 42 small cells randomly deployed, following a ratio of 2 small cells per macro area. The initial conditions of the simulation are defined by 1/3 of the users dropped on each macro coverage area while the remaining 2/3 are confined within circular areas of 50 m radius around each small cell. In total, 30 users per macro area are deployed. All users are initially connected to the cell with highest RSRP regardless of the cell type. For each simulation time-step the down-link SINR is calculated taking into account the propagation characteristics of all links. The SINR-throughput mapping is according to an abstract layer which includes the effect of scheduling and link adaptation. At the end of each step the KPIs are collected. Users are moving in different set of simulations at 3 km/h or 50 km/h.

The offered load per macro area varies from 18 Mbps (low-load) to 34 Mbps (high-load). The whole simulation time is 1000 s or 50 s for user speeds of 3 km/h or 50 km/h respectively. Three simulation cases are investigated. First, a baseline scenario is defined in order to explore the performance when inter-frequency handovers triggered by the A3 event and based on RSRQ balance the load between both layers. In this case, handover parametrization follows recommendations from [10]. Traffic Steering – Option 1 and 2 define the other two simulation cases. Whenever any traffic steering implementation is enabled, mobility parameters are set to a more relaxed configuration to avoid the radio handovers redoing traffic steering decisions. This configuration also targets to minimize RLFs for users in bad conditions. The performance is evaluated by comparing the three cases. A complete definition of the simulation parameters is shown in Table H.1. The utilized system level simulator has been used in various 3GPP studies. As a reference, additional HetNet mobility performance results produced by the simulator can be found in [13].

Table H.1: Simulation Parameters

Parameter	Value
Scenario	3GPP HetNet Scenario 2a [12]
Number of macro cells	21
Number of pico cells	42 (2 small cells per macro area)
Macro Inter-Site Distance (ISD)	500 m
Frequencies	Macro: 1800 MHz. Pico: 2600 MHz
Bandwidth	Macro: 10 MHz. Pico: 10 MHz
Transmitted Power	Macro: 46 dBm. Pico: 30 dBm
Number of UEs	630 (30 per macro area)
Users speed	3 km/h or 50 km/h
Packet call size	Negative exponential distributed with 10 Mbits mean
Intra-Frequency Mobility	Baseline: A3 RSRP-based. 2dB offset. 160 ms TTT TS ON: A2 RSRQ-based. -16 dB thr. 480 ms TTT
Inter-Frequency Mobility	Baseline: A3 RSRQ-based. 4dB offset. 160 ms TTT TS ON: A2 RSRQ-based. -16 dB thr. 480 ms TTT
Inter-Frequency Meas	A2 RSRQ-based. -10 dB threshold
Simulation Time	1000 s (3 km/h) or 50 s (50 km/h)
Simulation Time Step	50 ms
Triggering Period	TS - Option 1: 50ms. TS - Option 2: When necessary

5 Simulation Results

Figure H.2 shows the average session throughput of all users moving at 3 and 50 km/h in different offered traffic conditions per macro area. Although the algorithms base

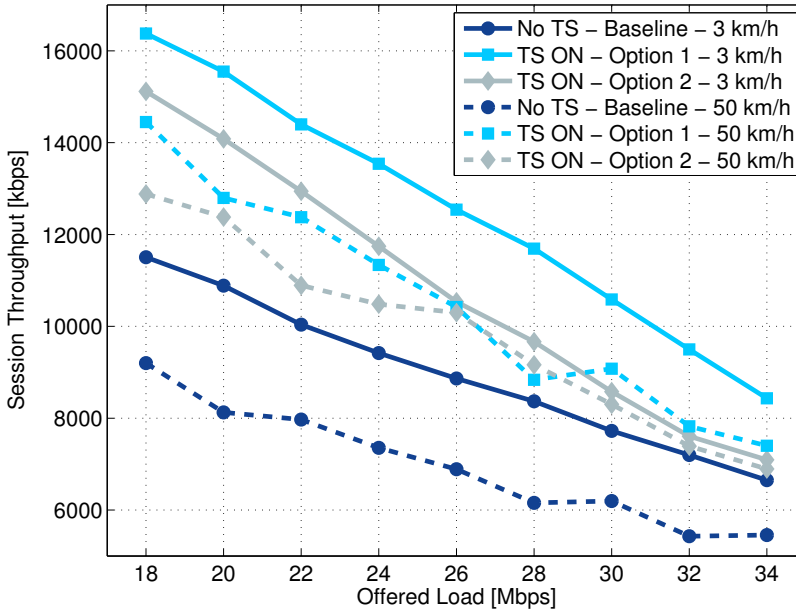


Fig. H.2: Averaged UE session throughput for each simulated offered load case with users moving at 3 and 50 km/h.

their decisions on the instantaneous user throughput, the impact to the end-user is analyzed by examining the session throughput. The best performance is given by Traffic Steering – Option 1, closely followed by Option 2. As the different simulated speed cases are under the same handover parameterization, the performance of the baseline case drops when increasing the user speed. Despite the speed difference, traffic steering brings gains in both cases. The observed fluctuations at 50 km/h are due to the limited number of collected samples as the simulation is set to 50 s. Nevertheless, a clear tendency can be extracted from the chart.

Figure H.3 depicts the session throughput gains for both traffic steering implementations, compared to the baseline case, and the number of traffic steering handovers for both methods. As Traffic Steering – Option 1 tracks the fast traffic fluctuations of the network by always trying to obtain the best user throughput, this implementation achieves the best gains. However, this performance comes with the high price of performing a large number of handovers. On the other hand, by applying the condition of moving users, if and only if, there is an augmentation in the sum of the user throughput, Traffic Steering – Option 2 reduces considerably the number of necessary handovers. Although this improvement in signaling has a cost in terms of achievable gain, the results do not show big losses in performance. For instance, when users are moving at 3 km/h in a system with 26 Mbps of offered load, a reduction of 41 % in the number of traffic steering handovers implies only a reduction of 22 % point in the session throughput gain. As a reference, the maximum number

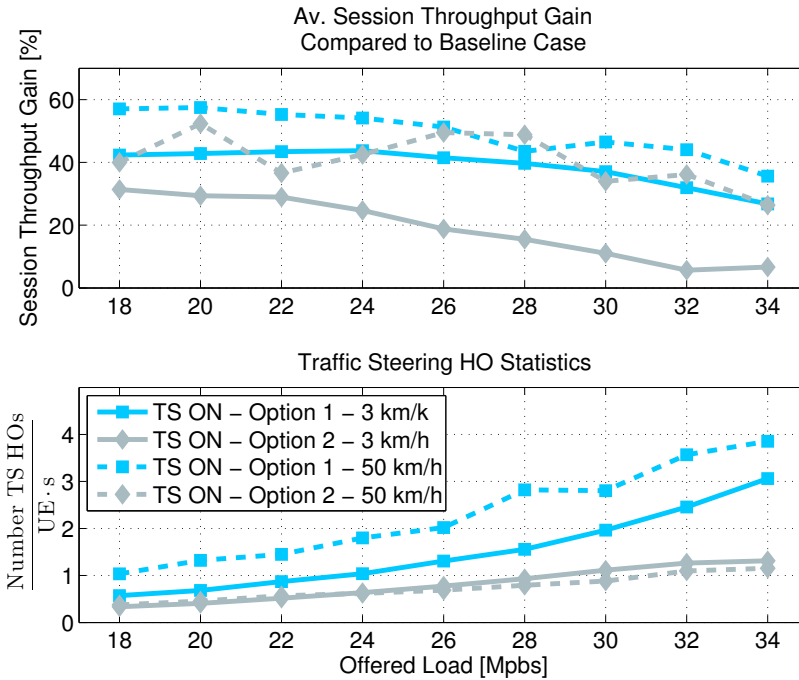


Fig. H.3: UE session throughput gains and number of traffic steering handovers for each simulated offered load case with users moving at 3 and 50 km/h.

of handovers in the baseline case is observed at low-load with an absolute value of 0.37 handovers per user per second. Regarding the gain of the fifth-percentile session throughput at 3 km/h, the values obtained for Option 1 and 2 are: 107 % and 69 % for low-load, 98 % and 36 % for medium-load (26 Mbps), and 90 % and 18 % for high-load conditions.

The average macro and pico PRB utilization for 3 km/h case is depicted in Figure H.4. As it can be noticed, for the baseline case, the PRB utilization tends to be equalized in both layers as the load increases. This is due to the fact that the RSRQ radio handovers already steer some users towards the pico layer. However, for high-load cases, the macro layer is close to overload. Traffic steering decreases considerably the overall load of the system bringing gains in the user throughput and hence, reducing the duration of each session. Traffic Steering – Option 1 brings the biggest gain due to the elevated number of handovers however, the contribution of Option 2 with less signaling rate, is worthy to highlight. Some RLFs are observed when users are moving at 50 km/h in the baseline case nevertheless, they are eliminated whenever any of the traffic steering implementations are switched-on.

5.1 Throughput Estimation Error

As both of the considered traffic steering algorithms are based on throughput estimations, the accuracy of these have been assessed as well. For the sake of simplicity, we here present the throughput estimation accuracy for Traffic Steering – Option 2, where the sum throughput is estimated. Let us denote the estimated sum throughput as \hat{r}_{sum} and the real experienced sum throughput after performing the traffic steering decisions as r_{sum} . Given those, the relative estimation error is expressed as $\epsilon = \frac{\hat{r}_{sum} - r_{sum}}{r_{sum}}$. During the simulations, statistics for ϵ reveals that the sum throughput estimate is unbiased as the sample mean of ϵ is practically zero. Furthermore, the standard deviation of the relative estimation error is found to be rather modest, taking values of 2.1 % and 2.9 % for 3 km/h and 50 km/h respectively.

6 Conclusions

In this paper two different methods of a throughput-based traffic steering algorithm are proposed. One that forces the handover of the active users on each time step towards the cell where the highest achievable throughput is predicted, and a second method which forces the handover if, and only if, an augmentation in the sum of the overall user throughput is estimated. Exhaustive system level simulations of a dual-layer HetNet scenario are conducted to evaluate their performance. Results show that the first scheme achieves better performance in terms of the average user session throughput and overall PRB utilization at the cost of a large numbers of handovers. More promising is the second implementation as it reduces the number of handovers by 41 %, while still offering session throughput gains of 19 % for medium-load at 3 km/h.

Given the attractive gains of the presented traffic steering algorithms, it is suggested to further study the details of the required inter-Evolve Node B (eNodeB) signaling, the related eNodeB-to-UE signaling for the handovers, as well as the impact on the associated data interruption times. It is also recommended to analyze the time complexity of the algorithms and its applicability in practical cellular networks with different user traffic requirements.

References

- [1] J. Andrews, “Seven ways that HetNets are a cellular paradigm shift,” *IEEE Communications Magazine*, vol. 51, no. 3, pp. 136–144, March 2013.
- [2] P. Fotiadis, “Load-based traffic steering in heterogeneous LTE networks: A journey from Release 8 to Release 12,” Ph.D. dissertation, 2014.
- [3] P. Munoz, R. Barco, D. Laselva, and P. Mogensen, “Mobility-based strategies for traffic steering in heterogeneous networks,” *IEEE Communications Magazine*, vol. 51, no. 5, pp. 54–62, May 2013.
- [4] J. Suga, Y. Kojima, and M. Okuda, “Centralized mobility load balancing scheme in LTE systems,” in *8th International Symposium on Wireless Communication Systems (ISWCS)*, Nov 2011, pp. 306–310.

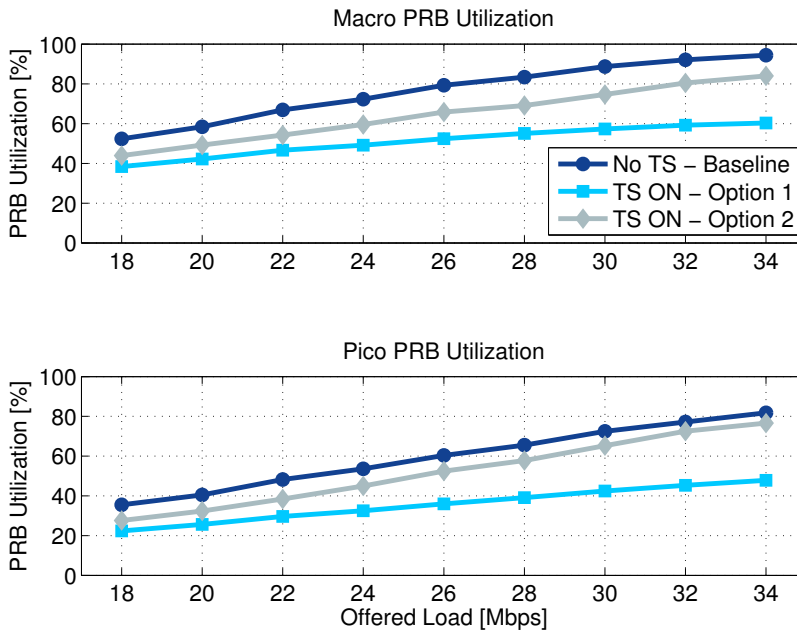


Fig. H.4: Macro and Pico PRB utilization. 3 km/h simulation case.

- [5] S. Eduardo, A. Rodrigues, A. Mihovska, and N. Prasad, "Cell load balancing in heterogeneous scenarios: A 3GPP LTE case study," in *3rd International Conference on Wireless Communications, Vehicular Technology, Information Theory and Aerospace Electronic Systems (VITAE)*, June 2013, pp. 1–6.
- [6] P. Fotiadis, M. Polignano, L. Chavarria, I. Viering, C. Sartori, A. Lobinger, and K. Pedersen, "Multi-layer traffic steering: RRC idle absolute priorities & potential enhancements," in *IEEE 77th Vehicular Technology Conference (VTC Spring)*, June 2013, pp. 1–5.
- [7] *3GPP Technical Specification (TS) 36.423. Evolved Universal Terrestrial Radio Access Network (E-UTRAN); X2 Application Protocol (X2AP)*, v 12.4.2, February 2015.
- [8] J. Andrews, S. Singh, Q. Ye, X. Lin, and H. Dhillon, "An overview of load balancing in HetNets: old myths and open problems," *IEEE Wireless Communications*, vol. 21, no. 2, pp. 18–25, April 2014.
- [9] J. Andrews, S. Buzzi, W. Choi, S. Hanly, A. Lozano, A. Soong, and J. Zhang, "What will 5G be?" *IEEE Journal on Selected Areas in Communications*, vol. 32, no. 6, pp. 1065–1082, June 2014.
- [10] *3GPP Technical Report (TR) 36.839. Evolved Universal Terrestrial Radio Access (E-UTRA); Mobility enhancements in heterogeneous networks (Release 11)*, v 11.1.0, December 2012.

- [11] I. Viering, M. Döttling, and A. Lobinger, "A mathematical perspective of self-optimizing wireless networks," in *IEEE International Conference on Communications (ICC)*, June 2009, pp. 1–6.
- [12] *3GPP Technical Report (TR) 36.872. Small cell enhancements for E-UTRA and E-UTRAN - Physical layer aspects (Release 12)*, v 12.1.0 , December 2013.
- [13] S. Barbera, P. Michaelsen, M. Saily, and K. Pedersen, "Mobility performance of LTE co-channel deployment of macro and pico cells," in *IEEE Wireless Communications and Networking Conference (WCNC)*, April 2012, pp. 2863–2868.

Part V

Additional Studies and Collaborations

Additional Studies and Collaborations

This part of the thesis brings together the most relevant findings from some of the articles that were published in collaboration with other research groups during the course of the PhD studies.

The level of participation differs from article to article. In some of the papers the PhD student has collaborated actively by running simulations, analyzing results, performing measurements, and writing part of the content. However, in others, the participation has been limited providing feedback on the development of the work. Therefore, the PhD student cannot take credit for the whole content of these articles. The intention of this part is to briefly present the main findings within the framework of mobility in cellular networks. Consequently, the papers are not integrated within the main core of this dissertation. However, the full content of the articles can be found in Appendix A for additional reference.

Comparison and Extension of Existing 3D Propagation Models with Real-World Effects Based on Ray-Tracing (Collaboration 1)

This journal article proposes propagation models that include different propagation effects such as the impact of the base station antenna tilt and the multi-floor height gain. The models are based on the analysis of outdoors and indoors path-loss maps predicted using a ray-tracing tool in an urban scenario in Germany.

The most common procedure for computing the received power inside buildings at different floors begins with the calculation of the received power at street level. Afterwards, a gain of certain dBs per floor is applied to calculate the received power at a certain height. Commonly, a constant gain of 0.6 dB/m is used, with a constant floor height of approximately 3.1 m per floor [1]. In other words, a constant height gain of 1.86 dB/floor is applied. This gives the received power outside the building at an specific altitude. To compute the received power indoors it is necessary to subtract the penetration loss due to the outside wall and an additional losses of 0.6 dB/m, according to the distance between the UE and the outside wall. While this method provides an understanding of how the signal propagates at different floors, there are

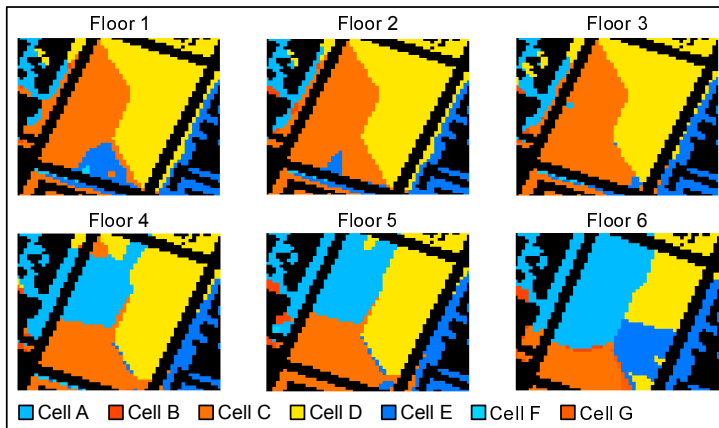


Fig. 5.1: Multi-floor cell dominance area in a real urban scenario predicted by a ray-tracing tool [2].

some limitations that should be considered when applying the model for mobility purposes.

The model above provides different values of received power from each cell among stories in absolute terms. However, due to the constant nature of the height gain, the received power between cells in relative terms is exactly the same for all floors. Consequently, this height gain model predicts exactly the same cell coverage area at each floor. Moreover, since the model takes the street level as a reference, this method concludes that indoor users in upper stories experience the same cell coverage area map than those located at the ground floor.

Instead of applying the constant height gain model, this journal uses a ray-tracing tool for predicting the cell coverage in a multi-floor scenario. Figure 5.1 illustrates the cell dominance area produced by path loss maps predicted at different heights. Concretely, the figure shows the coverage areas of different cells inside a building for each floor. As can be seen, two users positioned at the same location, but in different floors, are not necessarily connected to the same cell. The coverage area of each cell changes among stories, producing a different best-server map for each floor. The different heights of the surrounding buildings produces changes in the LOS and NLOS conditions when transiting from one floor to another. As a result, some cells may vanish whereas new cells may appear dominating the coverage map.

From these studies, it is concluded that the buildings layout and the changes in the LOS probability among floors result in a non-constant height gain among stories. Due to these variations, the ground-level network planning is not sufficient for predicting and understanding the user-association and the mobility at different altitudes for both, outdoors and indoors scenarios.

The results also suggest some mobility challenges for the upcoming applications. Unmanned aerial vehicles in smart cities or elevated railways are some examples of use cases that can be impacted by these effects. A user traveling in an elevated train may experience more handovers than those that the mobile operator registered during the

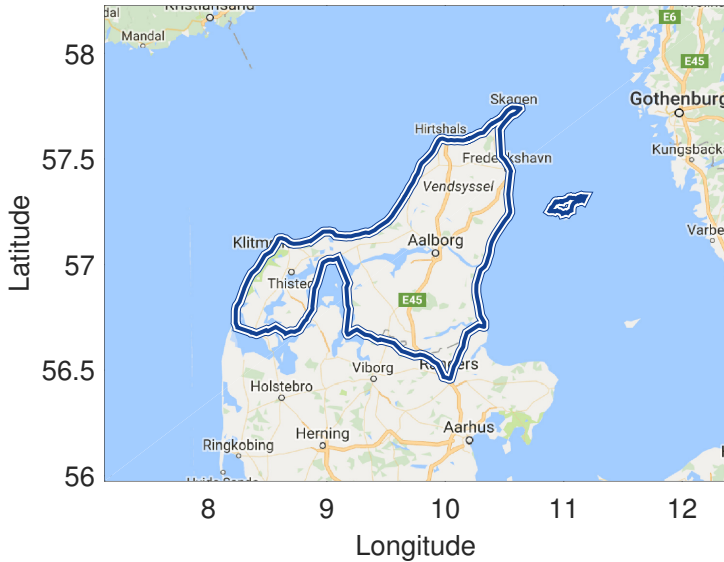


Fig. 5.2: Illustration of the measurements area in Northern Jutland.

drive tests at street level. Moreover, a drone connected to the cellular network that ascends or descends vertically must be able to perform fast handovers and deal with new interfering cells that appear due to the changes in the LOS probability.

From LTE to 5G Connected Mobility (Collaboration 3)

This magazine article evaluates how operational LTE networks perform compared with the initial LTE design requirements. To this end, measurements collected via 19000 km of drive tests in the region of Northern Jutland (Denmark) are processed. Among other KPIs, the magazine is focused on analyzing samples of the LTE handover execution time measured under the operational networks deployed by four Danish mobile operators.

The measurements area is illustrated in Figure 5.2. The article extends the LTE studies conducted in Part II to a broader variety of scenarios, covering networks deployed in rural, suburban, and urban areas. The handover execution times were measured at different speeds (from 30 to 130 km/h) in urban streets, rural roads, and highways. A total of four smart-phones were used for the measurements (one per operator) and configured to periodically perform File Transfer Protocol (FTP) transfers in both, up-link and down-link. When finalizing an FTP data transfer, each phone was set to stay idle for 10 seconds. To emulate a real operational behavior, the phones were not restricted to any frequency nor technology. Moreover, the phones were allowed to perform carrier aggregation (CA) operations where available.

Figure 5.3 shows the cumulative density function (CDF) of the measured handover execution time split among operators. By the time the measurements were

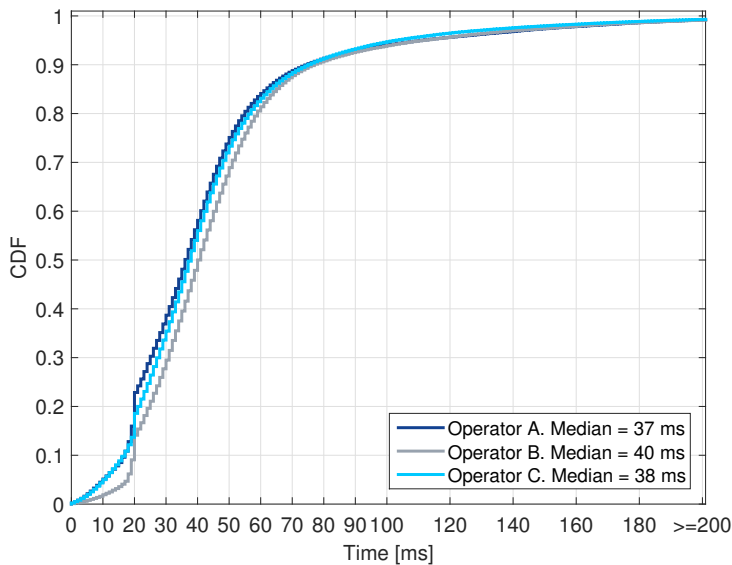


Fig. 5.3: CDF of the handover execution time measured during the drive tests, split among mobile operators [3].

performed, two of the operators shared the same network infrastructure. Therefore, the samples collected under the networks of those two operators were combined into one. The measurements represent a combination of different LTE releases, handover types (intra-/inter-frequency and intra-/inter-site), network deployments, and scenarios. Whereas the measured median values of the handover execution times met the LTE design target of 30-60 ms, the analyzed networks were far from meeting the 5G requirements. As can be seen, an important percentage of the samples registered times larger than 100 ms. Moreover, for 1 % of the samples the execution time is found to be larger than 200 ms, reaching a maximum value of approximately 5-6 s. These extreme cases represent handover failures.

The parametrization of the network was concluded to be the reason why it took several seconds for the phone to declare the failure and initiate the connection re-establishment. The analysis of the RRC messages revealed that the timer used for detecting handover failures (T_{304}) was configured to 1-2 s, depending on the operator and target cell. Moreover, the timer for the connection re-establishment (T_{311}) was set to 3-5 s. Consequently, the operators allowed the UE to spend up to 6 s performing the handover. This configuration provides the UE sufficient time for recovering from problems during the handover (e.g. poor radio-conditions towards the target cell), thereby reducing the handover failure statistics of the network. However, with this parametrization the operators were also allowing a data interruption time up to 6 s.

These results indicate that apart from design requirements and standardized features, the configuration the operators use in the network plays an important role in the experienced handover execution time, the data interruption time, and in the overall mobility performance. Naturally, there is a trade-off between the maximum time

allowed for the handover execution and the number of failures. Lowering the UE timers constitutes a more aggressive option that may increase the number of handover failures and signaling overhead in the network. Nonetheless, it also allows the UEs to perform earlier re-establishments, thereby reducing the data interruption.

Measurement-based Evaluation of the Impact of Large Scale Vehicle Shadowing on V2X Communications (Collaboration 4)

The studies presented in Part II showed that the utilized system-level simulator was not able to completely replicate the influence of surrounding vehicles in the signal propagation. Although this was not a critical issue for studying the number of mobility events relative to different simulation cases, the signal blockage produced by vehicles is an important effect that cannot be disregarded for evaluating the absolute number of events and their precise locations.

To understand the effect of surrounding vehicles in the signal propagation, this article presents measurements and ray-tracing predictions of the shadowing produced by large vehicles in vehicle-to-vehicle (V2V) and vehicle-to-infrastructure (V2I) communications. The measurements considered several transmitters deployed at different locations, emulating other vehicles and road-side-units (RSUs). The large scale vehicle used for obstructing the signals was a truck. Samples of the received power from the different transmitters were collected varying the position of the truck relative to the receiver throughout an area that replicates a 4-lanes road scenario.

The obtained results showed that the impact of being obstructed by a large vehicle was more significant for V2V communications than for V2I. For instance, for V2I the minimum shadowing value was measured around 21-23 dB, while in the V2V case, the minimum registered value was 27 dB.

The analysis of the measurements revealed that the height of the transmitters, the materials used in the truck, the reflections in the ground, and the number of lanes, produced a signal propagation footprint that should be considered for mobility studies. The shadow produced by large vehicles changed the LOS conditions of the scenario, modifying the received signal from the different cells, and also altering the number and location of the mobility events.

This effect constitutes a challenge, particularly in the highway. For example, let's consider the dual connectivity scenario of Part III and a car that overtakes a convoy of trucks. Due to the 21-23 dB of shadowing produced by the trucks, and the high-speed of the vehicles, the user traveling in the car (or the car itself if considering self-driving cars) will experience a fast degradation of the link served by the small cell. This situation may lead not only to a large number of SeNB removals and additions, but also to undesired RLFs that should be avoided by guarantying a fast transition between cells.

References

- [1] J.-E. Berg, *COST Action 231. Digital mobile radio towards future generation systems. Final report. Propagation Prediction Models. Building Penetration.* European Commission. EUR 18957, 1999.
- [2] D. W. Kifle, L. C. Gimenez, B. Wegmann, I. Viering, and A. Klein, "Comparison and extension of existing 3D propagation models with real-world effects based on ray-tracing," *Wireless Personal Communications*, vol. 78, no. 3, pp. 1719–1738, 2014.
- [3] M. Lauridsen, L. C. Gimenez, I. Rodriguez, T. B. Sørensen, and P. Mogensen, "From LTE to 5G for connected mobility," *IEEE Communications Magazine*, March 2017.

Part VI

Conclusions

Conclusions

1 Summary of the Main Findings

The current development of the fifth-generation (5G) new radio (NR) calls for new stringent and ambitious design requirements in terms of mobility performance. Concretely, 5G networks should support seamless handovers between cells with zero-data interruption time. This zero mobility disruption should be guaranteed for both pedestrian users in urban environments and for users in high-mobility scenarios moving at speeds up to 500 km/h [1].

In order to understand and characterize what current networks can achieve, the first part of this dissertation was focused on analyzing measurements of the mobility performance under an operational LTE network deployed by a major Danish operator. The studies focused on an urban and in a highway scenario. The analysis of the measurement results showed a good LTE macro mobility performance with a low rate of failures. The results also revealed that current networks are far from fulfilling the requirement of zero-data interruption at handovers. The measured median handover data interruption time meets the maximum values of [40-60] ms set by the International Telecommunication Union (ITU) for LTE [2]. However, a non-negligible amount of samples revealed values larger than 100 ms, constituting the handover data interruption time one of the main challenges to address in these studies.

The field-measurements were additionally used for calibrating and validating the system-level simulator used during the entire studies. Therefore, it was necessary to provide new features and capabilities to the system-level simulator in order to model the exact real-scenarios where the measurements were performed. This modeling included the capability of managing operational network parametrization and buildings and street layouts. Furthermore, a three-dimensional (3D) version of each analyzed scenario was replicated in a ray-tracing tool in order to predict the signal propagation considering additional effects than statistical models can provide in the studied environments. The generated path loss maps were also imported into the simulator. A one-to-one comparison of the measurements and simulations results revealed that the methodology for simulating real-scenarios provided trustful mobility performance results comparable to what was experienced in the field.

After identifying the main issues in the LTE mobility performance and validating the output of the system-level simulator, the next step was to analyze the mobility in LTE-Advanced (LTE-A) scenarios with dual connectivity (DC). The evaluation was

performed by means of a sensitivity analysis in 3GPP scenarios and in more sophisticated urban areas. From the detailed analysis of the results, it was observed that whereas simulations of generic 3GPP scenarios are a valuable technique for an initial evaluation of features in a cellular network, the standardized scenarios do not include the explicit modeling of building and street layouts, thereby lacking of specific radio-propagation conditions such as the street canyon and the corner effect that play an important role in the mobility performance. Therefore, it is concluded that 3GPP studies should be complemented with the explicit modeling of site-specific scenarios for fully characterize the mobility performance.

The highway stretch studied in the field-measurements was selected for analyzing the mobility data interruption time in LTE-A with DC. The scenario imported in the system-level simulator was upgraded with an extra layer of small cells deployed at both sides of the highway as road-units. Two different connectivity modes were studied: single-node connectivity and DC. The analysis of the results showed that for single-node connectivity a user traveling along the highway stretch suffered from data interruption during approximately 5 % of the duration of the trip. For implementing DC in the network, 3GPP standardized two user-plane architectures under the name of secondary cell group (SCG) and split bearer. The system-level simulations allowed the formulated hypothesis regarding the variability of the data interruption time with the adopted architecture for DC to be validated. The results demonstrated that whereas SCG architecture increased the overall interruption up to 7 % of the traveling time, split bearer architecture offered all the benefits of aggregating additional links with a data disruption that lasted only 0.8 % of the duration of the trip. However, the data interruption still persisted, leading to the conclusion that LTE-A DC is not sufficient for meeting the upcoming 5G requirements. The benefits brought by DC came also with the cost of an increased number of mobility events, and a higher signaling overhead, constituting a new additional issue to be addressed in this thesis. This issue is particularly important in the highway scenario where the number of mobility events is much higher due to the high-speed of the users.

To reduce the amount of signaling, this thesis analyzed the benefits of deviating from traditional network-controlled mobility, towards a UE autonomous mobility approach for the small-cell layer in the highway. With this approach, the Radio Resource Control (RRC) signaling for SeNB additions and SeNB changes was completely eliminated. For the SeNB release, the amount of RRC messages were reduced by 33 % compared to the traditional implementation. Moreover, the amount of signaling in the back-haul was reduced by 50 %, 42 % and 33 % for each SeNB addition, change and release, respectively. The UE autonomous mobility for DC requires the small cells to be prepared in advance. Instead of preparing all the cells in the highway, this thesis proposed a method that takes advantage of the linear topology of the scenario, where a window of prepared cells surrounds the UE and follows its movement. The results proved that is not necessary to prepare a large number of cells at the same time to reduce the overall signaling overhead. For instance, by setting up a window of 10 prepared cells that follows the UE as it advances through the highway, the total amount of signaling was reduced up to 30 % over the air and up to 82 % in the back-haul.

The thesis also studied the possibilities of the synchronous random access (RA)-less handover and the make-before-break technique for completely eliminate the mo-

bility data interruption time. The RA-less handover is designed for a time-synchronous network where the RA at each handover can be avoided, reducing the data disruption and the overall handover latency. The analyzed results indicated that due to non-negligible UE and eNB processing times, UE reconfiguration delays and the required signaling exchange, the zero interruption time requirement is not fulfilled. Moreover, in the RA-less handover the data forwarding between the source and the target cell takes place after commanding the handover to the UE. As the data forwarding is affected by the latency of the interface that connects the eNBs, the UE could complete the reconfiguration before the source forwards the content of its buffer to the target, increasing the data disruption. To minimize this effect, this thesis proposed an enhanced selective data forwarding where the source cell estimates the amount of data that should be forwarded to the target based on channel quality reports. Consequently, the data forwarding in the RA-less handover can be performed before commanding the handover to the UE, reducing the overall handover latency.

Furthermore, the thesis proposed an integration of the synchronous handover and the make-before-break technique, where the UE receives data from both the source and target cell simultaneously during the entire handover procedure. To avoid additional delays due to the radio-frequency (RF) retuning in an inter-frequency handover, the thesis also proposed duplicated receiver chains at the UE, so it can still receive data from the source cell while reconfiguring towards the target. The analysis showed that the proposed synchronous make-before-handover fulfills the 5G design specifications with independence of the handover steps, and the time each network entity takes for executing a successful handover.

Finally, to increase the user experience for media-applications, a user association algorithm that selects the most suitable target cell based on throughput estimates was proposed. Two algorithms were evaluated by means of simulations of a 3GPP HetNet scenario. The results showed minimum gains in the average user session throughput of 32 %, 18 % and 7 % at low-, medium- and high-load network conditions with users moving at a speed of 3 km/h.

Recommendations

The following recommendations can be made from the presented conclusions:

- a) Complement the studies of standardized 3GPP simulations with the analysis of site-specific scenarios to fully characterize the mobility performance.
- b) When upgrading the network with DC, implement the user-plane with the split bearer architecture to obtain all the benefits of aggregating additional links and minimize the mobility data interruption time.
- c) Also for DC, deviate from traditional network-controlled mobility and adopt the UE autonomous cell management approach at the secondary cell layer to reduce the signaling overhead while maintaining a stable anchor point with the network at the MeNB.
- c) For synchronous RA-less handovers, adopt the proposed enhanced data forwarding technique during the handover preparation to avoid additional data interruption.

- d) Implement the make-before-break technique with duplicated receiver chains at the UE to perform the reconfiguration towards the target cell while receiving data from the source, thereby completely eliminating the data interruption without increasing the overall handover latency.

2 Future Work

The work presented in this dissertation opens up many possibilities for future research directions that were not able to be addressed due to the limited time of the PhD study.

The thesis presented two different policies for preparing cells in the highway scenario. However, these are not the only approaches that can be adopted. For example, the network could utilize uplink measurements of the reference signals periodically sent by the UE to follow its movement and update the set of prepared cells included in the window. The presented studies can be complemented by analyzing the performance with other cell preparation techniques.

The handover latencies and data interruption time studies have been performed under a distributed architecture. A possible future research path is to investigate the performance under semi- and fully centralized architectures. In these cases, the exchange of messages between the UE and the access points should be forwarded to the centralized entity that implements the upper layers (RRC, PDCP, RLC...), modifying the presented latency values. Moreover, it is recommended to study different data forwarding approaches for avoiding data disruption in these architectures.

The make-before-break studies can be complemented with protocol and system-level simulations to analyze non-ideal cases with packet loss during the data forwarding, and cases where the source cell is not able to transmit data to the UE due to degraded radio-link conditions. Furthermore, it is advised to evaluate performance of a multi-connectivity solution in the highway scenario with split-bearer architecture that integrates all the presented solutions. In particular, synchronous make-before-break handover for the macro-layer and UE autonomous cell management operations for the small-cell layer, eliminating the data disruption and reducing the amount of signaling overhead.

As a final future research path, it is suggested to analyze the mobility performance of the presented ideas and others considering a decoupled link, where the UE is served by one node in the downlink and by a different one in the uplink, and a cell-less design. In the later, rather than adopting traditional RRC procedures the mobility could rely on physical-layer signaling, following an antenna-switching approach. The decoupled link design opens the doors to new schemes where partly-independent handover decisions for the two links can be implemented.

References

- [1] 3GPP Technical Report (TR) 38.913. *Study on Scenarios and Requirements for Next Generation Access Technologies. V.0.4.0*, June 2016.

- [2] *Report ITU-R M.2134. Requirements related to technical performance for IMT-Advanced radio interface(s)*, 2008.

Appendix A

Paper I – (Collaboration 1)

Comparison and Extension of Existing 3D
Propagation Models with Real-world Effects Based
on Ray-tracing. A Basis for Network Planning and
Optimization

Dereje W. Kifle, Lucas Chavarría Giménez, Bernhard Wegmann,
Ingo Viering, Anja Klein

Published in
Wireless Personal Communications. Springer. 2014.

© 2014 Springer

Reprinted with permission. The layout has been revised.

Abstract

The next generation of cellular network deployment is heterogeneous and temporally changing in order to follow the coverage and capacity needs. Active Antenna Systems allows fast deployment changes by cell shaping and tilt adaptation which have to be controlled in self-organized manner. However, such kind of automated and flexible network operation require a Self Organizing Network algorithm based on network performance parameters being partly derived from the radio measurements. Appropriate radio propagation models are not only needed for network planning tools but also for simulative-lab tests of the developed Self Organizing Network algorithm controlling the flexible deployment changes enabled by Active Antenna Systems. In this paper, an extension of the existing 3D propagation model is proposed in order to incorporate the the propagation condition variation effects, not considered so far, by changing antenna beam orientation like antenna tilting or when users are distributed in the third dimension (height) in multi-floor scenarios. Ray tracing based generated propagation maps that show the realistic propagation effect are used as 3D real world reference for investigation and model approval.

1 Introduction

Cellular system design requires an in depth understanding of the characteristics of the propagation environment. Therefore, accurate and robust prediction models are needed to be able to predict the characteristics of the physical radio channel where the cellular system is going to be deployed. A very good prediction of the radio channel ensures more reliability in delivering high system capacity with high efficiency and provides more flexibility in further optimization. As the impact of the propagation environment is determined by several factors, including the operating frequency the radio signal and varying clutter type, its modeling is the most difficult task. Plenty of propagation models and prediction scheme have been proposed for various case scenarios and are being utilized in order to approximate all those effects and predict the signal power loss in the course of propagation [1] [2] [3] [4].

The total propagation loss for a signal can be modeled as a distance dependent path loss and an additional random variable component which depends on the nature of the propagation environment characteristics. The path loss component $L(\bar{x})$, also known as distance dependent path loss, gives the average signal attenuation level and it is exponentially proportional to the shortest distance r between \bar{x} and the transmitter antenna, $L \propto r^\beta$. Where β is called the path loss component and its value depends on the clutter type of the propagation environment, particularly in the vicinity of the receiving mobile terminal, such as terrain, buildings, vegetation, etc. Different kinds of path loss models are available in literatures that are derived based on analytical and empirical approaches [2] [3]. The additional variability of the propagation loss component is caused by different physical phenomenon that the radio wave undergoes in the course of propagation; i.e., reflection, diffraction and scattering there by resulting in a signal fading. The large scale signal fading which is known as shadowing is typically modeled as a random variation of a signal attenuation level around the path loss caused by presence of obstructing objects on the path of the signal propagation [5] [6]

and therefore, it is location dependent.

Proper radio propagation models are not only needed for network planning tools but also in system level simulator being used to evaluate Self Organizing Network (SON) algorithms designed for flexible deployment changes enabled by Active Antenna Systems (AAS). Antenna beam characteristics can be fast adapted from simple tilt changes to more complicated beam shaping techniques like cell splitting [7]. Such types of network operation changes are implemented in system level simulator or network planning tool based the prediction of the expected network performances like coverage, signal to interference level, etc utilizing propagation models [6]. Hence, accurate propagation model that is able to reflect a very good approximation of the realistic propagation effect is essential. The existing models and assumptions are fair enough for application as used in non automated network planning tasks. However, automated traffic dependent network adaptation and optimization of the 3D antenna characteristics require a very high accuracy in the approximation of the realistic propagation condition. Due to this fact, the performance of a developed algorithm in the field is limited by the quality of the utilized models during the development phase to approximate the effect of the changes in the reality.

Shadowing effect is modeled as a log-normal distributed random variable with zero mean and a standard deviation 5 - 12 dB depending on the nature of the propagation environment. For fixed deployment, shadowing is assumed to be a Gaussian process that de-correlates exponentially with distance [5] [6]. However, in urban and dense urban deployment, when the antenna beam orientation is changed, the radio signal experiences a different propagation behavior for the same user location resulting from changed path way of the radio wave. The received signal change does not only result from changing antenna beam direction but also from a change in shadowing effect [5] [6]. This variability of the shadowing effect and existence of its dependency with respect to antenna tilt is presented in [8] and , therefore, a new tilt dependent shadowing model approach is needed.

This paper provides more detailed study of the shadowing effect variability with respect to antenna tilt changes and a new shadowing model is introduced that statistically approximates the tilt dependency of the shadowing process based on the propagation statistics generated using a ray tracing based network planning tool that employs 3D model for a typical European urban deployment scenario. Moreover, the paper also investigates the height gain variation in the propagation loss associated to difference clutter type experience for a signal at a different height level. This height gain effect becomes necessary when considering in-door users in multi-floor building scenarios. Thus a height dependent propagation model is also presented utilizing a ray tracing based propagation maps generated at different floor height levels.

The rest of the paper is organized as follows. Section 2 formulates the problem and the proposed propagation models are presented in Section 3. The scenario description, site layout and other settings used in the ray tracing tool are described in Section 4. Section 5 discusses and evaluates the performance of the proposed models using propagation statistics from ray tracing. The impact of the tilt and height models in planning and optimization is discussed in Section 6. And Section 7 concludes the work.

2 Problem Formulation

2.1 Tilt Dependency of Propagation Model

Assuming the antenna beam has a tilt setting of Θ_o , a pixel point in a network located at \bar{x} with respect to the base station site and at a height of h_o above the ground, i.e. \bar{x}_{h_o} , the total propagation loss from the transmitting antenna to \bar{x}_{h_o} is described by $L_t(\bar{x}_{h_o}, \Theta_o)$. In the existing propagation model the $L_t(\bar{x}_{h_o}, \Theta_o)$ is given by:

$$L_t(\bar{x}_{h_o}, \Theta_o) = L(\bar{x}_{h_o}) - G_a(\bar{x}_{h_o}, \Theta_o) + S(\bar{x}_{h_o}) \quad (I.1)$$

where $L(\bar{x}_{h_o})$ is the distance dependent path loss and $S(\bar{x}_{h_o})$ is a log-normal random variable with zero mean and standard deviation of σ , $S(\bar{x}_{h_o}) \sim \mathcal{N}(0, \sigma^2)$, that gives the shadowing fading effect. The term $G_a(\bar{x}_{h_o}, \Theta_o)$ is the total antenna gain at \bar{x}_{h_o} and it is given by the sum of the dBi gain of the antenna A_{dBi} and the three dimensional radiation pattern loss $B_p(\Phi, \Theta_o, \phi, \theta)$ normalized to 0 dB value and given in terms of the azimuth and elevation angular location of \bar{x}_o , (ϕ, θ) , the antenna beam azimuth orientation Φ and the elevation tilt Θ_o : i.e. $G_a(\bar{x}_{h_o}, \Theta_o) = A_{dBi} + B_p(\Phi, \Theta_o, \phi, \theta)$.

When the elevation tilt configuration is changed from Θ_o to Θ_i the total propagation loss at \bar{x}_{h_o} with respect to the new tilt configuration Θ_i $L_t(\bar{x}_{h_o}, \Theta_i)$ is described by the existing model as shown in Equation I.2.

$$L_t(\bar{x}_{h_o}, \Theta_i) = L(\bar{x}_{h_o}) - G_a(\bar{x}_{h_o}, \Theta_i) + S(\bar{x}_{h_o}) \quad (I.2)$$

According to the model, the associated change in the total propagation loss \bar{x}_{h_o} due to the change in the tilt configuration is described by only by the difference in the total antenna gain value $\Delta G_a(\bar{x}_{h_o}, \Theta_i, \Theta_o)$ experienced at the same location before and after applying the tilt change where $\Delta G_a(\bar{x}_{h_o}, \Theta_i, \Theta_o) = G_a(\bar{x}_{h_o}, \Theta_i) - G_a(\bar{x}_{h_o}, \Theta_o)$. Whereas the $L(\bar{x}_{h_o})$ is not affected as it is dependent only on the distance and the shadowing effect is assumed to be identical and hence always the same shadowing is assumed independent of the tilt. Accordingly, the total propagation loss after a tilt change is expressed in terms of the total propagation loss before the change and the difference in the total antenna gain at \bar{x}_{h_o} associated to the applied tilt change in Equation I.3:

$$L_t(\bar{x}_{h_o}, \Theta_i) = L_t(\bar{x}_{h_o}, \Theta_o) + \Delta G_a(\bar{x}_{h_o}, \Theta_i, \Theta_o) \quad (I.3)$$

However, in reality, in the presence of obstructing building environments, the shadowing effect does not remain identical during tilt configuration change. The variability of the shadowing with respect to tilt change is observed based on a propagation map generated using a ray tracing tool that reflects the real propagation effect changes by employing a ray based prediction in a real based 3D model scenario in [8]. The ray tracing scenario and further scenario description are discussed in the forthcoming sections. Based on such propagation maps, it has been observed that the total propagation loss change during a tilt change is not equal to only the total antenna gain difference as described in the existing model in Equation I.3 but also on the shadowing effect change associated with the tilt applied tilt difference. The paper [8] also discusses the impact of tilt change on the shadowing process and it shows the existence of dependency of shadowing with tilt configuration. In [8] only the problem is discussed and tilt dependent shadowing model $S(\bar{x}_{h_o}, \Theta_i)$ is required in order

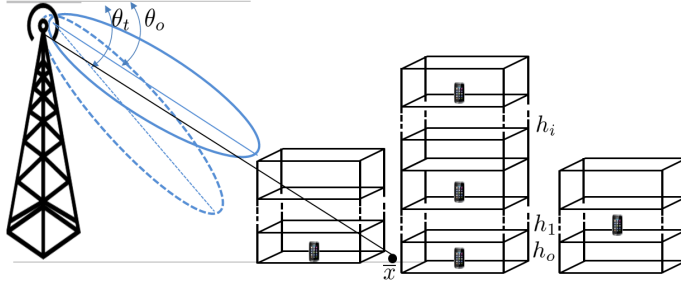


Fig. I.1: Please write your figure caption here

to properly include the shadowing effect change while carrying out tilt related system level simulation. As a consequence, during a tilt configuration change, the new propagation model should also include the corresponding variation with respect to the tilt dependent shadowing.

2.2 Height Gain

In urban areas of high rise buildings, users are not necessarily at the ground rather distributed at a different height level above the ground on different building floors as shown in Figure I.1. During a multi-floor building scenario, prediction of the total propagation loss for indoor users residing at different floors requires proper approximation of the outdoor propagation and the corresponding penetration loss. In many existing planning tools and models, the common approach to estimate the indoor propagation loss is to predict the outdoor propagation loss in the proximity of the buildings and then add some additional constant penetration loss [9] [10]. The corresponding outdoor propagation conditions is also dependent on the actual surrounding clutter type visible at that floor height level. Apparently, at a higher height levels, the clutter type gets better leading to a higher probability of line of sight visibility between the transmitter and the receiver. Consequently, this clutter level variation leads to a propagation gain with height. The existing propagation model approximates this height gain effect by modeling a floor height gain $H(\bar{x}_{h_i, h_o})$ and to include this value for the height level change from h_o to h_i . Hence, the existing model prediction of the total propagation loss $L_t(\bar{x}_{h_i}, \Theta_o)$ at h_i height level is done by applying the floor height gain to the total propagation loss at h_o as shown in Equation I.5

$$L_t(\bar{x}_{h_i}, \Theta_o) = L_t(\bar{x}_{h_o}, \Theta_o) + H(\bar{x}_{h_i, h_o}) \quad (\text{I.4})$$

In the existing models, $H(\bar{x}_{h_i, h_o})$ is accounted and approximated with a constant average floor height gain determined from different measurement statistics. In COST 231 [10], floor height gain of 1.5-2 dB/floor and 4-7 dB/floor has been reported for buildings with storey heights of 3 m and 4 – 5 m respectively. The floor height gains are translated to dB/m to be generally applied for floors with different floor height. Currently, an average height gain of 0.6 dB/m proposed by COST and different literatures is widely adopted [9] [10]. Previous studies [9] have also reported approximated average height gain of 0.6 dB/m and the investigations have also indicated that this

value is independent of the operating frequency and the relative distance from the corresponding base station.

However, since all these models recommends a constant average values independent of the type of the building scenario, in some cases this does not properly reflect the actual gain variation per height relative to what is assumed at the ground level. Hence, a height gain model that includes the floor height gain variation with respect to the ground floor is required to better reflect the the non constant height gain level in order to be able to predict an accurate propagation loss when dealing with a multi-floor building scenario in network planning and system level simulation setups.

3 Derivation of Tilt and Height Dependent propagation Model

3.1 Tilt Dependent Shadow Model

While an antenna tilt configuration tilt is changed from Θ_o to Θ_i , it is primarily intended to direct the beam orientation in a desired direction in order to have change in the total antenna gain with respect to each location \bar{x} in a network. During the tilt adjustment, the path loss component, however, is not affected due to the fact that it is rather dependent only on the relative distance of \bar{x} from the base station.

As stated in Section 2.1, the tilt setting change has an impact on the shadowing effect of the propagation environment particularly in urban clutter type case. Thus, the shadowing at a tilt Θ_i is modeled as tilt dependent, $S(\bar{x}_{h_o}, \Theta_o)$. In our shadowing model derivation, we have a shadowing map $S(\bar{x}_{h_o}, \Theta_i)$ extracted from the propagation map generated from with a ray tracing at Θ_i . The shadowing statistics extraction has been done for various tilt settings. In the case of a tilt configuration change the new propagation model includes the effect of the the experienced change in the shadowing $\Delta S(\bar{x}_{h_o}, \Theta_i, \Theta_o)$, where $\Delta S(\bar{x}_{h_o}, \Theta_i, \Theta_o) = S(\bar{x}_{h_o}, \Theta_i) - S(\bar{x}_{h_o}, \Theta_o)$, accordingly, the new total propagation loss $\hat{L}_t(\bar{x}_{h_o}, \Theta_i)$ after tilt change from Θ_i to Θ_o can be expressed as shown in Equation I.5.

$$\hat{L}_t(\bar{x}_{h_o}, \Theta_i) = L_t(\bar{x}_{h_o}, \Theta_o) + \Delta G_a(\bar{x}_{h_o}, \Theta_i, \Theta_o) + \Delta S(\bar{x}_{h_o}, \Theta_i, \Theta_o) \quad (I.5)$$

Since the shadowing process is modeled as log-normally distributed, the shadowing difference, $\Delta S(\bar{x}_{h_o}, \Theta_i, \Theta_o)$, can be also approximated to follow a log-normal distribution with zero mean and a standard deviation of $\sigma_{\Delta S}$. Ray tracing based data, to be discussed more in later section, have shown that, with the increase in the tilt configuration difference, $\Delta\Theta = \Theta_i - \Theta_o$, the shadowing effect experience becomes more different leading to a higher de-correlation between the shadowing values at a higher $\Delta\Theta$. The correlation between the shadowing statistics at two different settings, Θ_i and Θ_o is given by the correlation coefficient value $\rho^{\Theta_i, \Theta_o}$ and since the respective tilt shadowing statistics are assumed as a zero mean, the correlation coefficient is by:

$$\rho^{\Theta_i, \Theta_o} = \frac{\text{Exp}\{(S(\bar{x}_{h_o}, \Theta_i) - \mu_{\Theta_i})(S(\bar{x}_{h_o}, \Theta_o) - \mu_{\Theta_o})\}}{\sigma_{\Theta_i} \sigma_{\Theta_o}} \quad (I.6)$$

On the other hand, it has been indicated in [8] and also will be justified later that, the shadowing effect statistics standard deviation shows a very slight variation that the over all shadowing map has closely the same statistical distribution. Hence, it is reasonable to assume the same value of shadowing standard deviation at various tilt, i.e. $\sigma_{\Theta_i} \approx \sigma_{\Theta_o}$. According to the ray tracing based data statistics, the shadowing effect variability and statistical de-correlation of the shadowing values increases with the amount of $\Delta\Theta$ applied this in turn leads to an increase the standard deviation $\sigma_{\Delta S}$ of $\Delta S(\bar{x}_{h_o}, \Theta_i, \Theta_o)$.

The tilt dependent shadowing model proposes prediction a shadowing map of $\hat{S}(\bar{x}_{h_o}, \Theta_i)$ for Θ_i tilt configuration from a known shadowing map at a reference tilt Θ_o . In our investigation, $\hat{S}(\bar{x}_{h_o}, \Theta_i)$ is to be predicted from the $S(\bar{x}_{h_o}, \Theta_o)$ ray tracing data extracted at tilt of Θ_o . In this case, the new shadow predicting model should also maintain the correlation between the shadowing statistics at Θ_i and Θ_o tilt setting to a reasonable level. Hence, the cross correlation coefficient of the predicted shadowing statistics at Θ_i with the reference shadow map is given by $\hat{\rho}^{\Theta_i, \Theta_o}$. In order to estimate $\hat{\rho}^{\Theta_i, \Theta_o}$, the proposed model introduces a predictor function $f_s(\Delta\Theta)$ that approximate the corresponding correlation level between two shadowing statistics at whose tilt setting difference is $\Delta\Theta$.

$$\hat{\rho}^{\Theta_i, \Theta_o} = f_s(\Delta\Theta) \quad (I.7)$$

where $f_s(\Delta\Theta)$ is going to be derived empirically by using ray tracing based extracted tilt dependent shadowing statistics from a real world based 3D deployment scenario, from several sectors. The cross correlation coefficient value is expected to drop linearly with the $\Delta\Theta$. As a result $f_s(\Delta\Theta)$ can be approximated as a linear predictor with coefficients a and b such that $f_s(\Delta\Theta) = a \cdot \Delta\Theta + b$. The coefficients a and b are to be determined empirically based on the cross correlation coefficient data values $\hat{\rho}^{\Theta_i, \Theta_o}$ found from the ray tracing scenario extracted shadowing statistics.

During the tilt change of $\Delta\Theta$, the proposed model estimates the shadowing effect $\hat{S}(\bar{x}_{h_o}, \Theta_i) \sim \mathcal{N}(0, \hat{\sigma}_{\Theta_i}^2)$ at $\Theta_i = \Theta_o + \Delta\Theta$ from the shadowing value before the tilt change $S(\bar{x}_{h_o}, \Theta_o)$ and an additional uncorrelated Gaussian random variable $\Omega(\Theta_i, \Theta_o) \sim \mathcal{N}(0, \sigma_{\Omega}^2)$. Utilizing the predicted cross correlation coefficient $\hat{\rho}^{\Delta\Theta}$, the resulting shadowing is modeled as:

$$\hat{S}(\bar{x}_{h_o}, \Theta_i) = \hat{\rho}^{\Theta_i, \Theta_o} \cdot S(\bar{x}_{h_o}, \Theta_o) + \sqrt{1 - \hat{\rho}^{\Theta_i, \Theta_o}} \cdot \Omega(\Delta\Theta) \quad (I.8)$$

where:

$$\hat{\rho}^{\Theta_i, \Theta_o} = \frac{\text{Exp}\{(\hat{S}(\bar{x}_{h_o}, \Theta_i) - \hat{\mu}_{\Theta_i})(S(\bar{x}_{h_o}, \Theta_o) - \mu_{\Theta_o})\}}{\sigma_{\Theta_i} \sigma_{\Theta_o}} = f_s(\Delta\Theta) \quad (I.9)$$

As discussed earlier, $\hat{\sigma}_{\Theta_i} \approx \sigma_{\Theta_o}$. Thus, σ_{Ω} can be derived from the variance relationship as:

$$\text{Var}[\hat{S}(\bar{x}_{h_o}, \Theta_i)] = \text{Var}[S(\bar{x}_{h_o}, \Theta_o)] \quad (I.10)$$

$$\text{Var}[\hat{\rho}^{\Theta_i, \Theta_o} \cdot S(\bar{x}_{h_o}, \Theta_o) + \sqrt{1 - \hat{\rho}^{\Theta_i, \Theta_o}} \cdot \Omega(\Delta\Theta)] = \sigma_{\Theta_o}^2 \quad (I.11)$$

From the above expression the σ_{Ω} is:

$$\sigma_{\Omega} = \sqrt{1 + \hat{\rho}^{\Theta_i, \Theta_o}} \cdot \sigma_{\Theta_o} \quad (I.12)$$

Accordingly, the total propagation loss $\hat{L}_t(\bar{x}_{h_o}, \Theta_i)$ expression at Θ_i shown in Equation I.5 can be rewritten by including the predicted shadowing effect change $\Delta\hat{S}(\bar{x}_{h_o}, \Theta_i, \Theta_o)$ as,

$$\hat{L}_t(\bar{x}_{h_o}, \Theta_i) = L_t(\bar{x}_{h_o}, \Theta_o) + \Delta G_a(\bar{x}_{h_o}, \Theta_i, \Theta_o) + \Delta\hat{S}(\bar{x}_{h_o}, \Theta_i, \Theta_o) \quad (\text{I.13})$$

where:

$$\Delta\hat{S}(\bar{x}_{h_o}, \Theta_i, \Theta_o) = \hat{S}(\bar{x}_{h_o}, \Theta_i) - S(\bar{x}_{h_o}, \Theta_o) \quad (\text{I.14})$$

$$\Delta\hat{S}(\bar{x}_{h_o}, \Theta_i, \Theta_o) = (\rho^{\Theta_i, \Theta_o} - 1) \cdot S(\bar{x}_{h_o}, \Theta_o) + \sqrt{1 - \rho^{\Theta_i, \Theta_o}} \cdot \Omega(\Delta\Theta) \quad (\text{I.15})$$

The standard deviation of $\Delta\hat{S}(\bar{x}_{h_o}, \Theta_i, \Theta_o)$, $\hat{\sigma}_{\Delta S}$, can be found by evaluating the variance of equation above and using the relationship shown in above, and it becomes:

$$\hat{\sigma}_{\Delta S} = \sqrt{2 \cdot (1 - \rho^{\Theta_i, \Theta_o}) \cdot \sigma_{\Theta_o}} \quad (\text{I.16})$$

3.2 Height Gain Model

In this paper height gain model investigation, the height gain is evaluated from a propagation map generated at a different floor height level using the ray tracing tool. This investigation aimed at showing the floor height gain variation statistics and compare it with the current average constant height gain assumption of 0.6 dB/m [10] whereas in real case this constant gain deviates randomly. Hence, the proposed height gain model approximates the effect of the clutter type with an a better estimation of the height gain.

Accordingly, a non constant variable height gain of $\hat{H}(\bar{x}_{h_i, h_o})$ is determined by subtracting the ray tracing propagation map generated at h_i and h_o floor height levels. The total propagation value at $\hat{L}_t(\bar{x}_{h_i}, \Theta_o)$ at h_i height level can now be rewritten as

$$\hat{L}_t(\bar{x}_{h_i}, \Theta_o) = L_t(\bar{x}_{h_o}, \Theta_o) + \hat{H}(\bar{x}_{h_i, h_o}) \quad (\text{I.17})$$

where $\hat{H}(\bar{x}_{h_i, h_o}) = \hat{L}_t(\bar{x}_{h_i}, \Theta_o) - L_t(\bar{x}_{h_o}, \Theta_o)$ gives the corresponding floor height gain. The height gain model in this paper investigates the statistical variation of $\hat{H}(\bar{x}_{h_i, h_o})$ and compares it with the existing model assumption by utilizing a ray tracing based propagation map statistics generated for a multi-floor scenario in Section 5.

4 Ray Tracing Scenario Description and Statistics Extraction

4.1 Ray Tracing Scenario

In this investigation, a network planning tool that employs ray tracing technique for the propagation map prediction is used. A 3D city model and the urban clutter behavior of a typical European city is considered in the scenario. The scenario assumes 27 sectorized sites consists of 75 sectors where the site plan and system parameter configuration settings are done based on realistic site deployment information. In the

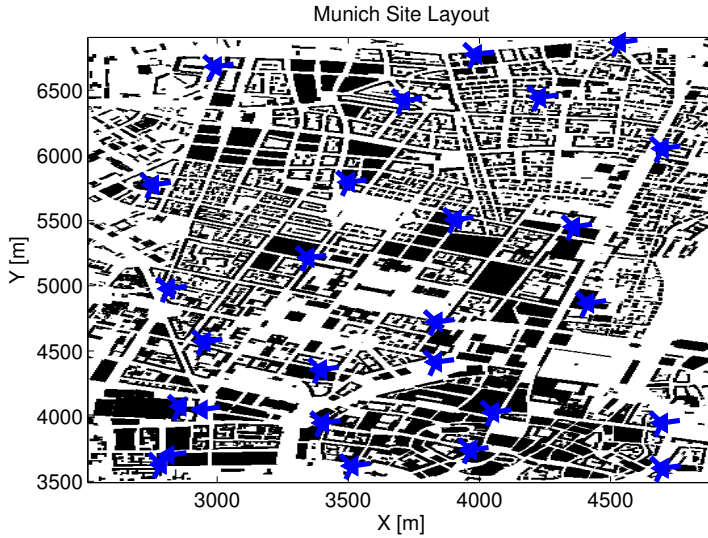


Fig. I.2: Munich Network Site Layout

ray tracing tool, Dominant path Prediction Model(DPM) is adopted where the propagation effect at point is predicted from a ray path taken by the dominant ray which brings most of the energy to the point of prediction. It has been shown in [11] [12] that DPM has as high accuracy as the prediction technique that employs several rays. The ray tracing technique along with the 3D models reflects the real propagation effects and an accurate prediction of the received signal at each pixel point using the employed prediction techniques. The propagation prediction is done for each sector antenna in a pixel based approach where the total network is divided in to a grid of pixels of 5 m resolution with a total prediction area of 3.4 km by 2.4 km. The site layout and the prediction area of the ray tracing scenario is shown in Figure I.2 and basic system parameters settings are summarized in Table I.1.

Two set of outdoor propagation maps are generated via ray based prediction of the received signal strength at each pixel point from each sector antenna. One set of prediction is done for ground floor at a 1.5 m user height level for different tilt settings varying from 4° to 14° in order to carry out the tilt dependent shadowing investigation. The other set of prediction has been carried out at a different floor height level and fixed tilt setting for the height gain study. The indoor propagation is estimated from the outdoor maps by adding a 10 dB penetration loss and an additional attenuation of 0.6 dB/m to the strongest ray detected around the building being considered [9] [10] [13].

4.2 Statistics Extraction

The total propagation loss $L_t(\bar{x}_{h_i}, \Theta_i)$ is obtained from the generated received power map by subtracting the total transmit power level used in the prediction, i.e. 43 dBm.

Table I.1: Basic Scenario Settings

Information	Settings
City	Munich
Network Size	3.4 km by 2.4 km
Site and Sector	27 sites, 75 sectors
Transmit power	20 W (43 dBm)
Antenna Gain	17.5 dBi
Radiation Beam	$\Phi_{3dB} = 62, \Theta_{3dB} = 5$
Sector Orientation	$[10^\circ, 250^\circ, 130^\circ]$
Mechanical Tilt	4°
Electrical Tilt	0° to 10° , step 1°
Prediction Height	Ground + 6 Floor
Floor height	3.1 m

The corresponding shadowing map statistics is extracted for each prediction setting scenario of Θ_i° tilt and h_i m height by using the empirical propagation model relation ship described in Equation I.2. Accordingly, $S(\bar{x}_{h_i}, \Theta_i)$ is:

$$S(\bar{x}_{h_i}, \Theta_i) = L_t(\bar{x}_{h_i}, \Theta_i) - L(\bar{x}_{h_i}) + G_a(\bar{x}_{h_i}, \Theta_i) \quad (\text{I.18})$$

However, since only $L_t(\bar{x}_{h_i}, \Theta_i)$ is available from Equation I.18, the path loss component $L(\bar{x}_{h_i})$ and the total antenna gain $G_a(\bar{x}_{h_i}, \Theta_i)$ values need to be determined. It is apparent that, $L(\bar{x}_{h_i})$ is the mean propagation loss whereas the $S(\bar{x}_{h_i}, \Theta_i)$ corresponds to the rest of the large scale attenuation over the mean, thus, the path loss plus shadowing statistics can be evaluated from Equation I.18 as:

$$S(\bar{x}_{h_i}, \Theta_i) + L(\bar{x}_{h_i}) = L_t(\bar{x}_{h_i}, \Theta_i) + G_a(\bar{x}_{h_i}, \Theta_i) \quad (\text{I.19})$$

In this case, the path loss is approximated by the empirical path loss model as $L(\bar{x}_{h_i}) = \alpha + \beta \cdot \log_{10}(r)$ where α and β are the path loss loss coefficients and can be determined via linear regression estimation from the the path loss plus shadowing statistics and the coefficients correspond to the path loss offset and the path loss exponent respectively [5] [6].

Proper extraction of the shadowing statistics requires estimating and excluding the total antenna gain values with respect to each \bar{x} in Equation I.19. And this needs a beam pattern model that provides the antenna gain variation in the boresight direction. In this investigation, the beam pattern model from the 3rd Generation Partnership Project (3GPP) is employed where it approximates the two dimensional and total three dimensional patterns as shown in Equation I.20-I.22 where the variables $\Phi_o, \Theta_i, \Phi_{3dB}$ and Θ_{3dB} are the azimuth orientation, elevation tilt, azimuth and elevation half

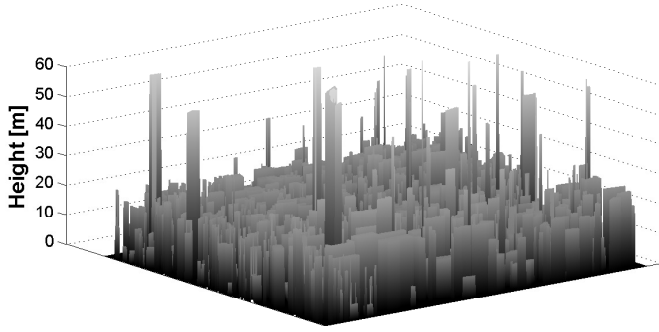


Fig. I.3: 3D City Building Layout

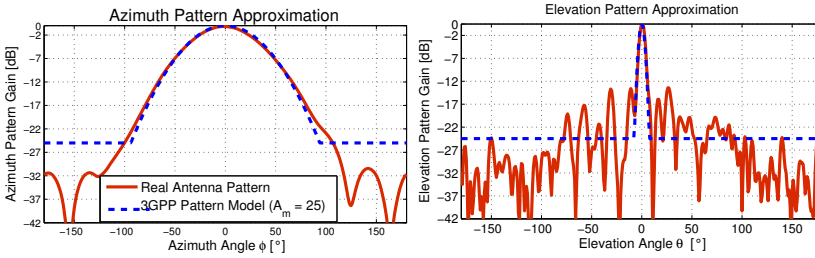


Fig. I.4: Approximation of The Real Antenna Radiation Pattern

power beam-widths respectively [6] [14]. Whereas ϕ and θ are the angular position of \bar{x} . The 3GPP pattern model estimates the main lobe radiation patterns and approximates the side and back lobe effect with a constant value of A_m known as backward attenuation factor. Figure I.4 depicts the estimated and real antenna elevation pattern behaviour for a typical value of $A_m = 25$ dB proposed by 3GPP [6].

$$B_H(\phi) = -\min \left\{ A_m, 12 \cdot \left(\frac{\phi - \Phi_o}{\Phi_{3dB}} \right)^2 \right\}, \Rightarrow \text{Azimuth} \quad (\text{I.20})$$

$$B_V(\theta) = -\min \left\{ A_m, 12 \cdot \left(\frac{\theta - \Theta_i}{\Theta_{3dB}} \right)^2 \right\} \Rightarrow \text{Elevation} \quad (\text{I.21})$$

$$B_{3D}(\phi, \theta) = -\min \{ A_m, -[B_H(\phi) + B_V(\theta)] \}, \Rightarrow \text{Total Pattern} \quad (\text{I.22})$$

However, the backward attenuation effect depends on the nature of the propagation environment as it attributes to the various physical phenomena that the signal wave undergoes during radiation like reflection, scattering and diffraction which determines the effective antenna gain behavior from side lobes [14]. As a consequence, A_m is characterized by the clutter type seen by each antenna and could have different values for each antenna in the same scenario. Hence, an exhaustive search optimization

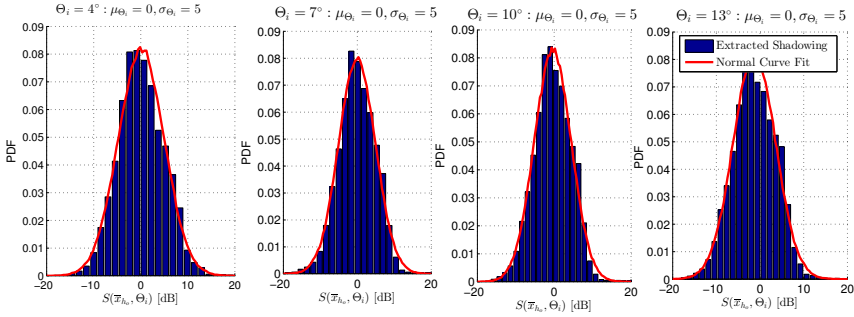


Fig. I.5: Shadowing Statistical Distribution For Different Tilt

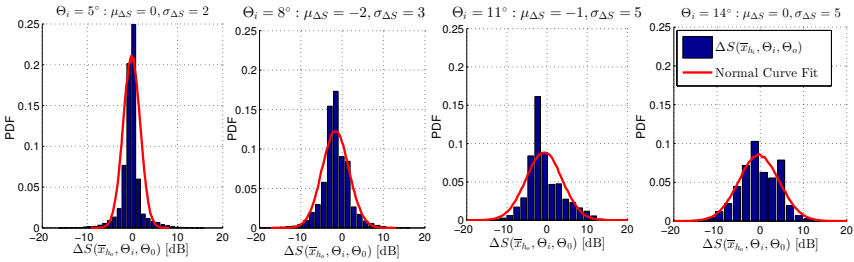


Fig. I.6: $\Delta S(\bar{x}_{\mu_0}, \Theta_i, \Theta_0)$ Statistical Distribution

has been carried out for a range of A_m values that will lead to a path loss plus shadowing statistics satisfying minimizing the standard deviation of the shadowing [8].

5 Model Coefficient Prediction and Performance Evaluation

5.1 Shadowing Statistics and Predictor Coefficients

Shadowing Statistics

The shadowing statistics extracted for each tilt Θ_i from the ray tracing data, $S(\bar{x}_{\mu_0}, \Theta_i)$, has been investigated for its statistical behavior and in-variability relationship along with the applied tilt change. Statistics observed from each site antenna confirmed that the extracted shadow map for each tilt settings have a Gaussian statistical distribution with closely the same standard deviation independent of the tilt. This is also illustrated in Figure I.5 where the shadowing map distribution is shown for a sample site for different tilt case validating the same shadowing statistics standard deviation assumption used in the Section 3.

As can be seen in the Figure I.5, the first and the second order statistical information are not depicting significant variation of the shadowing process for various

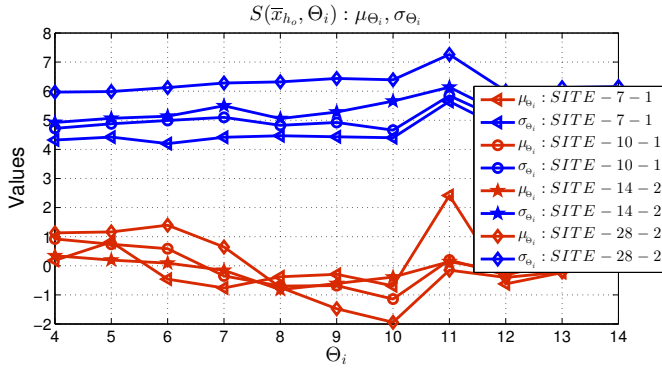


Fig. I.7: Mean and Standard Deviation of $S(\bar{x}_{h_0}, \Theta_i)$ at Different Θ_i

tilt. However, this does not guarantee the invariability of the shadowing effect with respect to tilt change. Hence, further investigation is done by evaluating the corresponding shadowing map change, $\Delta S(\bar{x}_{h_0}, \Theta_i, \Theta_0)$, at each pixel \bar{x} location in the prediction area for the applied tilt setting change. Figure I.6 shows the distribution of the shadowing value differences $\Delta S(\bar{x}_{h_0}, \Theta_i, \Theta_0)$ for various tilt differences evaluated per pixel showing that the shadowing effect indeed changes while tilt setting is varied. The figure confirms that $\Delta S(\bar{x}_{h_0}, \Theta_i, \Theta_0)$ also follows a Gaussian distribution with a mean value around zero and standard deviation, $\sigma_{\Delta S}$, which is increasing with $\Delta\Theta$ indicating that the actual shadowing experience has dependency on the tilt and the shadowing effect variation gets higher at a larger relative tilt change. Moreover, the statistical mean and standard deviation of the shadowing map are not changed considerably with tilt as discussed before, and this behavior is more depicted in I.7 for various tilt Θ_i

Shadowing Correlation and Predictor Coefficients

Due to its random behavior, the shadow fading effect at different locations are described in terms of the statistical correlation between them. The correlation property is also used in the existing shadowing model for system level simulations in order to generate a shadowing map with respect to each site [6]. Thus, in our investigation, the correlation statistical property is exploited in order to derive the relationship between the random shadowing process at different tilt settings. In the existing shadowing model, since the same shadowing effect is assumed irrespective the tilt setting, the shadowing random process is seen as fully correlated before and after a tilt change. In reality, however, the shadowing statistics extracted from the ray tracing propagation map data for different tilt settings show that the shadowing fading effect for any two different tilt settings does not remain the same and the variation increases with the increase in the tilt difference. This is illustrated in Figure I.8 where the shadowing correlation coefficient value is shown for the shadowing at a reference tilt, $\Theta_0 = 4^\circ$, and at a different tilt setting, Θ_i . This confirms the existence tilt dependency of the shadowing fading with respect to the antenna tilt setting. The figure also depicts

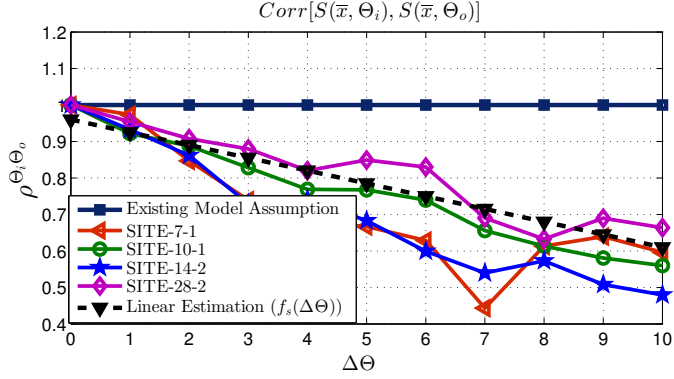


Fig. I.8: Shadowing Correlation Coefficients For Various $\Delta\Theta$

that the shadowing correlation level drops approximately linearly with the applied tilt change.

As discussed in Section 3, the new model introduced in this paper defines a linear function, $f_s(\Delta\Theta)$ as shown in Equation I.23, to predict the corresponding statistical correlation level of the shadowing effect at Θ_i and Θ_o , $\hat{\rho}^{\Theta_i, \Theta_o}$, for a tilt change of $\Delta\Theta$ from Θ_o to Θ_i . The coefficients of $f_s(\Delta\Theta)$ are determined from the shadowing correlation coefficients, $\rho^{\Theta_i, \Theta_o}$, evaluated from the ray tracing based shadowing statistics for various tilt settings using a linear curve fitting approach as shown in Figure I.8. The linear predictor function is given by Equation I.23 with coefficients a and b .

$$\hat{\rho}^{\Theta_i, \Theta_o} = f_s(\Delta\Theta) = a \cdot \Delta\Theta + b \quad (\text{I.23})$$

The predictor coefficients approximation is done using a linear least square method such that $f_s(\Delta\Theta)$ fits the correlation coefficient data, $\rho_{k,i}^{\Theta_i, \Theta_o}$, calculated from each sector k for different tilt change values, $\Delta\Theta_i$, at N number of sectors in our ray tracing scenario where $\Delta\Theta_i = \Theta_i - \Theta_o$. In this investigation, 19 sectors are randomly considered and at each sector, the tilt configuration, Θ_i , is changed from 4° up to 14° with 1° step for a total of $T = 11$ tilt settings. Thus, the coefficients that linearly best fit the data minimizing the error ϵ in Equation I.24 are calculated accordingly.

$$\epsilon = \sum_{k=1}^N \sum_{i=1}^T (\rho_{k,i}^{\Theta_i, \Theta_o} - (a \cdot \Delta\Theta_i + b))^2 \quad (\text{I.24})$$

Thus, based on the data from our ray tracing scenario, predictor coefficient value of $a = -0.035$ and $b = 0.96$ are found with error $\epsilon = 2.3$. The correlation coefficient predictor function is then given by $f_s(\Delta\Theta) = -0.035 \cdot \Delta\Theta + 0.96$ and its slop indicates that the shadowing correlation drops by approximately 3% per a tilt change.

Performance of The Proposed Model

In this subsection the performance of the proposed model is checked against with the ray tracing data. In this case, a new shadowing map of $\hat{S}(\bar{x}_{h_o}, \Theta_i)$ is generated

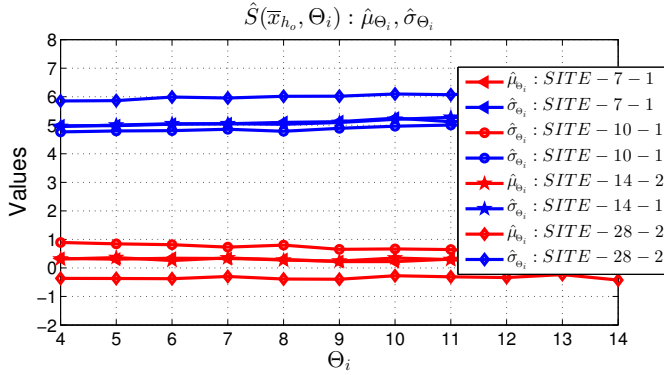


Fig. I.9: Mean and Standard Deviation of $\hat{S}(\bar{x}_{h_o}, \Theta_i)$ at Different Θ_i

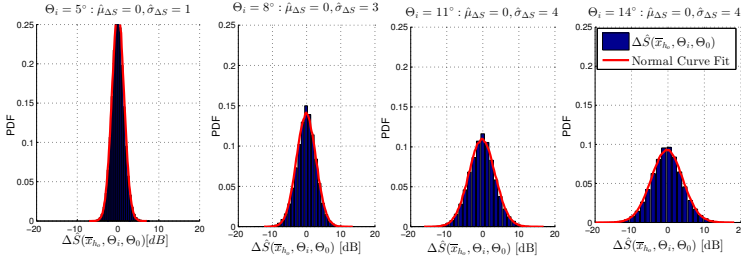


Fig. I.10: $\Delta \hat{S}(\bar{x}_{h_o}, \Theta_i, \Theta_0)$ Statistical Distribution

for a sector at a tilt setting Θ_i from the ray tracing propagation extracted shadowing map $S(\bar{x}_{h_o}, \Theta_0)$ of the same sector at the reference tilt, $\Theta_0 = 4^\circ$, by using the proposed model described in Equation I.7-I.15 and the correlation coefficient predictor function. The statistical correlation between the predicted $\hat{S}(\bar{x}_{h_o}, \Theta_i)$ and $S(\bar{x}_{h_o}, \Theta_0)$ is equal to $\hat{\rho}^{\Theta_i, \Theta_0}$ and it is the same as the value of $f_s(\Delta\Theta)$ evaluated for the respective tilt change. Thus, the correlation property is well approximated by the model as already demonstrated in Figure I.8. The mean $\hat{\mu}_{\Theta_i}$ and the standard deviation $\hat{\sigma}_{\Theta_i}$ of the newly generated shadowing map, $\hat{S}(\bar{x}_{h_o}, \Theta_i)$, at different tilt setting is also evaluated for selected sites. The standard deviation of the normally distributed random values, $\Omega(\Theta_i, \Theta_0)$, used while generating $\hat{S}(\bar{x}_{h_o}, \Theta_i)$ is also determined as described in Equation I.11 and in this case it is also assumed that independent random values are generated for pixel points separated by the same de-correlation distance as $S(\bar{x}_{h_o}, \Theta_i)$ and the other values in between are evaluated using interpolation. Spatial de-correlation distance of 40 m is assumed in our case during the generating the new shadowing map while validating the performance of our model.

Results shown in Figure I.9 has indicated that the $\hat{S}(\bar{x}_{h_o}, \Theta_i)$ has closely the same statistical distribution with the shadowing map $S(\bar{x}_{h_o}, \Theta_i)$ extracted from the ray tracing data. This is illustrated by comparing the corresponding mean and standard deviation values for the extracted and the newly generated shadow map depicted in

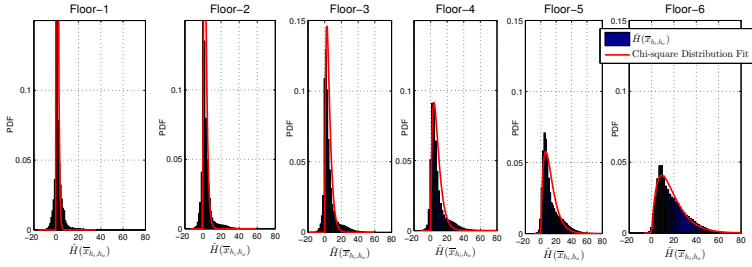


Fig. I.11: $\hat{H}(\bar{x}_{h_i, h_0})$ Statistical Distribution With respect to the Ground Floor

Figure I.7 and Figure I.9 respectively at different tilt settings.

Moreover, it is also interesting to show how close the model predicts the corresponding shadowing effect change, $\Delta\hat{S}(\bar{x}_{h_o}, \Theta_i, \Theta_o)$, that happens during the tilt configuration change from Θ_i to Θ_o which is found by subtracting the shadowing values at each pixel, \bar{x}_{h_o} , at the respective tilt settings, i.e. $\Delta\hat{S}(\bar{x}_{h_o}, \Theta_i, \Theta_o) = \hat{S}(\bar{x}_{h_o}, \Theta_i) - S(\bar{x}_{h_o}, \Theta_o)$. Thus, this value is checked with the corresponding shadowing difference values evaluated from the ray tracing data at the respective tilt settings, i.e. $\Delta S(\bar{x}_{h_o}, \Theta_i, \Theta_o) = S(\bar{x}_{h_o}, \Theta_i) - S(\bar{x}_{h_o}, \Theta_o)$. The comparison between distribution curves and standard deviation values shown in Figure I.6 and Figure I.10 demonstrate that the proposed model predicts the shadowing variation with respect to tile changes closely to what is observed from the ray tracing data.

5.2 Statistical Behavior of Height Gain

The height gain effect is investigated by using the propagation maps generated using a ray tracing tool for the considered 3D urban model scenario depicting a typical European city clutter type as shown in Figure I.3. In this case the total propagation loss $L(\bar{x}_{h_i}, \Theta_o)$ is predicted at a different floor height level using the ray tracing tool where the tool considers the propagation effects experienced in real life by using the employed 3D model scenario during the propagation map prediction. Thus, various propagation map is generated with the ray tracing tool for 7 different height levels, i.e. ground floor at 1.5 m high and 6 higher floors with 3.1 m height difference between the them.

Accordingly, the height gain $\hat{H}(\bar{x}_{h_i, h_0})$ at at each pixel points \bar{x} at a floor height level of h_i with respect to the ground floor height h_o is evaluated from the ray tracing propagation maps, predicted for each floor height, as shown in Equation I.25.

$$\hat{H}(\bar{x}_{h_i, h_0}) = L(\bar{x}_{h_i}, \Theta_o) - L(\bar{x}_{h_i}, \Theta_o); \quad (I.25)$$

The evaluated $\hat{H}(\bar{x}_{h_i, h_0})$ statistics from each pixel points are analyzed for different sectors. $\hat{H}(\bar{x}_{h_i, h_0})$ statistical distribution is presented in Figure I.11 for one sample sector from the ray tracing scenario. It can be seen from the figure that, the height gain value is different at different location and this value even deviates significantly from the corresponding average height gain value at the respective floor height level. The deviation is due to the fact that the clutter effect experienced at various points at a

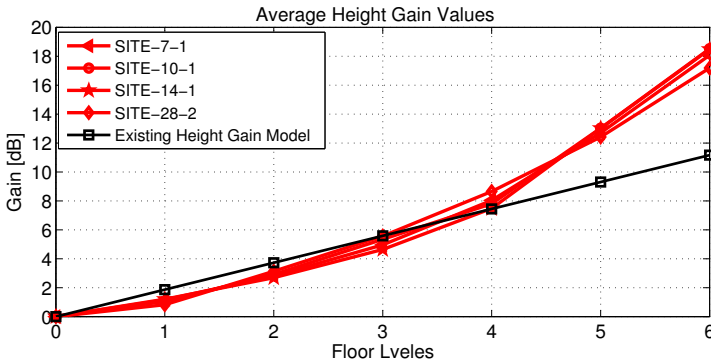


Fig. I.12: $\hat{H}(\bar{x}_{h_i, h_0})$ Statistical Distribution With respect to the Ground Floor

certain floor height level different at different location. The average height floor height gain level is also evaluated for various sector propagation cases and it is compared with the exiting 0.6 dB/m gain in Figure I.12. The same kind of statistical distribution behavior is observed for the height gain values evaluated with respect to various sector from the ray tracing scenario. It has been also shown in Figure I.11 that this height gain statistics follows a chi-square distribution and fits well in the figure with a chi-square distribution curve for 4 degree of freedom, i.e. $\hat{H}(\bar{x}_{h_i, h_0}) \sim \chi_4^2$, centered at different mean for each floor height level.

As can be seen in Figure I.12, the average height gain found from the ray tracing data fits quite well till the 4th floor and a height gain corresponds to the existing model declines for higher floors. This could be a specific clutter nature of the scenario considered in our ray tracing. However, the average height gain from different sites shows quite similar trends.

6 Impact of Tilt and Height Based Models in Network Planning and Optimization

The proposed tilt dependent shadowing model and the floor height gain investigation results have shown that a more tuning is required in the existing propagation model in order to accurately reflect the real time propagation effects. As discussed in earlier section, in network planning and optimization tasks, the planning and optimization tool should be able to properly estimate the changes that occurs in reality due to any applied change in network parameter. The antenna tilt is one of the significant radio parameters which is used in order to ensure network coverage and also to control the co-channel interference level in the system. In dynamic and flexible cell lay out deployment, supported by the AAS features, the antenna beam orientation is adapted to the traffic situations in the network. Hence, developing and evaluation such network operation mechanisms and algorithms in system level simulators and network planning tools, respectively, should include the impact of tilt and corresponding clutter

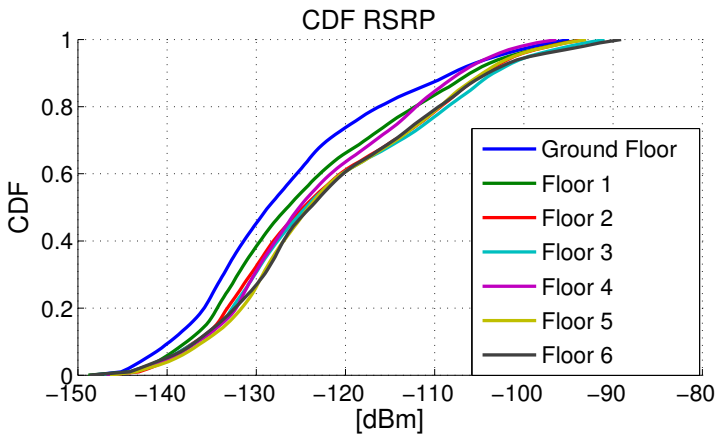


Fig. I.13: RSRP statistics CDF From Ray Tracing Scenario

type variation experience.

In the case of multi-floor building scenario, using a constant floor height gain, as proposed by the existing model, always leads to a gain in that increase with floor height level as depicted in Figure I.12. However, in real case, the floor height gain value is highly dependent on the relative position of a user location with respect to the corresponding transmitting antenna and also the the line of sight probability for the signal reception at respective floor height level. Consequently, the height gain is not always experienced and could disappears after a certain height level. In this paper, this is illustrated in Figure I.13 where the height gain is exhibited in the Reference Signal Received Power (RSRP) level cdf indoor statistics taken from the ray tracing scenario. Thus, the floor height gain is observed up to 3rd floor in some cases and disappears after that, and at the lower percentile the CDF, it can be seen also that the height gain does not disappear but stops showing further gain while increasing the floor level. This is due to the fact that, the line of sight probability and the clutter experience of some locations gets worse with height due to their geographical location with respect the transmitting antenna. The presence of various height gain experience in real network results in a different RSRP level reception at each floor. This will lead a different cell coverage and serving cell dominance per floor.

According to the the existing floor height gain model, however, the signal received from any transmitting antenna will have the same amount of height gain, therefore it predicts the same server map plot for each floor at certain location. However, the best server map plot found from the ray tracing data and shown in Figure I.14 demonstrates that, due to the random variation of the height gain value, a certain location could experience different floor height gain on the RSRP value detected from different transmitting sector antennas. As a consequence, a user could experience a different serving sector at the same 2D geographical location but at different floor heights. It is also well illustrated in Figure I.14 that while changing the floor a new sector could merge and dominate and other sectors also changes either their coverage dominance area or disappear.

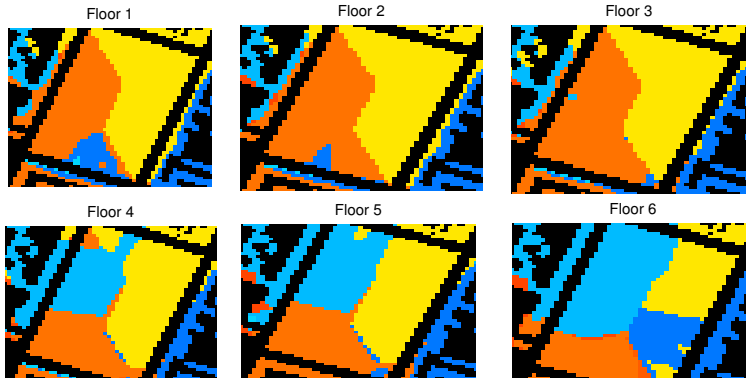


Fig. I.14: Best Server Map Plot at Different Floor Levels

7 Conclusion

In this paper, a new tilt dependent shadowing model is proposed as an extension to the existing propagation model. The tilt dependent shadowing model predicts the shadowing effect variation that could be experienced in real propagation environment while a tilt change is applied. During when a tilt is changed, the proposed model predicts and generates a new shadowing fading process from the shadowing effect assumed before the tilt with a certain statistical correlation level and the amount of tilt change applied. The level of the shadowing effect change with the applied tilt difference and the corresponding de-correlation of the shadowing process can be also predicted by the the proposed tilt dependent shadowing model. The model is derived and validated with a ray tracing based generated propagation maps that for a 3D model of a typical European city urban clutter type. Though a sample site results are presented in the paper, the investigation has been carried out randomly for 75 different sectors and closely the same prediction performance is observed for the proposed model.

Furthermore, the floor height gain variation and its effects has been investigated and discussed in this paper. It has been found out that the height gain variation is deviates from the mean value with an increase in height level. Moreover, it has been demonstrated that, in real deployment, the floor height gain does not actually exist and it leads a different server map experience for a service area depending on the its relative location with respect to the transmitting antenna. This suggests to use a random variable floor height gain than a deterministic gain value as stated in the existing model.

The proposed tilt dependent model, is derived based on the propagation map data from the considered typical scenario. The scenario dependent parameter introduced here is the correlation prediction function $f_s(\Delta\Theta)$ whose coefficients are evaluated based on this specific scenario. Therefore, there could be deviation on the coefficient values. Hence, the authors would like to put this limitation as an outlook.

References

- [1] J. Walfisch and H. L. Bertoni, "A theoretical model of UHF propagation in urban environments," *IEEE Transactions on Antennas and Propagation*, vol. 36, no. 12, pp. 1788–1796, Dec 1988.
- [2] F. Ikegami, S. Yoshida, T. Takeuchi, and M. Umehira, "Propagation factors controlling mean field strength on urban streets," *IEEE Transactions on Antennas and Propagation*, vol. 32, no. 8, pp. 822–829, Aug 1984.
- [3] M. Hata, "Empirical formula for propagation loss in land mobile radio services," *IEEE Transactions on Vehicular Technology*, vol. 29, no. 3, pp. 317–325, Aug 1980.
- [4] J.-E. Berg, *COST Action 231. Digital mobile radio towards future generation systems. Final report.* European Commission. EUR 18957, 1999.
- [5] G. L. Stüber, *Principles of Mobile Communication. 3rd Edition.* Springer-Verlag New York, 2011.
- [6] *3GPP Technical Report (TR) 36.814. Further advancements for E-UTRA physical layer aspect. V.9.1.0*, Dec 2016.
- [7] O. N. C. Yilmaz, S. Hamalainen, and J. Hamalainen, "System level analysis of vertical sectorization for 3GPP LTE," in *6th International Symposium on Wireless Communication Systems*, Sept 2009, pp. 453–457.
- [8] D. W. Kifle, B. Wegmann, I. Viering, and A. Klein, "Impact of Antenna Tilting on Propagation Shadowing Model," in *IEEE 77th Vehicular Technology Conference (VTC Spring)*, June 2013, pp. 1–5.
- [9] H. Okamoto, K. Kitao, and S. Ichitsubo, "Outdoor-to-Indoor Propagation Loss Prediction in 800-MHz to 8-GHz Band for an Urban Area," *IEEE Transactions on Vehicular Technology*, vol. 58, no. 3, pp. 1059–1067, March 2009.
- [10] J.-E. Berg, *Propagation Prediction Models (building penetration). COST Action 231. Digital mobile radio towards future generation systems. Final report.* European Commission. EUR 18957, 1999.
- [11] G. Wölfle, R. Wahl, P. Wertz, P. Wildbolz, and F. Landstorfer, "Dominant path prediction model for indoor scenarios," *German Microwave Conference (GeMic)*, 2005.
- [12] S. Burger, *AWE Communications Technical Report. Accuracy of Winprop 3D Intelligent Ray Tracing*, 2003.
- [13] T. S. Rappaport and S. Sandhu, "Radio-wave propagation for emerging wireless personal-communication systems," *IEEE Antennas and Propagation Magazine*, vol. 36, no. 5, pp. 14–24, Oct 1994.
- [14] F. Gil, A. R. Claro, J. M. Ferreira, C. Pardelinha, and L. M. Correia, "A 3d interpolation method for base-station-antenna radiation patterns," *IEEE Antennas and Propagation Magazine*, vol. 43, no. 2, pp. 132–137, Apr 2001.

Paper J – (Collaboration 2)

Verification of 3G and 4G Received Power
Measurements in a Crowdsourcing Android App

Mads Lauridsen, Ignacio Rodríguez, Lars Møller Mikkelsen,
Lucas Chavarría Giménez, Preben Mogensen

Published in
IEEE Wireless Communications and Networking Conference (WCNC) 2016.

© 2016 IEEE

Reprinted with permission. The layout has been revised.

Abstract

Many crowdsourcing Android applications are available for measuring network Key Performance Indicators such as received power, latency, and throughput. The data is useful for end-users, researchers, and Mobile Network Operators, but unfortunately the applications' accuracy are rarely verified.

In this paper we verify the crowdsourcing Android application NetMap's ability to measure LTE Reference Signal Received Power by analyzing the Root Mean Squared Error, being 2-3 dB, and cross-correlation coefficient, being above 0.8, with measurements obtained by use of a professional radio network scanner and measurement phones. In addition, the application is applicable, but less accurate, for 3G Received Signal Code Power measurements. The studies are made for various device speeds and in different scenarios including indoor, urban, and highway, where the NetMap application is showed to perform well.

1 Introduction

Obtaining Key Performance Indicators (KPIs), such as received power, latency, throughput, and mobility performance for mobile networks is of interest to the end-user, researchers, and Mobile Network Operators (MNOs) [1]. The end-user can use the KPIs when selecting MNO subscription, while access to the KPI data enables researchers to study network problems and develop potential solutions. Finally the KPIs can assist MNOs in optimizing their network deployment and setup.

The KPIs can be measured using drive tests, dedicated test beds, network-side-only tools, or user-deployed applications, [1]. The first 3 solutions often rely on professional tools, only cover a limited area, and require many man-hours of work to be conducted. On the contrary the user-deployed applications enable both the end-user, researchers, and MNOs to obtain the KPIs, reflecting the real end-users experience and mobility, at a low cost. Many applications, e.g. [2–6], have started using crowdsourcing i.e. spreading the applications among many users to gather as much data as possible.

The aforementioned applications are able to measure a large number of parameters including received power, latency, throughput, location, mobility performance, and energy consumption. In addition, they are able to cover a larger geographical area as compared to what drive tests and dedicated test beds can, but unfortunately the developers rarely verify whether the measurements are accurate. In [2] the authors study how accurate the latency and energy consumption measurements are, while [4, 5] compare what they termed "manual measurements" and subsets of their own data without giving further details. In [6] the authors focus on the energy consumption of running the application, which is of high importance as crowdsourcing will be difficult if the application has a reputation of excessive energy consumption. The quality of the received power measurements is discussed in [3] which observed that measurements are averaged by the phone and that some phones seem to report inaccurate numbers. Related to that, the authors of [7] state that it is likely that different phones report with different level of resolution, but the authors don't examine it in further detail.

The received power is important for understanding other network KPIs such as latency and throughput, because it will affect the applied modulation and coding scheme, and the number of retransmissions. However, according to the survey in [1] only 14 of 29 surveyed tools are able to produce coverage maps or report the received power. In fact, the conclusion of [1] specifically mentions that the accuracy of the tools is difficult to compare. This entails a root cause analysis of the observed network KPIs may be difficult to perform.

The contribution of this paper is to verify the received power measurement accuracy of our crowdsourcing Android application, named NetMap, which uses the Android API [8]. Having verified and accurate received power measurements enables researchers and MNOs to understand other KPIs such as latency and throughput in further detail. We perform the verification by comparing the NetMap measurements with 2 professional measurement phones and a radio network scanner in 4 different scenarios including indoor, urban, and highway at speeds from pedestrian to 110 km/h.

The paper is structured as follows; first the NetMap application is described in Sec. 2 with focus on how received power measurements are made, then the verification methodology including tools, scenarios, data processing, and evaluation is presented in Sec. 3. Selected results are presented together with a discussion and future use of the application in Sec. 4 and 5 respectively, followed by the conclusion in Sec. 7.

2 The NetMap Application

The NetMap Android application is designed to capture network performance on the application layer and Radio Access Technology (RAT) specific parameters that affect the end-user experience [9]. The application captures information for 2G, 3G, and 4G while also logging user position via GPS.

The default NetMap application logs throughput, connectivity, network context state, Round Trip Time (RTT) and received power [9]. In this work, a simplified version logging the two latter parameters was applied. Both the RTT and received power measurement are collected with a frequency of approximately 1 Hz, which entails the mobile terminal is always expected to be actively connected to the serving cell. In between the measurements the application is in a sleep state to reduce the effect on battery life and general resource usage.

The RTT measurement is initiated when the application sends a UDP packet, with a payload containing a packet ID of a maximum of 1024 bytes, to a server at Aalborg University (AAU). When the response is received at the application layer the total RTT is logged. This is implemented using the DatagramPacket and the DatagramSocket APIs in Android [8]. A timeout of 1 s is set on the socket to capture long RTTs.

Every time a RTT measurement is performed the received power is also sampled as illustrated in Fig. J.1. When 60 measurements are completed a report is generated after which 60 new measurements are initiated as soon as possible. Depending on the RAT it varies how the received power is calculated and which Application Programming Interface (API) must be used. Furthermore, depending on the state of the phone's screen the APIs act differently, and in addition, different APIs are available in different versions of the Android operating system.

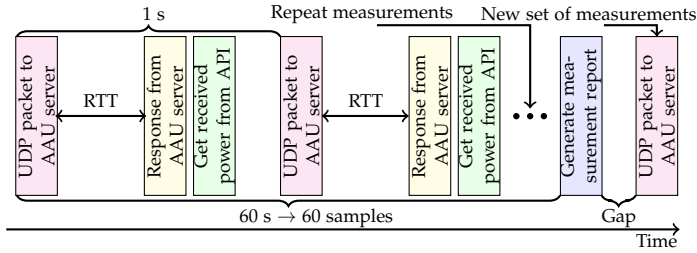


Fig. J.1: NetMap activity chart.

There are two APIs that can be used for extracting the received power values; SignalStrength and CellInfo [8]. The SignalStrength API has been available since Android SDK version 7 (Android 2.1). This API offers a wide range of received power related information, and for 3G measurements NetMap reads the GsmSignalStrength via the call `getGsmSignalStrength()`. The 3G received power is reported via this API because Android decided it is convenient that the received power for different RATs is reported in the same place. The call returns an Arbitrary Strength Unit (ASU) value representing the 3G Common Pilot Channel Received Signal Code Power (RSCP), and valid values are (0-31, 99) as defined in [10]. The conversion to RSCP is defined as:

$$\text{RSCP} = \text{ASU} - 120 \quad [\text{dBm}] \quad (\text{J.1})$$

For Long Term Evolution (LTE) the call `LteRsrp` returns the Received Signal Reference Power (RSRP) defined as: [10]

$$\text{RSRP} = \text{ASU} - 140 \quad [\text{dBm}] \quad (\text{J.2})$$

Unfortunately the SignalStrength API only report updates while the screen is ON, and therefore the CellInfo API is used while the screen is OFF. The CellInfo API was made available in Android SDK version 17 (Android 4.2), but the subclass CellInfoWcdma was not added until SDK version 18 (Android 4.3) [8]. For 3G the CellInfoWcdma is used to extract received power values via the call `.getCellSignalStrength().getDbm()`. For LTE the subclass CellInfoLte is used with the call `.getCellSignalStrength().getAsuLevel()` which returns an ASU value defined between 0-97, and where 99 is unknown [10].

During development and measurements we have observed that the behavior of received power values from the CellInfo API varies from phone to phone from different manufacturers in terms of update frequency and availability. This indicates that different manufacturers implement the received power reported to the Radio Interface Layer from the network modem differently, as also observed by [3, 7].

3 Methodology

The purpose with this work is to verify that NetMap, using the Android APIs on a commercial smartphone, is able to accurately measure 3G RSCP and LTE RSRP received powers. Our methodology is to compare the NetMap measurements, made in 4 different scenarios, with quality references obtained by use of professional measurement tools consisting of a Rohde & Schwarz radio network scanner, from now on referred as the scanner, and 2 Qualipoc measurement smartphones from SwissQual. The details of the tools and scenarios are given in the following Sec. 3.1. This allows for the following three comparisons:

i *Radio network scanner vs. NetMap*

The scanner has the best measurement resolution and sampling time, but it is a passive device unable to connect to a specific network. The scanner is often favored for drive tests due to its ability to monitor multiple carrier frequencies at once. However, it will not reflect the end-user experience, including handover settings, traffic steering, and cell load conditions, as NetMap will.

ii *Qualipoc vs. NetMap running on the same phone*

Running NetMap on the measurement phone entails NetMap and the Qualipoc software should report the same received power, because they have the same origin. However, the measurement phone is rooted and the Qualipoc software optimized to provide better resolution and sampling time as compared to the commercial phone.

iii *Qualipoc vs. NetMap running on a different phone*

Running NetMap on a different phone is expected to result in received power differences, because the two phones will not experience the same fast fading. In addition, the Radio Frequency (RF) front ends and application layers are different. However, since both phones are connected to the same MNO the measurements should be comparable and reflect the accuracy that can be obtained in practice.

3.1 Tools and Scenarios

The list of phones and measurement tools as well as their key characteristics are given in Table J.1. To illustrate NetMap's potential to crowdsource coverage, latency, and other network KPIs the application was installed on 3 identical, commercial phones (A,B,C), which were connected to 3 major MNOs (X,Y,Z) in Denmark. The measurement phones (D,E) were connected to operator X, while the scanner (F) passively monitored the received power from all 3 MNOs simultaneously.

As indicated in Table J.1 NetMap's resolution is 10-100 times worse than the professional tools (D-F), and therefore it especially interesting to analyze whether the received power measurements are comparable, because NetMap will then provide a cheap and easily deployable alternative. NetMap's sampling time is also lower than Qualipoc's and the scanner in LTE mode. For 3G the scanner, used in high accuracy mode, has a sampling time similar to NetMap because it monitors a large number of bands. NetMap's lower sampling time and resolution may be more of an issue in some scenarios than in others and therefore the 6 devices were deployed in 4 different

Table J.1: KEY PARAMETERS FOR THE PHONES AND MEASUREMENT TOOLS. RAT SPECIFIC PARAMETERS ARE GIVEN AS 3G; LTE.

ID	Model	Software	Android version	Operator & bands	Sampling time [s]	Resolution [dB]
A	Google Nexus 6	NetMap	5.1.1	X: 900,2100; 800,1800,2600	1; 1	2; 1
B	Google Nexus 6	NetMap	5.1.1	Y: 900,2100; 800,2600	1; 1	2; 1
C	Google Nexus 6	NetMap	5.1.1	Z: 2100; 1800,2600	1; 1	2; 1
D	Samsung GS3	Qualipoc 13.0.0.25	4.1.2 [†]	X	0.32; 0.52	1; 0.1
E	Samsung GS5	Qualipoc 15.0.0.53	4.4.4 [†]	X	0.29; 0.53	1; 0.1
F	R&S TSMW radio scanner	Romes 4.82	-	passive X,Y,Z	1.1; 0.11	0.1; 0.01

[†] SwissQual provided a modified version of Android to run Qualipoc

Table J.2: SCENARIO DETAILS WITH SPECIFIC PARAMETERS AVERAGED FROM QUALIPOC PHONES (D,E). RAT SPECIFIC PARAMETERS ARE GIVEN AS 3G; LTE.

Scenario	AAU	AAU	Aalborg	Highway
Parameter	indoor	outdoor	city center	E45
Fig. reference	J.2a yellow	J.2a green	J.2b	J.2c
Device speed [km/h]	6 (pedestrian)	6	30	110
Distance [km]	0.44	0.35	2.7	5.7
Observed cells [-]	2; 1	2; 1	14; 12	9 ; 6
Minimum power [dBm]	-100; -110	-87; -96	-96; -114	-106; -117
Maximum power [dBm]	-61; -72	-62; -79	-41; -56	-47; -62

scenarios; indoor & outdoor at AAU campus, in Aalborg city center, and on the local highway. The details of the scenarios are listed in Table J.2 and they clearly provide different propagation conditions as reflected by the device speed, number of observed cells, and dynamic range of the received signal. The number of observed cells and received powers are based on reports from the Qualipoc phones (D,E). Fig. J.2 illustrate the measurement routes in the 4 scenarios. Note that the yellow line in Fig. J.2a corresponds to the indoor scenario, while the green line is the outdoor scenario.

In order to eliminate effects of the devices moving differently or experiencing different gains due to hand grip effects [11], the devices were mounted in a measurement rack and then moved either by use of a trolley (in the AAU scenarios) or car

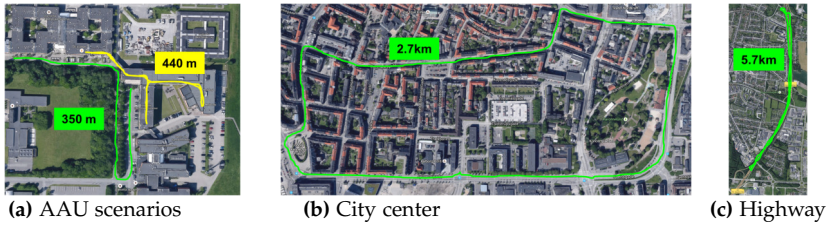
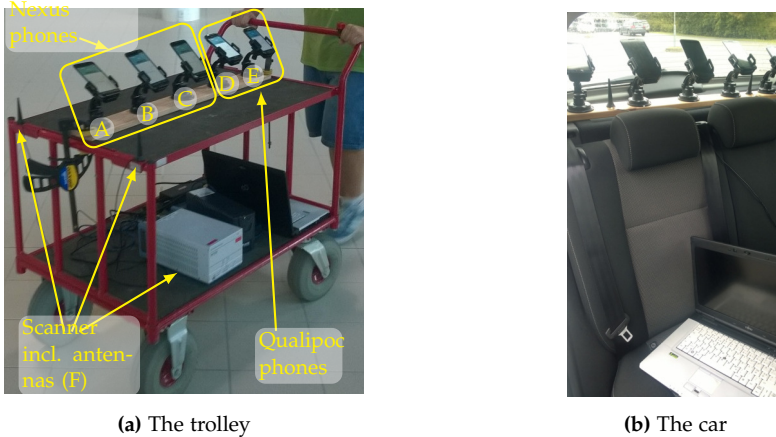


Fig. J.2: The measurement routes in the 4 scenarios.



(a) The trolley (b) The car
Fig. J.3: The measurement tools and transportation devices.

(city center and highway) as illustrated in Fig. J.3.

3.2 Data Processing and Evaluation

After the measurements are completed they are post-processed in Matlab to determine how well NetMap's measurements match those of the Qualipoc phones and the scanner. The processing procedure is as follows:

1. data from the Qualipoc phones and the scanner (devices D-F) are filtered to remove any fast fading effects, because the purpose is to verify whether NetMap captures the overall coverage (mean path loss level) and shadow fading (slow variations of the path loss).
2. data from devices D-F is downsampled (if necessary) to fit the sampling rate of NetMap.
3. comparisons according to the methodologies (i,ii,iii), described in Sec. 3, are performed as follows:
 - i NetMap phones (A-C) are compared with the scanner (F) capturing all 3 MNOs (X,Y,Z). The results are averaged across operators for each of the 4 scenarios. The scanner measures the received power of all cells within its dynamic range while NetMap only measures the received power of the current serving cell. The NetMap measurements are therefore compared with the maximum received

power of the scanner, which is determined sample by sample. A hysteresis of 5.5 dB and 3 dB is used for 3G and LTE respectively, to emulate a handover margin between the current serving cell and a stronger neighbor cell.

- ii NetMap measurements of phones D and E are compared with the Qualipoc measurements of the same phones. The results are averaged for the two Qualipoc phone D and E connected to MNO X.
 - iii NetMap in phone A is compared with Qualipoc measurements of phones D and E. The 3 phones are connected to the same operator (X), but they may experience small differences in fading, in addition to the different RF front end and antenna gains.
4. the comparisons are based on a parameter search to determine the time- and power-offset between NetMap and reference data. This is necessary because the 6 devices were not started simultaneously and due to the devices' different antenna and RF front end gains.
 5. the best fit, depending on the time- and power-offset, is the one resulting in the lowest Root Mean Squared Error (RMSE) and the highest cross-correlation coefficient ρ . Definitions of these metrics are given in the appendix.

Fig. J.4 illustrates the original data after it is time-aligned (thin line) and after it has been filtered (thick line), but not compensated for power-offset. The Fig. also illustrates a potential handover case, where carrier 2 observed by the scanner is stronger than carrier 1. However, during the measurements (not illustrated in Fig. J.4) it was observed that NetMap and Qualipoc phones may be connected to a carrier with lower received power as compared to the maximum value observed by the scanner. The reason is traffic steering and handover policies implemented by the MNO to suit the specific scenario, and differences in antenna and RF front end gains.

The power-offset calibration coefficients for NetMap on phone A vs Qualipoc phone D and E are given as an example in Table J.3. In order for the measurements to be valid the power-offset should be constant across the scenarios when compared with a specific device for a specific RAT, because the power-offset only depends on antenna and RF front end gains. The results in Table J.3 reflect this as the standard deviation is around 1 dB for 3G, while it is only about 0.2 dB for LTE i.e. a very constant offset is applied for all scenarios in LTE. In the city center scenario phone A, connected to operator X, performed a handover from LTE to 3G shortly after the measurement was initiated. Therefore the result, marked with *italic*, is unreliable and not included in the calculation of average values. It is not possible to force the phones to LTE, because Voice over IP is not fully implemented in Denmark yet and therefore it would make voice calls to the specific LTE-only phone impossible.

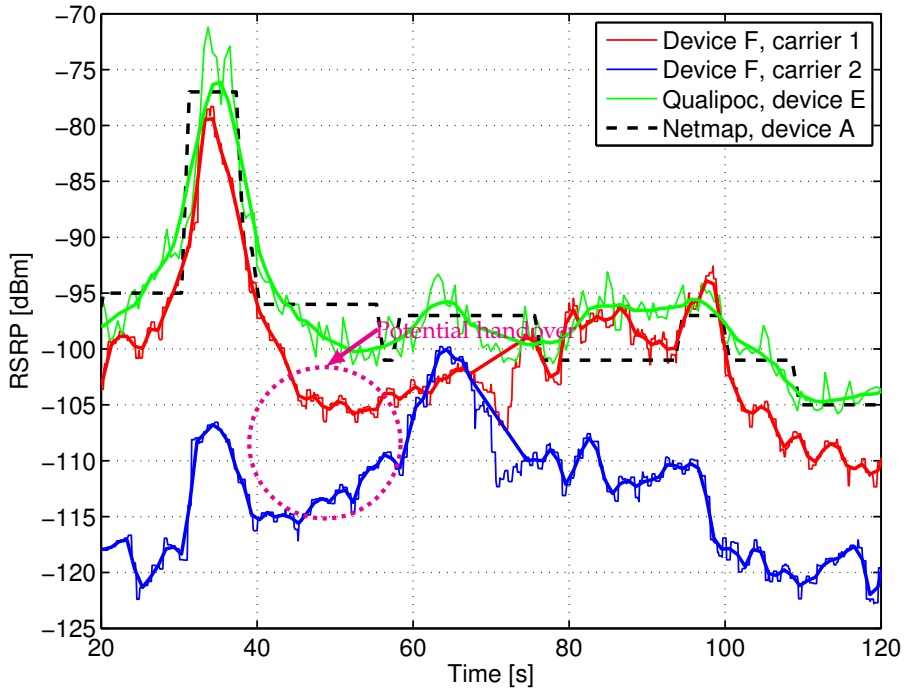


Fig. J.4: Data processing steps. Thin lines are original, time aligned data. Solid lines are filtered and downsampled data. The scenario is indoor LTE.

Table J.3: CALIBRATION COEFFICIENTS FOR NETMAP ON PHONE A VS QUALIPOC PHONES D AND E. VALUES IN DB.

Scenario	Phone	3G		LTE	
		D	E	D	E
Indoor		-8.5	-4.8	-0.8	0.7
Outdoor		-8.3	-5.2	-0.5	1.0
City center		-6.2	-5.9	2.5	1.6
Highway		-8.5	-4.5	-0.9	0.8
Average		-7.9	-5.1	-0.73	0.83
Standard deviation		1.12	0.61	0.21	0.15

Table J.4: NETMAP 3G MEASUREMENTS COMPARED WITH SCANNER AND QUALIPOC.

Comparison	i (scanner)		ii (same phone)		iii (different phone)	
	RMSE	ρ	RMSE	ρ	RMSE	ρ
Indoor	4.1 dB	0.52	2.1 dB	0.88	3.7 dB	0.68
Outdoor	4.8 dB	0.57	1.8 dB	0.73	3.3 dB	0.44
City center	6.1 dB	0.72	2.3 dB	0.97	7.0 dB	0.66
Highway	6.8 dB	0.71	4.3 dB	0.92	4.6 dB	0.87
Average	5.4 dB	0.63	2.6 dB	0.88	4.6 dB	0.66

4 Results

In this section the RMSE and cross-correlation coefficient ρ results are presented for the 3 comparisons defined in Sec. 3. The 2 KPIs: RMSE and ρ are defined in the appendix.

The results for the 4 scenarios when using 3G is given in Table J.4. As expected comparison ii (NetMap and Qualipoc on the same phone) results in the best fit with an average RMSE close to NetMap's resolution of 2 dB (see Table J.1), and a high cross-correlation coefficient of 0.88. The comparisons i and iii with the scanner and Qualipoc running on a different phone yield less accurate results for 3G as the correlation on average is below 0.7 while the RMSE is above 4 dB.

The indoor and outdoor AAU scenarios show the smallest dynamic range of the received power according to Table J.2, and this is reflected in the results in Table J.4 where those scenarios result in the lowest RMSE. However, on average the smaller variations also entail a lower cross-correlation coefficient as compared to the city center and highway scenarios.

The results for LTE are given in Table J.5. As in 3G the comparison ii provides the best results, but for LTE the comparisons i and iii also provide accurate results with an average cross-correlation coefficient around 0.8 i.e. a good match between NetMap and the professional tools.

Fig. J.5 illustrates the filtered, downsampled, and time- and power-offset results for Qualipoc and NetMap measurements on phone E compared with NetMap measurements on phone A i.e. all connected to the same operator (X). The scenario is indoor LTE. The NetMap measurement on phone E seems to vary slightly more than the NetMap measurement on phone A. Since NetMap was configured to provide one measurement per second for both phones, see Table J.1, the difference is expected to be due to the model and configuration of the chipset and processor.

Table J.5: NETMAP LTE MEASUREMENTS COMPARED WITH SCANNER AND QUALIPOC.

Comparison	i (scanner)		ii (same phone)		iii (different phone)	
Scenario	RMSE	ρ	RMSE	ρ	RMSE	ρ
Indoor	3.0 dB	0.83	2.1 dB	0.88	2.6 dB	0.87
Outdoor	3.0 dB	0.72	0.8 dB	0.93	2.0 dB	0.67
City center	5.8 dB	0.80	1.9 dB	0.99	4.5 dB	0.85
Highway	7.3 dB	0.74	1.8 dB	0.99	4.5 dB	0.91
Average	4.7 dB	0.77	1.7 dB	0.95	3.4 dB	0.83

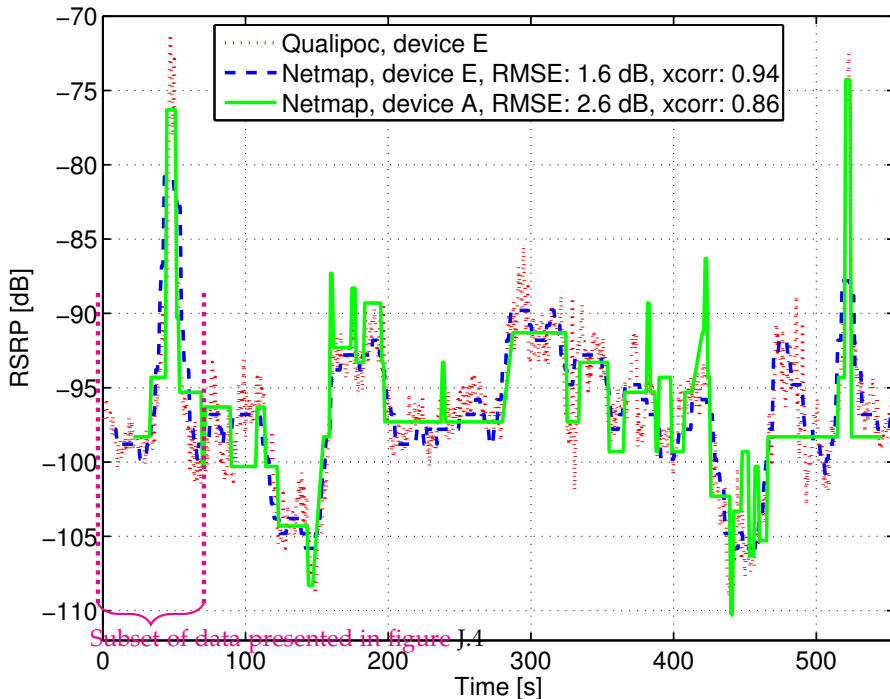


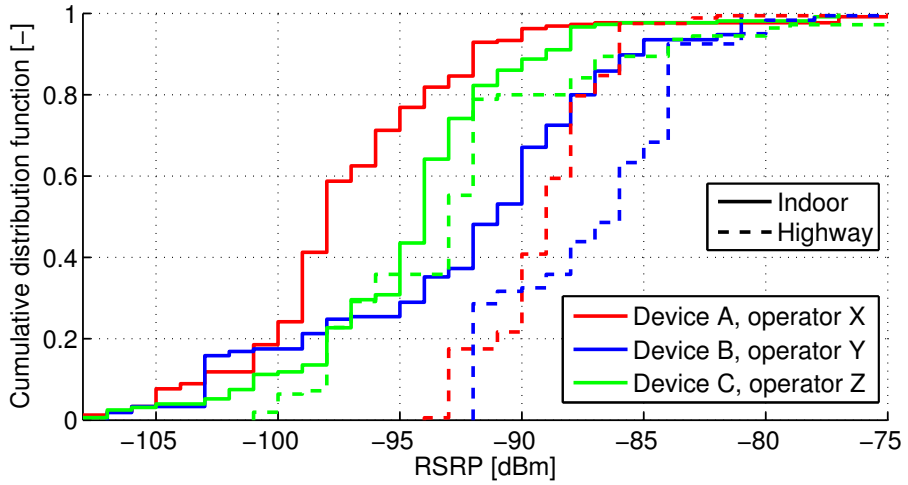
Fig. J.5: NetMap measurements from Qualipoc phone E and commercial phone A compared with the Qualipoc measurement. The scenario is indoor LTE.

5 Discussion

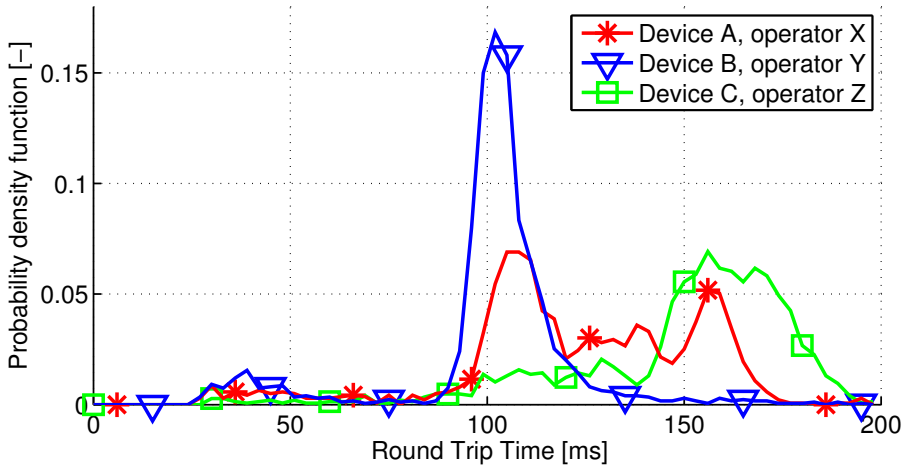
The results, presented in the previous section, verified that NetMap, running on a commercial smartphone, is able to measure LTE RSRP with sufficient accuracy to track shadow fading and path loss. It provides a cheap alternative to the professional tools even though the resolution and sampling time are significantly lower. In addition, NetMap reports the measurements of a connected phone as opposed to the scanner, which in some cases may overestimate the coverage, because it is not able to capture phenomena caused by MNO traffic steering. NetMap's 3G measurements are less accurate, partly due to the Android API, but still reliable. The RMSE of 3-5 dB (see Table J.4) is not critical when considering that empirical path loss models and ray-tracing tools compared with received power measurements may result in RMSEs of 4-6 dB [12].

The NetMap measurements were calibrated towards either the scanner or the Qualipoc phones and therefore the power-offset is relative to the antenna and RF front end gain of these devices. This entails the absolute values are not accurate, while the relative measurements are calibrated. This is especially important for the crowdsourcing results, because as the measurements show the average power-offset in Table J.3 is as high as 8 dB between phones A and D. Thus, there may be significant differences in crowdsourced data from different phones, which must be compensated in the final analysis. This variability was also observed by [3, 7].

Having verified the NetMap received power is an important achievement, because it enables the further analysis of statistics such as latency and throughput, and why those parameters in some cases are worse than expected. In addition, the received power measurements can be used to study and compare the coverage of various MNOs. As an example Fig. J.6a shows the Cumulative Distributive Function of the received power for phones A-C connected to operators X, Y, and Z respectively. The measurements are made for LTE in the indoor AAU and highway scenarios. Operators X and Y seem to benefit from having a sub-GHz carrier in the highway scenario, while operator Y in general provides the best coverage for both scenarios. Fig. J.6b illustrates the combined NetMap LTE RTT measurements for each of the 3 operators averaged across the 4 scenarios. Significant variations can be observed and if low RTT is of importance to the end-user, operator Y seems like the best choice. Future work includes a correlation analysis of the RSRP and RTT measurements. In addition, the authors of [7] also noted that the use of the signal-to-interference-and-noise ratio metric can be useful, when correlating RTT and throughput measurements with coverage.



(a) NetMap RSRP for LTE indoor and highway scenarios.



(b) NetMap RTT for all LTE scenarios combined.

Fig. J.6: NetMap LTE measurements.

6 Conclusion

NetMap is an Android application developed for crowdsourcing Mobile Network Operator statistics as observed by the user, e.g. received power, latency, and throughput.

The purpose of this work, being a measurement campaign, was to verify the ability of NetMap to correctly measure received power in 3G and LTE cellular networks. Received power is important when analyzing metrics such as latency and throughput because it affects the modulation and coding scheme that can be applied and the number of retransmissions.

The measurements were performed by connecting commercial smartphones running NetMap to 3 operators in Denmark, while also monitoring the received power using professional measurement phones from SwissQual and a Rohde & Schwarz radio network scanner. The diverse measurement scenarios included indoor & outdoor pedestrian speed traces, and driving on the highway and in the city center of Aalborg.

The results show that NetMap yields accurate LTE measurements with a Root Mean Squared Error of 2-3 dB and cross-correlation coefficient above 0.8, even for high speeds. The 3G measurements result in an error of 3-5 dB and a cross-correlation coefficient of 0.6-0.8, partly due to lower measurement resolution in the Android API. Furthermore, the results show a constant power-offset between NetMap and the professional tools and thus indicate consistent measurements.

Future work includes recording the cell ID concurrently with received power measurements, and presenting the measurement results to the end user, e.g. a coverage map. This will help attract new users, which is vital for crowdsourcing.

Appendix

The Root Mean Squared Error is defined as:

$$\text{RMSE}(x, y) = \sqrt{\frac{1}{N} \sum_{i=1}^N (x_i - y_i)^2} \quad [\text{dB}] \quad (\text{J.3})$$

where x and y are the signal of interest and reference, respectively i.e. a NetMap measurement and a scanner or Qualipoc measurement. The length of the signals is N .

The cross-correlation coefficient ρ is defined as:

$$\begin{aligned} \rho(x, y) &= \frac{\text{cov}(x, y)}{\sqrt{\sigma_x^2 \sigma_y^2}} \quad [-] \\ &= \frac{E[(x - \mu_x)(y - \mu_y)]}{\sqrt{E[(x - \mu_x)^2] E[(y - \mu_y)^2]}} \quad [-] \end{aligned} \quad (\text{J.4})$$

where $\text{cov}(x, y)$ is the covariance of x and y , σ_x^2 is the variance of x , E is the expectation, and μ_x is the mean defined as $\mu_x = \frac{1}{N} \sum_{i=1}^N x$ for discrete values.

Acknowledgment

This work was supported by Innovation Fund Denmark.

References

- [1] U. Goel, M. P. Wittie, K. C. Claffy, and A. Le, "Survey of End-to-End Mobile Network Measurement Testbeds," *CoRR*, vol. 1411.5003, 2014.
- [2] A. Nikraves, H. Yao, S. Xu, D. Choffnes, and M. Mao, "Mobilyzer: An open platform for controllable mobile network measurements," in *Proceedings of MobiSys*, May 2015.
- [3] S. Sonntag, J. Manner, and L. Schulte, "Netradar - Measuring the wireless world," in *11th International Symposium on Modeling Optimization in Mobile, Ad Hoc Wireless Networks*, May 2013, pp. 29–34.
- [4] S. Rosen, S.-J. Lee, J. Lee, P. Congdon, Z. Mao, and K. Burden, "MCNet: Crowdsourcing wireless performance measurements through the eyes of mobile devices," *Communications Magazine, IEEE*, vol. 52, no. 10, pp. 86–91, October 2014.
- [5] J. Yoon, S. Sen, J. Hare, and S. Banerjee, "WiScope: A Framework for Measuring the Performance of Wide-Area Wireless Networks," *Mobile Computing, IEEE Transactions on*, vol. 14, no. 8, pp. 1751–1764, 2015.

- [6] N. Haderer, F. Paraiso, C. Ribeiro, P. Merle, R. Rouvoy, and L. Seinturier, "A Cloud-Based Infrastructure for Crowdsourcing Data from Mobile Devices," in *Crowdsourcing*, ser. Progress in IS, W. Li, M. N. Huhns, W.-T. Tsai, and W. Wu, Eds. Springer, 2015, pp. 243–265.
- [7] J. Cainey, B. Gill, S. Johnston, J. Robinson, and S. Westwood, "Modelling download throughput of LTE networks," in *Local Computer Networks Workshops, IEEE 39th Conference on*, 2014, pp. 623–628.
- [8] Google Inc., "Developers' reference," Sep. 3 2015. [Online]. Available: <http://developer.android.com/reference>
- [9] L. M. Mikkelsen, S. R. Thomsen, M. S. Pedersen, and T. K. Madsen, "NetMap - Creating a Map of Application Layer QoS Metrics of Mobile Networks Using Crowd Sourcing," in *Internet of Things, Smart Spaces, and Next Generation Networks and Systems*, ser. Lecture Notes in Computer Science, S. Balandin, S. Andreev, and Y. Koucheryavy, Eds. Springer International Publishing, 2014, vol. 8638, pp. 544–555.
- [10] 3GPP, "UMTS;LTE AT command set for UE, TS 27.007 v.10.3.0 release 10," April 2011.
- [11] E. Buskgaard, A. Tatomirescu, S. Del Barrio, O. Franek, and G. Pedersen, "Effect of antenna bandwidth and placement on the robustness to user interaction," in *Antenna Technology: Small Antennas, Novel EM Structures and Materials, and Applications*, 2014, pp. 258–261.
- [12] I. Rodriguez, H. Nguyen, T. Sørensen, J. Elling, M. Gentsch, M. Sørensen, L. Kuru, and P. Mogensen, "A Geometrical-Based Vertical Gain Correction for Signal Strength Prediction of Downtilted Base Station Antennas in Urban Areas," in *Vehicular Technology Conference*, 2012.

Paper K – (Collaboration 3)

From LTE to 5G for Connected Mobility

Mads Lauridsen, Lucas Chavarría Giménez, Ignacio Rodríguez,
Troels B. Sørensen, Preben Mogensen

Accepted for publication in
IEEE Communications Magazine. 2017.

© 2017 IEEE

Reprinted with permission. The layout has been revised.

Abstract

The Long Term Evolution, 4th generation of mobile communication technology, has been commercially deployed for about 5 years. Even though it is continuously updated through new releases, release 13 or LTE Advanced Pro being the latest one, the development of the 5th generation has been initiated. In this article, we measure how current LTE network implementations perform in comparison with the initial LTE requirements. The target is to identify certain Key Performance Indicators which has suboptimal implementations and therefore lends itself to careful consideration when designing and standardizing next generation wireless technology. Specifically we analyze user and control plane latency, handover execution time, and coverage, which are critical parameters for connected mobility use cases such as road vehicle safety and efficiency.

We study the latency, handover execution time, and coverage of four operational LTE networks based on 19.000 km of drive tests covering a mixture of rural, suburban, and urban environments. The measurements have been collected using commercial radio network scanners and measurement smartphones. Even though LTE has low air interface delays, the measurements reveal that core network delays compromise the overall round trip time design requirement. LTE's break-before-make handover implementation causes a data interruption at each handover of 40 ms at the median level. While this is in compliance with the LTE requirements, and lower values are certainly possible, it is also clear that the break-before-make will not be sufficient for connected mobility use cases such as road vehicle safety. Furthermore, the measurements reveal that LTE can provide coverage for 99 % of the outdoor and road users, but the LTE-M or NarrowBand-IoT upgrades, as of LTE release 13, are required in combination with other measures to allow for additional penetration losses, as e.g. experienced in underground parking lots.

Based on the observed discrepancies between measured and standardized LTE performance, in terms of latency, handover execution time, and coverage, we conclude the paper with a discussion on techniques that need careful consideration for connected mobility in the 5th generation mobile communication technology.

1 Introduction

The 3rd and 4th generations (3G and 4G) of mobile communication technologies are widely deployed, providing voice and mobile broadband as their main services. However, due to the increasing demand for higher data rates and larger system capacity [1] in addition to the emergence of new Internet of Things use cases, the 5th generation (5G) is currently being discussed. The 5G is expected to be standardized and deployed in 2018 and 2020, respectively. A key scenario for 5G is connected mobility, which utilizes vehicular communication for e.g. infotainment, safety, and efficiency [2]. The two latter use cases impose new and challenging requirements in terms of low latency, zero handover interruption time, and ultra-high radio signal reliability [3].

While these requirements are already in the scope of 5G standardization, the ability to meet the requirements in practice is more important than ever in view of the criticality of the safety-oriented connected mobility use cases. These cases rely on vehicular communication for e.g. platooning, cooperative awareness, and self-driving

cars [2]. In this sense, there are learnings to be made from network testing on the already established 4G Long Term Evolution (LTE) infrastructure, to see if the original LTE requirements are met in practice, and if not, evaluate whether the current 5G developments are likely to minimize the gap between requirements and commercial implementation. In this paper, we look at the initial design requirements of 4G LTE and the observed performance in terms of user and control plane latency and LTE handover execution time. In view of this, we discuss how 5G may be designed to address the latency and handover requirements of connected mobility use cases such as vehicular communication for safety and efficiency. Our analysis is based on an extensive measurement campaign of LTE performance in four cellular networks in Northern Jutland, Denmark. The campaign included 19.000 km of drive test with commercial radio network scanners and specialized measurement smartphones. Furthermore, we use the measurements to calibrate a radio wave propagation tool to study radio coverage, because it is a prerequisite for good latency and handover performance.

The LTE latency and handover performance has previously been studied e.g. in [4], [5], [6], and [7]. However, the scope of our measurement campaign in terms of number of studied operators, network configurations and topologies, device speeds, and scenario areas is unprecedented to the best of our knowledge. Specifically we study 4 commercial operators covering both rural, urban, and suburban areas, totaling 19.000 km of drive test at speeds from 30 to 130 km/h using specialized measurement smartphones, which provide information on not only application layer performance but also Radio Resource Control (RRC) messages. This is a significant statistical improvement compared to [4], which is based on 3 days of measurements in a single, lightly loaded, urban network with line-of-sight connection; [5], which is based on 35 km of urban drive test; and [6], which is based on field trials, where the Core Network (CN) was located close to the trial area to reduce the latency. The report [7] relies on data collected in the Nordic countries from 22.000 users via a smartphone application in January through March 2016, but it only provides information on data rates and user plane latency. Therefore, the statistical representation of our measurement data and the availability of network parameters ensures a solid comparison with the design requirements, enabling us to identify any discrepancies.

The article is structured as follows: first we describe the extensive measurement campaign. Then the latency and handover performance observations are presented. Next we present the LTE coverage and discuss how it can be extended. Then we identify discrepancies and areas for improvement by comparing the LTE requirements with the observed performance, and discuss how the 5G development can address these issues.

2 Measurement Campaign

The extensive measurement campaign was conducted in the region of Northern Jutland in Denmark. The region has about 585.000 inhabitants over an area of 8000 km². A large part of the region is rural area with small villages and farmland, and only few larger cities with population size in the 10-20.000 range and one major city of 130.000 inhabitants. The wireless infrastructure in the region is well developed. As it was re-

vealed in the measurement campaign, at least one operator provides all technologies over the full region. If two operators are required for 3G/4G coverage, about 60 small areas (of 0.5-4 km radius) experience limited or no coverage.

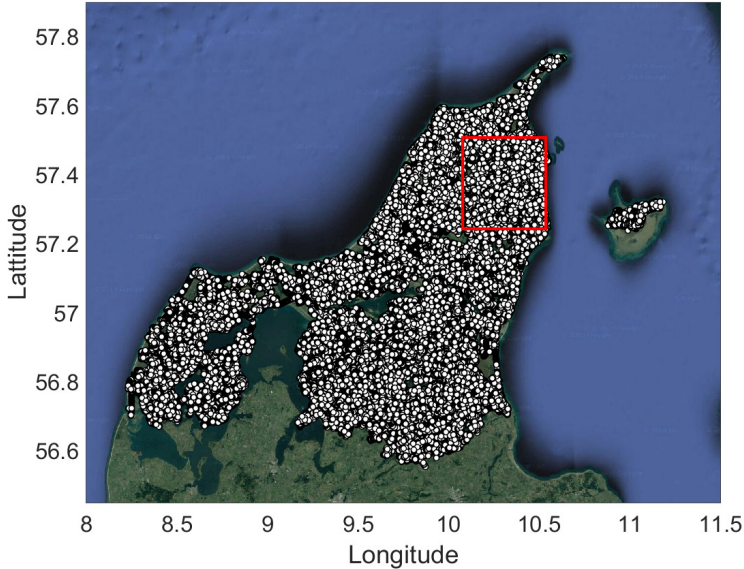


Fig. K.1: Overview of measurement locations in Northern Jutland. The red rectangle indicates the area, which is examined in the coverage study.

The drive test measurements were made using two cars covering about 19.000 kilometers of city roads, rural roads, and highways within the region, and therefore includes measurements in the range 30-130 km/h. During the drive test, samples of received signal power, data rate, round trip time (RTT) and radio access network (RAN) specific parameters were collected simultaneously for the four main operators in Denmark. The road coverage, based on more than half a million collected data points, is illustrated in Fig. K.1. The measurements were made during the daytime Monday through Friday in the period from November 2015 to May 2016. Note that the status of the four networks may have changed during the long measurement campaign, both in terms of deployed base stations and equipment, but also in terms of number of users and network load. However, this information is not publicly available and therefore the measurement campaign reflects the performance at the specific time of measurement.

Each car, moving according to local traffic rules, was equipped with a roof box containing a Rohde & Schwarz FreeRider III system. The system consists of four Samsung Galaxy S5 Plus smartphones, running specialized QualiPoc measurement software, and a TSME radio network scanner. The smartphones reflect the user experienced performance and, in addition, they are able to record relevant network parameters such as RRC messages. Each phone was connected to one of the four

main mobile network operators of Denmark using either 3G or 4G depending on the current signal levels and operator traffic steering policies, while the scanner was passively monitoring the allocated frequency bands for 2G, 3G and 4G communication from 700 MHz to 2.7 GHz. We only report results for 4G in this work. The smartphones and the scanner measured the received signal power from the serving cell and all observable neighbor cells, respectively. The scanner was equipped with an external, omni-directional Laird TRA6927M3NB-001 antenna, which was mounted in the roof box on a separate ground plane. In addition the position was logged per measurement sample via GPS, and used to generate averages of the received signal power over 50 m road segments.

Each smartphone was continuously performing a series of data measurements consisting of four fixed duration File Transfer Protocol (FTP) transfers in uplink and downlink (alternating link directions i.e. eight transfers in total), each 20 seconds long to estimate the broadband coverage. The FTP transfers were followed by a 10 s idle period and preceded by two ping measurements occurring with 1 s separation. The ping and FTP measurements were made towards a server located at Aalborg University (AAU). The server was connected via 10 Gbps fiber to the Danish Research Network, which is connected to the Danish Internet Exchange Point via another 10 Gbps fiber, and thus the link between the Internet and the server is expected to have minimal impact on the measurements. Ping measurements made from a computer located at AAU towards the server, passing through the Danish Research Network, result in average RTTs of 7.5 ms with a standard deviation of 0.6 ms. Figure K.2 emphasizes the Key Performance Indicators (KPIs) considered in this paper; RTT, handover execution time, and received signal power, and how the KPIs relate to the network configuration in the measurement campaign. Notice that each of the operators have a direct link to the Danish Internet Exchange Point. Furthermore, two of the operators share their networks and therefore their measurement results are combined in this work.

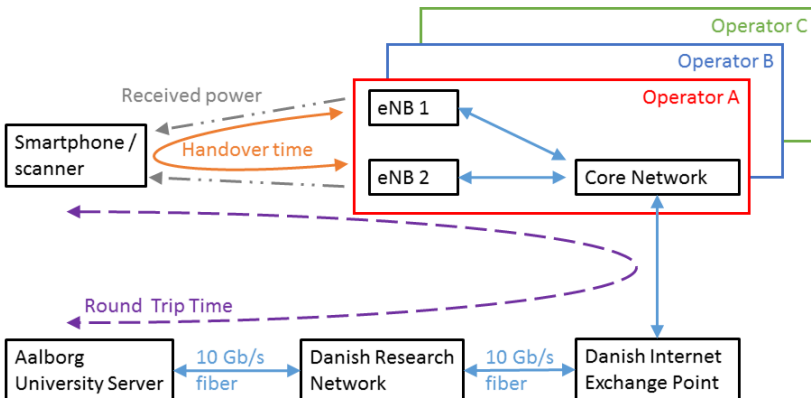


Fig. K.2: The measurement configuration including network connectivity and KPIs.

3 Latency Performance

Latency or RTT performance is a KPI for user Quality of Experience. The emergence of the connected mobility use cases for safety makes it even more critical to deliver data and responses with low latency [2]. Latency can be divided into control plane latency that is the time it takes the device to transfer from the RRC Idle state to the RRC Connected state and be able to transfer data; and user plane latency, which is equal to the RTT of a data packet and its associated acknowledgment from the target layer, assuming the device is connected with the network. In LTE the control plane latency target is 100 ms, while the user plane latency target is 20 ms [8].

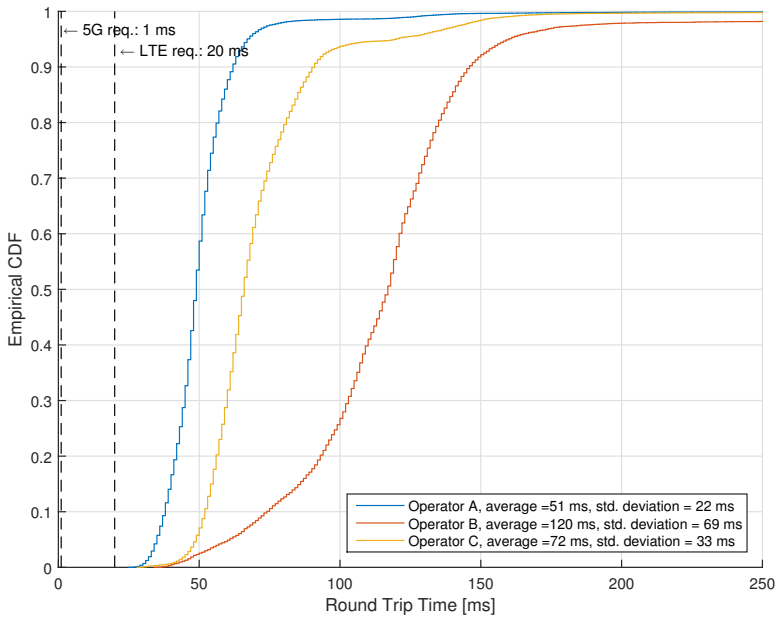
Figure K.3 shows the Cumulative Distribution Function (CDF) of the two ping measurements performed using LTE. The second ping, performed 1 s after the first ping, is a good measure of the user plane latency, because the 1 s delay allows sufficient time for entering an RRC Connected and schedulable state. According to [6] the RTT of LTE, excluding the CN delay, is approximately 19 ms when the UE does not have pre-allocated resources, and therefore a scheduling request in uplink is triggered. During high network load and/or poor radio signal conditions this value will increase due to scheduling delays, low data rates, and retransmissions. As mentioned previously, the AAU server to Danish Research Network RTT, illustrated in Fig. K.2 was measured to be 7.5 ms, and furthermore the RTT between the Danish Research Network and the Danish Internet Exchange Point is estimated to be 1 ms. The total latency, excluding the CN is thus about 27.5 ms, which fits with the observation of Fig. K.3a where the lowest observed RTT is 28 ms. Scheduling delays, low data rates due to network load and insufficient coverage, and retransmissions contribute to the 95-percentile being 67, 160, and 120 ms for operators A, B, and C, respectively. However, even the best 5-percentile experience latencies 7.5, 33.5, and 21.5 ms above the expected 27.5 ms for operators A, B, and C, respectively. Clearly the CN latency, which is the time it takes the packet to transfer from the S1 interface between eNB and the Serving Gateway through the operator's backhaul to the Danish Internet Exchange Point, is a major limitation, especially for operator B whose best 5-percentile users experience latencies more than 100% higher than the expected 27.5 ms. The observed delays are significantly longer than [4], which noted an average LTE user plane latency of 36 ms and CN latency of 1-3 ms. However, those measurements were made in a network with limited number of users and from a static, line-of-sight measurement position. The average user plane latency was noted to be 45 ms in [7], but it is not clear how the users were distributed geographically (and whether they were indoor or outdoor) as the coverage was claimed to be less than 80% even for the best operator. This is in contrast with our finding of approximately 99% outdoor LTE coverage, which is described later.

In general operator A provides the lowest user plane latencies and this is correlated with the fact that operator A provides the best LTE coverage in the area. The standard deviation of the latency of operator B is 69 ms, and significantly larger than operators A and C, being 22 and 33 ms respectively. The reasons for the latency jitter may include varying load across the network and thus varying scheduling delays and data rates, but also a less consistent routing of packets in the CN. Independently of the reason it is an issue for safety-critical connected mobility, which requires predictable

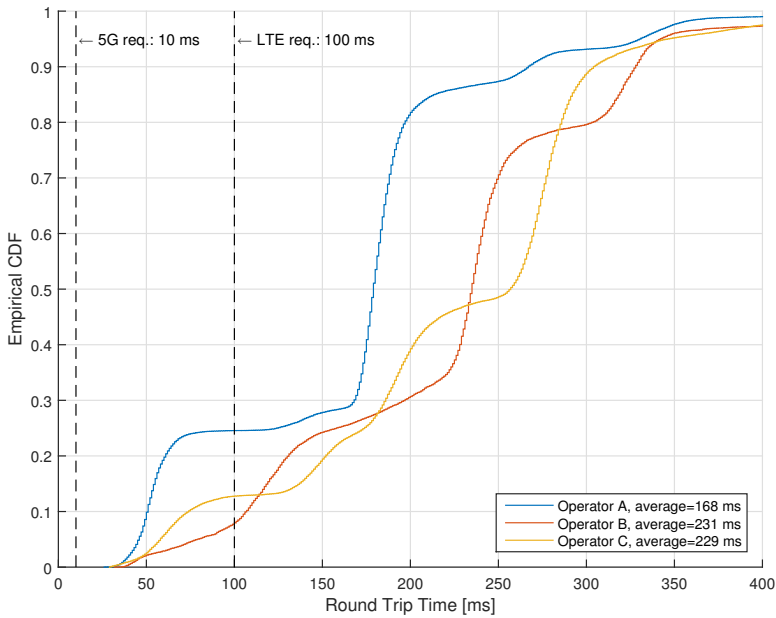
and steady latency performance.

The first ping, which is performed after 10 s of idle time and illustrated in Fig. K.3b, is a measure of the control plane latency combined with the user plane latency of Fig. K.3a. After the first measurement the smartphones have a cached Address Resolution Table with the AAU server's MAC address. The measurement smartphones' default Address Resolution Table renewal timer is 60 s and since a new FTP or ping measurement is initiated every 20 s the timer will always be reset before expiry, and therefore, the Address Resolution Protocol does not cause additional delays. Furthermore, the Domain Name System service is not used because the server is addressed via IP.

The inactivity timer of LTE, that is the time between the last data transfer and until the network moves the UE to RRC Idle, is in the order of 5-10 s for most networks and this explains why some UEs in the CDF of ping 1 in Fig. K.3b experience performance similar to ping 2. Excluding the UEs who seem to be RRC connected when ping 1 is initiated, and subtracting the average RTT observed in Fig. K.3a the lowest control plane latency is in the order of 120 ms for operators A and B and 80 ms for operator C. Some users experience longer latencies, which may be due to a failed Random Access (RA) procedure in addition to the aforementioned RAN contributors. Independent of the operator there are some distinctive steps, which occur with intervals of 40 and 80 ms. This corresponds well with the periodicities of System Information Block 1 and 2, which are needed by the UE to perform cell access and RA [9]. Similar to the user plane latency result in Fig. K.3a operator A performs best in Fig. K.3b, but when the user plane latency is subtracted from the measurements the three operators perform very similar.



(a) CDF of ping 2 - user plane latency.



(b) CDF of ping 1 - control plane latency.

Fig. K.3: The LTE ping measurement results. Note the AAU server RTT is 7.5 ms, which must be added to the LTE requirement line for result interpretation.

4 Handover Execution Performance

LTE implements the break-before-make handover, where the UE breaks data exchange with the serving cell before establishing the connection towards the target cell. As a result, the UE experiences a service interruption at each handover for a short period of time. Upon the reception of the handover command or the RRC Connection Reconfiguration message that includes the mobility control information [9], the UE proceeds to reconfigure Layers 2 and 3, terminating any data exchange with the network. Afterwards, it performs the radio frequency retuning and attempts the RA towards the target cell. When completed, the UE sends the RRC Connection Reconfiguration Complete message to confirm the handover, informing the target cell that the data-flow can be restored. The stage that encloses the procedures in between both RRC messages is called handover execution [6]. In order to detect problems during the handover execution, the UE initiates the timer T_{304} after receiving the handover command. If the MAC layer successfully completes the RA procedure, the UE stops the timer. However, if the timer T_{304} expires before the handover has been completed, a handover failure is declared and the UE shall perform connection re-establishment [9].

Ideally, the time it takes to perform the handover execution is a lower-bound of the handover service interruption time. In practice, there are additional delays such as UE and eNB processing times and propagation delays that may increase the overall service interruption. Current 3GPP studies on LTE latency report a typical handover execution time of 49.5 ms [10], while the ITU target is 30-60 ms [8].

The QualiPoc measurement smartphones collect the RRC signaling exchanged with the network. Therefore, the handover execution time is determined by analyzing the time-stamp of the RRC messages at each handover. Figure K.4 depicts the CDF of the handover execution times measured on each of the analyzed networks. The number of registered handovers differ between networks: 161313, 46517, and 148011 handovers for operator A, B, and C, respectively. However, the measured handover execution times are similar across them. As illustrated in Fig. K.4 the extracted times are below 75 ms in 90 % of the cases with a median value of approximately 40 ms, which is in line with the expected typical value of 49.5 ms reported by the 3GPP [10] and the 30-60 ms target of ITU [8]. The average handover execution time is reported to be 30 ms in [5], but the measurement only covers 35 km of urban drive test. Similarly [6] reports average times around 25 ms, but for a field trial where the CN was located close to the trial area.

Figure K.4 also illustrates handover execution times larger than 200 ms, and some are due to unsuccessful handovers (approximately 1 % of the total number of samples). In these cases, a handover failure is declared and the connection re-establishment increases the data interruption time up to several seconds. These extreme values show that the LTE handover execution with a break-before-make implementation may become an issue for the safety-critical connected mobility use cases with stringent latency requirements.

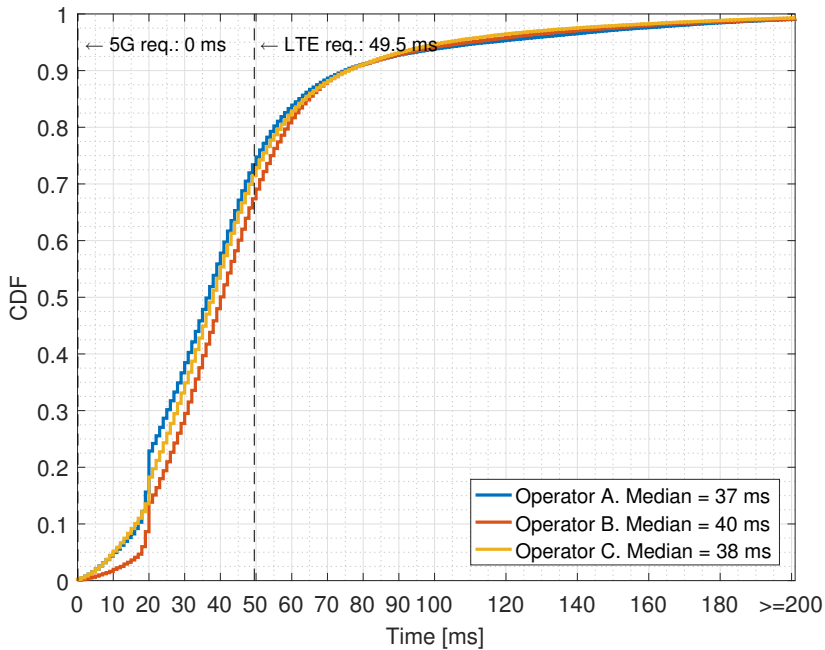


Fig. K.4: CDF of the handover execution time measured during the drive tests for each operator.

5 Coverage Performance

The requested latency and handover performance cannot be achieved without sufficient radio coverage. As mentioned earlier the 4G coverage is good in the region, but since the measurements are performed as drive tests they only indicate road coverage. However, the connected mobility use cases focused on vehicular communication for safety and efficiency also require indoor coverage, e.g. for underground parking lots and integral garages. Therefore the extensive measurement campaign was used for calibration of a radio wave propagation tool, in order to estimate the received signal power for a selected rural area of the region. The area under study is approximately 800 km² and is based on a local operator's commercial deployment of 71 eNB sectors operating in LTE band 20 (~800 MHz). The area is illustrated with a red rectangle in Fig. K.1. An elevation map, obtained from Kortforsyningen [11], is imported to account for terrain variations and combined with a log-normal shadow fading of 8.7 dB variance, which was estimated using the received power values from the measurement campaign. The area is divided into 50x50 m pixels and the coupling loss is then determined between each pixel and the 71 eNB sectors. The coverage is evaluated for different users groups, which are assigned to specific pixels based on public database information. The first set is outdoor users, located in pixels that contain a house number based on Open Street Map, and road users, located in pixels that contain a road segment [11]. The other group consists of indoor users, which are also identified

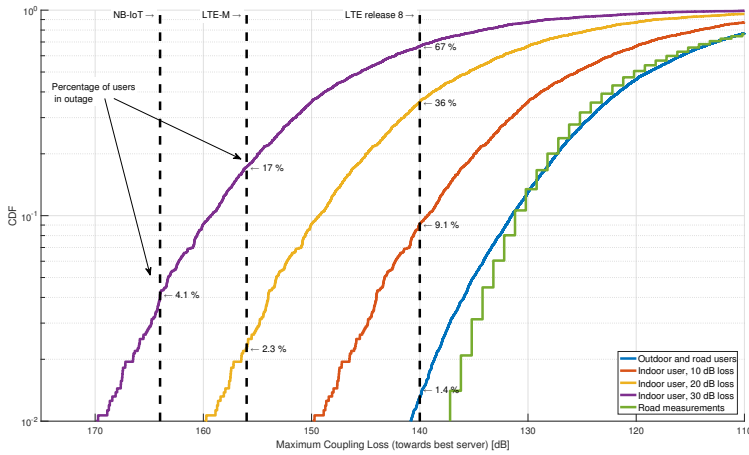


Fig. K.5: Coverage performance for LTE, LTE-M, and NB-IoT. Based on Fig. 3 of [11].

by house numbers. The indoor users are divided into 3 subgroups, experiencing 10, 20, and 30 dB penetration loss in addition to the observed coupling loss. The indoor groups are generated to study a light indoor scenario, where a user e.g. is located close to a window and thus only experience 10 dB additional loss, and deep indoor scenarios, where a user for example is located in a basement such as an underground parking lot and therefore suffers 20-30 dB additional loss [12]. For further details on the simulation setup refer to [11].

Figure K.5 shows the coupling loss between the UE and the serving cell, which is selected based on the strongest received signal. The three dashed, vertical lines indicate the supported Maximum Coupling Loss (MCL) for LTE release 8 (140 dB), LTE-M release 13 (156 dB), and NarrowBand-IoT (NB-IoT) release 13 (164 dB) [13]. The two latter technologies achieve the higher MCL by applying repetitions in time (at the cost of latency!) and Power Spectral Density boosting in smaller transmission bandwidths of 1.4 MHz for LTE-M and 200 kHz for NB-IoT. Note that NB-IoT does not apply handovers, but only cell reselection. Figure K.5 also contains road measurements obtained in the area indicated by the red rectangle in Fig. K.1. The curve shows a good fit with the simulation of outdoor and road users, and the minor difference is attributed to remote houses, in the area, that are located far from the road measurements.

The results in Fig. K.5 indicate that LTE release 8 provides sufficient coverage for 99% of the outdoor and road users. If indoor coverage is needed LTE release 8 provides coverage for only approximately 90% of the light indoor users, experiencing 10 dB additional penetration loss. For deep indoor users NB-IoT is required and can provide coverage for about 95% of the users. However, for most of the safety and efficiency use cases the outdoor and road users can rely on LTE release 8, and thus also benefit from the larger bandwidth and lower latency of this technology.

6 Enabling Connected Mobility in 5G

The connected mobility use cases, focused on road vehicle safety and efficiency, demand low latency, high reliability, and zero handover execution time [2, 3]. These parameters were also defined for LTE, but using different values since mobile broadband and voice applications were mainly targeted. In Table K.1 the LTE requirements are compared with the results of the extensive measurement campaign, which represents what is achievable in commercially deployed networks. In addition, the current 5G targets are listed together with highlights of ongoing 5G research on how the mobile communication system can improve as compared to LTE and address the discrepancies between standardized and measured performance. These comparisons are important in order not to experience similar performance discrepancies, when 5G is deployed.

The measured LTE user plane latency, see Fig. K.3a, is significantly higher than the 20 ms target, [8], for all operators. However, the key observation is that there is an even larger difference (51 vs 121 ms) between two operators. Since the air interface is the same and assumed to have comparable loads it is clear that RAN setup, routing, and CN architecture have a major impact on user plane latency. When designing 5G, it is therefore important to minimize the probability and impact of poor RAN and CN implementations on the envisioned new and optimized air interface. In addition, 5G research is targeting a reduction of the user plane latency to 1 ms, [3], by use of shorter Transmit Time Intervals (TTI), bundling of scheduling request and data, decreased processing times obtained due to technology improvements, and potentially semi-persistent scheduling. Fortunately, work is also ongoing to optimize the RAN and CN. For example the use of Mobile Edge Computing, where processing and decision making is moved towards the eNB is studied. Moreover the 5G network is expected to rely on a flexible slicing of the RAN and CN, and splitting of tasks between edge and central clouds to accommodate the requirements of the different use cases [14]. The control plane latency of LTE was targeted to be 100 ms or less, [8], and one operator fulfills this, achieving 80 ms on average, while the two other operators require approximately 120 ms as illustrated in Fig. K.3b. However, subsequent access attempts are delayed significantly due to the 80 ms or higher periodicity of the System Information Blocks, which provide the information the UE needs in order to access the network. The 5G target is 10 ms, [3], and therefore the required access information must occur more frequently at the cost of increased control overhead. Additionally, work is ongoing to develop new RA and registration methods to enable the UE to connect faster and with more consistent performance. The control plane latency will also benefit from the use of network slicing, e.g. by applying faster RA schemes to time critical applications and by using different control channel modulation and coding schemes for different applications; and Mobile Edge Computing, e.g. by letting the eNB handle some of the tasks currently performed by the Mobility Management Entity in LTE.

The LTE handover execution time target is 49.5 ms [10]. The measurement results in Fig. K.4 show that the operators on average fulfill this target with a median of 40 ms. However, a Radio Link Failure occurs in approximately 1 % of the measurements

Table K.1: Comparison of requirements, measured performance, and potential techniques for improvement.

Parameter	LTE requirement	Measured LTE performance	5G target	Potential techniques
User plane latency (RTT)	20 ms	Average: A: 51 ms, B: 121 ms, C: 72 ms. Even the users in best radio signal conditions are affected by long core network latency	1 ms	Semi-persistent scheduling and combining of requests and data, processing time reduction, shorter TTIs, mobile edge computing, network slicing
Control plane latency (Idle-to-Active time)	100 ms	A and B require 120 ms, while C completes in 80 ms. Subsequent access attempts are delayed by long System Information Block periods	10 ms	Optimized Random Access and security setup, periodicity of System Information Blocks, network slicing and mobile edge computing
Handover execution time	49.5 ms	Similar median LTE values for all the operators of ~40 ms	0 ms	Make-before-break, multi-cell connectivity, UE autonomous cell management, synchronized handover
Supported maximum coupling loss	140 dB	LTE release 8 provides coverage for 99% of the outdoor and road users in the rural area under study	164 dB	Micro and macro diversity, TTI bundling, cell densification, Power Spectral Density boosting

and the subsequent connection re-establishment procedure extends the handover execution time to several seconds. The connected mobility use cases targeting safety and efficiency require 5G to provide zero service interruption time and therefore a significant amount of work is needed in this area [3]. One proposed solution is to apply make-before-break connectivity where the UE connects to the target cell before disconnecting from the serving cell. In 5G this may be expanded to multiple connections due to the expected use of multi-cell connectivity. The cost is increased UE complexity and simultaneous utilization of resources in multiple cells. This concept is similar to the Dual Connectivity Split Bearer Architecture of LTE, which potentially can be combined with the UE autonomous cell management. The latter concept allows the UE to autonomously add and release different radio-links, reducing the control signaling overhead. Finally, 5G may also utilize synchronized handover which is a Random Access-less procedure where the synchronized UE and cells agree on when the handover shall occur.

The supported MCL of a mobile communication system defines the radio signal availability together with the network deployment and load. The LTE release 8 MCL is 140 dB and the calibrated simulation in Fig. K.5 of a rural area showed that a commercially deployed network would provide coverage for approximately 99% of the outdoor and road users. However, the connected mobility use cases focused on safety must also work in deep indoor scenarios such as underground parking lots with higher coupling loss [12]. Therefore, a certain slice of 5G must support a higher MCL, potentially similar to the 164 dB of NB-IoT. Similar to NB-IoT the 5G design can thus rely on TTI bundling that is repetitions of transmissions in the time domain, which however will harm the latency, and use of Power Spectral Density boosting, which may harm the Signal-to-Interference ratio of other users. Therefore, 5G will preferably utilize the expected network of ultra-dense small cells, macro cell densification, and micro and macro diversity to improve the received signal power and reliability [15].

7 Conclusion

In this study we examined the performance of four LTE operators in an extensive measurement campaign of 19.000 drive test kilometers. The goal was to identify gaps between LTE requirements and achievable performance in order to avoid similar discrepancies when 5G is standardized and deployed. The 5G will be able to support connected mobility use cases focused on vehicular communication for road safety and efficiency, but improvements are needed in the areas of user and control plane latency, handover execution time, and radio signal availability.

The LTE user plane latency is observed to be twice as long as the requirement due to core network latencies, and thus diminishes the effect of an optimized air interface. For 5G it will be of key importance that the operators focus on the latency of the core architecture in order to achieve the 1 ms RTT target. The studied networks roughly achieve the LTE control plane latency requirement, but since 5G requires it to be 10 times lower the amount of Random Access, connection and security setup signaling must be reduced. For both latency targets the use of mobile edge computing and network slicing will be beneficial.

The LTE handover execution time requirements and observed performance are

similar, but since the connected mobility use cases targeting safety and efficiency require zero service interruption time the 5G design must utilize new mobility methods such as make-before-break, multi-cell-connectivity and synchronized handovers.

The simulated LTE outdoor and road coverage is sufficient for 99 % of the users but in order to ensure the connected mobility operation it is suggested that 5G target a significant cell densification and use of macro and micro diversity to improve the radio signal availability.

Acknowledgment

The authors would like to thank the reviewers and the editor for their useful comments. Furthermore, the authors would like to thank Business Region North Denmark for providing access to the measurement data. The work was partly funded by Innovation Fund Denmark.

References

- [1] Cisco, "Visual networking index: Global mobile data traffic forecast update, 2015 - 2020," White paper, 2016.
- [2] 5G Infrastructure Public Private Partnership, "5G Automotive Vision," White paper, 2015.
- [3] 3GPP, "Study on scenarios and requirements for next generation access technologies," TR 38.913 V0.3.0, March 2016.
- [4] M. Laner et al., "A comparison between one-way delays in operating HSPA and LTE networks," in *Modeling and Optimization in Mobile, Ad Hoc and Wireless Networks (WiOpt)*, 2012 10th International Symposium on, May 2012, pp. 286–292.
- [5] A. Elnashar and M. A. El-Saidny, "Looking at LTE in practice: A performance analysis of the LTE system based on field test results," *IEEE Vehicular Technology Magazine*, vol. 8, no. 3, pp. 81–92, Sept 2013.
- [6] H. Holma and A. Toskala, *LTE for UMTS - Evolution to LTE-Advanced*, 2nd ed. John Wiley & Sons, Ltd., 2011.
- [7] O. Signal, "State of mobile networks: Nordics," May 2016, report, accessed on Dec. 12 2016. [Online]. Available: <https://opensignal.com/reports/2016/05/nordic/state-of-the-mobile-network/>
- [8] International Telecommunication Union, "Requirements related to technical performance for IMT-Advanced radio interface(s)," ITU-R M.2134, November 2008.
- [9] 3GPP, "Radio Resource Control Protocol specification," TR 36.331 V13.1.0, April 2016.
- [10] —, "Study on latency reduction techniques for LTE," TR 36.881 V14.0.0, June 2016.

- [11] M. Lauridsen et al., "Coverage and Capacity Analysis of LTE-M and NB-IoT in a Rural Area," in *2016 IEEE 84rd Vehicular Technology Conference (VTC Fall)*, September 2016, pp. 1–5.
- [12] H.C. Nguyen et al., "A simple statistical signal loss model for deep underground garage," in *2016 IEEE 84rd Vehicular Technology Conference (VTC Fall)*, September 2016, pp. 1–5.
- [13] Nokia, "LTE-M — Optimizing LTE for the Internet of Things," White paper, 2015.
- [14] A. Colazzo, R. Ferrari, and R. Lambiase, "Achieving low-latency communication in future wireless networks: the 5G NORMA approach," in *European Conference on Networks and Communications (EuCNC)*, June 2016, pp. 1–5.
- [15] G. Pocovi et al., "Signal quality outage analysis for ultra-reliable communications in cellular networks," in *IEEE Globecom Workshops*, Dec 2015, pp. 1–6.

Paper L – (Collaboration 4)

Measurement-based Evaluation of the Impact of Large Vehicle Shadowing on V2X Communications

Ignacio Rodríguez, Erika P. L. Almeida, Mads Lauridsen,
Dereje A. Wassie, Lucas Chavarría Giménez, Huan C. Nguyen,
Troels B. Sørensen, Preben Mogensen

Published in
Proceedings of the 22nd European Wireless Conference (EW'2016).

© 2016 IEEE

Reprinted with permission. The layout has been revised.

Abstract

Upcoming applications, such as autonomous vehicles, will pose strict requirements on the vehicular networks. In order to provide these new services reliably, an accurate understanding of propagation in the vehicular scenarios is needed. In this context, this paper presents a measurement-based evaluation of large vehicle shadowing at 5.8 GHz in V2X scenarios. The receiver antenna height is fixed to average vehicular height (1.5 m), while the transmitter antennas are located at different heights (1.5, 5, and 7 m) in order to investigate both V2V and V2I scenarios. A truck was used to obstruct the LOS between transmitter and receiver, and a large number of geometrical combinations of the scenario were explored. The statistical analysis of the measurement shows how in the V2V case, the experienced shadow levels are approximately 5 dB higher than in the V2I scenarios, where the shadow levels depend on the transmitter antenna height, reaching maximum values of 21-23 dB. The statistical analysis also shows that the differences in shadow level due to the non-symmetries of the obstacle truck are in the order of approximately 2 dB. A simple 3D ray-tracing simulation is validated against the measurements, showing a good match with a RMSE of 4.1 dB. Based on both measurements and ray-tracing data, a simple deterministic shadowing model, useful for implementation in system level simulators, is presented, as a first step towards a more dynamic and scalable shadowing model.

1 Introduction

Autonomous vehicles and safety-improving driving applications, such as warnings of hazardous road conditions and overtaking vehicles, expected in the near future, are to be enabled by vehicular communications. These new use cases impose strict requirements to the communication link in terms of reliability of 99.999 % and latency below 5 ms [1]. The vehicular communication will rely on both vehicle-to-vehicle (V2V) and vehicle-to-infrastructure (V2I) communication, combined termed as V2X. Due to the reliability and latency requirements of the V2X communication and the criticality of the use cases, even the shortest obstruction of the communication link is an issue. Therefore, the characteristics of the communication channel and, especially, the shadow loss due to large vehicles, are of renewed interest for many researchers.

Until recently, dedicated short range communication radio access technologies (RATs) such as 802.11p have been the key focus area for vehicular communication. These technologies mainly rely on V2V communication and, therefore, channel models where both transmitter and receiver are mobile and have similar heights, have been studied extensively. In previous works, large scale propagation is modeled by single and dual slope log-distance path loss models, geometry-based models or ray-tracing techniques [2]. Specifically addressing the shadow fading caused by large vehicles, previous studies, based on both real measurements and ray tracing predictions [3, 4], reported an additional loss of 12-20 dB depending on the distance between transmitter, receiver, and the vehicle obstructing the line-of-sight (LOS).

Nowadays, the V2I scenario is under discussion. As opposed to V2V case, this scenario may benefit from a higher transmitter position and thus be less prone to large vehicle shadowing. Unfortunately, this temporary shadowing condition has

not been as extensively investigated as in the V2V case [2]. Due to the stringent reliability and latency requirements, critical to vehicular communications, an accurate characterization of the shadowing phenomena is still needed in the unexplored V2I scenarios, in order to determine whether, for example, autonomous vehicles can be supported by the infrastructure. In this direction, existing ray-tracing studies have examined road side unit (RSU) scenarios with blind corners [5] without providing specific results for large vehicle shadow loss. Measurements have also been conducted in real RSU scenarios, however the focus was done on small scale fading models [6], and packet delivery rate evaluations [7]. These evaluations show that non-line-of-sight (NLOS) conditions caused by large vehicles, buildings and vegetation, are the most critical issue for vehicular communication, thus underlining the necessity of understanding V2I large vehicle shadowing. This is also evident from the recent V2X surveys [2, 8, 9], which identify large vehicle shadowing as a key area for future research.

In this context, this paper complements the previous work by presenting a measurement based evaluation of large vehicle shadowing in a controlled scenario. An extensive measurement campaign was performed for different combinations of transmitter positions and heights (1.5, 5 and 7 m), with a receiver located at 1.5 m, emulating both V2V and V2I links in a 4-lane road scenario at 5.8 GHz. This particular frequency band is the selected band for road safety and traffic efficiency applications [10]. A truck was placed in different positions obstructing the LOS between transmitters and receiver, creating many different shadowing situations. A statistical analysis is performed over the measurement data in order to quantify and compare the different shadow levels and dynamics expected in the diverse V2V and V2I scenarios. The measurements are compared to ray-tracing simulations, providing valuable input for accurate modeling of V2X communication scenarios. Based on both the measurements and the ray-tracing simulations, an initial version of a deterministic shadowing model, useful to be used in system level simulations, is presented. The future research directions towards a complete realistic dynamic shadowing model are presented in the paper as well.

The rest of the paper is structured as follows: Section 2 describes the different aspects related to the measurement campaign. Section 3 presents the statistical analysis of the measurement results and the discussion based on the different V2X scenarios. Section 4 introduces the ray-tracing simulations and the comparison with the measurements. Section 5 presents the road-map towards a complete realistic and dynamic shadowing model, including an initial version of a deterministic large vehicle shadowing model. Finally, Section 6 concludes the paper.

2 Measurement Campaign

2.1 Measurement Scenario

The measurement campaign was performed in a driving school located a few kilometers north from Aalborg, Denmark. A dedicated V2X propagation scenario was reproduced over a rectangular flat paved area of approximately 45x95 m. The layout of the considered scenario is an 80 m long section of a 4-lane road, resembling

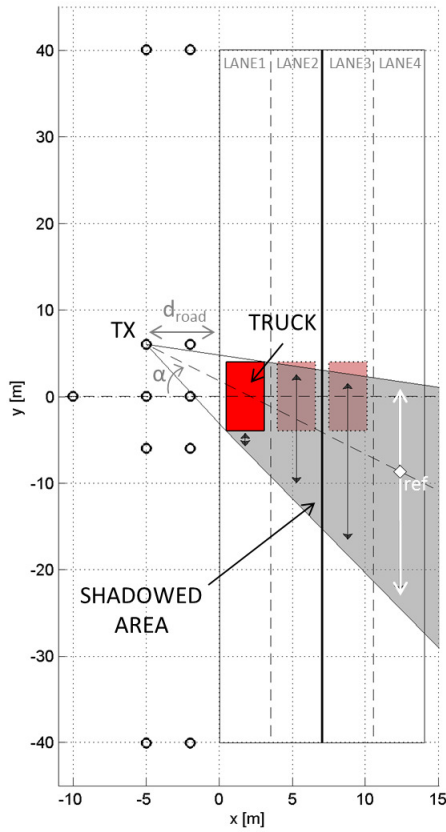


Fig. L.1: Overview description of the measurement scenario.

the typical wide-street vehicular case in any mid-sized European city, with 2 lanes per driving direction. Each of the lanes was marked by using traffic cones, considering a lane width of 3.5 m (which is the European average width for all types of pathways: urban, rural and highways [11]). A set of 6 transmitter (TX) antennas was deployed at different heights (h) on a mast (7, 5 and 1.5 m), a van (7 and 5 m) and a trolley (1.5 m), emulating different RSUs, and re-deployed several times by swapping them across the 11 different positions illustrated in Figure L.1. A single receiver (RX) antenna was mounted on a trolley at average vehicular height (1.5 m) [12], emulating a car roof antenna. By considering this setup, various V2X combinations are explored. This includes both the V2I and V2V cases, as detailed in Table L.1.

The V2X link measurements were performed by driving the RX trolley at walking speed (5 km/h in average) along each of the 4 lanes, recording simultaneously the signal strength from the 6 different transmitters, each of which was transmitting an independent narrow-band continuous wave (CW) signal. The selected orthogonal frequencies of operation (f_c) are detailed in Table L.1.

The different V2X links were obstructed by placing the large vehicle (truck), shown

Table L.1: Summary of the V2X TX/RX configurations and TX positions considered during the measurement campaign.

TX	f_c [MHz]	Link type	h_{TX} [m]	h_{RX} [m]	TX re-deployment positions [x,y] - shown on Figure L.1					
					1	2	3	4	5	6
Mast_1	5800	V2I	7	1.5	[-2,0]	[-2,-6]	[-2,-40]	[-5,-40]	[-5,-6]	[-10,0]
Mast_2	5801	V2I	5	1.5	[-2,0]	[-2,-6]	[-2,-40]	[-5,-40]	[-5,-6]	[-10,0]
Mast_3	5802.2	V2V	1.5	1.5	[-2,0]	[-2,-6]	[-2,-40]	[-5,-40]	[-5,-6]	[-10,0]
Van_1	5803.6	V2I	7	1.5	[-2,+40]	[-2,+6]	[-5,+6]	[-5,0]	[-5,+40]	[-5,+40]
Van_2	5805.2	V2I	5	1.5	[-2,+40]	[-2,+6]	[-5,+6]	[-5,0]	[-5,+40]	[-5,+40]
Trolley_1	5807	V2V	1.5	1.5	[-2,+6]	[-2,+40]	[-5,+40]	[-5,+6]	[-5,0]	[-5,0]



Fig. L.2: Obstacle truck (in the foreground), and mast/van containing part of the transmitters (in the background).

in Figure L.2, in the central part of the road section as depicted in Figure L.1. The dimensions of the truck were approximately 8x2.6x3.6 m (length x width x height). Diverse shadowing conditions were created over the different lanes, depending on the geometry of the scenario: dimensions of the obstacle, position of the obstacle (e.g. lane number over which the truck is placed), height of the TX, distance of the TX to the first lane (d_{road}), height of the RX, position of the RX (e.g. lane number over which the RX is located), and interaction angle (α) between TX and obstacle (defined as the angle relative to the direction of normal incidence on the left side of the truck).

In order to make the study more statistically significant, a large number of different scenario situations were created. Each of the aforementioned re-deployments across the 11 different TX positions was independently performed for the obstacle truck located on lanes 1, 2, and 3. All in all, by considering the 3 different truck positions, 3 antenna height combinations, 11 TX positions, and 4 lanes covered by the RX, the measurement examined a total of 176 different geometrical combinations.

2.2 Setup, Calibration & Data Processing

At the TX side, NI USRP-2953R devices were used to generate each of the CW signals with a constant output RF power (P_{TX}) of 10 dBm. These signals were fed into the correspondent TX antenna by using coaxial cables of different lengths depending on the TX antenna height. All the TX antennas were standard dipoles with a gain (G_{TX}) of approximately 3.5 dBi. Only vertical polarization was explored.

At the RX side, an omnidirectional antenna H+S SWA 0859/360/4/10/V of approximately 6 dBi of gain (G_{RX}) was used. A jumper cable was used to transfer the received signals into the receiver. A R&S TSWM universal radio network analyzer was used as RX, recording the signal strength of all the different CWs simultaneously at a sampling rate of 10 Hz. An average of approximately 576 received power (P_{RX}) samples were recorded per driven lane. In order to remove fast-fading effects, the received power samples were averaged over chunks of 1 m distance (20 wavelengths), resulting in 80 samples per lane.

The combined cable loss (L_c) was measured and calibrated, resulting in 3.7 dB for

the links with TX antenna at 1.5 m, 8.4 dB for the links with TX antenna at 5 m, and 9.5 dB for the links with TX antenna at 7 m. The sensitivity of the scanner used in the measurement was -115 dBm, which combined with the previous values according to (L.1) leads to maximum measurable path loss (PL_{meas}) of 138-144 dB.

$$PL_{meas} = P_{TX} - P_{RX,meas} + G_{TX} + G_{RX} - L_c \quad [\text{dB}] \quad (\text{L.1})$$

To characterize the shadowing effect, excess path loss (ΔPL) is defined in (L.2) as the difference between the measured path loss and free space path loss ($FSPL$). In the scenario explored, with only the obstacle truck obstructing the line-of-sight (LOS) between TX and RX, a negative excess path loss ($\Delta PL < 0$) would indicate favorable contributions to the received signal, most likely due to reflections on the truck. While, on the other hand, positive excess path loss ($\Delta PL > 0$) would indicate negative contributions to the propagation, mainly due to the obstruction by the truck and suggesting that the RX is in a shadowed area. The latest is the main focus of this paper.

$$\Delta PL = PL_{meas} - FSPL \quad [\text{dB}] \quad (\text{L.2})$$

In order to further calibrate the system and the calculations, a LOS measurement (without the obstacle truck) was performed along all the 4 lanes (+3 extra, in order to enlarge the calibration range) with the transmitters in re-deployment configuration 6. In the end, the calibration measurement covered distances between 5 and 120 m, including a large number of both elevation and azimuth angles. From the result, it was possible to verify that the calibrated LOS path loss obtained matched quite well the theoretical FSPL with an average root mean square error (RMSE) of 4.4 dB, considering data from all the different TX antenna heights. This result validates the use of the FSPL as a correct reference for the excess path loss calculation, over the entire measurement area defined.

3 Measurement Results

All the measurement cases were independently post-processed using (L.1) and (L.2) to obtain the excess path loss in the different situations. A statistical analysis was performed on the entire set of resulting empirical data.

First, the overall excess path loss per scenario was explored. Figure L.3 presents the cumulative distribution functions (CDF) of the measured excess path loss for the different V2I scenarios with TX antennas at 5 and 7 m, V2V scenarios with TX antenna at 1.5 m, and the combined V2X scenario that includes all the measurement data from all the different TX antenna heights. These empirical distributions are taken to model the probability of large vehicle shadowing being above or below a certain threshold. As it can be seen, the probability of being above any particular threshold value is higher for lower TX antenna heights. This means that, in case of being shadowed by a large vehicle, the impact is more significant for the V2V scenario than for the V2I scenario. For example, in the V2V scenario, the probability of experiencing a shadow level higher than 10 dB is 50%, while in the V2I scenario this probability is reduced to 35% and 20% for TX at 5 and 7 m, respectively. The maximum shadowing values experienced in the measurement were 21-23 dB for the V2I scenario and 27 dB for the

V2V scenario. In the case of considering the entire V2X scenario as a whole, without distinguishing between different TX antenna heights or type of links (V2V/V2I), it can be seen, how the resulting shadow level probability is very similar to the one for the intermediate TX antenna height.

The extensive measurement campaign, performed with transmitters in different positions, allowed to analyze other geometrical characteristics of the shadowing. Figure L.4 presents the same distributions as before, but separated for positive and negative interaction angles (α). These results allow to understand what is the impact of the non-symmetrical structure of the obstacle truck. As it can be seen, for the V2I scenario at both TX antenna heights, higher shadow levels are in general experienced for negative interaction angles ($\alpha < 0$). This is due to the fact that, for these angles, the container is the closest part of the truck to the TX, which is approximately 0.5 m taller than the cabin and, therefore, causes larger shadowing. In average, the differences in shadow level due to the non-symmetry of the obstacle truck are found to be in the order of approximately 2 dB. In the case of the V2V scenario, the non-symmetry impact is even smaller.

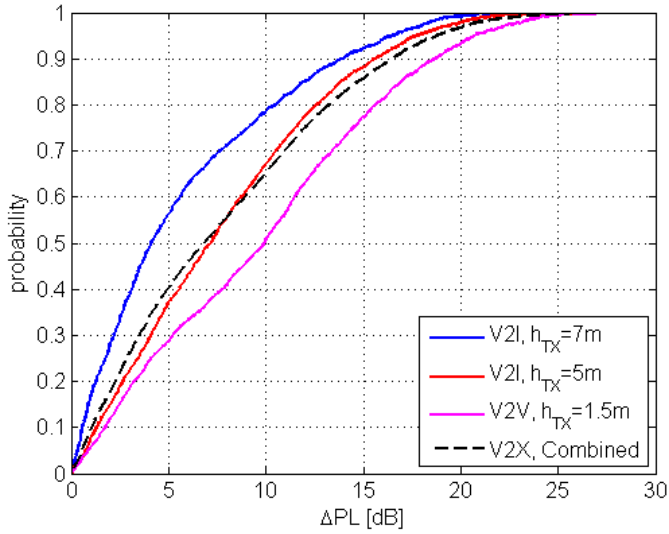


Fig. L.3: Shadow level probabilities for the different V2V, V2I and combined V2X scenarios.

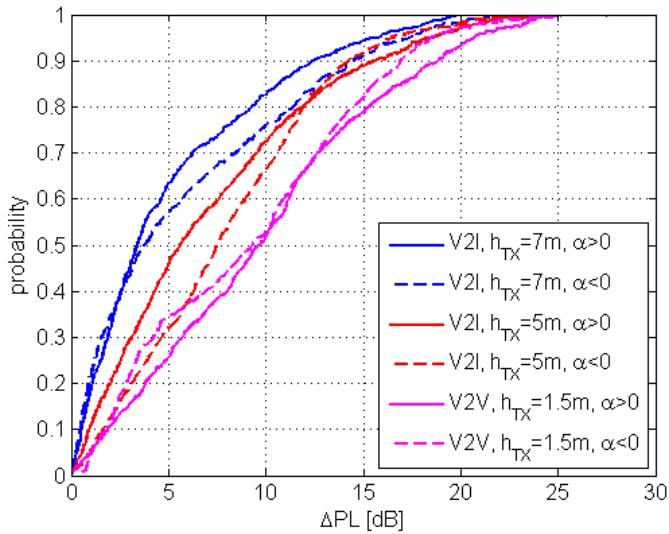


Fig. L.4: Shadow level probabilities for the different V2V and V2I scenarios classified per interaction angle.

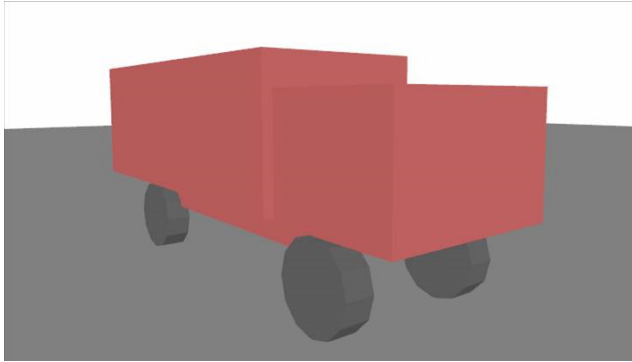


Fig. L.5: Simple 3D ray-tracing model of the obstacle truck.

4 Comparison with Ray-tracing

In order to gain further insight on the different possibilities for large vehicle shadowing characterization, the measurement campaign was reproduced in a commercial ray-tracing tool [13]. Figure L.5 shows the simple 3D model of the measurement scenario composed of a flat surface of dimensions 100x60 m and a simplified block model of the obstacle truck. Both the ground surface and the truck were modeled with standard materials available in the tool database: medium dry floor and metal, respectively.

The simulations for computation of path loss were performed with 3D standard ray-tracing, with a resolution of 0.25 m and basic simulation settings: LOS path loss exponent of 2, reflection and diffraction losses based on default permittivity and conductivity values of the different materials, and maximum 2 ray interactions.

Figures L.6 and L.7 show two examples of measurements (M) compared to ray-tracing (RT) predictions. They are similarly arranged in 4 sub-figures. Sub-figure a) displays the averaged excess path loss with a resolution of 1 m (80 samples per lane), computed from the measurements by following the procedures previously mentioned in Section II. Sub-figure b) contains the processed ray-tracing results, and it is directly comparable with Sub-figure a). In this case, the averaged excess path loss per lane has been computed by translating the original ray-tracing predictions with a resolution of 0.25 m, displayed in Sub-figure c), to the lane resolution of 1 m by applying exactly the same averaging procedures as to the measurements. In practice, the processed results are more representative of the shadow levels that a car would experience in the real world, due to potential RX antenna pattern irregularities and the different ray contributions to the received signal. Finally, Sub-figure d) presents an individualized comparison of the measurement and ray-tracing data per different lane, including RMSE values and cross-correlation coefficients (xcorr), giving a numerical indication on how good is the match between measurements and simulations.

With focus on the results now, in Figure L.6, one of the V2V cases with the obstacle truck placed on lane 1 is presented. The 1.5 m height TX antenna was located at position [-2,0], with an interaction angle of zero, which means that the incident angle

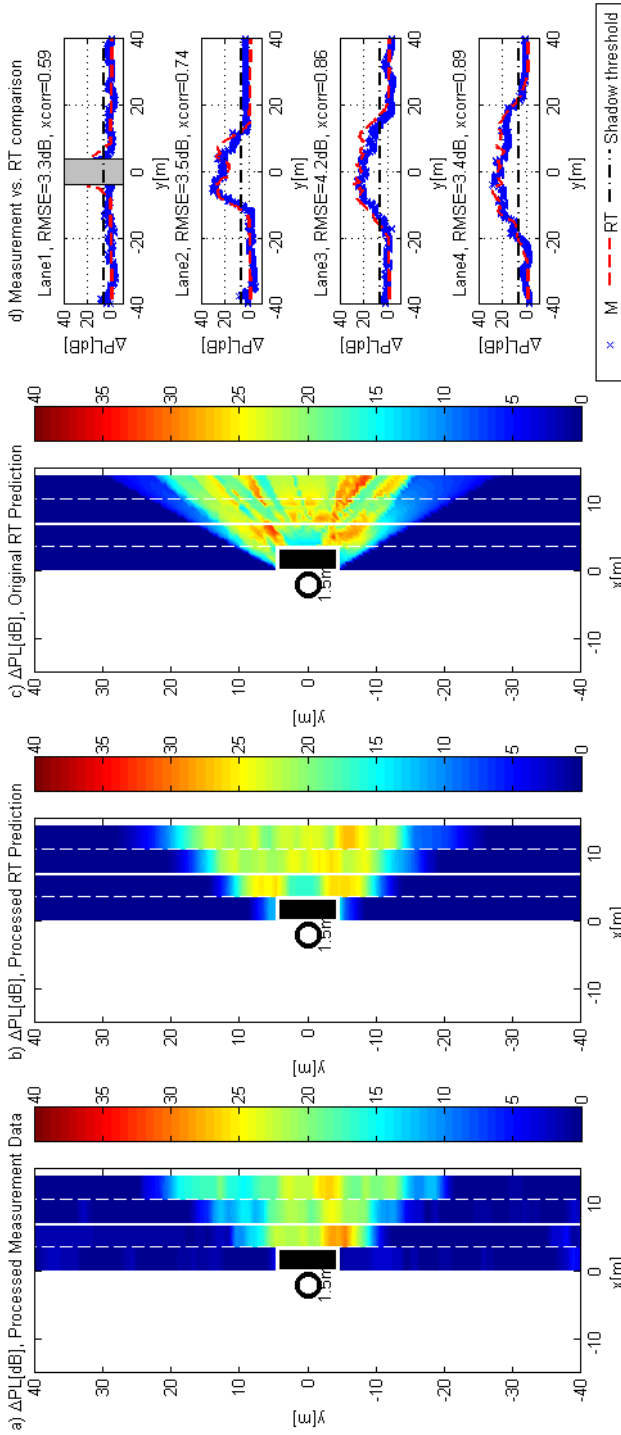


Fig. L.6: Comparison of measurements with ray-tracing for one of the V2V cases explored ($l_{TX} = 1.5$ m, $l_{RX} = 1.5$ m, $d_{road} = 2$ m, $\alpha = 0^\circ$, obstacle truck on lane 1).

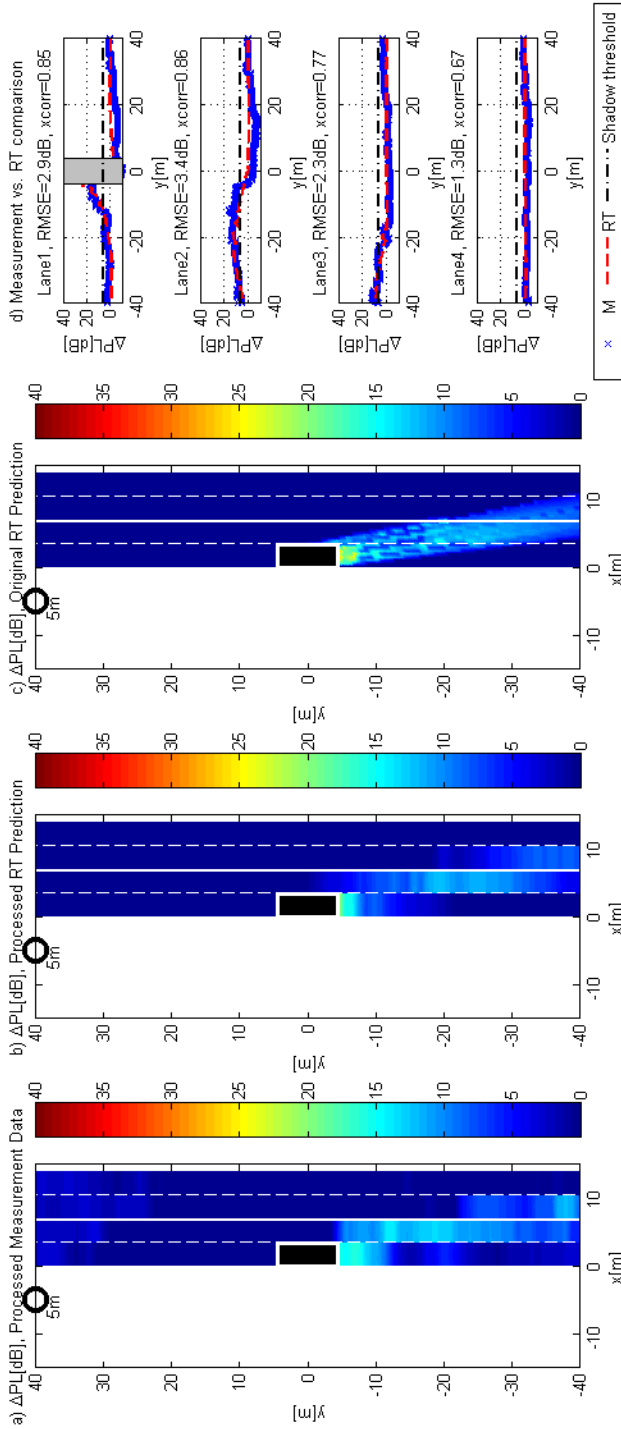


Fig. L.7: Comparison of measurements with ray-tracing for one of the V2I cases explored ($l_{rx} = 5$ m, $h_{road} = 1.5$ m, $d_{road} = 5$ m, $\alpha = 80^\circ$, obstacle truck on lane 1).

is perpendicular to the left side of the truck. As it can be seen from all sub-figures a), b) and d), the ray-tracing predictions show a good match to the measurements. For this particular case, an average RMSE of 3.6 dB and xcorr coefficient of 0.77 were obtained. This was the explored case with the strongest shadowing conditions, and some details can be observed. One of them is that, by looking at the data from lane 2 in sub-figure d), it can be seen how both the measurement and ray-tracing excess path loss present a small valley (reduction of approximately 6 dB) at the central position. This is due to the positive contribution of reflections of the signal on the ground below the truck between wheel axes. This also appreciable in the heatmaps. The second detail that is worth to be mentioned is that, especially in the measurement data from lanes 2 and 3, it is noticeable that, in shadowed areas, the excess path loss is slightly smaller for lane positions with positive ordinate ($y > 0$). This is due to the aforementioned fact that the obstacle truck was not symmetric, and the cabin shadows a few dB less than the container. Under this particular V2V configuration, cars driving on shadowed areas of the lanes would experience maximum shadow levels of approximately 22-27 dB.

The second case, in Figure L.7, presents a V2I example. The TX antenna was located at 5 m in position [-5,+40]. The obstacle truck was still placed on lane 1, as in the previous V2V example. In this case, the average RMSE was 2.5 dB, with a xcorr coefficient of 0.79. While in the previous case shadowing on the first lane was negligible, meaning that a car will experience no shadow impact by driving close in-front/behind the truck in the same lane. In this case, due to the larger interaction angle, some shadowing is created over the lane on which the obstacle truck is positioned (lane 1). The results illustrate the benefit of having elevated TX antenna positions in the V2I scenario. Even though larger areas are shadowed, the shadow levels, measured in excess path loss, are smaller than in the previous V2V scenario. In this case, the maximum shadow levels experienced per lane were in the range 0-18 dB.

It is nontrivial to present individually all the different cases considered in the study, but the conclusion is that with very simple ray-tracing simulations, with not very detailed 3D models or material characterization, it is still possible to achieve a quite accurate level of prediction of both geometry and shadow levels. Considering all the different combinations explored, the overall RMSE was 4.1 dB, while the average xcorr coefficient was 0.65.

5 Dynamic & Scalable Shadowing Model

The results and observations presented in this paper are part of the initial study towards the development and calibration of a dynamic and scalable shadowing model for system level simulation of V2X communications. As a first step, it is possible to propose a stochastic model based on the empirical distribution in Figure L.3, or the corresponding sample-based distribution from ray-tracing simulations. The approach, illustrated in Figure L.8, can be useful for simple static snap-shot based system level simulations where one wants to ignore the geometric detail, and instead apply the shadowing state by probabilistic means. It is envisaged here that the state of being shadowed can be determined probabilistically based on the traffic density, since denser traffic implies a higher probability of being shadowed. If shadowed, the ac-

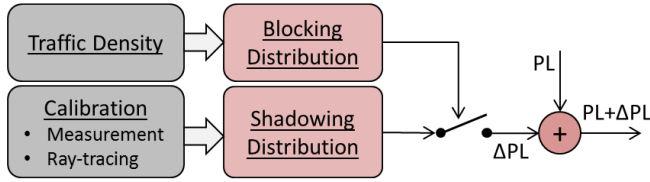


Fig. L.8: Overview of the intended future dynamic and scalable shadowing model for V2X communications.

tual fading state (ΔPL) can be determined from the distributions in Figure L.3 using the inverse percentile transformation method, and added to the overall link path loss (PL).

A more deterministic model, based on the actual geometry of the link and the obstructing vehicle, can be computed from more detailed information extracted from the measurements. For instance, based on the different combinations of V2V and V2I TX antenna height (h_{TX}), distance from the TX to the first lane of the road (d_{road}), interaction angle between the TX and the truck (α), target lane ($\#_{lane,RX}$), and lane where the obstacle truck is located ($\#_{lane,truck}$), the model output can be summarized in terms of the shadowing path loss (fading state) over a particular lane, and the spatial length over which this occurs (fading state duration). Such a model can be tailored for time-dynamic system level simulations.

The model output, defined in (L.3), is given as a look-up table in Table L.2 in terms of shadow amplitude (SA, in dB) and shadow length (SL, in m), relative to the central position (ref) defined by the intersection between the target lane and the interaction angle (α) - see lane 4 on Figure L.1 for visual reference. The pairs of values have been determined by applying a 6 dB reference threshold on the data, from either measurements (M) or ray-tracing (RT) simulations, so that a bounded region results for the shadowing length. Each corresponding pair (SA,SL) is defined over the length of the lane where measured or simulated data exceeds this threshold, as depicted in Figure L.9.

$$(SA, SL) = f(h_{TX}, d_{road}, \alpha, \#_{lane,RX}, \#_{lane,truck}) \quad (L.3)$$

As an example on how the SA and SL coefficients have been calculated, the 6 dB shadow threshold has been plotted as a reference in Figures L.6.d and L.7.d, and the corresponding output values have been highlighted in Table L.2. The reference value for the threshold was selected due to the fact that, for the explored scenario, diffraction on the truck wedges is the main propagation mechanism into the shadowed areas, and 6 dB is the minimum knife-edge diffraction loss when half of the TX antenna beam is blocked by the truck [14]. A sensitivity analysis was performed on the selected reference threshold value, finding very similar values for 0 dB and 3 dB thresholds, with small average SA differences of 0.2 dB and slightly larger (1.2-2.5 m) SL values.

It should be noticed that the interaction angles in Table L.2 have been classified as 0, ± 60 and ± 90 degrees. Each of them encompass the different TX positions with ordinate (y) 0, ± 6 and ± 40 m, respectively. This has been done for simplification of the model, to make a clearer distinction in interaction angle (normal incidence, intermediate condition, and grazing angle). This initial look-up approach of the model

Table L.2: Model look-up table with the different measured (M) and simulated (RT) shadow lengths (SL) in m and shadow amplitudes (SA) in dB at 5800 MHz.

d_{road} [m]	α [°]	h_{rx} [m]	Obstacle truck on lane 1				Obstacle truck on lane 2				Obstacle truck on lane 3				
			Lane 1 [m] / [dB]	Lane 2 [m] / [dB]	Lane 3 [m] / [dB]	Lane 4 [m] / [dB]	Lane 1 [m] / [dB]	Lane 2 [m] / [dB]	Lane 3 [m] / [dB]	Lane 4 [m] / [dB]	Lane 1 [m] / [dB]	Lane 2 [m] / [dB]	Lane 3 [m] / [dB]	Lane 4 [m] / [dB]	
2	90	M	14 / 11.3	4 / 7.1	0 / 0	0 / 0	9 / 15.4	13 / 8.3	0 / 0	0 / 0	6 / 12	14 / 9.9	14 / 9.9	14 / 9.9	
		RT	12 / 11.5	0 / 0	0 / 0	0 / 0	7 / 12.6	15 / 9.1	0 / 0	0 / 0	5 / 12.8	14 / 9.3	14 / 9.3	14 / 9.3	
		M	14 / 10.4	27 / 9.4	2 / 27.5	0 / 0	9 / 13.5	22 / 10.1	5 / 6.7	5 / 6.7	4 / 11.8	19 / 10.6	19 / 10.6	19 / 10.6	
		RT	12 / 10	22 / 8.8	0 / 0	0 / 0	7 / 12.1	25 / 9.3	12 / 7.3	12 / 7.3	4 / 15	20 / 8.6	20 / 8.6	20 / 8.6	
		1.5	M	3 / 10.9	4 / 9.8	0 / 0	0 / 0	11 / 12.7	13 / 10.4	6 / 8.9	6 / 8.9	0 / 0	16 / 12.3	16 / 12.3	16 / 12.3
		RT	11 / 12.1	1 / 6.2	0 / 0	0 / 0	9 / 11	11 / 8.2	3 / 6.5	3 / 6.5	5 / 12.6	12 / 8.9	12 / 8.9	12 / 8.9	
	60	M	3 / 11.9	9 / 12.3	4 / 7.2	0 / 0	4 / 11.6	10 / 12.6	10 / 8.8	10 / 8.8	4 / 11.9	6 / 11.7	6 / 11.7	6 / 11.7	
		RT	2 / 10.5	9 / 9.6	0 / 0	0 / 0	1 / 8.5	10 / 16.6	0 / 0	0 / 0	1 / 6.3	10 / 14.8	10 / 14.8	10 / 14.8	
		M	6 / 15.3	15 / 16	14 / 11.6	2 / 6.2	4 / 18.2	11 / 17.4	13 / 14.8	13 / 14.8	6 / 12.5	11 / 15.2	11 / 15.2	11 / 15.2	
		RT	4 / 13.3	14 / 19.6	0 / 0	0 / 0	2 / 7.8	13 / 19.4	13 / 11.6	13 / 11.6	1 / 8	12 / 17.4	12 / 17.4	12 / 17.4	
		1.5	M	15 / 10.1	22 / 16.5	42 / 18.1	40 / 14.6	3 / 17.5	11 / 18.3	18 / 14	18 / 14	5 / 12.5	11 / 16.9	11 / 16.9	11 / 16.9
		RT	5 / 12.9	25 / 17.8	36 / 13.6	40 / 16.4	2 / 11.8	16 / 19	20 / 12.9	20 / 12.9	1 / 10.1	14 / 16.5	14 / 16.5	14 / 16.5	
-60	0	M	7 / 11.2	7 / 12.7	3 / 7.3	3 / 8.3	1 / 6.1	13 / 11	8 / 8.7	8 / 8.7	0 / 0	12 / 13	12 / 13	12 / 13	
		RT	2 / 9.1	9 / 9.4	0 / 0	0 / 0	0 / 0	11 / 15.3	0 / 0	0 / 0	0 / 0	11 / 13	11 / 13	11 / 13	
		M	6 / 14.3	22 / 12.1	8 / 11.7	2 / 8	0 / 0	16 / 13.3	15 / 13	15 / 13	1 / 7.5	9 / 15.4	9 / 15.4	9 / 15.4	
		RT	3 / 8.3	15 / 16.6	0 / 0	0 / 0	0 / 0	14 / 15.6	12 / 11.9	12 / 11.9	0 / 0	12 / 15.1	12 / 15.1	12 / 15.1	
		1.5	M	2 / 8.2	23 / 14.6	31 / 15.8	42 / 17.7	0 / 0	13 / 17.6	16 / 14.7	16 / 14.7	0 / 0	10 / 15.3	10 / 15.3	10 / 15.3
		RT	4 / 10.6	24 / 20	33 / 19.7	43 / 19	1 / 15.5	15 / 24.6	20 / 16	20 / 16	1 / 9.6	12 / 20.3	12 / 20.3	12 / 20.3	
	-90	M	4 / 12.1	5 / 7	0 / 0	3 / 9.9	4 / 17.9	10 / 12.4	0 / 0	0 / 0	5 / 15.4	11 / 15.2	11 / 15.2	11 / 15.2	
		RT	4 / 11.4	8 / 8.6	0 / 0	0 / 0	2 / 10.3	12 / 13.7	0 / 0	0 / 0	1 / 12	12 / 12.2	12 / 12.2	12 / 12.2	
		M	2 / 12.7	15 / 9.9	0 / 0	0 / 0	5 / 16.3	12 / 14.4	13 / 9.9	13 / 9.9	4 / 17.5	11 / 15.3	11 / 15.3	11 / 15.3	
		RT	6 / 10.4	18 / 13.5	0 / 0	0 / 0	2 / 11.9	15 / 15.5	14 / 10.5	14 / 10.5	1 / 14.4	14 / 14.9	14 / 14.9	14 / 14.9	
		1.5	M	5 / 15.4	26 / 16.1	26 / 11.3	41 / 16	1 / 12.1	11 / 14.1	14 / 12.4	14 / 12.4	0 / 0	9 / 15.2	9 / 15.2	9 / 15.2
		RT	6 / 14.9	23 / 18.2	35 / 14	41 / 17.1	2 / 18.9	15 / 19.5	20 / 13.3	20 / 13.3	1 / 18.4	13 / 17	13 / 17	13 / 17	
-90	M	15 / 11.4	0 / 0	0 / 0	0 / 0	8 / 12.3	15 / 9.7	0 / 0	0 / 0	2 / 13.6	11 / 11.8	11 / 11.8	11 / 11.8		
	RT	16 / 10.7	0 / 0	0 / 0	0 / 0	9 / 11.3	19 / 8.8	0 / 0	0 / 0	6 / 11.7	18 / 8.7	18 / 8.7	18 / 8.7		
	M	36 / 9.2	30 / 11.6	1 / 7.2	0 / 0	13 / 9.9	31 / 10	19 / 7.8	19 / 7.8	2 / 12.7	17 / 10.1	17 / 10.1	17 / 10.1		
	RT	16 / 9.5	23 / 8.8	0 / 0	0 / 0	7 / 12.1	27 / 9.4	8 / 7.1	8 / 7.1	5 / 12.9	21 / 8.7	21 / 8.7	21 / 8.7		
	1.5	M	19 / 11.3	25 / 8.8	3 / 7.1	0 / 0	4 / 16.1	19 / 10.4	16 / 9.3	16 / 9.3	5 / 13.1	19 / 11	19 / 11	19 / 11	
	RT	12 / 13.8	1 / 6.1	0 / 0	0 / 0	9 / 13.5	11 / 8.2	6 / 6.7	6 / 6.7	5 / 16.2	15 / 8.3	15 / 8.3	15 / 8.3		

d_{road} [m]	α [°]	h_{TX} [m]	Obstacle truck on lane 1								Obstacle truck on lane 2								Obstacle truck on lane 3																									
			Lane 1		Lane 2		Lane 3		Lane 4		Lane 2		Lane 3		Lane 4		Lane 3		Lane 4																									
			[m]	[dB]	[m]	[dB]	[m]	[dB]	[m]	[dB]	[m]	[dB]	[m]	[dB]	[m]	[dB]	[m]	[dB]	[m]	[dB]	[m]	[dB]																						
5	90	M	7 / 13.2	10 / 8.2	0 / 0	0 / 0	0 / 0	0 / 0	5 / 11.4	13 / 9.7	0 / 0	4 / 9.1	13 / 11.2	M	9 / 11.4	20 / 9.9	15 / 7.4	0 / 0	5 / 11	18 / 9.8	21 / 8.6	2 / 9.6	16 / 10.1	M	8 / 12	16 / 8.5	0 / 0	5 / 13	18 / 10.1	0 / 0	4 / 11.9	16 / 9.9												
		RT	8 / 12	16 / 8.5	0 / 0	0 / 0	0 / 0	0 / 0	5 / 13	18 / 10.1	0 / 0	4 / 9.1	13 / 11.2	M	8 / 11.4	26 / 9.2	14 / 8	0 / 0	5 / 13.3	23 / 9	18 / 8.8	3 / 14.2	17 / 9.3	M	9 / 11.4	26 / 9.2	14 / 8	0 / 0	5 / 13.3	23 / 9	18 / 8.8	3 / 14.2	17 / 9.3											
		M	13 / 8.5	18 / 10.3	12 / 9.6	0 / 0	4 / 9.8	18 / 10.4	25 / 9.5	2 / 9.2	16 / 11.4	M	10 / 10.7	11 / 7.7	4 / 6.3	0 / 0	5 / 12.7	15 / 10.9	7 / 6.4	3 / 13.9	14 / 10.4	M	4 / 14.7	8 / 14.9	0 / 0	0 / 0	15 / 12.8	7 / 11.3	0 / 0	11 / 14.5	11 / 14.5													
		RT	10 / 10.7	11 / 7.7	4 / 6.3	0 / 0	5 / 12.7	15 / 10.9	7 / 6.4	3 / 13.9	14 / 10.4	M	4 / 14.7	8 / 14.9	0 / 0	0 / 0	15 / 12.8	7 / 11.3	0 / 0	11 / 14.5	11 / 14.5	M	1 / 9.6	10 / 16.1	0 / 0	1 / 6.4	10 / 17.1	0 / 0	0 / 0	10 / 15.6	10 / 15.6													
	60	M	5 / 17.1	12 / 17.4	11 / 13.1	12 / 8.1	1 / 7.3	13 / 14.4	12 / 14.5	0 / 0	10 / 15.9	M	5 / 17.1	12 / 17.4	11 / 13.1	12 / 8.1	1 / 7.3	13 / 14.4	12 / 14.5	0 / 0	10 / 15.9	M	2 / 8.1	13 / 12.6	7 / 6.6	1 / 10.1	9 / 13	M	6 / 12	10 / 13.1	9 / 8.1	0 / 0	2 / 8.1	13 / 12.6	7 / 6.6	1 / 10.1	9 / 13							
		RT	2 / 8.3	13 / 20	13 / 12.3	0 / 0	1 / 8.2	12 / 16.9	13 / 14.3	0 / 0	12 / 17.5	M	6 / 12	10 / 13.1	9 / 8.1	0 / 0	2 / 8.1	13 / 12.6	7 / 6.6	1 / 10.1	9 / 13	M	6 / 12	10 / 13.1	9 / 8.1	0 / 0	2 / 8.1	13 / 12.6	7 / 6.6	1 / 10.1	9 / 13	M	1 / 6.3	11 / 14.9	0 / 0	0 / 0	11 / 13.1	11 / 13.1						
		M	4 / 18.3	15 / 17.4	19 / 14.7	26 / 14	0 / 0	12 / 17.2	14 / 14.3	0 / 0	10 / 15	M	4 / 18.3	15 / 17.4	19 / 14.7	26 / 14	0 / 0	12 / 17.2	14 / 14.3	0 / 0	10 / 15	M	6 / 12	10 / 13.1	9 / 8.1	0 / 0	2 / 8.1	13 / 12.6	7 / 6.6	1 / 10.1	9 / 13	M	6 / 14.4	16 / 13.7	20 / 11.3	13 / 9	3 / 8.1	12 / 14.6	14 / 12.5	1 / 6.6	10 / 13.8			
		RT	2 / 12.8	17 / 19	21 / 13.7	26 / 11.2	1 / 10.7	13 / 19.4	16 / 11.9	0 / 0	12 / 17.5	M	4 / 18.3	15 / 17.4	19 / 14.7	26 / 14	0 / 0	12 / 17.2	14 / 14.3	0 / 0	10 / 15	M	1 / 6.3	11 / 14.9	0 / 0	0 / 0	11 / 13.1	M	1 / 6.3	14 / 16.1	12 / 12.9	0 / 0	0 / 0	12 / 15	14 / 13	0 / 0	12 / 14.3	12 / 14.3						
	0	M	7 / 17.2	12 / 16	18 / 15.3	21 / 12.6	2 / 7.4	10 / 17.5	13 / 15.2	2 / 7	10 / 16.2	M	7 / 17.2	12 / 16	18 / 15.3	21 / 12.6	2 / 7.4	10 / 17.5	13 / 15.2	2 / 7	10 / 16.2	M	4 / 15.6	8 / 13.7	2 / 6.7	0 / 0	4 / 16.5	11 / 13.8	5 / 7.6	0 / 0	9 / 12.8	8 / 16.4	M	4 / 15.6	8 / 13.7	2 / 6.7	0 / 0	4 / 16.5	11 / 13.8	5 / 7.6	0 / 0	9 / 12.8	8 / 16.4	
		RT	2 / 11.2	15 / 25.7	20 / 17.6	25 / 13.7	1 / 10.2	12 / 23.1	16 / 13.2	1 / 6.4	12 / 17.2	M	2 / 11.2	15 / 25.7	20 / 17.6	25 / 13.7	1 / 10.2	12 / 23.1	16 / 13.2	1 / 6.4	12 / 17.2	M	2 / 10.6	12 / 13.2	0 / 0	0 / 0	1 / 12.3	12 / 14	0 / 0	1 / 12.3	12 / 12.7	M	4 / 17.4	13 / 14.4	13 / 11.6	7 / 6.7	4 / 17.9	13 / 14.5	14 / 12.8	0 / 0	8 / 16.4	8 / 16.4		
		M	4 / 15.6	8 / 13.7	2 / 6.7	0 / 0	4 / 16.5	11 / 13.8	5 / 7.6	0 / 0	9 / 12.8	M	4 / 15.6	8 / 13.7	2 / 6.7	0 / 0	4 / 16.5	11 / 13.8	5 / 7.6	0 / 0	9 / 12.8	M	4 / 17.4	13 / 14.4	13 / 11.6	7 / 6.7	4 / 17.9	13 / 14.5	14 / 12.8	0 / 0	8 / 16.4	8 / 16.4	M	2 / 12.1	16 / 15.1	14 / 11.3	0 / 0	1 / 14.3	13 / 15.6	13 / 12.9	1 / 15.2	12 / 16.6	12 / 16.6	
		RT	3 / 15.5	16 / 19.5	20 / 14.5	25 / 11.8	1 / 19.4	13 / 19.2	15 / 12.5	1 / 14.8	12 / 17	M	4 / 14.8	12 / 14.7	14 / 12.7	18 / 12.9	0 / 0	10 / 16.5	13 / 12.2	0 / 0	8 / 16.6	M	2 / 10.6	12 / 13.2	0 / 0	0 / 0	1 / 12.3	12 / 14	0 / 0	1 / 12.3	12 / 12.7	M	4 / 17.4	13 / 14.4	13 / 11.6	7 / 6.7	4 / 17.9	13 / 14.5	14 / 12.8	0 / 0	8 / 16.4	8 / 16.4		
-60	M	11 / 13	14 / 10.3	0 / 0	0 / 0	6 / 18.2	16 / 11.9	3 / 7	5 / 11.9	17 / 11.5	M	11 / 13	14 / 10.3	0 / 0	0 / 0	6 / 18.2	16 / 11.9	3 / 7	5 / 11.9	17 / 11.5	M	11 / 13	14 / 10.3	0 / 0	0 / 0	6 / 18.2	16 / 11.9	3 / 7	5 / 11.9	17 / 11.5	M	11 / 13	14 / 10.3	0 / 0	0 / 0	6 / 18.2	16 / 11.9	3 / 7	5 / 11.9	17 / 11.5				
	RT	10 / 11.1	20 / 8.3	0 / 0	0 / 0	6 / 11.8	19 / 10.5	0 / 0	5 / 11.8	17 / 11.5	M	10 / 11.1	20 / 8.3	0 / 0	0 / 0	6 / 11.8	19 / 10.5	0 / 0	5 / 11.8	17 / 11.5	M	10 / 11.1	20 / 8.3	0 / 0	0 / 0	6 / 11.8	19 / 10.5	0 / 0	5 / 11.8	17 / 11.5	M	10 / 11.1	20 / 8.3	0 / 0	0 / 0	6 / 11.8	19 / 10.5	0 / 0	5 / 11.8	17 / 11.5				
	M	17 / 11.9	34 / 11	16 / 9.2	0 / 0	6 / 14.5	22 / 9.9	5 / 15.8	5 / 11.8	15 / 9.1	M	17 / 11.9	34 / 11	16 / 9.2	0 / 0	6 / 14.5	22 / 9.9	5 / 15.8	5 / 11.8	15 / 9.1	M	17 / 11.9	34 / 11	16 / 9.2	0 / 0	6 / 14.5	22 / 9.9	5 / 15.8	5 / 11.8	15 / 9.1	M	17 / 11.9	34 / 11	16 / 9.2	0 / 0	6 / 14.5	22 / 9.9	5 / 15.8	5 / 11.8	15 / 9.1				
	RT	7 / 12.2	29 / 9.3	11 / 7.8	0 / 0	5 / 13	21 / 9.4	22 / 8.4	5 / 11.8	13 / 12	M	7 / 12.2	29 / 9.3	11 / 7.8	0 / 0	5 / 13	21 / 9.4	22 / 8.4	5 / 11.8	13 / 12	M	7 / 12.2	29 / 9.3	11 / 7.8	0 / 0	5 / 13	21 / 9.4	22 / 8.4	5 / 11.8	13 / 12	M	7 / 12.2	29 / 9.3	11 / 7.8	0 / 0	5 / 13	21 / 9.4	22 / 8.4	5 / 11.8	13 / 12				
-90	M	8 / 11.1	23 / 10.5	20 / 8.8	0 / 0	0 / 0	0 / 0	0 / 0	4 / 11	13 / 12	M	8 / 11.1	23 / 10.5	20 / 8.8	0 / 0	0 / 0	0 / 0	0 / 0	4 / 11	13 / 12	M	8 / 11.1	23 / 10.5	20 / 8.8	0 / 0	0 / 0	4 / 11	13 / 12	M	8 / 11.1	23 / 10.5	20 / 8.8	0 / 0	0 / 0	4 / 11	13 / 12	M	8 / 11.1	23 / 10.5	20 / 8.8	0 / 0	0 / 0	4 / 11	13 / 12
	RT	10 / 13	12 / 7.5	5 / 6.9	0 / 0	5 / 16.6	14 / 11.1	8 / 6.6	5 / 14.5	14 / 10.3	M	10 / 13	12 / 7.5	5 / 6.9	0 / 0	5 / 16.6	14 / 11.1	8 / 6.6	5 / 14.5	14 / 10.3	M	10 / 13	12 / 7.5	5 / 6.9	0 / 0	5 / 16.6	14 / 11.1	8 / 6.6	5 / 14.5	14 / 10.3	M	10 / 13	12 / 7.5	5 / 6.9	0 / 0	5 / 16.6	14 / 11.1	8 / 6.6	5 / 14.5	14 / 10.3				

d_{road} [m]	α [°]	h_{TX} [m]	Obstacle truck on lane 1				Obstacle truck on lane 2				Obstacle truck on lane 3			
			Lane 1 [m] / [dB]	Lane 2 [m] / [dB]	Lane 3 [m] / [dB]	Lane 4 [m] / [dB]	Lane 2 [m] / [dB]	Lane 3 [m] / [dB]	Lane 4 [m] / [dB]	Lane 3 [m] / [dB]	Lane 4 [m] / [dB]	Lane 3 [m] / [dB]	Lane 4 [m] / [dB]	
10	0	M	5 / 12.2	10 / 12.3	9 / 10	2 / 8.5	1 / 7	11 / 12.2	10 / 10.8	0 / 0	10 / 13	0 / 0	10 / 15.1	
		RT	0 / 0	11 / 14	9 / 8.3	0 / 0	0 / 0	10 / 14.1	9 / 10	0 / 0	10 / 15.1	0 / 0	10 / 15.1	
	5	M	6 / 11.6	11 / 14	12 / 12.5	15 / 11.1	0 / 0	12 / 12.4	11 / 12.4	0 / 0	9 / 13.5	0 / 0	11 / 16.6	
		RT	0 / 0	12 / 14	14 / 13.2	12 / 10.8	0 / 0	11 / 16.3	12 / 13.4	0 / 0	11 / 16.6	0 / 0	11 / 16.6	
	1.5	M	4 / 16.4	11 / 15.4	12 / 12.2	13 / 11.5	0 / 0	12 / 13.7	11 / 11.9	0 / 0	8 / 13.7	0 / 0	10 / 18.8	
		RT	1 / 8.6	12 / 20.2	14 / 12.7	14 / 10.3	0 / 0	11 / 19.7	10 / 12.6	0 / 0	10 / 18.8	0 / 0	10 / 18.8	

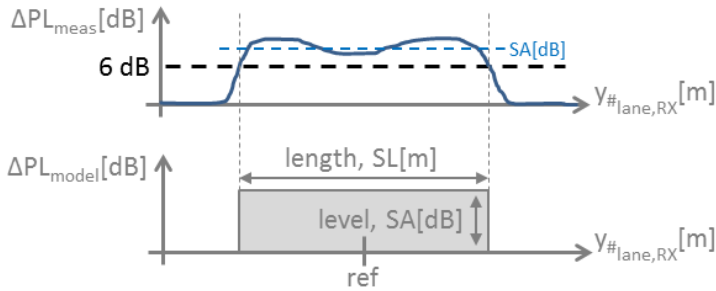


Fig. L.9: Initial deterministic shadow model: calculation of the SA and SL coefficients and application example.

has some limitations, due to the size of the scenario explored. In this respect, shadow lengths may be larger in reality than what is given in the table, for TX positions at large interaction angles. However, a minor error is expected in shadow amplitude. This can be easily understood from, for example, the V2I example presented in Figure L.7, where the shadow would be further extended on lanes 2-3 for positions with ordinate smaller than -40 m. The average difference between the coefficients calculated over the measurement data or the ray-tracing data is approximately 0.4 dB in shadow amplitude, and smaller than 1 m in shadow length.

With this initial version of the model, it is possible to simulate only very basic V2X scenarios and situations (e.g. a car overtaking a truck). However, for that particular situation, it would be already possible to perform a sensitivity analysis of different V2I deployment configurations considering, for example, different RSU inter-site distances and antenna heights, for various car speeds. This will provide some initial insights on how the shadowing due to large obstacles may affect the reliability of the link, even though it is only for a short period of time. The future model will, of course, consider more complex situations, including more dynamic aspects of the scenario.

6 Conclusions

This paper presented a measurement-based evaluation of the impact of large vehicle shadowing on V2X scenarios at 5.8 GHz. An extensive measurement campaign was performed by considering several V2V and V2I configurations in a practical 4-lane road section scenario. The RX antenna height was fixed to average vehicular height (1.5 m), and the TX antenna heights were fixed to 5 and 7 m for the V2I scenarios, and 1.5 m for the V2V cases. Different shadow conditions were created by placing a large truck at different positions, obstructing the LOS between TX and RX.

The analysis of the measurement data shows how, in case of being shadowed by a large vehicle, the impact is more significant in the V2V scenario than in the V2I scenario, which benefits from the elevated TX antenna position. The maximum shadowing levels experienced were 27 dB in the V2V scenario, 23 dB in the V2I scenario with TX antenna height at 5 m, and 21 dB in the V2I scenario with TX antenna height 7 m. The empirical distributions are given in the paper, and are useful for statistical characterization of the V2X scenario. The impact to the shadow level due to non-symmetries of the obstacle truck was also evaluated, finding small average variations of approximately 2 dB.

The measurements were compared to 3D ray-tracing simulations, showing a good match with a RMSE of 4.1 dB. From these results it can be concluded that ray-tracing simulations, based on 3D models with limited details and material characterization, can still result in accurate levels of predictions of both geometry and shadow levels.

The future work was also introduced in the paper, presenting the roadmap towards a dynamic and scalable shadowing model suitable for simulation of V2X communication systems. As an alternative initial approach, a look-up table-based deterministic shadowing model was presented. The different coefficients of the model, computed from both the measurements and the ray-tracing simulations, can be used to characterize the areas shadowed by a truck inside a 4-lane road scenario.

Acknowledgment

The authors would like to thank Køretekniisk Anlæg Nørresundby for providing access to the area and the truck. The authors would also like to express their gratitude to Kristian Bank, Assistant Engineer from the Department of Electronics Systems, Aalborg University, for his effort and support with the measurement setup. This work was supported by Innovation Fund Denmark.

References

- [1] G. Poci, M. Lauridsen, B. Soret, K. I. Pedersen, and P. Mogensen, "Automation for on-road vehicles: Use cases and requirements for radio design," in *IEEE 82nd Vehicular Technology Conference (VTC-Fall)*, Sept 2015, pp. 1–5.
- [2] W. Viriyasitavat, M. Boban, H. M. Tsai, and A. Vasilakos, "Vehicular communications: Survey and challenges of channel and propagation models," *IEEE Vehicular Technology Magazine*, vol. 10, no. 2, pp. 55–66, June 2015.
- [3] R. He, A. F. Molisch, F. Tufvesson, Z. Zhong, B. Ai, and T. Zhang, "Vehicle-to-vehicle propagation models with large vehicle obstructions," *IEEE Transactions on Intelligent Transportation Systems*, vol. 15, no. 5, pp. 2237–2248, Oct 2014.
- [4] R. Meireles, M. Boban, P. Steenkiste, O. Tonguz, and J. Barros, "Experimental study on the impact of vehicular obstructions in VANETs," in *IEEE Vehicular Networking Conference*, Dec 2010, pp. 338–345.

- [5] A. Chelli, R. Hamdi, and M. S. Alouini, "A vehicle-to-infrastructure channel model for blind corner scattering environments," in *IEEE 78th Vehicular Technology Conference (VTC-Fall)*, Sept 2013, pp. 1–6.
- [6] G. Acosta-Marum and M. A. Ingram, "Six time- and frequency- selective empirical channel models for vehicular wireless LANs," *IEEE Vehicular Technology Magazine*, vol. 2, no. 4, pp. 4–11, Dec 2007.
- [7] J. Gozalvez, M. Sepulcre, and R. Bauza, "IEEE 802.11p vehicle to infrastructure communications in urban environments," *IEEE Communications Magazine*, vol. 50, no. 5, pp. 176–183, May 2012.
- [8] C. F. Mecklenbrauker, A. F. Molisch, J. Karedal, F. Tufvesson, A. Paier, L. Bernado, T. Zemen, O. Klemp, and N. Czink, "Vehicular Channel Characterization and Its Implications for Wireless System Design and Performance," *Proceedings of the IEEE*, vol. 99, no. 7, pp. 1189–1212, July 2011.
- [9] D. W. Matolak, *V2V Communication Channels: State of Knowledge, New Results, and What's Next*. Berlin, Heidelberg: Springer Berlin Heidelberg, 2013, pp. 1–21. [Online]. Available: http://dx.doi.org/10.1007/978-3-642-37974-1_1
- [10] K. Dar, M. Bakhouya, J. Gaber, M. Wack, and P. Lorenz, "Wireless communication technologies for ITS applications [topics in automotive networking]," *IEEE Communications Magazine*, vol. 48, no. 5, pp. 156–162, May 2010.
- [11] F. C. M. Wegman and M. Slop, *Safety Effects of Road Design Standards in Europe. The European Market for Infrastructural Projects*, September 2016.
- [12] "The international council on green transportation," European Vehicle Market Statistics. Pocketbook, 2014.
- [13] A. Communications, "Wave propagation and radio network planning," <http://www.awe-communications.com/>, [Online; accessed February 2016].
- [14] W. C. Y. Lee, *Mobile Communications Engineering. 2nd Edition*. McGraw Hill, 1983.

Paper M – (Collaboration 5)

A Simple Statistical Signal Loss Model for Deep
Underground Garage

Huan Cong Nguyen, Lucas Chavarría Giménez, István Z.
Kovács, Ignacio Rodríguez, Troels Bundgaard Sørensen,
Preben Mogensen

Published in
IEEE 84th Vehicular Technology Conference (VTC Fall). 2016.

© 2016 IEEE

Reprinted with permission. The layout has been revised.

Abstract

In this paper we address the channel modeling aspects for a deep-indoor scenario with extreme coverage conditions in terms of signal losses, namely underground garage areas. We provide an in-depth analysis with regard to the path loss (gain) and large-scale signal shadow fading, and propose a simple propagation model which can be used to predict cellular signal levels in similar deep-indoor scenarios. The measurement results indicate that the signal at 800 MHz band penetrates external concrete walls to reach the lower levels, while for 2000 MHz wall openings are required for the signal to propagate. From the study it is also evident that the shadow fading between different levels of an underground garage are highly correlated. The proposed frequency-independent floor attenuation factor (FAF) is shown to be in the range of 5.2 dB per meter deep.

1 Introduction

The telecommunication industry is adopting new radio technologies, moving from 2G/3G to 4G systems, and within next 10 years the first commercial 5G networks are also expected to be available [1–3]. This technology evolution is heavily driven by the introduction of new services and a steady increase of the number of mobile users. In addition to mobile voice and broadband (MBB) services, new emerging applications based on Machine Type Communications (MTC) will increase significantly both the number of devices connected to the mobile radio network and also the geographical area which requires service coverage [2, 3]. For this reason, Mobile Network Operators (MNOs) are planing their radio networks to provide close to 100 % (probability) service coverage across the different frequency bands, cell types (macro, micro, pico) and technologies (2G, 3G, 4G, WLAN) deployed. To achieve this target, the required radio network planing has become a very complex task in recent years and will remain an important part of the 5G network deployments optimization as well. Further, the network deployment scenarios not sufficiently investigated in past for 2G/3G/4G systems due to their infrequent occurrence in real-life MNO deployments, will need to be analyzed and characterized in terms of radio channel propagation conditions. A typical example for this is the case of growing MTC services where applications rely on the large scale deployment of devices such as, environmental sensors, remote controlled units, industrial actuators, which were not available in the past or were not operating connected to wireless networks. [1].

In this paper we address the channel modeling aspects for a deep-indoor scenario with extreme coverage conditions in terms of signal losses, namely underground garage areas. Typically today, in these use cases, MNO provide voice services by means of a combination of cell types (macro and micro, indoor) and/or technologies, tailored for the expected traffic load. Although penetration loss and indoor attenuation models have been studied widely in the literature [4–9], to the best of our knowledge none of them discusses the rate of attenuation across floor for underground structures.

In this paper, our investigations are based on radio channel measurements of deployed (live) urban 3G and 4G networks, which provide radio coverage outside

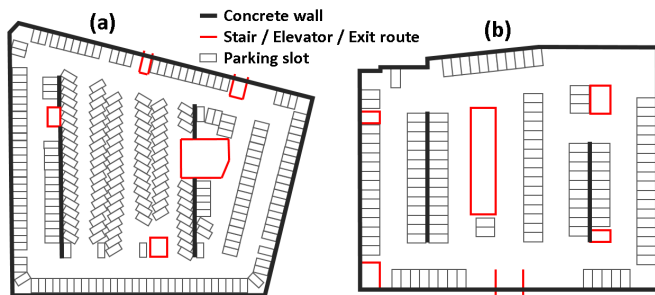


Fig. M.1: The layouts of the two deepest underground parking garages in Denmark: (a) Friis, level -3 and (b) Dalgashus, level -1.

and inside selected underground garage locations. We provide an in-depth analysis in terms of path loss (gain) and large scale signal shadowing and, propose simple propagation models which can be used to predict cellular signal levels in similar deep-indoor scenarios. Our study also highlights the indoor radio coverage limitations of current network deployments.

The paper is organized as follows: In Section 2 the scenarios, measurement setup and procedures are discussed. The results are analyzed in Section 3, and finally the conclusions are drawn in Section 4.

2 Measurement Campaign

2.1 Scenarios

The measurement campaign took place at the two deepest underground car parks in Denmark, which belong to Friis and Dalgashus Shopping Center. Located at the heart of Aalborg city, Friis is a modern building complex consisting of a shopping center, hotel, offices, business center and car park. Its parking lot is built over an area of approximately 60 x 70 meters and has 4 levels with the capacity of 850 parking spaces. The first level is around 4 meters underground, while all remaining are approximately 2.5 meters deep each. This makes the garage almost 12 meters below ground. Dalgashus is a shopping center and residential building in the center of Herning city. Its parking lot is also 4 levels deep, but the last level is for its residents only and hence inaccessible during our measurement. Dalgashus car park is smaller than Friis', approximately 50 x 60 meters in size and can accommodate around 480 cars. The average floor height of the garage is 2.2 meters; however its first level is half-submerged with small open windows along one side of the building, near its entrance. Figure M.1 shows the layouts of the two garages, which is very similar across levels of each garage. Both garages are constructed with thick concrete walls and floors. Visitors can access the garage via exits / entrance marked in red in the figure.

2.2 Measurement Setup and Procedures

A Rhode & Schwartz TSMW Universal Radio Network Analyzer is used to record all radio signals from surrounding live Universal Mobile Telecommunications System (UMTS) and Long-Term Evolution (LTE) cells at the frequency bands of interest, i.e. 800 and 2000 MHz. The device is connected to a Global Positioning System (GPS) antenna for marking outdoor locations, and two omni antennas with 0 dBi gain for receiving the signals. The antennas are placed on top of our car, which is traveling at an average speed of 10 km/h. For indoor locations we relied on a set of markers placed at every turn the car made. The radio signal strength is measured differently between LTE and UMTS: The LTE power measurement is extracted from the Secondary Synchronization Signal (S-Sync), which is transmitted every 5 ms on 62 sub-carriers. The sensitivity for the LTE power measurement is -127 dBm. The UMTS power is based on Received Signal Code Power (RSCP) measurement and has sensitivity of -123 dBm. The RSCP measurement is performed every 10 ms on Common Pilot Channel (CPICH).

Being at the heart of the city, next to the pedestrian and shopping streets, gives the two car parks the advantage of having very good cellular coverage. As a result, during the measurement we are able to identify signals from at least 10 macro cells inside both garages. To make it easier for plotting together the different power levels due to non-identical cell location, transmitting power, antenna pattern and technology, the indoor received power is normalized to its maximum value and hereafter is referred to as the *indoor attenuation*. Let $P_{Rx,i}(x, y, z')$ be the received signal power in dBm from the i^{th} macro cell at the indoor location defined by $[x, y, z']$ coordinates:

$$\Gamma_i(x, y, z') = P_{Rx,i}(x, y, z') - P_{Rx,i}(x_r, y_r, z'_r) \quad (M.1)$$

$$P_{Rx,i}(x_r, y_r, z'_r) = \max[P_{Rx,i}(x, y, z')] \quad (M.2)$$

where $\Gamma_i(x, y, z')$ is the indoor attenuation in dB and the *reference point*, $[x_r, y_r, z'_r]$, is the location where the maximum received signal power is observed indoor. It is important to note that such normalization does not change the distribution of the observed power samples, nor the slope of the Least-Square (LR) analysis presented in the next section. To ensure a reasonable deep indoor coverage during the measurement, we discarded all cells whose maximum indoor received signal power was lower than -80 dBm. This guarantees that we have at least around 50 dB of dynamic range for deep underground indoor attenuation measurement. In order to model the rate of attenuation across floors, we also normalize the absolute depths z' to the depth of the reference point z'_r :

$$z = z' - z'_r \quad (M.3)$$

From this point onwards all reference to depth means the relative depth z , unless otherwise stated.

In general, the total path loss, PL_{total} , between an outdoor cell and a deep underground user equipment (UE) can be expressed as follows:

$$PL_{total} = PL_{out} + W + PL_{in} - z \times L_{FAF} \quad (M.4)$$



Fig. M.2: The received signal power outside Friis from cell A at 800 MHz.

where PL_{out} is the loss up to the external wall, W is the penetration loss due to the external wall(s) and PL_{in} is the additional loss from the outer wall to the indoor location. All these terms are in dB. The term L_{FAF} is the Floor Attenuation Factor (FAF), which is measured in dB/m and represents the additional loss due to the increasing depth z . The main focus of this paper is to derive the L_{FAF} statistically from measurement.

3 Result analysis

3.1 Propagation into Underground Building Structure

The COST 231 [4] assumes that radio waves penetrate building's external wall that is in direct view of the base station, while in [6] the authors argue that the outdoor-to-indoor paths are possible only through wall openings such as door or windows. In this section, we look into how the signal propagates from outdoor to underground building structure.

Figure M.2 shows the received signal power from the LTE cell A at 800 MHz outside Friis Shopping Center. The area highlighted in pink is the Friis' building, and the black triangle marker is the cell's location. The cell points directly towards Friis, illuminating the area between the two black lines. The square and diamond marker denote the two potential entries for the signal into the underground parking lot: The first is the building corner closest to and in direct view of cell A. The latter is the entrance to the underground parking lot. In Figure M.3 the indoor attenuation from cell A is plotted in 3D. The diamond and square marker in this figure corresponds to the same markers in Figure M.2. Warm colors indicate strong received signal strength, and cold ones mean that the signal is weak. We observe that the signal has penetrated the concrete wall at the square marker, and the received signal strength here is higher than that of the triangle marker. At the square marker, the signal is measured -43

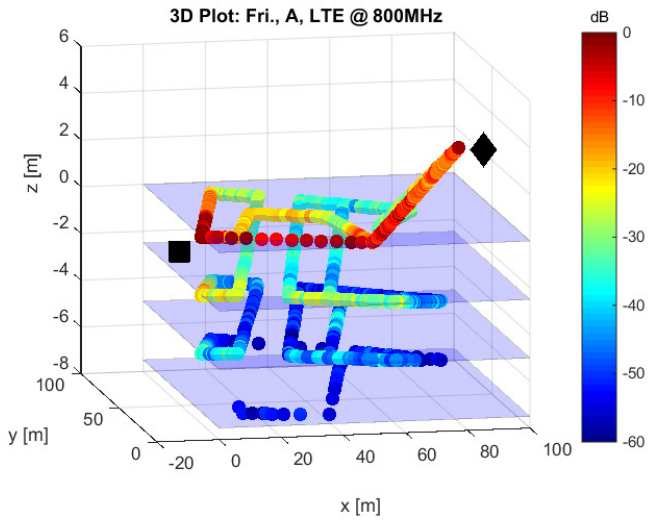


Fig. M.3: The measured indoor attenuation in Friis from cell A at 800 MHz.

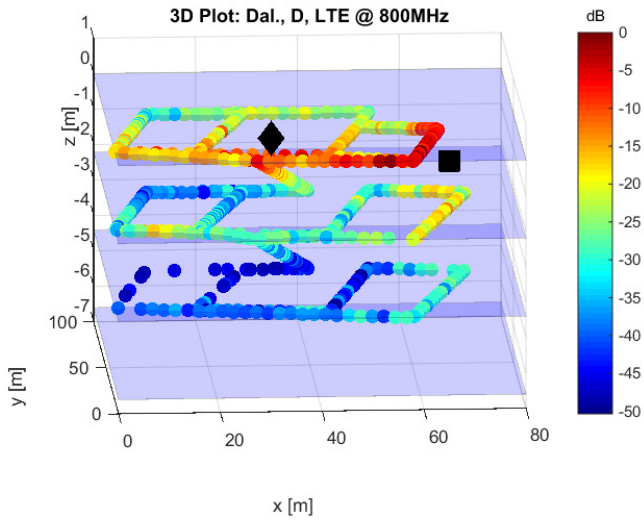


Fig. M.4: The measured indoor attenuation in Dalgashus from cell D at 800 MHz.

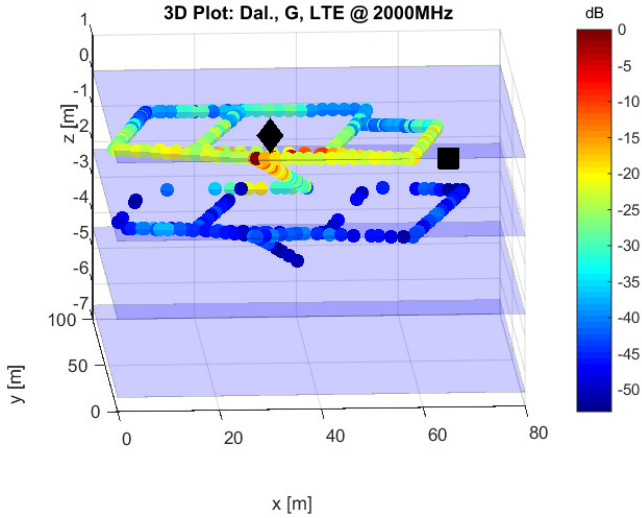


Fig. M.5: The measured indoor attenuation in Dalgashus from cell G at 2 GHz.

dBm outdoor, and -68 dBm indoor, putting the estimated outdoor-to-indoor penetration loss at 25 dB. Typically, the penetration loss for concrete walls is less than 10 dB at 800 MHz [5, 9], but in this case the signal has to penetrate also 4 meters underground. Similarly, in Dalgashus the main propagation path is through the concrete wall, marked by the black square in Figure M.4, which is in direct view with the cell under measurement, and the outdoor-to-indoor penetration loss is approximately 20dB. However, as the frequency increases in Figure M.5, the penetration loss of the concrete wall also rapidly increases [5, 9], and the path going through the garage entrance becomes dominant.

Before the measurement campaign, we expected that the stairs and elevator shafts inside the two building complexes could be paths for signal to propagate down to the underground levels. However, there is no clear evidence supporting this assumption from the measurement data. The reason might be that the stairs and elevator shafts are surrounded by concrete or glass walls, and/or they are located too deep inside the complexes, making it difficult for the signal to propagate down to the lower levels via these paths.

From Figure M.3 and M.4, the shadowing maps seem to be highly correlated over floors. To measure this, we extract data separately from the driving routes on three levels (L-1, L-2 and L-3), matching them point-by-point across levels, and then compute the correlation coefficient between them. The correlation coefficient is between $[-1, +1]$, where $+1$ indicates a perfect direct correlation, -1 in case of a perfect anti-correlation, and other value showing the degree of linear dependence between the variables. The results are presented in Table M.1, with value ranging from 0.66 to 0.91, confirming the high correlation between floors.

Table M.1: Correlation between levels

Description	Correlation coefficient		
	L-1 vs L-2	L-2 vs L-3	L-1 vs L-3
Friis: A (LTE)	0.91	0.76	0.73
Dalgashus: D (LTE)	0.66	0.69	0.83

3.2 Floor Attenuation Factor

In this section we derive the FAF statistically from all valid data sets from our measurement campaign, as shown in Table M.2. Each row of the table represents data from an unique macro cell, identified by its location (Friis or Dalgashus), cell's pseudonym, frequency band (800 or 2000 MHz) and technology (LTE or UMTS). The "Samples" column indicates how many indoor samples were collected during the measurement, and the "Min. z" is the deepest level relative to the reference point that the signal can still be observed. In order to extract the FAF, the Least-Square LR is applied separately to each data set using the following equations:

$$\beta = \frac{\sum_{i=1}^N (\Gamma_i - \bar{\Gamma})(z_i - \bar{z})}{\sum_{i=1}^N (\Gamma_i - \bar{\Gamma})^2} \quad (\text{M.5})$$

$$\alpha = \bar{z} - \beta \times \bar{\Gamma} \quad (\text{M.6})$$

$$\epsilon = \sqrt{\frac{1}{N} \sum_{i=1}^N [\Gamma_i - (\beta \times z_i + \alpha)]^2} \quad (\text{M.7})$$

where Γ_i is the indoor attenuation value and z_i is the depth of the i^{th} measurement point ($i = 1, 2, \dots, N$). $\bar{\Gamma} = \frac{1}{N} \sum_{i=1}^N \Gamma_i$ and $\bar{z} = \frac{1}{N} \sum_{i=1}^N z_i$ is the average indoor attenuation and average depth of the entire data set, respectively. The term β and α are the slope and the intercepting point of the least-square LR fitting curve, respectively. The root mean square error (RMSE), or ϵ , between the measurement data and the LR fitting curve is also computed and shown here, because it serves two purposes: first, it is an indication of how well a model fits with the measurement data, and secondly it represents the fluctuation due to obstacles and other random propagation effects, which can be useful for establishing the shadow fading model for underground garages.

Figure M.6 shows the dependency between the indoor attenuation and the depth from cell A, D and G, which has the most number of indoor samples for each pair of location and frequency band. The slopes of the fitting curves indicate the rate at which the loss increases with the decrease of the relative depth, or the FAF. From Table M.2 we observe that the FAF values extracted from different cells are similar if they are measured in the same environment: In Friis the FAF value ranges from 3.8 to 4.3 dB/m, while in Dalgashus it is from 5.5 to 5.8 dB/m at 800 MHz band. The reason for higher FAF in Dalgashus is that its first garage level is not completely underground, and therefore the mean indoor attenuation of that floor is lower than those of the other floors. This affects the slope of the fitting curve. Another interesting observation is that the 2 GHz measurement in Dalgashus shows similar FAF values as those measured at 800 MHz, indicating that the FAF does not seem to change sig-

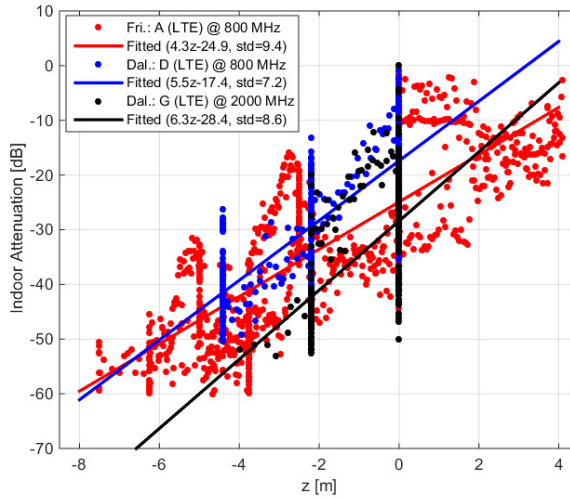


Fig. M.6: Example of measurement data and linear regression fitting curves.

Table M.2: Deep underground indoor attenuation in Friis and Dalgashus

Description Location: Cell (Tech)	Samples	Min. z [m]	Linear Regression		
			β	α	ϵ
800 MHz band					
Friis: A (LTE)	1,037	-7.50	4.3	-24.9	9.4
Friis: B (LTE)	360	-9.58	4.1	-13.7	6.6
Friis: C (UMTS)	222	-8.87	3.8	-19.4	8.6
Friis, combined			4.1		9.4
2000 MHz band					
Dalgashus: D (LTE)	591	-4.40	5.5	-17.4	7.2
Dalgashus: E (UMTS)	247	-4.40	5.7	-23.4	5.9
Dalgashus: F (UMTS)	231	-4.40	5.8	-24.0	7.2
Dalgashus, combined			5.7		7.2
2000 MHz band					
Dalgashus: G (LTE)	382	-3.99	6.3	-28.4	8.6
Dalgashus: H (LTE)	374	-3.81	5.8	-29.9	8.1
Dalgashus, combined			6.1		8.6

nificantly with the increase of frequency. This is somewhat coherent with the findings in [8], where the in-building attenuation rate in horizontal plane is also frequency-independent and measured at 0.6 dB/m for frequencies ranging from 800 MHz to 18 GHz.

By averaging all slopes from the data sets measured in Friis at 800 MHz, we

obtained a FAF of 4.1 dB/m for this scenario. Similarly, FAF values of 5.7 and 6.1 dB/m are derived for Dalgashus at 800 and 2000 MHz, respectively. Combining all cases, regardless of different scenario and frequency band, gives an average FAF of 5.2 dB/m. The attenuation rate in the z dimension therefore is much higher than the 0.6 dB/m in-building attenuation in the x and y dimension, and also the 0.6 dB/m height gain [8]. The RMSE is 9.4 dB for Friis and 7.2 dB for Dalgashus, which is in agreement with the WINNER II model C4 NLOS outdoor to indoor macro cell with shadow fading's standard deviation of 10 dB [10].

4 Conclusions

A measurement campaign was carried out at two deepest underground garages in Denmark to investigate the feasibility of using outdoor cellular network to serve deep underground devices, such as in the future MTC. Our study shows that the signal at 800 MHz band is able to penetrate the external concrete wall to reach the lower levels, while at 2000 MHz band it would require wall openings such as door or windows for the signal to enter the lower levels. There is evidence that the shadowing at different levels are highly correlated. We propose a simple signal loss prediction formula that is derived based on the measurement results. The proposed FAF is shown to depend mainly on building structure, not frequency. The average FAF is approximately 5.2 dB per meter deep, which is much higher than the horizontal indoor attenuation or the height gain, which are approximately 0.6 dB/m as measured in the literature. In the worst scenario, more than 60 dB of additional loss was observed at 12 meters deep, which indicates that outdoor-to-underground coverage can be challenging at such depth.

References

- [1] "Ericsson Mobility Report," Ericsson, Tech. Rep., 2015.
- [2] "5G White Paper," Next Generation Mobile Networks (NGMN), Tech. Rep., 2015. [Online]. Available: https://www.ngmn.org/uploads/media/NGMN_5G_White_Paper_V1_0.pdf
- [3] "5G masterplan – five keys to create the new communications era," Nokia Networks, Tech. Rep., 2016. [Online]. Available: <http://gsacom.com/paper/5g-masterplan-five-keys-create-new-communications-era/>
- [4] "COST Action 231: Digital Mobile Radio Towards Future Generation System, Final Report," European Commission, Tech. Rep., 1999. [Online]. Available: https://books.google.com/books/about/COST_Action_231.html?id=setUHQAAAJ
- [5] I. Rodriguez, H. C. Nguyen, N. T. K. Jorgensen, T. B. Sorensen, and P. Mogensen, "Radio propagation into modern buildings: Attenuation measurements in the range from 800 mhz to 18 ghz," in *2014 IEEE 80th Vehicular Technology Conference (VTC2014-Fall)*, Sept 2014, pp. 1–5.

- [6] Y. Miura, Y. Oda, and T. Taga, "Outdoor-to-indoor propagation modelling with the identification of path passing through wall openings," in *Personal, Indoor and Mobile Radio Communications, 2002. The 13th IEEE International Symposium on*, vol. 1, Sept 2002, pp. 130–134 vol.1.
- [7] E. Suikkanen, A. Tölli, and M. Latva-aho, "Characterization of propagation in an outdoor-to-indoor scenario at 780 mhz," in *21st Annual IEEE International Symposium on Personal, Indoor and Mobile Radio Communications*, Sept 2010, pp. 70–74.
- [8] H. Okamoto, K. Kitao, and S. Ichitsubo, "Outdoor-to-indoor propagation loss prediction in 800-mhz to 8-ghz band for an urban area," *IEEE Transactions on Vehicular Technology*, vol. 58, no. 3, pp. 1059–1067, March 2009.
- [9] E. Semaan, F. Harrysson, A. Furuskär, and H. Asplund, "Outdoor-to-indoor coverage in high frequency bands," in *2014 IEEE Globecom Workshops (GC Wkshps)*, Dec 2014, pp. 393–398.
- [10] "Deliverable 1.1.2: WINNER II Channel Models," WINNER, Tech. Rep., 2007.

ISSN (online): 2446-1628
ISBN (online): 978-87-7112-891-8

AALBORG UNIVERSITY PRESS